NEUTRONS
FOR SCIENCE

2002

We thank all the people who helped make this report.

In particular, we gratefully acknowledge the help of:
H. Börner, R. Currat, A. Hewat,
M. Johnson, H. Schober and P. Timmins

Editors: Giovanna Cicognani and Christian Vettier
Design and Typesetting: Lignes droites communication (38 Echirolles)
Photography by Serge Claisse (ILL) and Artechnique – artechnique@wanadoo.fr
Printing: Imprimerie du Pont-de-Claix – April 2003

Further copies can be obtained from:
Institut Laue-Langevin
Scientific Coordination Office (SCO)
BP 156 - F-38042 Grenoble Cedex 9 (France)
Tel: +33 (0)4 76 20 72 40 - Fax: +33 (0)4 76 48 39 06
email: kjenkins@ill.fr or sco@ill.fr
Web: www.ill.fr

ANNUAL REPORT.

The Institut Laue-Langevin

The Institut Laue-Langevin (ILL) is an international research centre using neutrons to probe the microscopic structure and dynamics of a broad range of materials from the molecular, atomic and nuclear point of view. The ILL is directed by three founding countries - France, Germany and the United Kingdom - whose grants to the Institut's budget of approximately 60 million € per year are enhanced by Scientific Membership contributions from Austria, the Czech Republic, Italy, Russia, Spain and Switzerland.

The ILL was founded to provide scientific communities in its member countries with a unique flow of neutrons and a matching suite of experimental facilities (some 40 instruments) for use in fields as varied as solid-state physics, materials science, chemistry, the biosciences and the earth sciences as well as nuclear physics and engineering. The Institut has ever since been an exceptional centre of excellence and a fine example of successful co-operation in Europe. It operates the most intense neutron source in the world. Over 2 000 visiting scientists, performing a total of 750 experiments per year, bear witness to the scientific success of the facility.

An exceptional centre of excellence and a fine example of successful co-operation in Europe

Directors directing

On Wednesday, 4 December at the French Ministry of research in Paris, the Fourth Protocol of the Intergovernmental Convention was signed by Mme Claudie Haigneré, Minister for Research and New Technologies (centre), Mr. Fritjof von Nordenskjöld, the German Ambassador to France (left), and Sir John Holmes, the British Ambassador to France (right). The Protocol prolongs the duration of the Convention and related subsequent agreements to the year 2014, thus guaranteeing continuity in the field of fundamental and applied research with neutrons at the ILL.

Mme Claudie Haigneré with Christian Vettier.

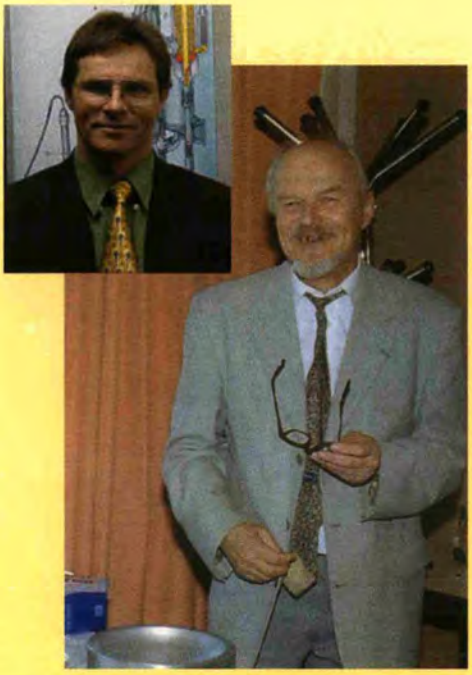

Mr Ben Lahcen, "Proviseur" of the International School of Grenoble, with Colin Carlile and Christian Vettier during his visit in November.

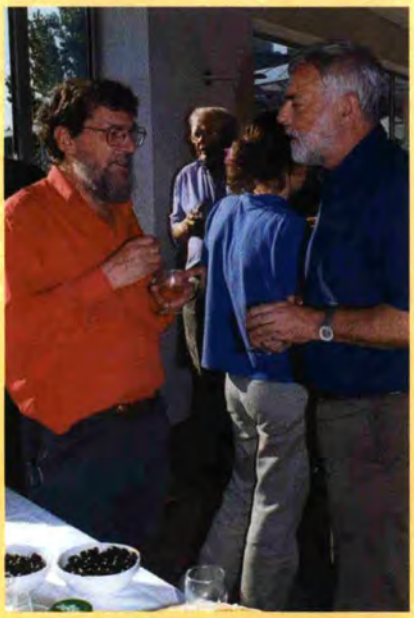

Werner Press discussing with Ted Forgan (left, University of Birmingham), Chairman of the ILL Scientific Council as from 2003.

Witness change in the reactor division
A long page of ILL's history turns over: Ekkehardt Bauer – Head of the Reactor Division – left the Institute after 27 years. Our new Head of the Reactor Division, Hervé Guyon (inset), arrived at the ILL on 11 October, after having been Head of the Orphée reactor in Saclay.

Contents

Director's report

An air of renewal pervades the Institut on all levels. This process started with the setting in place of the Millennium Programme in the year 2000 but its origins can perhaps even be traced back to the rebuild of the reactor which was completed in 1994.

The year has been dominated by the ten-yearly review of sûreté *of the ILL's installations in parallel with a review of our vulnerability to external aggression. The pushing up the political agenda of such matters is, of course, a direct result of the world events of autumn 2001 – one wilful and one accidental – in New York and Toulouse.* Sûreté *is a French word which – like* bricolage *or* terroir *– has no proper equivalent in the English language but which expresses the idea of safety, security and reliability in a single word and is a quality which the man in the street quite correctly expects the ILL to possess. We at the ILL are committed to the concept of sûreté, but not only the concept. Concepts must be translated into visible and operational reality and that is what has resulted from the 2002* sûreté *review, known colloquially as the* Groupe Permanent. *Following the many interactions with the* Groupe Permanent, *the ILL has committed itself to a refit programme which will protect the installations of the Institut from aggression either of a natural kind such as posed by earthquakes or of a pre-meditated nature. This refit renewal programme involves the fabric of the reactor building itself, the possibility that the buildings adjacent to the reactor shell – the experimental halls and the offices – could threaten the integrity of the shell itself as well as matters related to redundant control circuitry and treatment of the by-products of running a research reactor. This work programme has been costed at 20 M€ and will be implemented to a strict 3-year schedule terminating in early 2006. In order to incorporate this large programme of work into the ILL's already busy life, it has been necessary to reduce operations to 3 cycles per year – 150 days instead of the 200 to 225 days normally expected. The ILL has, however, pledged itself to protect both the scientific output of the Institut and the Millennium Programme of instrument and infrastructure renewal. We are committed to delivering 80% of the beam-days to our 9 Scientific Partner nations which we have delivered in recent years. Our 3 Associate nations are fully supportive of this initiative which safeguards the ILL for scientific research for the foreseeable future, and have undertaken to top up by 9 M€ the 11 M€ savings from the ILL's budget to fund the refit programme.*

We at the ILL are committed to the concept of sûreté

We are committed to delivering 80% of the beam-days to our 9 Scientific Partner nations

In parallel, the ILL's scientific life has progressed apace. Two examples spring to mind – the detection of quantised states of the neutron in the gravitational field of the earth, and real time studies on the millisecond frame of chemical synthesis kinetics. Many more examples are cited in this document where the depth and increasing breadth of our scientific output is evident. Our scientists are increasingly playing their part in defining the future directions for neutrons whether it be as representatives in national societies or on the European stage. They have a lot to contribute to this debate and we encourage them to do so.

Future dreams are founded on present realities

The May meeting in Bonn to present the European Spallation Source to a waiting world was attended by, quite literally, a bus-load of ILL scientists. None of the European nations, apart from the host country, had a larger delegation than that from the ILL. The meeting was a great success for neutrons and we congratulate the organisers. Future dreams, however, are founded on present realities and the deliberations of the European Strategy Forum on Research Infrastructures indicate, even using favourable conditions for new sources, that barring unforeseen events, the ILL cannot be overtaken in high quality scientific output until the second half of the next decade – 2015 at the earliest.

The ILL cannot be overtaken in high quality scientific output until 2015 at the earliest

Which is why we are vigorously pursuing the mutual benefits which partnerships will bring to the ILL – as Christian Vettier says **"more than simply neutrons".** *We have signed the agreement between ESRF, EMBL, IBS and ILL to launch a Partnership for Structural Biology – building work begins shortly, we have formally opened the Facility for Materials Engineering FAME 38 between ESRF and ILL, and we have signed the EIROforum charter – a linking together of the resources of CERN, EMBL, ESA, ESO, ESRF, JET and ILL to lobby for the support of basic sciences – in the presence of M. Busquin the European Research Commissioner at the FP6 launch in Brussels.*

The continuation of the ILL's International Convention until 31st Dec. 2013

Finally, as a Christmas present for ILL staff and users, in Paris on 4th December the continuation of the ILL's International Convention until 31st December 2013 was signed by Mme Claudie Haigneré, astronautess and French Research Minister. Could this event, symbolic in many ways, possibly be surpassed by anything? Well, yes... and that was the winning of the Atomiades Winter Olympics by a team of fifty ILL staff and family members against the might of 25 other European scientific centres.

Colin Carlile

European Conference ESS in Bonn

The European Spallation Source project was presented to the public and to politicians in Bonn on 15-17 May.
About 50 people from the ILL attended the meeting, participating with oral presentations and contributing to 51 posters.

Christian Vettier, during his plenary talk *"Fluctuations in solids: the global view"*.

Waiting for the bus

Werner Press, Helmut Schober and Thomas Hansen at the French Neutron Scattering Society meeting.

The signing of the EIROforum Charter (Brussels, 11-13 November)

The directors of the seven organisations during the signing of the EIROforum chart with Mr Philippe Bousquin, the European Research Commissioner.

The seven members of the EIROforum organisation (www.eiroforum.org) – CERN, EMBL, ESA, ESO, ESRF, ILL and JET – sealed their partnership on 12 November with the formal signing of a common EIROforum Charter.
This event took place during the 'multiple dimension' EU-conference on "European Research 2002 - The European Research Area and the Framework Programme 6", held in Brussels between 11 and 13 November.

Valery Nesvizhevsky and Prof. Marco Fontana (University of Parma) in a heavy discussion about Gravity.

The South-African Research Minister (right) visiting the ILL stand.

Eddy Lelièvre-Berna, Giovanna Cicognani and Giovanni Bruno: A rose between two thorns.

We are the Champions!
ILL wins the 2002 Winter Atomiades (Feldberg, 3-9 March)

The 8th Winter Atomiades 2002 took place in Feldberg (Germany). The ILL team of our 50 people did us proud by carrying off the overall Best Team Trophy.

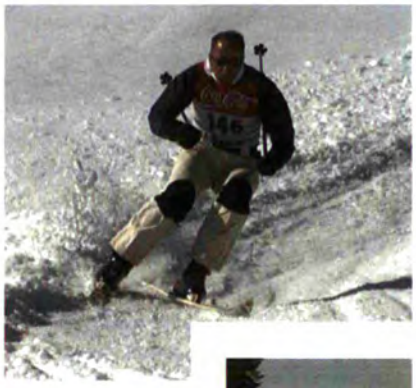

Thierry Martinet in full flow.

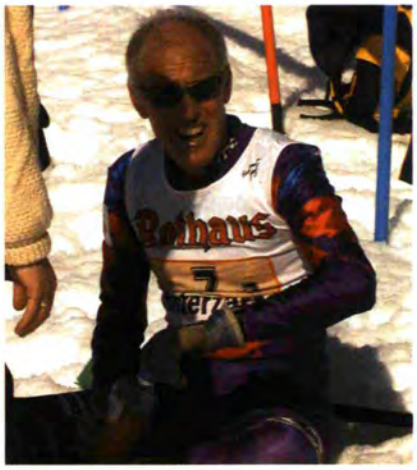

Adrian Perkins during his well deserved rest.

Jean-Marie Perotto, the winner of the cross-country competition.

The three ILL teams in the cross-country ski relay.

The Isaac Newton of the new millennium?

Fête de la Science

The 11th anniversary of 'La Fête de la Science', the France-wide science festival, was held this year from the 16 to 20 October. The ILL's stand included demonstrations on the effect of the gravitational force, animated presentations for the youngest visitors and posters highlighting the ILL activities and its way of operating. People from the ILL who manned the stand were able to explain in a friendly context the contributions being made by the ILL to science and research.

Alain Filhol explaining the principles of neutron detection to a group of young visitors.

Albert Wright checks the safe arrival of the ILL model under the watchful eye of Roland Gähler.

What is the ILL ?

Formally, the ILL is a non profit-making French company under civil law, which is governed by an International Convention signed at Foreign Ministry level by three countries - France, Germany and the United Kingdom. Our Associates - the CNRS and the CEA representing France, the FZ Jülich representing Germany and the EPSRC representing the United Kingdom - own and administer the Institut. They are also responsible for all liabilities and eventual decommissioning costs. With the signing of the Fourth Avenant of the ILL Intergovernmental Convention on 4 December 2002, the ILL's life has been formally extended until at least 31 December 2013.

Although the ILL is an international organisation, its staff are not paid tax-free salaries, but instead they are enveloped within the French tax, employment and social security systems which has marked advantages but also marked disadvantages from whichever point of view you look at it. The Institut is answerable to French legal bodies and to French security authorities. We exist and operate within the French "loi de travail". Our staff representative bodies are those laid down by French law and are a significant presence in the ILL's daily life. We have strong links to the Mairie of Grenoble and surrounding communities, to the Préfecture of the Isère and to the Council of the Rhône-Alpes Region.

The ILL also benefits from the scientific partnerships of six other nations

Whilst our Associates own the facility and contribute the largest amount to the more than 60 M€ annual operating costs, the ILL also benefits from the scientific partnerships of six other nations - Austria, the Czech Republic, Italy, Spain, Switzerland and Russia – who together contribute ~15% of the operational costs of the Institut. All nine partner countries in addition can and do contribute to capital projects at the Institut, within the Institut's priorities but according to their own priorities also.

Our governing body is the Steering Committee which meets twice-yearly and is made up of representatives of the Associates and the Scientific Partners together with Directors and Staff Representatives. Within the framework of the International Convention, the Steering Committee has the ultimate responsibility for determining operational and investment strategies for the Institut.

The Institut has a Director and two Associate Directors, one from each of the Associate countries, appointed on short-term contracts normally of 5 years. The Director's role is in general taken alternately by the German and British appointee. The two Associate Directors are also responsible respectively for the Science Division and the Projects and Techniques Division. The Head of the Administration Division is also appointed on a short-term contract, whereas the Head of the Reactor Division is a permanent ILL employee. These five people together constitute the Management Board of the Institut and are responsible for its day-to-day operation.

The scientific life of the Institut is guided by the Science Policy Board, with input from the ILL's nine scientific colleges. A Scientific Council, comprising 17 external scientists from the member countries, advises the Directors on scientific directions for the Institut, on the evolution of the instrument suite to best meet the needs of the programme,

Our interactions with our user community have been enhanced in the past three years

and to assess the scientific output of the Institut. It is helped in this process by the Instrument Sub-Committee and by the Chairmen of the 8 Scientific Sub-Committees which twice-yearly peer review the experiment proposals.

Our community of users is world-wide but scientists from non-partner nations have access only by collaboration with colleagues from partner nations. This use enriches the scientific life of the Institut but has been increasing of late thanks to the improved instrumentation. From 2003 onwards, this non-partner use is limited to 10%. Our interactions with our user community have been enhanced in the past three years in order to be better informed of their needs and to be more responsive to emerging demands. The Millennium Symposium in April 2001 was a major event in this process, but our informal series of User Forums at which researchers on site on a given day are invited to a meeting with Directors and ILL group leaders

Why Neutrons ?

Neutron beams have the power, when directed at samples of materials, to probe what is invisible using other radiations. Neutrons can appear to behave either as particles or as waves or as microscopic magnetic dipoles. Their specific properties enable them to reveal information which is often impossible to access using other techniques.

Electrically Neutral – neutrons are non-destructive and can penetrate deep into matter making them an ideal probe for biological materials and samples under extreme conditions.

Microscopically Magnetic – they possess a magnetic dipole moment which makes them sensitive to magnetic fields generated by unpaired electrons. Precise details of the magnetic behaviour of materials at the atomic level can be investigated. In addition, the nuclear scattering amplitude (of the neutrons) depends on the orientation of their spin offering a way to detect the nuclear spin order.

Wavelengths of Ångstroms – their wavelengths range from 0.1 Å to 1000 Å making them an ideal probe of atomic and molecular structures ranging from single atomic species to complex biopolymers.

Energies of millielectronvolts – their energies are of the same magnitude as the energies of diffusive motions in solids and liquids, the coherent waves in single crystals (phonons and magnons) and the vibrational modes in molecules. An energy exchange between the incoming neutron and the sample of between 1μeV (even 1 neV with spin-echo) and 1eV can readily be detected.

Randomly sensitive – the variation of scattering power from nucleus to nucleus in a sample can vary in a quasi-random manner. This means that light atoms are visible in the presence of heavy atoms and neighbouring atoms can be distinguished. In addition, isotopic substitution (for example D for H, or one nickel isotope for another) can allow contrast to be varied in certain samples. The neutron is particularly sensitive to hydrogen atoms.

have also been important. We are transforming our interactions to electronic means – proposals are now 100% electronic as are feedback forms. Much of our communication with users is now electronic although the Annual Report will remain in printed form for some time yet.

The ILL is composed of four Divisions, each with its distinct role and, it is true to say, its own culture. Efforts have been made to bring those cultures closer together whilst recognising the need for differences. The Science Division staffs the instruments and delivers the science; the Projects and Techniques Division designs and builds new instruments, develops new concepts and maintains beamlines and instruments operational; the Reactor Division delivers the neutrons, operates and mans the reactor 24 hours per day every day of the year and has responsibility for all aspects of security; the Administration Division deals with Personnel matters particularly being responsible for interactions with staff representative bodies, with Purchasing and with Finance and with Site and Building maintenance; and the Director's Services deal with Radiological safety, with conventional safety and with Health and Working Practices – 2002 has seen a significant strengthening of the safety culture of the Institut which will continue.

The ILL's neutron source is the finest in the world, being based on a single element 58.3 MW nuclear reactor designed for high brightness. The main moderator is the ambient D_2O coolant surrounding the core which delivers intense beams of thermal neutrons to 11 beamlines and to four neutron guides. A graphite hot source operating at 2400 K delivers hot neutrons – energies up to 1 eV and wavelengths down to 0.3 Å – to 3 beamlines. A renewal project will result in the installation of a new hot source and beam tubes during 2003. Two liquid deuterium cold sources at 25 K deliver cold neutrons – energies down to 200 μev and wavelengths up to 20 Å – to 1 beamline and 9 neutron guides. An ultra-cold neutron source fed from the top of one of the cold sources delivers neutrons vertically through the reactor pool to 5 instruments on the operational floor of the reactor. In all there are more than 50 measuring stations, 25 of which have full public access.

The ILL monitors the papers published as a result of the use of our facilities. This indicates about 500 papers per year. Every third year a more rigorous search is done which uncovers a further 300 papers. The average number of papers published per year is therefore ~ 600. With an annual budget of ~ 60 M€, the cost per paper is around 100 k€. We pay particular attention to papers published in high impact journals. Data indicate ~ 80 such papers per year which, interestingly, is equivalent to the output of ESRF.

Beam days delivered for science equals 5 753 for 2002. The cost per beam day of science therefore stands at a very cost effective 11 k€ per day.

"Offering more than simply neutrons" *(Christian Vettier)*

The Partnership for Structural Biology (PSB)

Located close together on the Polygone Scientifique in Grenoble, the ESRF, the ILL, the EMBL and the IBS, are creating a structural biology centre unique in the world.

The PSB brings together expertise in state-of-the-art molecular biology with the investigatory power of synchrotron radiation, neutron scattering and nuclear magnetic resonance necessary to pursue an integrated European Programme in Structural Biology.

Mme Fioraso, Adjointe to the Mayor of Grenoble, at the PSB Opening Ceremony.

Colin Carlile (ILL), Bill Stirling (ESRF) and Fotis Kafatos (EMBL) sign the PSB charter.

FaME38- the Facility for Materials Engineering ▶

The formal opening ceremony of FaME38 (cf. pages 92-93) – set up jointly by ILL/ESRF - took place on 26 November. FaME38's aim is to provide the extra support required to enable engineers to make the best use of neutron and X-ray beam facilities.

From the left: Peter Webster, Colin Carlile and Michael Harloe - Vice-Chancellor of Salford University – inaugurate the FaME38 Lab.

◀ As part of their strategy for the expansion of the life sciences programme in neutron scattering, the ILL and the EMBL have set up a **Biomolecular Deuteration Laboratory** (cf. page 62) for the deuteration of biological molecules. Access to the Deuteration Laboratory is gained through a peer review process analogous to that used for access to any central facility instrument. Two proposals have already been accepted in 2002. In the photo, the Deuteration Lab Team!

SCIENTIFIC HIGHLIGHTS.

The selection of highlights presented below represents a small glimpse of the tremendous range of high-quality science achieved at ILL instruments. The summaries proposal by Colleges describe the multiple facets of neutrons which make them so powerful in exploring properties of Matter and Materials. Magnetism as a field of research is still rapidly evolving: new materials are discovered and exciting problems are contemplated such as quantum phase transitions and the interplay of superconductivity and magnetism. The study of vortex lattices in superconductors has been pushed farther by means of both elastic and inelastic neutron scattering. Chemistry and Materials have witnessed the developments of time-resolved experiments with time-scale ranging from seconds to days, together with fast survey of diffraction patterns using the Laue method on the newly constructed instrument VIVALDI. Soft condensed matter science exploits neutrons to investigate large-scale structures (polymer melts, surfactants, colloidal suspensions...) in sophisticated sample environment and is moving towards bio-inspired problems. The Laboratory for deuteration/labelling of biological macromolecules has been set up to take advantage of the full power of neutron scattering methods in Biology; indeed, diffraction studies either at low resolution or at atomic resolution as well as observations of the dynamics of macromolecules benefit greatly from the isotopic substitution methods.

A small glimpse of the tremendous range of high-quality science

In contrast with the small number of instruments dedicated to this field, nuclear and particle physicists explore phenomena which involve an enormously wide range in energy scale covering the four fundamental forces. Finally, the blend of Theory and Modelling has become more and more visible. Numerical simulations allow to select relevant ingredients required to capture observed effects and can serve as a guide to help theoreticians to build full models to predict new phenomena.

Progress in science combines creativity, ingenuity but also ever increasingly sophisticated methods. Accordingly, the ILL has developed a full suite of instruments which allows scientists in Europe to achieve the core aims of their research programmes using neutron methods. We are very grateful to our many collaborators who have eagerly submitted their highlights in order to demonstrate the breadth of research performed at ILL. I personally wish to thank most warmly all of you who have contributed to this year's version and, more especially, those whose contributions could not be included.

Christian Vettier

Magnetic personalities

Well shielded ^{3}He co-ordination. From the left: Vladimir Hutanu (HMI), Eddy Lelièvre-Berna and David Jullien.

Markus Braden (Köln University), Louis-Pierre Regnault (CEA, Grenoble) and Cyrille Boullion, during their experiment on IN22.

Arnd Gildemeister (Heidelberg) working on neutron tomography.

Magnetic personalities: (from the left) Oscar Moze (Modena University), Caterina Petrillo (Politecnico di Milano) and Francis Tasset.

Chris Ling, College 5B Secretary
http://www.ill.fr/pages/science/groups/dif_1.html
Ross Stewart, College 4 Secretary
http://www.ill.fr/colleges/C4/index.htm

Magnetism

Technologies based on magnetic materials have been among the most influential in modern history, from the invention of the compass, through the discovery of electricity, to modern electronic computers. The high-tech industries of today are totally reliant on well-understood magnetic materials for their present operations, and on the discovery of new magnetic materials for their future development.

The spin of the neutron, the property that allows it to interact directly with the spin and orbital angular momentum of atoms, is consequently one of the fundamental driving forces behind the construction and operation of neutron research facilities. Magnetic materials have been studied using neutrons for over 50 years, and core experiments such as the use of diffraction to study spin order and the use of inelastic scattering to study spin dynamics continue to dominate the demand for beamtime at the ILL.

Enormous increases in neutron flux, detector efficiency, computing resources and experience mean that extremely difficult pioneering experiments can now be done in a few hours, and that problems previously considered intractable are being solved every year. In parallel with these increases in speed and power, there have been equally great improvements in the range and performance of sample environment apparatus, giving scientists access to previously unattainable temperature, pressure and magnetic field regimes. Furthermore, the ability to polarize neutrons with ever greater efficiency allows the microscopic natures of magnetic materials to be determined even more accurately and unambiguously.

Nevertheless, magnetic neutron scattering is far from settling back comfortably as a field of routine "production line" experiments. New scientific problems are constantly appearing, and the ILL continues to take up and meet the technical challenges accompanying them, as illustrated by the Scientific Highlights presented by magnetism researchers in this year's Annual Report. This year has seen a resurgence of neutron time-of-flight mapping of magnetic excitations, with 3 out of the 5 inelastic magnetism highlights being performed on the IN6 time-focussing TOF spectrometer. This has been largely the result of the provision of the ILL's 2.5 T vertical cryomagnet on IN6, which has made possible studies of field driven quantum critical points, quantum spin-chains and the study of the magnetically mediated superconducting material $YbSnPd_2$ presented in this report. Polarized neutron techniques – pioneered at the ILL – are used in 3 out of the 7 magnetism articles in this year's annual report, demonstrating their usefulness in the unambiguous determination of magnetic structures and dynamics.

The study of magnetism at the ILL promises to be equally exciting in 2003, with many important and novel experiments already approved for the first half of the year. For example, two experiments were highlighted by the scientific council concerning vortex lattices in superconductors. In particular, measurements of the velocity distributions of vortex lattices using a novel time-of-flight neutron spin-echo technique will be carried out this year. Crucial experiments on the interplay of superconductivity and magnetism will continue this year, specifically, work is continuing on the UGe_2 class of ferromagnetic superconductors in order to fully characterise the spin-triplet pairing mechanism proposed for these materials. Finally, the prediction of a magnonic Bose-Einstein condensate in the magnetic dimer compound $Cs_3Cr_2Br_9$ will be investigated on IN14 in the coming year. The fact that the experimental topics and techniques described in these Scientific Highlights change greatly from year to year underlines the range and depth of magnetism research using neutrons at the ILL.

Short-range magnetic correlations in tapiolite revealed by Laue diffraction

E.M.L. Chung, M.R. Lees, G. Balakrishnan, D. Visser, D.McK. Paul
(University of Warwick)
G.J. McIntyre and C. Wilkinson
(ILL)

Difference Laue diffraction patterns on VIVALDI, the first instrument of the Millennium Programme, reveal with striking clarity the 2D magnetic ordering in the mineral tapiolite. Complementary temperature-dependent monochromatic data suggest the ordering is two-stage, first to a 2D paramagnet, then to a 2D antiferromagnet.

Named after the god Tapio of Finnish mythology, tapiolite ($FeTa_2O_6$) is one of a group of naturally occurring minerals with general formula $A^{2+}B_2^{5+}O_6$. The crystal structure can be described as the conventional rutile unit cell tripled along the tetragonal c-axis. The trirutile structure arises from the ordering of the divalent and pentavalent cations, and results in each layer of Fe^{2+} cations being separated from the next by two sheets of diamagnetic Ta^{5+} ions (figure 1). This results in a highly convoluted magnetic exchange pathway, and favours 2D magnetic ordering.

Past reports of the magnetic properties of $FeTa_2O_6$ are based almost exclusively upon the analysis of polycrystalline samples. Early researchers mistakenly reported the long-range ordering temperature as coinciding with the maximum in the magnetic susceptibility at $T(\chi_{max}) \approx 14$ K. In fact, a single thermodynamic quantity is not sufficient to characterise the magnetism fully, and measurements of other properties such as the heat capacity are required to show that the true Néel temperature occurs at $T_N \approx 8.5$ K. Broadening of the susceptibility maximum above T_N arises from short-range correlations, and is now acknowledged to be a classic signature of 2D magnetic ordering. Combined interpretation of data from Mössbauer spectroscopy and neutron powder diffraction indicated that the 3D ordered phase consists of anti-ferromagnetic planes of Fe <110> moments with adjacent planes rotated by 90°, consistent with the local co-ordination of oxygen atoms. To investigate the 2D ordering we undertook magnetisation and neutron diffraction experiments on a single crystal of $FeTa_2O_6$.

Figure 1: Schematic of the $FeTa_2O_6$ structure. Fe and Ta are both octahedrally coordinated to O atoms at the vertices of the volumes shown. Fe is in the centre of each brown octahedron, Ta in the centre of each green.

Although it is possible to find natural crystals of tapiolite growing in granite pegmatites, these tend to contain impurities such as Mn^{2+} and Nb^{5+}, and exhibit a substantial reduction in cation ordering. Our sample was cut from a crystalline boule grown in an optical floating-zone furnace. Magnetisation data with the field along the <100>, <110> and <001> indicated high anisotropy between the a-b plane and the c direction. Our single-crystal data have clear points of inflection at $T_N = 8.0(1)$ K, but the ratio $T_N/T(\chi_{max})$ depends on the orientation of the crystal relative to the field, with $T_N/T(\chi_{max}) = 0.92(3)$ for H along <001> and $T_N/T(\chi_{max}) = 0.54(2)$ for the field along <110> or <100>; evidence that short-range order is prevalent within the a-b plane at elevated temperatures.

Can we obtain more detail of the 2D ordering by neutron diffraction?

The obvious choice is monochromatic neutron diffraction on an instrument like D10. The first step was to verify the 3D ordered structure by collection of extensive diffraction data at 2 K, which confirmed the model of planes of antiferromagnetic <1 1 0> Fe moments with a 90° rotation between successive planes. Significant moments were also detected on both bridging oxygen sites, indicative of the importance of the next-nearest neighbour super-exchange.

To search for evidence of 2D order above T_N, extended scans were made around the positions of the stronger magnetic reflections of the form $h+0.5\ k\ l+0.5$ or $h\ k+0.5\ l+0.5$.

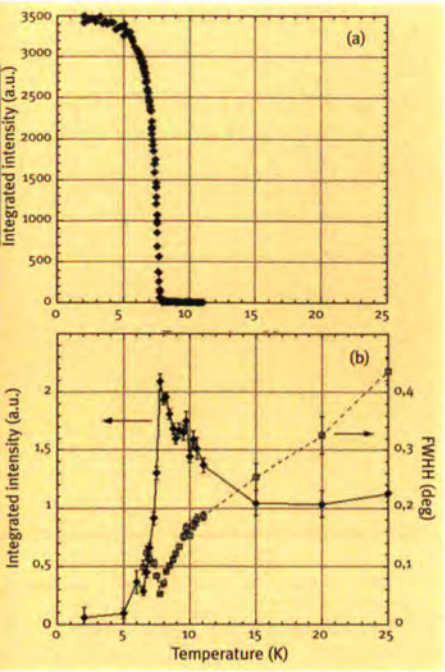

Figure 2: Temperature dependence of (a) the integrated intensity of the 0.5 0 1.5 magnetic reflection, (b) the integrated intensity and full-width-at-half-height in a scan across the 1-D rod at 0.5 0 2.5.

Well-defined rods of scattering were observed extending along c*, decreasing monotonically in intensity with increasing *l*, characteristic of greatly reduced ordering between the antiferromagnetic planes. The evolution with temperature of the intensity and the width (in k) of the rod 0.5 0 l at $l = 2.5$ are superimposed on the intensity variation of the 0.5 0 1.5 magnetic reflection in figure 2. Below 3 K the ordering is completely 3D. Between 5 K and $T_N = 7.95$ K there is a gradual cross-over from 3D to 2D order; the spins remain antiferromagnetically ordered within the planes but there is a reduction in correlation between planes. Between T_N and 9.5 K (the inflection in figure 2b), there is little or no correlation between planes, but still considerable order within each plane. Above 9.5 K the structure evolves towards a 2D paramagnet where the moments remain within the a-b plane, but become more disordered and mobile. As the temperature is further increased the structure gradually changes to the 3D paramagnetic state.

While the presence of 2D order is indisputable from the monochromatic D10 data, we were guided by magnetisation data in our search. In the white-beam Laue method the next best thing to a point-like Bragg reflection should be a rod of scattering. What can the new thermal-neutron Laue diffractometer VIVALDI reveal? The Laue diffraction pattern at 2 K (figure 3a) shows clearly the additional magnetic reflections between pairs or rows of structural reflections. At 10 K only the structural reflections remain (figure 3b), but we can also see additional extended streaks radiating from the straight-through beam, as well as the triangular fans from preferred orientation in the cryostat heat shields. These additional streaks are more evident in the difference Laue diffraction pattern (figure 3c), and are the projections of several of the 1D diffuse rods that extend along c*. Again we did know where to look for diffuse rods in the Laue experiments, but the additional 1D scattering in the Laue diffraction patterns, especially in the difference pattern, is very obvious; yet another advantage of the global view afforded by the Laue method. Modelling the scattering is complicated by chromatic overlap, nevertheless comparison of patterns above and below transitions should be routine in all studies of magnetic structures by the Laue method.

This is only one of many recent experiments that show the unique importance of the neutron Laue method for exploring the whole of Q-space as a function of temperature, pressure, etc. A white beam from a continuous neutron source can provide an exceptionally high average flux on the sample, and this, combined with the very large solid angle of the detector, makes this a powerful instrument that will not easily be bettered, even on the new pulsed sources.

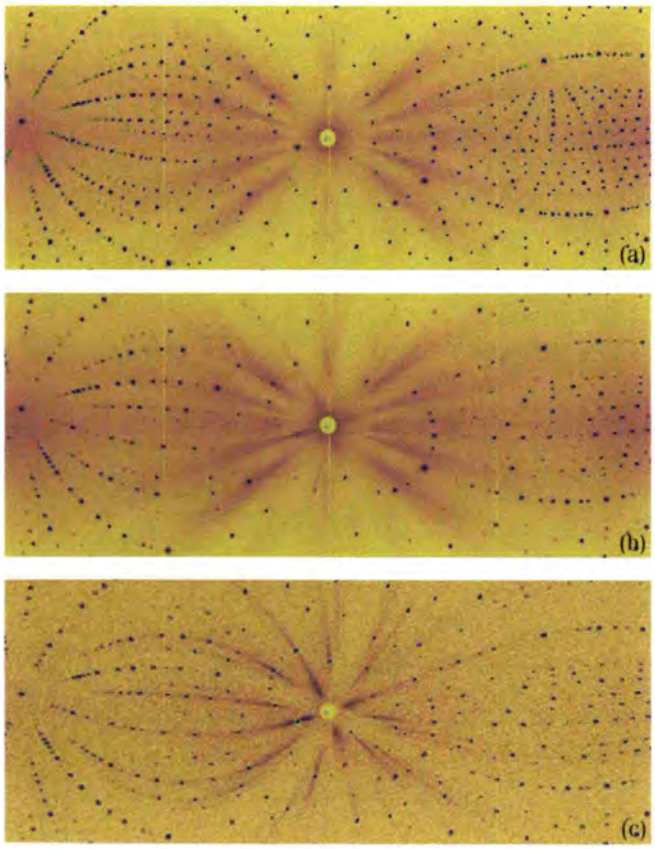

Figure 3: Laue diffraction patterns observed on VIVALDI for $FeTa_2O_6$, (a) at 2 K, with the structural reflections marked by +, (b) at 10 K, and (c) the difference between the patterns at 10 K and 2 K. Neutron waveband: 0.8 – 3.5 Å.

a: 2 K with predicted nuclear pattern superimposed

b: 10 K - a hint of diffuse scattering at low Q

c: 10 K minus 2 K -> rods of magnetic scattering along *l*

Super-exchange interactions enhanced through spin delocalisation in $K_2FeCl_5 \cdot H_2O$

J. Campo and F. Palacio
(ICMA Zaragoza and ILL)
J. Luzón and G.J. McIntyre (ILL)

Super-exchange acquired its name because of the relatively large distances, often more than 4 Å, between interacting magnetic ions. In the superexchange mechanism, magnetic ions modify the wave functions of connecting "ligands" giving them a magnetic character, allowing exchange interactions with neighbouring ions.

Two experimental facts related to the super-exchange mechanism attracted our attention to $K_2FeCl_5 \cdot H_2O$. First, the essential feature observed in the super-exchange pathway of this compound is that propagation is not via a diamagnetic intermediary linking the metal ions, such as in FeOFe or FeClFe [1]. Instead, propagation is via two or three non-magnetic atoms, such as FeCl···HOFe, FeCl···ClFe or variants, and includes combinations of through-bond or through-space pathways. Interestingly enough, even with such long and apparently weak pathways, where distances between neighbour Fe ions can be as large as 6.752 Å, the Neél temperature is remarkably high, e.g. $T_N = 14.06$. This indicates efficient propagation of the magnetic interactions, where the presence of hydrogen bonds seems to play an important role in the enhancement of magnetic coupling.

Another interesting result was that the neutron powder-diffraction experiments performed at 1.5 K on $K_2FeCl_5 \cdot H_2O$ showed that the magnetic moment on the Fe ions for each sublattice is 3.9(1) μ_B [2]. This value is far below the 5 μ_B expected for the saturated magnetic moment of Fe^{3+}. Spin delocalisation due to covalence in the FeCl and the FeO bonds would be the most likely origin of the moment reduction at the Fe sites.

In order to explore such a hypothesis, we have undertaken the examination of the magnetisation density in $K_2FeCl_5 \cdot H_2O$ by polarized neutron diffraction (PND) techniques. The aim is to obtain detailed experimental information about the spatial distribution of the unpaired spin density. Such studies will allow us to find how the spin delocalisation, due to covalence effects, enhances the super-exchange mechanism and consequently the propagation of magnetic interactions.

Experiments have been performed on a single crystal (about 5x3x1 mm^3) of $K_2FeCl_5 \cdot H_2O$. The compound is orthorhombic (Pnma) with cell parameters 13.4389, 9.6925 and 6.9789 Å at 20 K. The unit cell is formed by four Fe^{3+} cations in octahedral coordination, with five chlorine atoms, and the oxygen atom of the water molecule. Figure 1 shows the crystal structure with the coordination octahedra of the iron atom and the strongest super-exchange pathways between neighbour irons.

The polarized-neutron diffraction experiment was performed at 20 K on the D23 lifting-counter diffractometer at the ILL. A pyrolitic graphite (002) crystal and a Heusler (111) polarizer were used to monochromate the incoming neutron beam at a wavelength of 1.329 Å

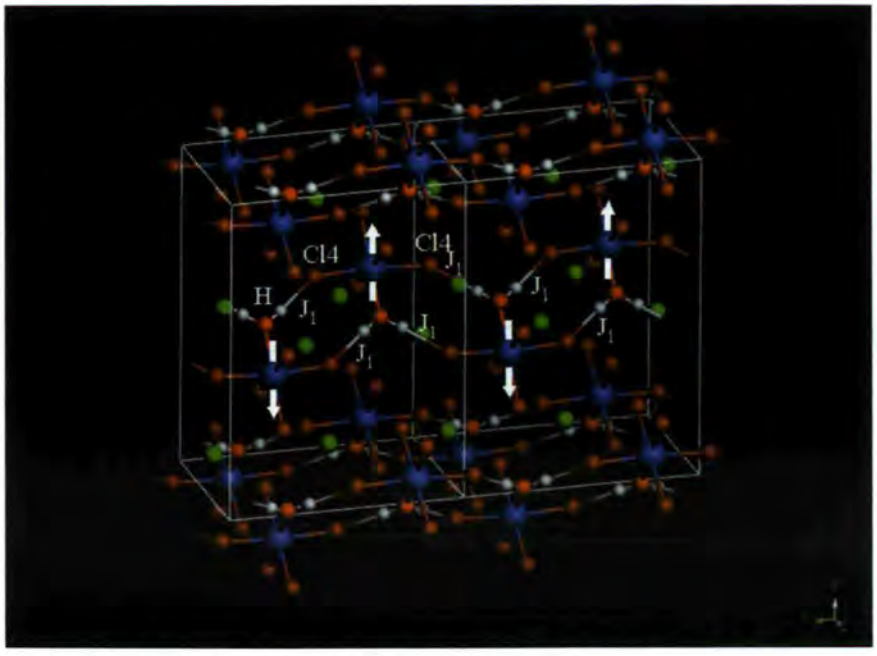

Figure 1: Unit-cell representation of $K_2FeCl_5 \cdot H_2O$ showing the J_1 super-exchange pathway.

and with a polarization of 0.9479(2). A flipper with 98% efficiency switched the polarization between parallel and anti-parallel to the vertical magnetic field of 5.5 T. The $K_2FeCl_5 \cdot H_2O$ crystal was mounted in two different orientations relative to the applied magnetic field. Absorption, extinction, Lorentz geometrical and multiple scattering corrections were applied to the measured intensities (D9) and flipping ratios (D23), and programs from the CCSL suite and MOLLY program [3] were used to analyse the data.

The spin-density distribution in the unit cell, as determined from the magnetic structure factors, has been analysed in terms of a simplified multipolar model. To a first approximation, the iron atom has a spherical distribution ($^6A_1$: $t^3_{2g}e_{2g}$), and the effect of the ligands can be considered to decrease the iron spin-density symmetry to only C_4. Therefore, the spin-density distribution has been modelled by a hexadecapolar expansion-preserve the C_4 symmetry. Only monopolar contributions have been assumed in the analysis for the ligands. The hydrogen and potassium spin populations were below the experimental accuracy and were not included in the final model. As expected, the largest spin population was found on the iron atom (4.155(3) μ_B). Moreover, a significant spin delocalisation from the iron to the ligands is also observed. Spin populations of 0.158(2), 0.150(1), 0.141(3), 0.162(2) and 0.072(3) μ_B were found on the Cl1, Cl2, Cl3, Cl4 and O atoms respectively. The shorter the Fe-Cl distance, the higher the spin population observed on the chlorine atom, except for the Cl4 atom belonging to the hydrogen bond, which has the highest spin population even though its distance to Fe is not the shortest. The hydrogen bond seems to favour spin delocalisation from the iron atom to the ligand.

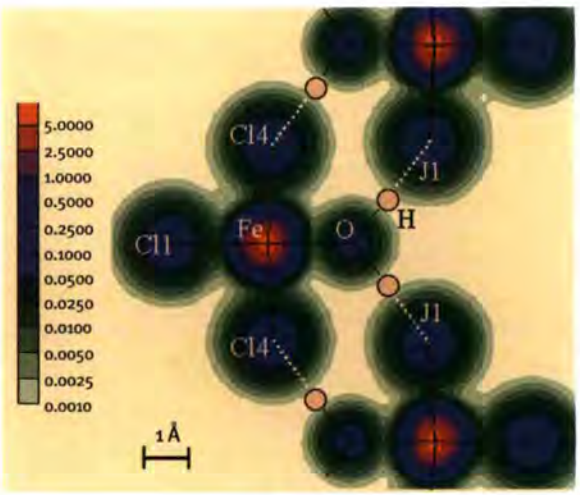

Figure 2: Projection of the spin-density reconstruction in the plane containing the FeCl···(H)OFe super-exchange pathway. Total density has been normalised to 5 μ_B per octahedron.

A projection of the spin-density reconstruction in the plane containing the FeCl···(H)OFe super-exchange pathway is shown in figure 2. This super-exchange pathway, as determined from inelastic neutron scattering experiments in ref. [4], has the strongest magnetic coupling constant, J_1=-0.184 meV, an order of magnitude greater than the next one J_2=0.016 meV.

Spin-delocalisation effects have been observed before in other coordination compounds of 3d metal ions [5]. Nevertheless, these phenomena are more pronounced in $[FeCl_5(H_2O)]^{2-}$ because it fulfils all the conditions favouring spin delocalisation due to covalence [6]: iron in this compound has the highest possible spin value (S=5/2), it has half-filled e_g orbitals allowing spin transfer through σ molecular orbitals, and it is a trivalent ion.

In the super-exchange mechanism, the magnetic orbitals are not completely localised on the magnetic atoms but they also have a contribution from the ligand atomic orbitals. This delocalisation of the magnetic orbitals allows them to overlap and, consequently, favours the magnetic interaction. In $K_2FeCl_5 \cdot H_2O$ we have observed that the magnetic orbitals include an important component from ligand atomic orbitals, which explains the relatively high ordering temperature.

Acknowledgements

We would like to thank the CICYT (grant MAT2000-1388-C03-03) for financial support.

REFERENCES

[1] R.L. Carlin and F. Palacio, Coord. Chem. Rev., 65 (1985) 141-165
[2] M. Gabás, F. Palacio, J. Rodríguez-Carvajal and D. Visser, J. Phys.: Condens. Matter., 7 (1995) 4725-4738
[3] N.K. Hansen and P. Coppens, Acta Crystallogr., Sec A 34 (1978) 909
[4] J. Campo, F. Palacio, C.C. Becerra, A.R. Wildes, L.P. Regnault, J.E. Lorenzo-Díaz, J. Magn. Magn. Matt., 261 (2001) 479
[5] R.J. Deeth, B.N. Figgis and M. Ogden, Chem. Phys 121 (1988) 115-113
[6] P.W. Anderson in Solid State Physics ed. by F. Seitz and D. Turnbull, Academic Press, New York 4 (1963) 99

The magnetic ground state of $CeFe_2$: resolving the paradoxes

L. Paolasini (ESRF)
B. Ouladdiaf (ILL)
N. Bernhoeft, J-P. Sanchez, P. Vulliet (CEA, Grenoble)
G. H. Lander (Institute for Transuranium Elements, Karlsruhe)
P. Canfield (Iowa State University)

Accurate single crystal neutron diffraction data, accumulated on the D10 diffractometer, taken in conjunction with results from inelastic neutron (LLB, Saclay and ILL) and resonant X-ray scattering (ESRF, Grenoble) experiments has enabled us to resolve longstanding controversies surrounding the magnetic ground state of $CeFe_2$.

Novel electronic ground states continue to attract much attention. Recent activity has focused on the appearance of simultaneous magnetic-superconducting systems both of the ferro- (F) and antiferromagnetic (AF) kind [1]. Here we explore a third type of ground state that exhibits the dynamic excitation spectra of a simultaneous antiferromagnetic-ferromagnetic system. As will become evident, the essential physics may be related to a fundamental dynamic nature of such ground states. In the following the focus is on the F-AF electronic phase as realised in particular in $CeFe_2$ and the preferential stabilisation of either the F, in undoped $CeFe_2$, or AF phase in the lightly doped $Ce(Co_{.07}Fe_{.93})_2$. The root of this rich behaviour lies in the anomalous nature of hybridisation between the Ce $4f$ shell and the $3d$ states of iron [2] which has lead to conflicting reports on the ground state of $CeFe_2$ and the magnitude of the Ce moment. The availability of single crystals (grown at Ames Laboratory, Iowa State University, Ames, Iowa, USA) allowed us to re-examine this challenging problem using a series of experimental techniques. We concentrate on diffraction experiments at a 7% Co doping on the Fe site which acts to stabilise the AF ground state below T_N (~ 69 K). This state is unusual in that it condenses out of an apparently F precursor phase which pertains for $T_N < T < T_c$ where T_c marks the transition to the paramagnetic state at 210 K. Inelastic neutron scattering, figure 1 (LLB, Saclay and ILL, Grenoble), brought the full, microscopic, nature of the paradox into focus. The lower panel, $T < T_N$, shows classic AF spin waves propagating away from the point [3/2 3/2 3/2] in the <111> direction as anticipated in a pure AF state. On the other hand, the upper panel, $T_N < T < T_c$, shows that in the F state there exist *both* ferromagnetic spin waves (originating from the zone centers [1 1 1] and [2 2 2]) as well as intense, *inelastic* AF excitations, focused around the zone center [3/2 3/2 3/2]. A similar situation pertains in $CeFe_2$ [3], *except* that in the pure compound the AF state remains dynamic to the lowest temperatures studied and no long-range order is found.

This paradox in the *dynamics* of the simultaneous F-AF excitation spectrum, was only compounded by experiments at the ID20 beamline at the ESRF Grenoble using resonance X-ray scattering (RXS) which revealed a paradoxical magnetic *structure*. Using incident X-ray energies tuned to the Ce L_3 edge (which is sensitive to the magnetic polarization at the Ce site) the intensity was measured as the sample was rotated around the scattering vector (azimuthal scans). As indicated in figure 2, the results dictate that the Ce ($4f$) moment must lie parallel to the <111> propagation vector of the magnetic structure. The difficulty is that *all* earlier neutron-diffraction and Möss-

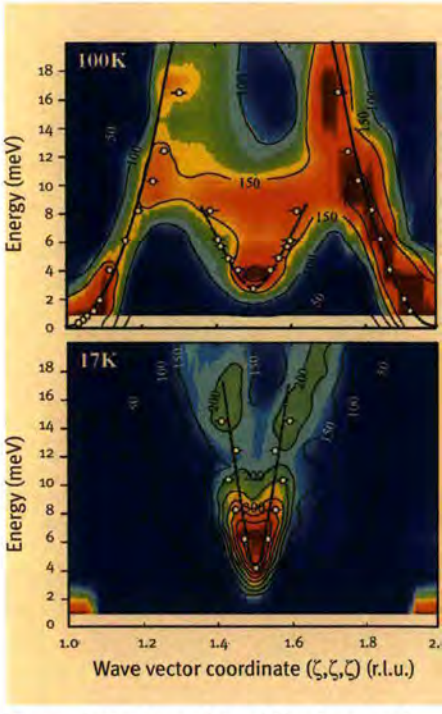

Figure 1: Contour plots of the dynamical magnetic susceptibility $\chi''(Q,\omega)$ determined by inelastic neutron scattering around the Brillouin zone boundary (3/2,3/2,3/2), and along the [111] direction. The thick lines are the fit of the parabolic F (continous lines) and of the linear AF (broken lines) spin wave dispersions. Measurements in different Brillouin zones establish that all the inelastic response is associated with the Fe spins [3].

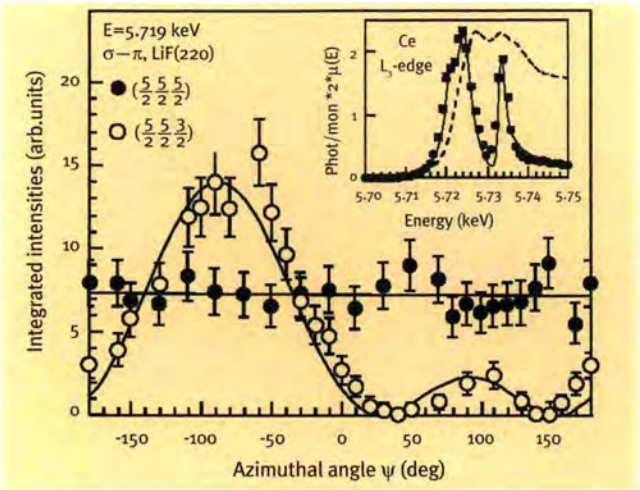

Figure 2: Azimuthal dependence of resonant magnetic X-ray scattering intensities of the reflections (5/2.5/2.5/2) (black points) and (5/2.5/2.3/2) (open points) at E = 5.719 keV taken at 12 K in the σ-π channel. The lines are the calculations of the angular dependence of the resonant intensities with the Ce moment directions aligned along [111]. The insert shows the energy dependence of the magnetic Bragg reflection (5/2.5/2.5/2) and the broken lines the absorption coefficients determined by fluorescence yield across the Ce L_3 edge.

bauer results are inconsistent with a simple collinear arrangement of the Fe moments [4, 5] and thus the polarization of the weak 4*f* moment (~ 0.2 μ_B) by the dominant Fe moments (~ 1.5 μ_B) is, apparently, inexplicable.

The opening of this *structural* paradox, which relies on the high sensitivity of X-rays to the Ce moments (the Fe K edge is too weak to determine the Fe moment orientation) and the fact that both the neutron and Mössbauer data are principally determined by the dominant Fe polarization, stimulated a new neutron experiment exploiting the full potential of D10. Using a single crystal, and gathering a data set approximately 2 orders of magnitude larger than previously collected with polycrystalline samples, showed unambiguously that the Fe moments are indeed *non*-collinear. The resulting magnetic moment configuration is shown in figure 3, where, in a given sub-lattice, the weak Ce moments lie parallel to a dominant [111] axis of magnetisation provided by the 'red' Fe moments (in agreement with the synchrotron experiments as shown in figure 2). However, in addition, the apical 'blue' Fe ion yields a *non*-collinear component with a smaller moment of 1.1 μ_B. The configuration, shown in figure 3, can also be used as a basis to interpret both the Mössbauer results and the paradoxical excitation spectrum of figure 1. Furthermore, it suggests an avenue towards an understanding of the ground state in $CeFe_2$, a possibility being that it comprises a set of dynamic, microscopic, blocks [6] based on the AF <111> structure of figure 3. Such a model may reconcile both the anomalous inhibition of a lattice distortion in the F state, which is then released by slow down and macroscopic domain growth on entering the AF phase in the doped compound, and the saturated magnetic moment of ~ 1.2 μ_B/Fe observed under high magnetic fields (1.6 x 3/4 = 1.2 μ_B/Fe) [7].

In conclusion, $CeFe_2$ realises a novel electronic ground state with the simultaneous excitation spectra of a dynamic ferromagnetic-antiferromagnetic phase [8]. The transition from F ground state with the resonant, dynamic, AF pole in pure $CeFe_2$ to a true AF ground state may be realised either, as in these experiments, by light doping on the Fe site or through the application of hydrostatic pressure [9]. Clearly then, there are many similarities with the phenomenology of both the Hi-Tc cuprates and the simultaneous ferro- and antiferromagnetic-superconducting systems. It remains as a challenge to see, whether, under conditions of sufficient purity and at low enough temperature, one may realise the transition to a truly exotic phase of simultaneous ferromagnetic-antiferromagnetic-superconducting dynamic order in such a material.

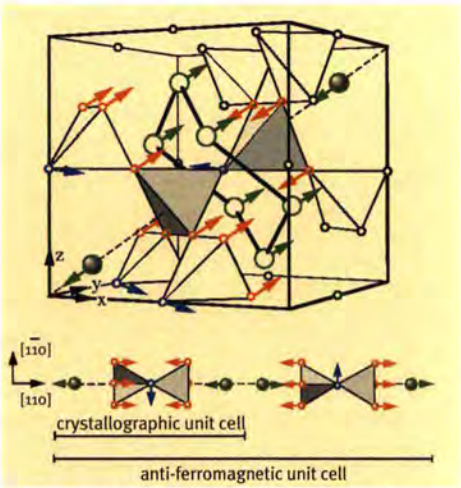

Figure 3: Magnetic structure in the AF state determined combining neutron and x-ray scattering results. The Fe sublattice has two inequivalent sites, with 3/4 of Fe having the magnetic moment direction parallel to [111] (red arrows) and 1/4 of Fe parallel to the [1-10] direction (blue arrows). The Ce magnetic moments point along the [111] direction (green arrows).

REFERENCES

[1] C. Geibel et al., Z Phys. B, 1 (1991) 84 ; N.D. Mathur et al., Nature 39-43 (1998) 394 ; S.S. Saxena et al., Nature 587 (2000) 406 ; C. Pfleiderer et al., Nature 58-61 (2001) 412 ; D. Aoki et al., Nature 613 (2001) 413

[2] O. Eriksson et al., Phys. Rev. Lett., 2523 (1988) 60

[3] L. Paolasini et al., Phys. Rev., 12117 (1998) B 58

[4] S. J. Kennedy and B. Coles, J. Phys. Cond. Mat., 1213 (1990) 2

[5] J-P. Sanchez et al., Hyperfine Int., 2 (2001) 133

[6] N. Bernhoeft, J Phys Conds. Matter, R 771 (2001) 13; ibid, J Phys. Soc. Japan, suppl. 17 (2002) 71

[7] H. Wada et al., J Phys. Soc. Japan, 1337 (1993) 62

[8] L. Paolasini et al., Phys. Rev. Lett. 057201 (2003) 90

[9] T. Fujiwara et al., Physica B, 336-338 (2002) 312

Spin dynamics in a stripe phase: the model system $La_{5/3}Sr_{1/3}NiO_4$

A.T. Boothroyd, D. Prabhakaran, P.G. Freeman, S.J.S. Lister (University of Oxford)
M. Enderle, A. Hiess, J. Kulda (ILL)

Over the past decade it has become increasingly apparent that charge carriers doped into antiferromagnetic oxides tend to form ordered structures with a stripe-like texture. These stripe phases, which represent a new form of electronic order in the solid state, are characterised by parallel lines of holes separating regions of antiferromagnetically ordered spins. While the static properties of stripe phases are now quite well understood, little is known about how the spins and charge carriers move. In this work we used polarized- and unpolarized-neutron inelastic scattering to explore the spin excitation spectrum of the simplest stripe-ordered compound, $La_{5/3}Sr_{1/3}NiO_4$. The measurements enabled us to determine the spin coupling both within a stripe domain and between adjacent stripes, and also provided insight into the way in which spin and charge degrees of freedom are coupled in stripe phases.

Stripe phases were actually predicted theoretically [1] several years before they were first identified in nature. The real explosion of interest, however, followed from the observation by Tranquada and coworkers [2] of spin-charge stripe order in a non-superconducting cuprate. Their discovery fuelled a debate about the role played by stripe correlations in the formation of the superconducting state in the high-T_c cuprates.

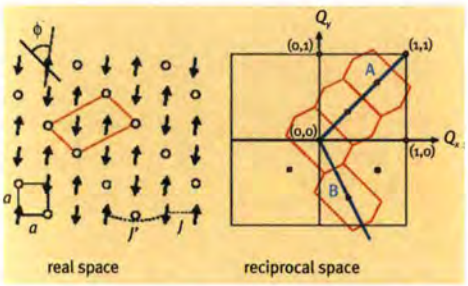

Figure 1: (a) Model for the stripe order found in the Ni–O layers of $La_{5/3}S_{1/3}NiO_4$. Arrows denote $S = 1$ spins on Ni^{2+} sites, and open circles represent Ni^{3+} holes. The O sites are not shown. Primitive unit cells of the NiO_2 square lattice and the stripe superlattice are indicated by the small square and parallelogram respectively. J and J' are the intra- and inter-stripe spin exchange couplings. (b) Diagram of reciprocal space showing several Brillouin zones for the stripe ordering.

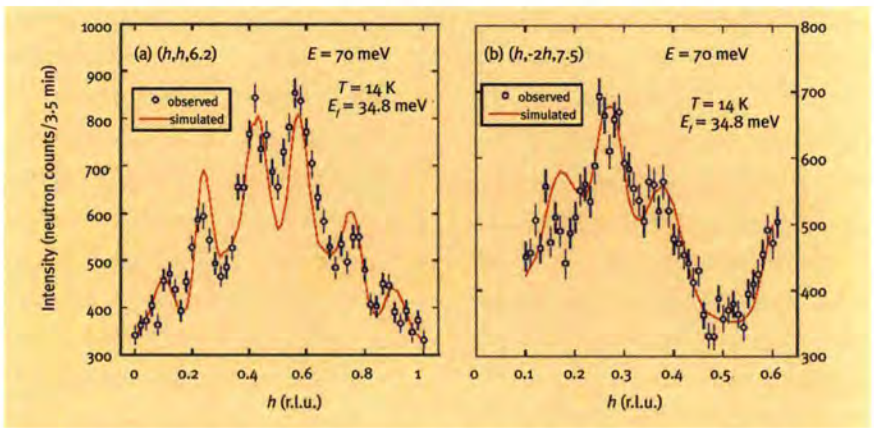

Figure 2: **Q** scans parallel to (a) $(h, h, 0)$ and (b) $(h, -2h, 0)$ at a constant energy of 70 meV, showing the magnetic scattering from $La_{5/3}Sr_{1/3}NiO_4$. The lines are scan simulations based on the spin-wave model.

Although the main impetus to learn about stripes arises from cuprate superconductivity, the most popular playground for studying stripe phenomenology has been the layered nickelate family $La_{2-x}Sr_xNiO_{4+\delta}$. This is because the stripes are more strongly localised and exist over a wider range of hole doping (controlled by the amount of Sr and excess oxygen) in nickelates than in cuprates. The stripe order is simplest and best correlated in $La_{5/3}Sr_{1/3}NiO_4$, and so this compound is an ideal system on which to establish the basic physics of stripes.

Figure 1(a) shows the arrangement of spins and holes observed in the Ni–O layers of $La_{5/3}Sr_{1/3}NiO_4$ at temperatures below ~200 K. The ordering of spins and holes is seen to form a superstructure whose periodicity is three times that of the underlying square lattice. A primitive unit cell of this stripe order is shown by the parallelogram. Fourier transformation of the stripe superlattice leads to the Brillouin zone geometry shown in figure 1(b).

To understand the existence and stability of stripe phases we need answers to a number of key questions: What are the values of J and J', the intra- and inter-stripe exchange couplings between Ni^{2+} spins? What are the characteristic frequencies of the col-

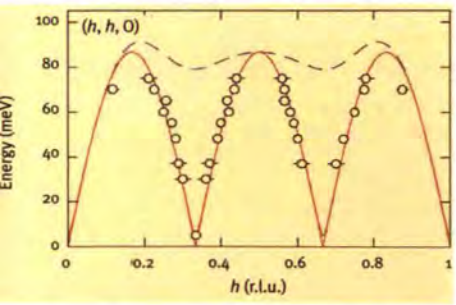

Figure 3: Dispersion of the magnetic excitations in $La_{5/3}Sr_{1/3}NiO_4$ parallel to (*h*, *h*, 0). The full and broken lines are the spin-wave model for two stripe twins oriented at 90° to one another.

lective motions of the lines of charges? How do the dynamics of the spins and charges couple to one another?

These questions motivated us to study the spin excitation spectrum of $La_{5/3}Sr_{1/3}NiO_4$ by neutron inelastic scattering on the triple-axis spectrometers IN20 and IN22 [3]. We probed the excitations mainly by scanning the neutron scattering vector **Q** at fixed energy along the lines marked A and B in figure 1(b). Figures 2(a) and (b) show two such scans, made at an energy of 70 meV, and figure 3 shows the dispersion of the observed spin excitations with wavevector along line A for energies above 30 meV. There is no measurable dispersion along the *z* axis.

What is interesting about these results is that the spin excitations apparently propagate as if the underlying charge-ordered superlattice were entirely static. In other words, in the energy range 30 – 85 meV the motion of the spins is independent of the motion of the holes. This surprising revelation means we can ignore the motion of the holes, at least for this energy range, and model the spin excitations very simply by linear spin-wave theory. Assuming only the two exchange parameters J and J' shown in figure 1(a) and a single-ion anisotropy energy K_c determined separately we followed the standard routine to calculate the spin-wave dispersion and cross-section. The lines drawn on figures 2 are simulations of the scans including the spectrometer resolution, and the calculated dispersion is compared with the data in figure 3 with parameters $J = 15$ meV, $J' = 7.5$ meV and $K_c = 0.07$ meV. The full model dispersion surface is plotted in figure 4.

For energies below 30 meV very strong scattering from phonons made it difficult to follow the magnetic excitations with unpolarized neutrons, and so to explore this energy range we employed polarization analysis. This enabled us to separate the magnetic from the non-magnetic scattering, and revealed that for energies between 10 meV and 25 meV there is a dramatic reduction in the spin-wave peak amplitude and a corresponding increase in width. Below 10 meV sharp spin wave peaks are again recovered.

We believe that the anomaly between 10 meV and 25 meV arises from a coupling between the spin waves and collective motions of the stripe domain wall. In other words, between these energies the lines of charge begin to oscillate in harmony with the spin waves. The lack of coupling below 10 meV suggests that the charges are to some extent pinned to the lattice, creating an energy gap for domain wall fluctuations.

These results provide several new insights into the spin dynamics of stripe phases. They show that the spin coupling between the stripe domains is about a factor two smaller than the spin coupling within the stripes. They also suggest that the motions of the spins and charges are essentially independent at high energies, but become intimately linked between 10 meV and 25 meV. Finally, we argue that a commensurability gap exists which freezes out certain collective charge modes at low energies. These findings, plus results from future neutron scattering experiments on other simple systems, will provide a critical test of theoretical models for stripe phases.

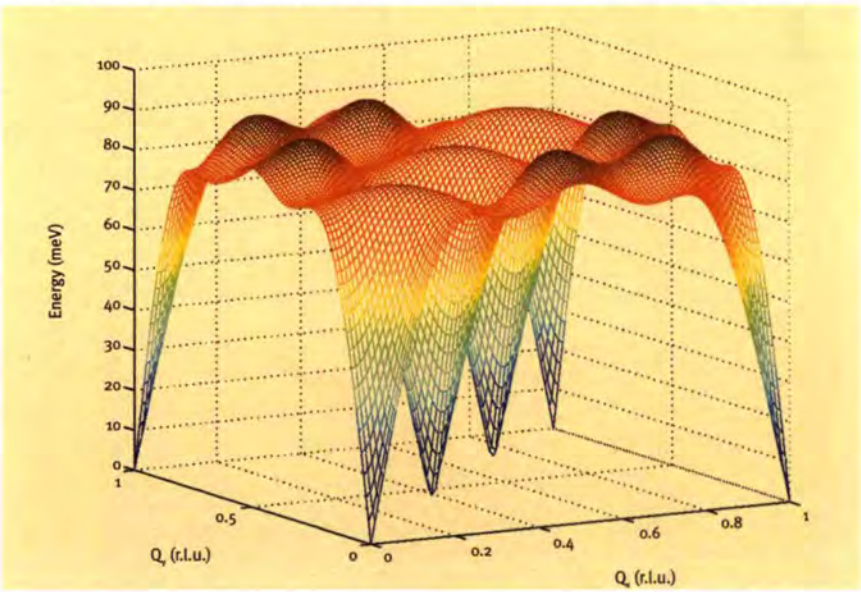

Figure 4: Two-dimensional dispersion surface for the spin-wave excitations in $La_{5/3}Sr_{1/3}NiO_4$.

REFERENCES

[1] J. Zaanen and O. Gunnarsson, Phys. Rev. B 40 (1989) 7391; D. Poilblanc and T.M. Rice, Phys. Rev. B 39 (1989) 9749

[2] J.M. Tranquada et al., Nature 375 (1995) 561

[3] A.T. Boothroyd et al., submitted to Phys. Rev. Lett.

β-manganese: an unconventional itinerant electron paramagnet

J.R. Stewart (ILL)
B.D. Rainford
(University of Southampton)
R. S. Eccleston (ISIS)
R. Cywinski (University of Leeds)

The Fermi-liquid picture of electron interactions in metals, developed by Landau in the mid 1950s [1] has, up to now, provided the basis for the understanding of the macroscopic thermodynamic and transport properties of metals. Recently, however, several metals have been discovered which show properties inconsistent with the Fermi-liquid model. We have observed non-Fermi-liquid (NFL) scaling behaviour in the elemental paramagnetic metal β-manganese – the first observation of such properties in a pure elemental metal. NFL properties of magnetic materials are caused by the existence of a distribution of relaxation times of the magnetic moments, which is normally brought about, by impurities or defects. However, this cannot be the case for β-Mn since it is a pure element.

β-Mn is the only stable form of elemental Mn which does not display magnetic order. The simple cubic β-Mn crystal structure consists of two inequivalent atomic sites, with eight site I and twelve site II Mn atoms per unit cell. Itinerant magnetic moments reside only on the site II positions. The bulk magnetic susceptibility of β-Mn is independent of temperature, indicating standard Pauli paramagnetic behaviour in this material. However, nuclear magnetic resonance and specific heat measurements of β-Mn have been performed, which indicate an antiferromagnetically correlated *quantum spin liquid* [2] ground state, in which the presence of geometrical magnetic frustration between the site II Mn atoms prevents long-range order at low temperatures. It has also been demonstrated that the itinerant moments in β-Mn are on the edge of moment stability [3]. Doping β-Mn with as little as 3 at% Al is sufficient to partially localise the Mn moments, and create a static spin-glass like magnetic ground state at low temperatures. In order to examine the electronic spin fluctuations in β-Mn we have performed quasi-elastic neutron time-of-flight studies of β-Mn in order to examine the dynamical magnetic susceptibility of this unconventional paramagnet [4].

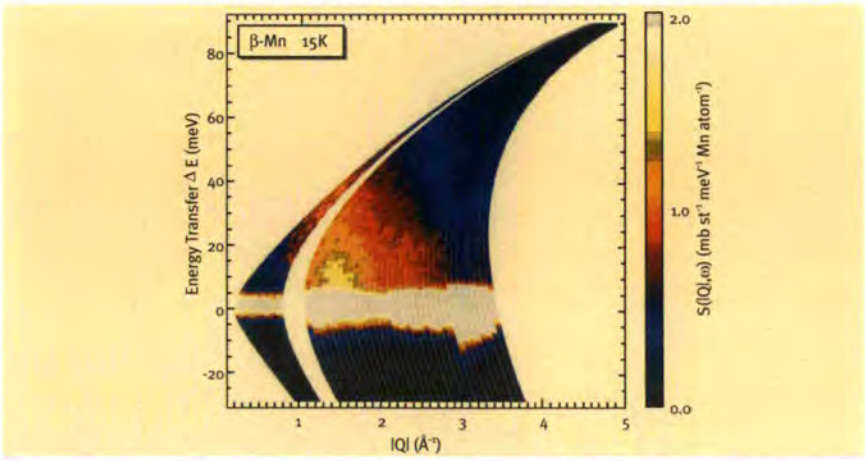

Figure 1: Contour plot of S(Q,ω) for β-Mn at 15K, taken on HET. The quasi-elastic spin fluctuation response is clearly visible, peaked around Q = 1.4 Å^{-1}. The spin fluctuation response is extremely broad extending out beyond 40 meV

Neutron scattering provides the only method for direct observation of the dynamical magnetic susceptibility as a function of energy and wavevector transfer, Q. For these studies we used the HET spectrometer at the ISIS spallation neutron facility, Didcot, UK, and the IN6 spectrometer at the ILL. Using these two spectrometers at incident neutron energies of 100 meV and 3.12 meV respectively, has enabled us to observe the dynamical susceptibility of β-Mn over almost four decades of energy between 0.08 meV and 40 meV. The dynamic structure factor S(Q,ω) for β-Mn at 15K measured on HET is shown in figure 1. It is immediately clear from the figure that even at low temperatures, there is significant magnetic intensity – centred at Q = 1.4 Å^{-1} extending to high energies on the neutron energy loss side of the spectrum. This is indicative of a strongly spin-fluctuating ground state as predicted by previous studies. On taking a cut through the data at the peak of the structure factor (at Q = 1.4 Å^{-1}) we find that the form of S(ω) does not follow a simple Lorent-

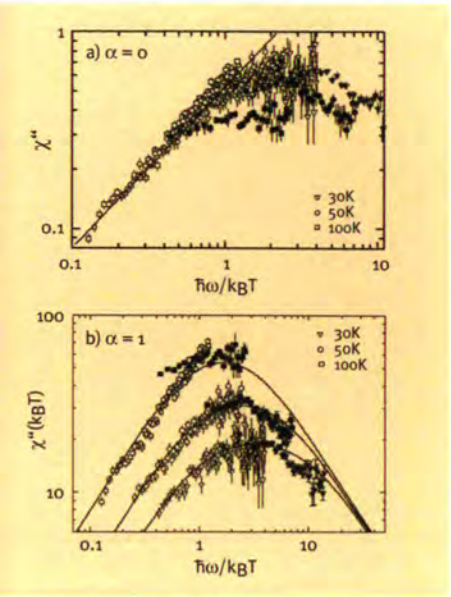

Figure 2: The observed $\hbar\omega/k_BT$ scaling relationship of the dynamical susceptibility of β-Mn plotted for the scaling exponents, a) $\alpha = 0$ and b) $\alpha = 1$. The HET data are shown as solid symbols and the IN6 data are shown as hollow symbols. The solid lines in b) are fits of the data to Eq. (1), from which the parameters shown in figure 3 were deduced. The low-frequency asymptote of the dynamical susceptibility is seen to scale well for $\alpha = 0$, while for $\alpha = 1$, the model fits to the data indicate scaling behaviour for the high frequency asymptote.

zian model. Instead we find that the data at each temperature are well described by the function,

$$\chi''(\omega) = \frac{u}{\Gamma_2 - \Gamma_1}\left[\tan^{-1}\left(\frac{\omega}{\Gamma_1}\right) - \tan^{-1}\left(\frac{\omega}{\Gamma_2}\right)\right] \quad (1)$$

where $\chi''(\omega)$ is the imaginary part of the dynamical magnetic susceptibility (related to $S(\omega)$) and $u = \Gamma\chi$ = constant. This form of the magnetic susceptibility is that predicted for a system where there is a broad distribution of spin relaxation rates between the upper limit Γ_2, and lower limit, Γ_1, rather than a unique relaxation rate, which would lead to a Lorentzian form to the susceptibility [5]. It is this distribution of relaxation rates which leads to the observation of non-Fermi liquid scaling. Figure 2 shows plots of $\chi''(\omega)(k_BT)^\alpha$ at $Q = 1.4$ Å^{-1} plotted as a function of $\hbar\omega/k_BT$, for two values of the exponent $\alpha = 0$ and $\alpha = 1$. In the case of classical Fermi liquid scaling, the data at each temperature should scale for $\alpha = 1$. It is clear from figure 2b that this is not the case, although at high values of $\hbar\omega/k_BT$ with $\alpha = 1$, the data are approaching scaling behaviour. In figure 2a we also notice that the data scale well at low values of $\hbar\omega/k_BT$ with $\alpha = 0$.

Figure 3 shows a plot of the high and low frequency limits Γ_2 and Γ_1 as a function of temperature, together with the fractional difference between them $(\Gamma_2 - \Gamma_1)/(\Gamma_2\Gamma_1)$ – the so-called NFL parameter. We see from figure 3 that Γ_2 is independent of temperature, whereas Γ_1 falls steadily with temperature. This behaviour leads to broadening of the distribution of relaxation rates as the temperature approaches zero, and hence to the large values of the NFL parameter. This then explains the scaling plots in figure 2. At high temperatures, the data approaches the Fermi liquid scaling regime, with a single relaxation rate $\Gamma_2 \sim \Gamma_1$. This is shown up in the approach to scaling behaviour at high frequencies in figure 2b with $\alpha = 1$ – as would be expected form the Fermi liquid model. As the temperature decreases and the distribution of relaxation rates broadens, we see a steady departure from Fermi-liquid behaviour, with the data scaling at the low frequency asymptote of figure 2a with $\alpha = 0$.

The question now remains as to what causes the distribution of relaxation times, leading to the observed NFL scaling of the magnetic susceptibility. Microscopically, we can understand the formation of such a distribution of relaxation rates as being due to either: spatial averaging over inhomogeneities (temperature, pressure gradients or intrinsic chemical disorder or defects), or an intrinsic *localised* distribution, independent of the above spatial averaging, giving rise to either a spatially correlated (wavevector dependent) or uncorrelated (wavevector independent) NFL state. Since we have no evidence to suggest the presence of atomic, chemical or defect disorder *in a pure element* we attribute the presence of NFL scaling in β-Mn to an intrinsic distribution of relaxation rates, independent of any spatial averaging over the sample. In other NFL compounds, the presence of atomic disorder cannot be ruled out to the same degree. In the case of $UCu_{5-x}Pd_x$ – even for the stochiometric case where $x = 1$ - there is evidence of Pd-Cu site disorder [6], while there is likely to be random site disorder in non-stochiometric $CeCu_{6-x}Au_x$ [7] and the doped rare-earth cuprates.

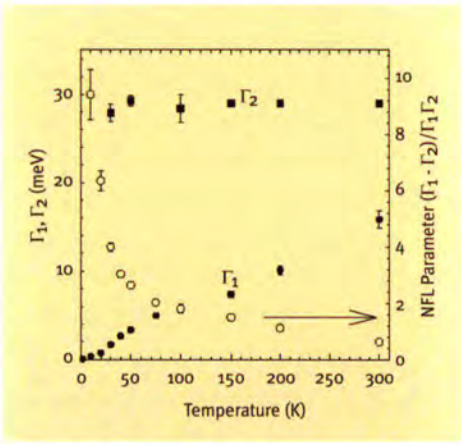

Figure 3: The temperature dependence of the high (Γ_2) and low (Γ_1) frequency limits of the spin relaxation rate distribution in b-Mn, found by fitting both the HET and IN6 quasielastic neutron scattering data to Eq. (1). The plot also shows the temperature dependence of the NFL parameter, which is seen to diverge at low temperatures.

REFERENCES

[1] L.D. Landau, Sov. Phys. -JETP 3 (1956) 920
[2] H. Nakamura, K. Yoshimoto, M. Shiga, et al., J. Phys. Condens. Matter 9 (1997) 4701
[3] J.R. Stewart, K.H. Andersen, and R. Cywinski, ILL Annual Report (1998) 26
[4] J.R. Stewart, B.D. Rainford, R.S. Eccleston, et al., Phys. Rev. Lett. 89 (2002) 186403
[5] N. Bernhoeft, J. Phys.: Condens. Matter 13, R (2001) 771
[6] M.C. Aronson, R. Osborn, R.A. Robinson, et al., Phys. Rev. Lett. 75 (1995) 725
[7] A. Schröder, G. Aeppli, E. Bucher, et al., Phys. Rev. Lett. 80 (1998) 5623

Evolution of low energy *antiferromagnetic fluctuations in superconducting $YbSnPd_2$*

P. Giudicelli
(ILL and CEA Grenoble)
B. Roessli, A. Amato and P. Fischer
(PSI Villigen)
A. Stunault and J. Ollivier (ILL)
A. Dönni (Niigata University)
H. Sugawara
(Tokyo Metropolitan University)
N. Bernhoeft (CEA Grenoble)

The Heusler compound $YbSnPd_2$ exhibits singular thermodynamic and transport properties, with coexistence of superconductivity and antiferromagnetism at low temperature. Using a cryomagnet with a dilution insert on IN6 we have studied the field and temperature dependence of the low energy fluctuations. At all temperatures, and for fields below 1 T, we observe a novel excitation characteristic of a magnetic fluid, in addition to the anticipated Zeeman doublet of a Γ_7 ground state.

The search for novel pairing mechanisms in the superconducting state has received a large impetus from the discovery of materials where superconductivity and long range magnetic order coexist. One actively pursued avenue, both theoretically and experimentally, focusses on exploring the possibility that the pairing mechanism is mediated by magnetic fluctuations. While residual magnetic correlations are destroyed by doping in the superconducting phase of high-T_c materials or by pressure in a set of recently investigated Ce compounds, it appears to persist in certain strongly correlated electron compounds such as UPd_2Al_3, URu_2Si_2, UGe_2 and $ZrZn_2$.

The Heusler compound $YbSnPd_2$ exhibits singular thermodynamic and transport properties. In zero field, a superconducting state sets in at $T_c = 2.3$ K, evolving into a simultaneous superconducting-antiferromagnetic state below $T_N = 220$ mK [1,2]. Note that antiferromagnetism occurs only at very low temperatures, deep in the superconducting phase. The upper critical field for $T \to 0$ is unusually small ($B_{c2} \approx 0.04$ T) and lies below the maximum critical field (≈ 0.05 T at 1 K). This peculiar behaviour has been cited as evidence for the interplay between superconductivity and antiferromagnetic fluctuations [3,4].

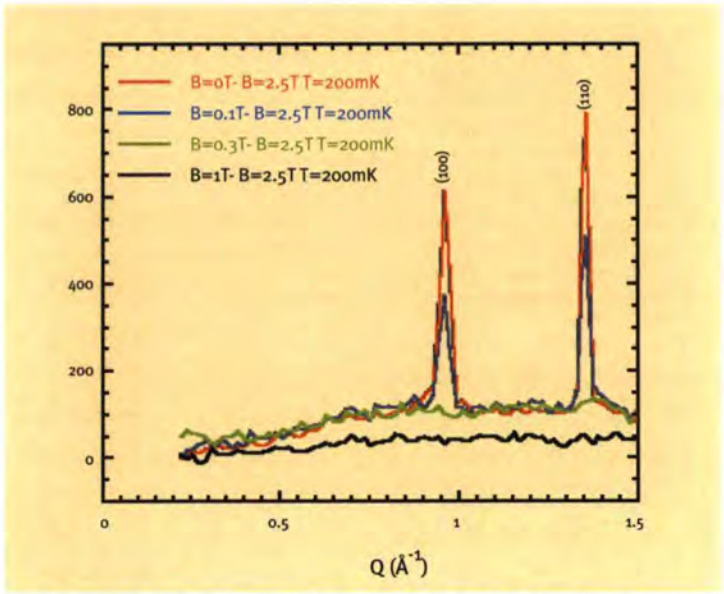

Figure 1: Q-dependence of magnetic scattering ($\Delta E = \pm 0.2$ meV) by field subtraction technique at 200 mK. The antiferromagnetic Bragg peaks disappear for $B > 0.3$ T, whilst the local magnetic fluid response persists to 1 T (see details in figure 3)

To clarify the connection between magnetism and superconductivity it is of interest to characterise the *dynamic* magnetic response at a microscopic level. We have therefore performed a systematic inelastic neutron scattering study of the magnetic field and temperature dependencies of the low energy magnetic fluctuations in $YbSnPd_2$.

A high-quality polycrystalline sample was used for these and complementary μSR studies [5]. Preliminary work on the IN14 (ILL) and TASP (SINQ) triple-axis spectrometers revealed (i) enhanced antiferromagnetic correlations in an energy window ± 0.2 meV for temperatures $10\,T_N < T < 50\,T_N$ and (ii) that an applied field of 2.5 T is sufficient to quench the magnetic response. Using a 2.5 T cryomagnet with a dilution insert on the IN6 time-of-flight spectrometer, where the extended array of detectors allows simultaneous measurements over the whole Brillouin zone, we inves-

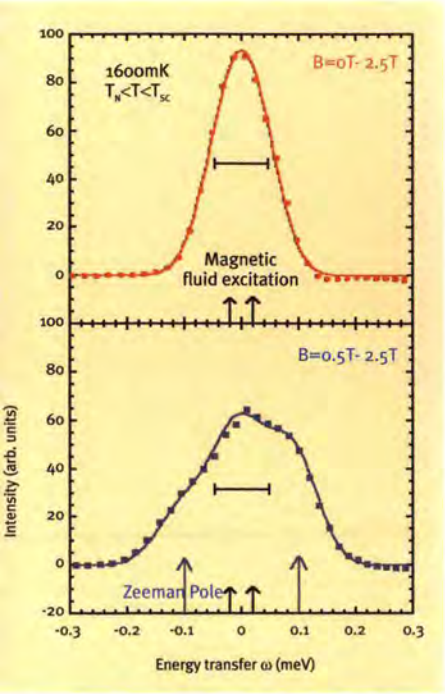

Figure 2: Inelastic magnetic scattering at 1.6 K as revealed by the field subtraction technique, in zero field (top panel) and in an applied field of 0.5 T (bottom panel). The poles of the magnetic fluid excitations are shown by black arrows and those of the field induced Zeeman doublet by blue arrows. The instrumental resolution is indicated by the horizontal bar.

tigated systematically the antiferromagnetic-superconducting and paramagnetic-superconducting ground states for 60 mK ≤ T ≤ 1.6 K (dilution stability limit), at fields between 0 and 2.5 T. Noting that the magnetic response within ± 0.2 meV is quenched at 2.5 T, we could deduce the magnetic part of the scattering at very low energy transfer by substracting the signal measured at 2.5 T (field subtraction technique). Figure 1 shows the field subtracted intensities at 200 mK, integrated over ± 0.2 meV. We observe Bragg scattering at angular positions corresponding to a propagation vector [001], confirming the antiferromagnetic structure below 0.3 T and 200 mK. Away from the Bragg positions, the wave-vector dependence is that of a magnetic fluid with a strong suppression of fluctuations at long wavelengths and a correlation radius of the order of the lattice parameter.

In applied magnetic fields below 1 T, the energy dependence of the magnetic fluid spectrum has two components as shown in the lower panel of figure 2 at T = 1.6 K, i.e. for $T_N < T < T_c$. First is the anticipated Zeeman doublet with splitting rate 200 μeV/T (moment 1.7 μ_B) confirming a Γ_7 CEF ground state [1-4]. The Stokes/anti-Stokes intensity ratio of this doublet provides an important *in situ* measurement of the sample temperature at these very low temperatures. In addition there is a *second*, low energy, ω_0 ~ 20 μeV, excitation, which exists for all fields below 1 T. The field dependent amplitudes at 200 mK, shown in figure 3, indicate that the excitation of the Zeeman term is reduced for fields below 1 T, whilst the magnetic fluid contribution is present. This observation gives a rational to the hitherto unexplained heat capacity anomalies, where the Schottky response of the Zeeman doublet is suppressed for applied fields of less than 1 T [3,4].
Our experiments, which confirm antiferromagnetic order, Q_{afm} = [001], below T_N ~ 220 mK and support a Yb^{3+} doublet [Γ_7] of effective moment 1.7 μ_B, reveal a novel ground state with excitations characteristic of an unexpected magnetic fluid. The superconducting state thus forms within, and appears to be supported by, a phase of strong magnetic correlations which range at least an order of magnitude above T_N. In view of the slow, dynamic, nature of the magnetic fluid correlations it appears eminently worthwhile to establish, by further experiments, if the nominal antiferromagnetic state occurring below T_N is indeed one of true static long range order or, alternatively, if it has the nature of a more fragile thermodynamic state such as appears to exist in, for example, URu_2Si_2 [6]. Technically, the novel combination of dilution temperatures and variable magnetic field have made it possible to examine very low energy magnetic excitations within the resolution window on IN6, with *in situ* temperature calibration. This will enable significant progress in the interpretation of the anomalous thermodynamic properties of $YbSnPd_2$.

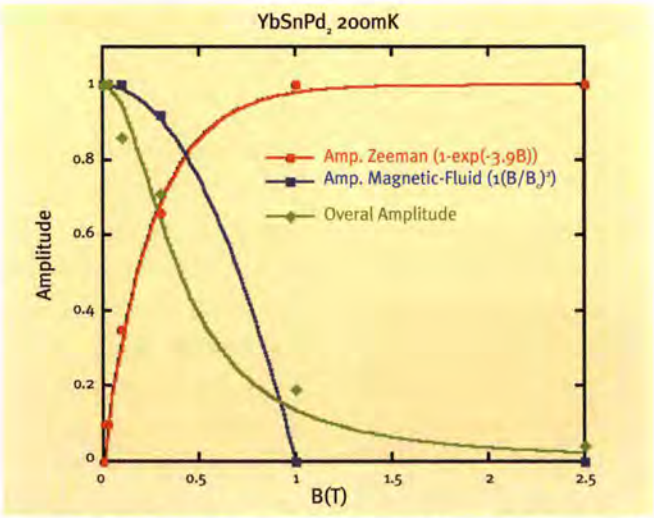

Figure 3: Relative intensities of the magnetic fluid and Zeeman poles at 200 mK together with the overall scattering amplitude.

REFERENCES

[1] H.A. Kierstead et al., Phys. Rev. B 32 (1985) 135
[2] A. Dönni et al., Physica B 259-261 (1999) 705
[3] Y. Aoki et al., J. Magn. Magn. Mater. 177-181 (1998) 559
[4] Y. Aoki et al., Physica C 333 (2000) 187
[5] A. Amato et al., Physica B 326 (2003) 369
[6] N. Bernhoeft et al., SCES-2002, Krakow, Poland (to be published)

Neutron spin-echo
and hot spin ice

J. S. Gardner (NRC, Chalk River)
G. Ehlers, M. Koza (ILL)
T. Fennell (The Royal Institution of Great Britain)
S. T. Bramwell (UCL London)

The drive towards ever smaller and faster electronic devices has forced scientists to consider quantum dynamics, which governs the interaction of particles on the atomic scale. The prospect of harnessing such dynamics in new technology has fueled interest in areas like spintronics, quantum algorithms and "large spin" magnets that show quantum tunnelling transitions between spin states. Examples of these magnets include the dipolar magnet $LiHoF_4$ and "single molecule magnets" such as "Mn_{12}". However, the inherently weak interactions in magnetism mean that tunnelling is usually only observed at millikelvin temperatures. Neutron spin-echo has now played a crucial role in unravelling the complex spin dynamics in another large spin system: $Ho_2Ti_2O_7$. This material shows a "spin ice" freezing transition near 1 K with unusually slow spin dynamics at higher temperatures. Neutron spin-echo clearly separates the various contributions to the dynamics and suggests that quantum tunnelling may be the dominant mechanism at temperatures up to 16 K. It appears that paramagnetic or "hot" spin ice represents a completely new class of quantum-dynamical magnet.

In quantum magnets, such as $LiHoF_4$ [1] and the "single molecule" magnets [2], the spin can be thought of as confined to a double-well potential of depth D. This situation may arise when the $(2J+1)$-fold degeneracy of the free ion groundstate is lifted by low symmetry of the crystalline electric field (CEF) to leave a groundstate doublet behind which is separated by D from the energy of the first excited state. At temperatures $T << D$, quasi-classical spin flips across this potential barrier are precluded, but spin relaxation can still exist and quantum mechanics has to be invoked. By analogy with dipolar molecular systems (e.g. the inversion of ammonia) this process can be described as "tunnelling", that may be resonant (a superposition of states) or thermally assisted (excitation between states). In $LiHoF_4$, these tunnelling processes are provoked by a transverse magnetic field, while in the single molecule magnets direct or thermally assisted tunnelling is also possible. Schemes exist to harness such effects for quantum computation [3], but as D is small (~10 K in $LiHoF_4$ [4] and ~50 K in Mn_{12} [5]) the temperatures involved are low, with "classical" processes dominating at $T > 1$ K.

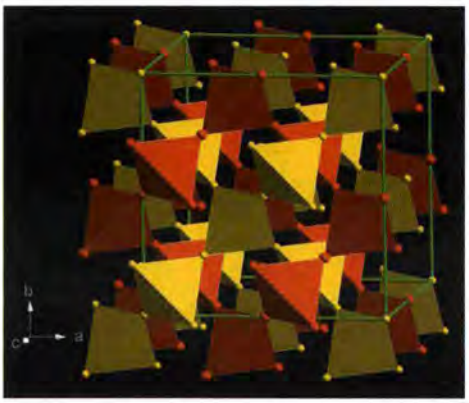

Figure 1: The two metal sublattices (red and yellow) of the oxide pyrochlore compound.

In the spin ice materials $Ho_2Ti_2O_7$, $Ho_2Sn_2O_7$ and $Dy_2Ti_2O_7$ [6], the magnetic rare earth ions occupy a cubic pyrochlore lattice of corner-linked tetrahedra (figure 1). The magnetic moments are constrained by the CEF to local <111> axes. This frustrates the dominant (effectively ferromagnetic) dipolar interactions in the system and leads to frozen, non-collinear, spin disorder below ~1 K. The spin ice state is analogous to the Pauling hydrogen disorder of water ice (H_2O), with each spin equivalent to a hydrogen displacement vector situated on the mid-point of an oxygen-oxygen line of contact [6]. The spin ice state can be described with great precision by a classical Ising model, but this is not to say that the dynamics are in any sense classical. Indeed, the single ion ground state of the spin ice materials is an almost pure quantum doublet, separated by over 200 K from the first excited state [6,7]. In this sense the spin ice materials must be among the most quantum mechanical of all magnets. They bear an obvious similarity to the quantum magnets discussed above, but in spin ice, the quasi-classical barrier is much higher - at least 200 K.

Neutron spin-echo (NSE) is a high energy-resolution probe that measures the intermediate scattering function $S(\mathbf{Q},t)$ in the time range $t \sim 10^{-12}$-10^{-7} s [8]. This can be related by Fourier transform to the generalised suscepti-

bility $\chi''(Q,\omega)$ which can then be extrapolated to $\nu < 10^5$ Hz for comparison with results of bulk ac-susceptibility measurements [9-11]. Figure 2 shows the normalised relaxation function $F(Q,t) = S(Q,t)/S(Q,0)$ measured for a polycrystalline sample of $Ho_2Ti_2O_7$ on IN11C using a neutron wavelength of 5.5 Å. At all temperatures between 0.05 K and 200 K the relaxation can be fitted with excellent precision to a simple exponential function

$$F(Q,t) = A \exp\{-\nu(T)\, t\},$$

where $A = 0.91 \pm 0.01$. The frequency $\nu(T)$ can be fitted to an Arrhenius expression $\nu(T) = 2\,\nu_0 \exp(-E_a/kT)$ with attempt frequency $\nu_0 = 1.1 \pm 0.2 \times 10^{11}$ Hz and activation energy $E_a = 293 \pm 12$ K (see inset to figure 2). The relaxation was found to be Q-independent and along with the fact that the activation energy is close to the first group of CEF levels [7], we conclude that it is a single ion spin flip process via one or more crystal field levels. The fact that $A \neq 1$ at ~10^{-12} s proves the existence of relaxation processes beyond the resolution of NSE. We suggest that these very fast processes might be associated with small incoherent oscillations of the spins about their <111> easy axes.

Transforming the relaxation function to the generalised susceptibility we find:

$$\chi(Q,\omega)=\chi(Q)\left\{\frac{\nu^2(T)}{\nu^2(T)+\omega^2}+\frac{i\omega\nu(T)}{\nu^2(T)+\omega^2}\right\},$$

where we have assumed $kT >> \hbar\omega$. This function was used to extrapolate the NSE response into the ac-susceptibility frequency window, suggesting that a peak of the bulk susceptibility χ' should be observed around 16 K. This peak has subsequently been detected by ac-susceptibility [12].

The NSE results prove that any classical Hamiltonian for $Ho_2Ti_2O_7$ must include a barrier to spin inversion of ~300 K. It therefore comes as some surprise that the ac-susceptibility χ' shows another maximum at lower temperature where the barrier is insurmountable. The spin flipping transitions in this range must involve quantum tunnelling between degenerate "spin up" and "spin down" states on Ho^{3+} ions. The susceptibility shows a second peak at ~1 K [6] associated with an activation energy $E_a' \approx 20$ K and attempt frequency $\nu_0' \sim 10^{10}$ Hz, due to a process taking place on a different energy scale. If this second process could be extrapolated into the NSE time window, it would be visible above ~4 K. The fact that it is not is consistent with dynamics that are slow and roughly temperature-independent in this range, a further signature of quantum tunnelling.

What is the origin of the quantum dynamics observed by NSE? In spin ice, neighbouring spins are fixed almost at right angles and subject each other to strong dipolar fields. We suggest that the transverse component of the effective dipolar field causes the single ion ground state to no longer be a pure doublet, inducing a finite rate of spin inversion that is approximately temperature-independent. These new quantum channels of relaxation are only possible in the "hot" paramagnetic phase where the mean field is zero. Freezing into the spin ice phase at ~1 K extinguishes these channels by establishing a mean field.

The unique interactions in spin ice are thus seen to play a crucial role in this process. Unlike $LiHoF_4$, the strong dipolar interactions in $Ho_2Ti_2O_7$ are frustrated by the enormous single ion anisotropy. This prevents the development of a correlation length and retains a strong transverse component of the instantaneous dipolar field. While quantum tunnelling in $LiHoF_4$ can only be introduced by applying a field, in $Ho_2Ti_2O_7$ the field is intrinsic. The large energy scales in $Ho_2Ti_2O_7$ also mean that quantum tunnelling persists to a higher temperature than in other quantum magnets. In short, NSE has revealed a completely new class of quantum dynamical magnet: "hot" spin ice.

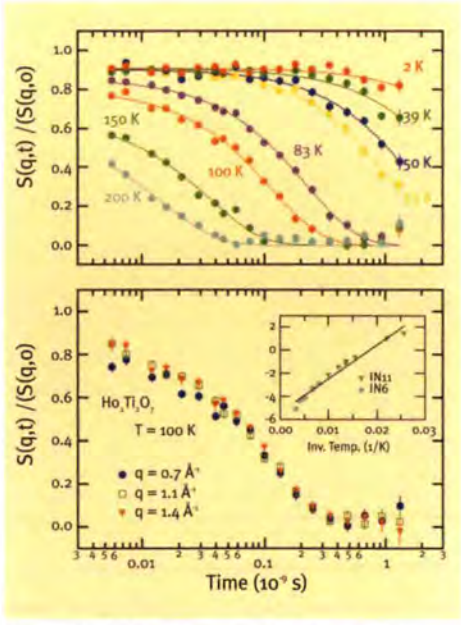

Figure 2: NSE results for $Ho_2Ti_2O_7$: (top) Integrated over all **Q** and fitted to an exponential function, (bottom) as a function of **Q**, indicating negligible Q-dependence. The inset shows the Arrhenius behaviour of this relaxation, with some data points added from an experiment performed at IN6.

REFERENCES

[1] D. Bitko, T.F. Rosenbaum and G. Aeppli, Phys. Rev. Lett. 77 (1996) 940
[2] J.R. Friedman et al., Phys. Rev. Lett. 76 (1996) 3830
[3] M.N. Leuenberger and D. Loss, Nature 410, (2001) 789-793
[4] P.E. Hansen, T. Johansson and R. Nevald, Phys. Rev. B 12 (1975) 5315
[5] R. Sessoli et al., Nature 365 (1993) 141-143
[6] S.T. Bramwell and M.J.P. Gingras, Science 294 (2001) 1495
[7] S. Rosenkranz et al., J. Appl. Phys. 87 (2000) 5914
[8] F. Mezei (editor), Neutron Spin-Echo, Lecture Notes in Physics vol. 128 (Springer-Verlag, Heidelberg 1980)
[9] K. Matsuhira et al., J. Phys. Condens. Matt. 12 (2000) L649-L656
[10] K. Matsuhira et al., J. Phys. Condens. Matt. 13, (2001) L737-L746
[11] J. Snyder, et al., Nature 413 (2001) 48-51
[12] A. Cornelius et al., unpublished results

Magnetic transitions in a Cr_8 antiferromagnetic ring

S. Carretta, E. Liviotti and G. Amoretti (INFM, Parma)
J. van Slageren, R. Sessoli and D. Gatteschi (Uni Firenze)
T. Guidi, F. Carsughi and R. Caciuffo (INFM Ancona)
C. Mondelli (INFM, Grenoble)

Inelastic neutron scattering has been used to determine exchange integrals and single-ion anisotropy parameters in a ring-shaped molecular cluster made by 8 Cr^{III} ions. Effects due to the mixing of different spin multiplets proved to be an important ingredient of the physics of this system. Evidence of decreasing lifetime with increasing energy of excited spin states was found.

Single Molecule Magnets (SMM) are clusters formed by a finite number of exchange-coupled transition-metal ions [1]. They exhibit many interesting properties, such as magnetic bistability and slow relaxation of the magnetisation. Macroscopic SMM samples are a collection of perfectly identical and weakly interacting clusters, allowing to observe quantum-mechanical effects through macroscopic measurements [2]. Moreover, these compounds are promising for several technological applications, such as quantum computing and high-density data storage.

A ring-shaped cluster consisting of eight Cr^{III} ions (chemical formula: $Cr_8F_8Piv_{16}$, where Piv = pivalic acid) has been recently synthesised [3]. Susceptibility measurements suggested an antiferromagnetic (AF) interaction between the Cr^{III} ions, with an energy splitting of about *0.8 meV* between the $S = 0$ ground state and the $S = 1$ first excited state. We have prepared 4 grams of non-deuterated polycrystalline sample using the procedure reported in [3], and checked the sample integrity by X-ray diffraction at room temperature. The molecular structure of the cyclic cluster is shown in figure 1. The system crystallises in the $P42_12$ tetragonal space group. The *Cr* ions form an almost perfectly planar octagon, with a slightly distorted octahedral environment and an average intramolecular *Cr-Cr* distance of *3.388 Å*. High-energy resolution inelastic neutron scattering experiments have been carried out on the time-focussing, time-of-flight spectrometer IN6 at ILL [4]. An energy-transfer range up to *4 meV* in neutron-energy-loss has been explored, with different spectrometer configurations corresponding to energy resolution from *50 μeV* to *170 μeV* at the elastic peak. The instrument covers a wide range of scattering angles (from *10* to *114* degrees), corresponding to a maximum momentum transfer of $Q = 2.6$ Å^{-1}. Isotropic exchange is the dominant interaction in these systems. The magnetic energy spectrum consists of many spin multiplets split by anisotropic interactions, such as the local crystal field and dipolar interactions [5]. Neutron spectroscopy provides direct access to the energies and wavefunctions of the different spin states of the magnetic clusters. The lowest energy levels for Cr_8 are shown in figure 2. The neutron spectra measured on IN6 with incident energies of *2.35*, *3.86*, and *4.86 meV* are shown in figure 3. With the sample at $T = 2$ K, the excited states are not populated. In the

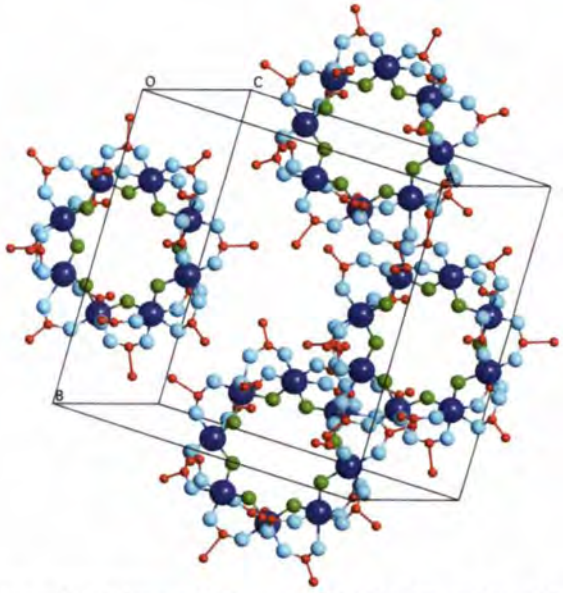

Figure 1: 3D view of the tetragonal Cr_8 unit cell (dotted line). Large blue spheres are Cr atoms, medium green and light-blue spheres are F and O atoms, respectively, and small red spheres are C atoms. H atoms, disordered solvent molecules and methyl groups are not shown for clarity.

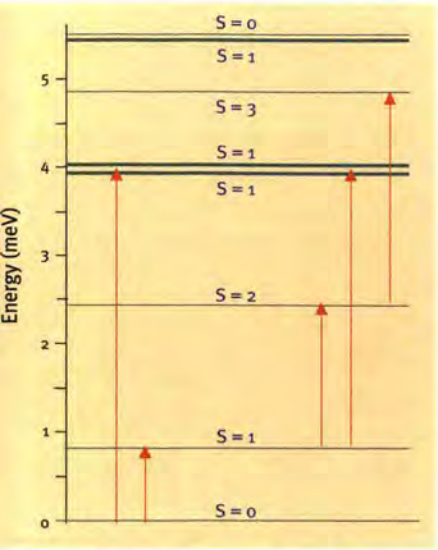

Figure 2: Lowest energy spin multiplets calculated for tetragonal Cr_8 assuming isotropic exchange interactions only, with parameters corresponding to the best fit of INS spectra.

energy range explored, the allowed transitions (with selection rule $\Delta S = 0,\pm1$ and $\Delta M = 0,\pm1$) are only those between the |S=0;M=0> ground state and the |S=1;M=0,±1> levels. The zero-field splitting of the first excited S=1 multiplet is well resolved. On increasing the temperature, the excited levels become progressively populated and transitions between them can be observed, offering the possibility of studying the details of the spin Hamiltonian and of determining the strength and topology of the exchange interactions. At $T = 12\ K$ and below *4 meV*, transitions from the |S=1> first excited state to |S=2> and to other |S=1> multiplet levels are clearly visible, together with a |S=2>→|S=3> transition. At higher temperatures, transitions from the ground state almost vanish, due to the thermal population of many excited levels.

The experimental spectra have been reproduced using a microscopic spin Hamiltonian and the parameters describing the intra-cluster interactions have been determined by a best-fit procedure. The most important effects due to the mixing between different spin multiplets have been taken into account. These effects have proved important in determining the details of the neutron results, in particular they change the ratio between the intensities of the peaks at *~0.7* and *~0.9 meV* by more than 20%. The spectra calculated using the best-fit parameters are shown by solid lines in figure 3. An interesting feature is the broadening of the transitions between excited multiplets, a signal that the lifetime of the excited states becomes shorter as the energy of the level increases.

To correctly reproduce the experimental data, a rhombic term [5] in the crystal-field Hamiltonian is necessary. In principle, this second-order in-plane anisotropy is not allowed by the C_4 symmetry exhibited by the cluster at room temperature, thus giving evidence that a low temperature distortion may take place. Preliminary neutron diffraction experiments confirm this assumption [6].

The detailed knowledge of the microscopic interactions in molecular magnetic clusters is essential to make possible a rational design of these systems. Indeed, a large Ising-type anisotropy barrier for spin reversal, U, is essential for the realisation of a single-molecule magnet to be used in information storage devices. The system with the highest barrier discovered so far is Mn12-acetate, for which U = 61 K. This value is far too small for practical applications, but the synthesis of magnetic clusters with sizeably higher anisotropy appears to be a difficult challenge. A deeper understanding of the origin of the magnetic anisotropy in SMM is necessary to achieve substantial progress and neutron scattering may prove to be an important tool to shed light in this matter.

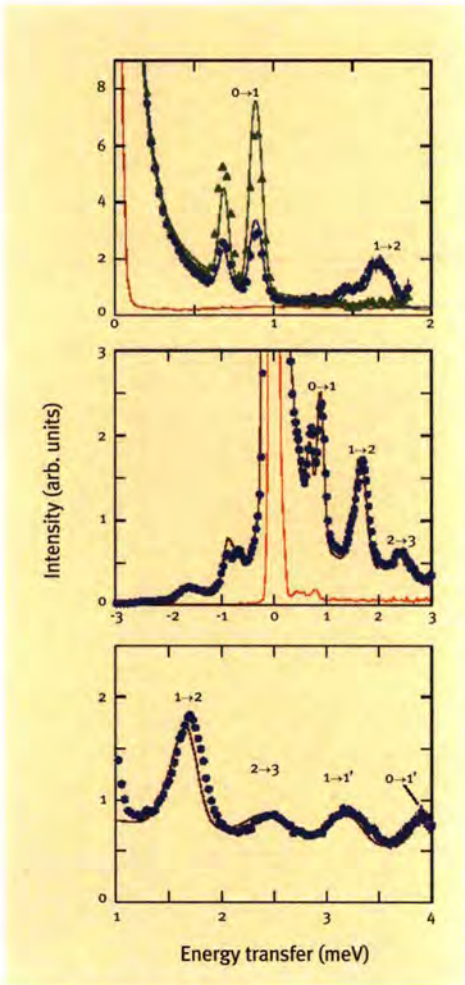

Figure 3: Inelastic neutron scattering results for Cr_8 at 2 K (red triangles) and 12 K (full circles), recorded on IN6 with an incident neutron energy of (upper panel) 2.35, (central panel) 3.86, and (lower panel) 4.86 meV. Intensities integrated over the whole scattering angle range are shown as a function of energy transfer. The empty sample-holder contribution (red line) has been subtracted after normalisation for absorption. Excitation peaks are labelled by indicating the total spin of the initial and final multiplet involved in the transition. The spectra calculated using the best-fit parameters are shown by solid lines.

REFERENCES

[1] D. Gatteschi et al., Science 265 (1994) 1054
[2] L. Thomas et al., Nature 383 (1996) 145
[3] J. van Slageren et al., Chem. Eur. J. 8 (2002) 277
[4] S. Carretta et al., Phys. Rev. B, in press (March 2003)
[5] A. Bencini and D. Gatteschi, EPR of Exchange Coupled Systems, Springer Verlag, Berlin (1990)
[6] T. Guidi et al., to be published

Structure matters

Participants in the IUCr-2002 Satellite Meeting: Crystal Chemistry of New Materials & Soft Matter studied by Synchrotron & Neutron Diffraction, held on the ILL/ESRF site in August 2002.

Colin Carlile checks the arrival of the new super-D2B detector from Eurocollimators, with Peter Cross and Pierre Thomas.

The S18 interferometer team: from left to right, Simon Mayer, Rudolph Loidl and François Dubus (Atominstitut Wien).

Andrew Wills, UCL, University of London.

Thomas Hansen,
College 5A Secretary

Chemistry and structure

Thermal neutrons are still, in many senses, unique probes for condensed matter research. This is not only the case for the exploration of magnetic structure, exploiting the neutron's magnetic moment, nor for the investigation of atomic dynamics, making use of its kinetic energy close to the energy range of collective excitations in solids and liquids. The neutron's zero-charge makes it an ideal probe for exploring atomic structures in condensed matter, particularly in crystalline materials (single crystals or polycrystalline samples). As the neutron interacts only through short-ranged nuclear exchanges, the interaction probability is small, and it can usually penetrate into the bulk of larger samples or through sample containers and shielding materials of complex sample environment, such as furnaces or fridges. Its zero-charge brings as a further advantage over X-ray or electron diffraction the independence of its scattering length to the number of electrons around an atom, which varies so arbitrarily over the periodic table and permits distinction of isotopes. Additionally there is a delivery of better information at high scattering angles, far in reciprocal space, as the nuclear scattering length is constant due to scattering at the nucleus, which can be considered as a point source.

As a brand new machine for single crystal diffraction, VIVALDI made its "debut" in 2002, and it was in fact a great comeback of the Laue method in the ILL's diffraction group, as shown, among many other examples, on the investigation of tiny crystals of vitamin B12 as an important part of a "*X-n*" investigation of the molecules electron density. Single crystal diffraction experiments on D19 permitted the precise localisation of hydrogen in different key compounds containing special hydrogen-bridge bonding systems. Together with D9 the temperature dependence of the thermal motion of naphthalene could be studied due to the neutron's ability to locate hydrogen and precise anisotropic displacement parameters.

High resolution powder diffraction performed on D1A or D2B elucidate the filling of zeolite cages with organic sorbates or the formation of copper-nitrosyl complexes by NO absorption in zeolites, or help to understand the amorphous polymorphism of water via its relation to liquid and high pressure crystalline phases.

Chemistry means not only the knowledge of the "static" localisation of atoms in a sample, but as well the understanding of the changes going on microscopically during a phase transition or a chemical reaction. High intensity powder diffraction on D1B and D20 allows for in situ investigations of phase transitions under the effect of temperature or pressure. The particularly high intensity of D20 allows for time-resolved studies on chemical kinetics, so in the continued work on the self-propagating high temperature synthesis of Ti_3SiC_2 where full diffraction patterns were recorded every 400 ms. The formation of methane- and CO_2 clathrates plays a role in problems of deep sea petrol drilling or might become interesting in view of a possible deep sea deposition of CO_2. The kinetics is an example for a slower, but rather complicated reaction mechanism, as different stages have to be distinguished on quite different time scales from seconds to days.

The upcoming year will see important upgrades to both powder diffractometers D2B and D20. D2B will become *super*-D2B, providing a gain of half an order of magnitude in detected intensity due to its new bank of more and higher single detectors. It will allow more easily to choose its very high resolution mode without spending too much time, or to perform a higher number of measuring points in multi-parameter space of temperature, pressure or chemical composition to map crystallographically phase transitions needing D2B's high resolution.

On the other hand, higher take-off angles, exploiting a new germanium monochromator, will become available on D20, providing higher resolution with a still high counting rate due to its large position sensitive detector. Both upgrades will close a gap between high intensity on D20 and high resolution at D2B, providing new scientific opportunities (and the need to know exactly the need in terms of wavelength, resolution and intensity of a powder diffraction experiment).

And, finally, D19 will be equipped with part of its new large position sensitive detector array, accelerating long experiments on complex organic and organometallic crystal structures and small samples already in 2003, and push fibre diffraction work at ILL.

We are confident that these upgrades will maintain a very lively research activity in chemistry and crystallography in spite of the reduced number of reactor cycles and the delay of hot neutrons in 2003!

Structural analysis of Li-ion conducting perovskites $Li_{0.5-x}Na_xLa_{0.5}TiO_3$

J. Sanz, J.A. Alonso (C.S.I.C., Madrid)
A. Varez (Univ. Carlos III, Leganés)
A. Rivera, C. León, J. Santamaría (Univ. Complutense, Madrid)
O. V'yunov, A. Belous (Ukrainian Academy of Sciences)
M.T. Fernandez-Diaz (ILL)

In order to understand the influence of the crystal structure on Li-ion conductivity of $Li_{0.5-x}Na_xLa_{0.5}TiO_3$ perovskites, ND patterns of $Li_{0.5}La_{0.5}TiO_3$, $Li_{0.3}Na_{0.2}La_{0.5}TiO_3$ and $Na_{0.5}La_{0.5}TiO_3$ samples have been analysed. The Rietveld analysis of these patterns shows that Li ions are located at the centers of the faces of the primitive perovskite unit cell, and La and Na ions are distributed randomly at A sites of the perovskite. Therefore the number of vacant A sites increases with lithium content but decreases with La and Na content. The sharp decrease observed in dc-conductivity when the sodium content increases above x = 0.2, is interpreted in terms of a three-dimensional percolation limited diffusion of lithium ions. This result confirms the important role played by vacant A-sites on Li mobility.

Interest in ionic conducting solids has increased in recent years because of their potential application as solid electrolytes in batteries, fuel cells and other electrochemical devices. $Li_yLa_{2/3-y/3}TiO_3$ perovskites, with $0<y<0.5$, are among the best Li-ion conductors, showing a dc conductivity of 10^{-3} S/cm at room temperature. Since the discovery of their outstanding electrical properties, several groups have investigated structural features of these perovskites; however, the conditions that enhance Li mobility have not been completely identified.

A previous study of perovskites $Li_yLa_{2/3-y/3}TiO_3$ showed that, depending on Li content, the symmetry of samples can be orthorhombic ($0.04<y<0.20$) or tetragonal ($0.20<x<0.5$) [1]. In this series, the distribution of La and vacant A sites becomes progressively ordered in alternating planes along the c-axis when the Li content decreases [2,3]. When samples are quenched from 1350ºC into liquid nitrogen, the structure becomes rhombohedral with unit cell parameters $\sqrt{2}$ a, $\sqrt{2}$ a, $3\sqrt{2}$ a [4]. In the former materials, two-dimensional displacements are favoured. However, in the latter compounds a three-dimensional behaviour is detected.

In the $Li_yLa_{2/3-y/3}TiO_3$ series, the conductivity value increases slightly with the lithium content, passing through a small maximum at y = 0.33. In the $Li_{0.5-x}Na_xLa_{0.5}TiO_3$ series, a sharp decrease in dc-conductivity was observed when the sodium content increased above x = 0.2, which has been interpreted in terms of a three-dimensional percolation limited diffusion of lithium ions [5,6].

In order to analyse the influence of two alkaline cations (Li, Na) on conductivity of $Li_{0.5-x}Na_xLa_{0.5}TiO_3$ perovskites, NPD patterns of $Li_{0.5}La_{0.5}TiO_3$, $Li_{0.3}Na_{0.2}La_{0.5}TiO_3$ and $Na_{0.5}La_{0.5}TiO_3$ samples were recorded at increasing temperatures (300-700 K) with the D1A diffractometer (λ = 1.913 Å). In all cases a rhombohedral *R-3c* symmetry was found, and the unit-cell parame-

	x = 0	x = 0.2	x = 0.5
a (Å)	5.4712 (3)	5.4799 (1)	5.4868 (1)
c (Å)	13.4046 (7)	13.4230 (7)	13.4239 (5)
V (Å^3)	347.49 (3)	349.08 (2)	349.999 (2)
R_p	5.18	5.86	5.29
R_{wp}	7.23	7.89	7.19
R_B	3.93	3.62	2.88
R_F	3.75	2.98	2.55
X^2	7.67	3.36	2.66
La occ	0.504 (10)	0.498 (10)	0.501 (11)
B_{iso}	0.10 (3)	0.25 (6)	0.68 (7)
3*(Li occ)	0.495 (40)	0.210 (30)	—
B_{iso}	10.1 (9)	9.2 (9)	—
Na occ	—	0.177 (20)	0.480 (20)
B_{iso}	—	0.25 (6)	0.68 (8)
Ti B_{iso}	1.08 (12)	0.51 (7)	0.48 (7)
O x	0.5317 (5)	0.5397 (3)	0.5396 (3)
B_{iso}	1.75 (8)	1.29 (9)	1.02 (8)
Ti-O	1.942 (2)	1.949 (2)	1.951 (2)
$(M-O)_{ab}$	2.739 (2)	2.744 (1)	2.744 (2)
$(Li-O)_{ab}$	1.939 (9)	1.943 (8)	—
$(O-O)_1$	4.121 (5)	4.190 (5)	4.192 (5)
$(O-O)_2$	3.632 (5)	3.584 (5)	3.588 (5)
Ti-O-Ti	169.8 (4)	167.3 (3)	167.4 (4)

Table 1: Structural information deduced from refinement of ND patterns of $Li_{0.5-x}Na_xLa_{0.5}TiO_3$ samples. Thermal factors of La and Na cations were constrained to vary together during refinement

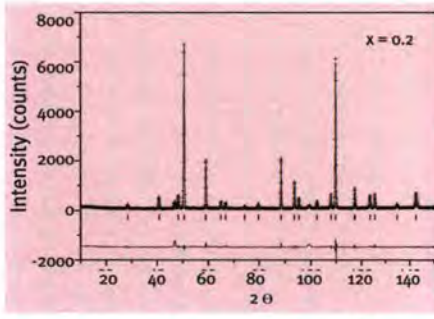

Figure 1: Rietveld refinement of the ND pattern of the $Li_{0.3}Na_{0.2}La_{0.5}TiO_3$ sample, recorded at 298K, assuming the R-3c space group. Bars correspond to Bragg peak positions. The difference profile is shown underneath.

ters remained essentially unchanged along the series. RB and Rwp factors obtained in the Rietveld analysis were always below 3.9% and 7.9% (see figure 1 and table 1).

The structural analysis of these samples showed that Li ions are located at the centers of the faces of the primitive perovskite unit cell, whereas La and Na ions are distributed at random at the A sites of the perovskite (figure 2). Location of lithium at the face-centers of the perovskite unit-cell implies that the amount of vacant A-sites involved in conductivity is considerably higher than that deduced from the structural formula. This fact explains high values of dc-conductivity measured in Li-rich perovskites.

The octahedral tilting ($a^-a^-a^-$ in Glazer's notation) produced Ti-O-Ti angles near 167° and an oblique distortion of unit cell faces that impeded Na ions from passing through the square windows that connect contiguous A sites of the perovskite. Thermal factors deduced for Li are considerably higher than those deduced for Na, indicating that the mobility of Li^+ ions is much more important than that of Na^+ ions (see table 1). In three analysed cases, octahedral tilting decreased when temperature increased.

Taking into account the fact that Na atoms preferentially occupy A-sites, we have considered a percolation model in which A sites associated with Li ions are vacant and participate in ionic diffusion, but La^{3+} and Na^+ ions occupy A sites blocking conduction pathways of the perovskite. In this model, the vacancy distribution is random and the dc conductivity is given by the expression $\sigma_{dc}=K(n-np)^2$, where n is the number of vacant A-sites and np is the percolation threshold for a three-dimensional cubic network ($n_p \approx 0.31$). In agreement with these

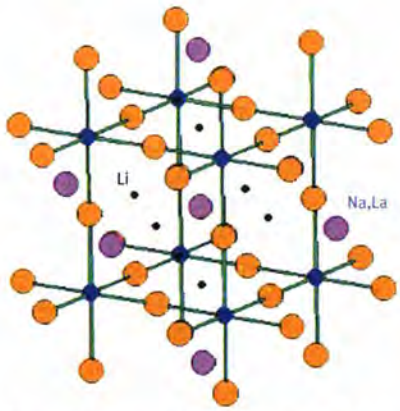

Figure 2: Elementary pseudocubic unit-cell of perovskites, indicating Li and Na locations.

predictions, the ion conductivity decreases drastically near the percolation threshold (see figure 3a).

Based on these structural results, the number of vacant A-sites should correspond to the sum of nominal vacancies plus Li content. From this fact, the number of vacancies that participate in lithium diffusion should be calculated as the sum of nominal vacancies plus the Li content, $n = [Li]+Ü$. Substitution of Li by Na ions reduces the number of vacant sites *n*. When the number of vacancies decreases below the percolation threshold, $n_p = 0.31$, the conductivity of $Li_{0.5-x}Na_xLa_{0.5}TiO_3$ perovskites decreases by six orders of magnitude, from 10^{-3} to 10^{-10} S/cm [5]. In the case of the $Li_yLa_{2/3-y/3}TiO_3$ series, where $n>0.31$, this situation is not reached. These considerations are illustrated in figure 3a, where we have plotted room temperature dc-conductivity data for both the $Li_yLa_{2/3-y/3}TiO_3$ and the $Li_{0.5-x}Na_xLa_{0.5}TiO_3$ series as a function of *n*. The results obtained confirm the important role played by the number of vacant A-sites on the Li conductivity of these perovskites. Above the percolation threshold, the number of conducting paths is important; however, below the percolation threshold only local motions are possible (see figure 3b).

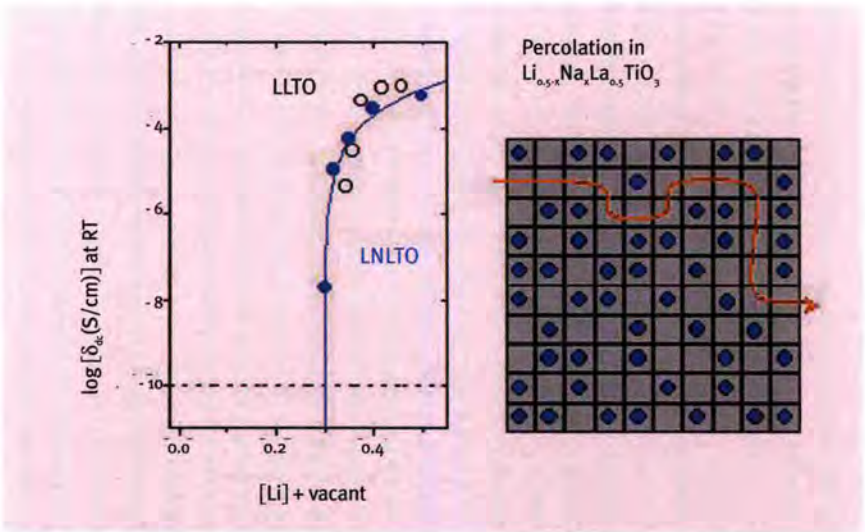

Figure 3: a) Room temperature dc conductivity of $Li_{0.5-x}Na_xLa_{0.5}TiO_3$ (blue circles) and $Li_yLa_{2/3-y/3}TiO_3$ (open circles) versus lithium plus vacant A-sites. RT dc-conductivity values are $<10^{-10}$ S/cm (our experimental resolution) for samples with n<0.3 b) Schematic illustration of lithium diffusion paths near the percolation threshold.

REFERENCES

[1] J. Ibarra, A. Varez, C. León, J. Santamaría, L.M. Torres-Martinez, J. Sanz, Solid State Ionics 134 (2000) 219

[2] J. Sanz, J.A. Alonso, A. Varez and M.T. Fernandez-Diaz, J. Chem. Soc. Dalton Trans. (2002) 1406

[3] Y. Inaguma, T. Katsumata, M. Itoh, Y. Morii, J. Solid State Chem. 166 (2002) 67

[4] J.A. Alonso, J. Sanz, J. Santamaría, C. León, A. Varez and M.T. Fernandez-Diaz, Angew. Chem. Int. Ed. 3 (2000) 619

[5] A. Rivera, C. León, J. Santamaría, A. Varez, O. V'yunov, A.G. Belous, J.A. Alonso and J. Sanz, Chem. Mater. 14 (2002) 5148

[6] Y. Inaguma, M. Itoh, Solid State Ionics 86 (1996) 257

Phase separation *in the manganite system* $CaMn_7O_{12}$

R. Przeniosło
(University of Warsaw and ILL)
I. Sosnowska
(University of Warsaw)
E. Suard and A. Hewat (ILL)
A.N. Fitch (ESRF)

The structural phase transition in $CaMn_7O_{12}$ has been investigated by using high resolution neutron powder diffraction. The measurements show a phase coexistence phenomenon between 410 K and 448 K, where two different crystallographic phases coexist in the material. The first, low temperature phase, is trigonal and it has charge ordering of the Mn^{3+} and Mn^{4+} ions, while the second, high temperature phase, is cubic and charge delocalized. The volume fraction of the high temperature phase increases with temperature from zero at 400 K up to 100% about 460 K. In the phase separation region both phases are built of domains with a size of at least 150 nm.

One of the most interesting phenomena observed in manganite perovskite systems is the so-called phase separation phenomenon. The competition of the electronic and lattice degrees of freedom can lead to the formation of sub-micrometer regions with different crystallographic structures in the lattice. Phase separation has been observed in several manganite oxides [1].

The unit cell of the high temperature crystal structure of $CaMn_7O_{12}$ is shown in figure 1. The low temperature phase is trigonal and it corresponds to a distortion of the cubic structure shown in figure 1. The unit cell is compressed along one of the <111> cube diagonals and the angle between the former cubic axis, called thereafter the pseudocubic angle, becomes larger than 90 deg. In the case of $CaMn_7O_{12}$ the pseudo-cubic angle is about 90.33 deg [2].

The neutron powder diffraction measurements have been performed on the high resolution diffractometer D2B, ILL Grenoble, operating at a wavelength of 1.594 Å [2]. Complementary studies were performed by taking advantage of the high resolution synchrotron radiation diffraction beamline BM-16 at ESRF. The advantage of SR diffraction is higher resolution and hence greater sensitivity to domain sizes. On the other hand neutron diffraction is more sensitive to the positions of the oxygen atoms. Representative parts of the neutron diffraction patterns are shown in figure 2. One can see that the peaks due to both the trigonal and cubic phases coexist in a large temperature interval between 418 K and 448 K. The Bragg peaks due to both phases are clearly separated, and from the width of the diffraction peaks one can estimate that the correlation length of both phases is at least 150 nm.

The concentration of the high-temperature phase is shown in figure 3a. Starting from zero at 400 K, the concentration increases linearly with temperature, approaching 50 % near 440 K. Then it starts to increase faster reaching finally 100 % at 460 K. This result should be compared with resistivity measurements of $CaMn_7O_{12}$ [3], which show a sharp decrease of one order of magnitude between 440 K and 450 K.

The unit cell volumes of both phases are shown in figure 3b and one can see that the unit-cell volume of the conducting high temperature phase is smaller that the corresponding unit-cell volume of the insulating low temperature phase. Since the number of ions is the same in both unit cells, the low temperature insulating phase has a smaller density. It is also interesting to note that the pseudocubic angle, shown in figure 3c has a minimum at about 440 K, i.e. when the concentration of the high temperature phase becomes larger than 50 %. This implies that

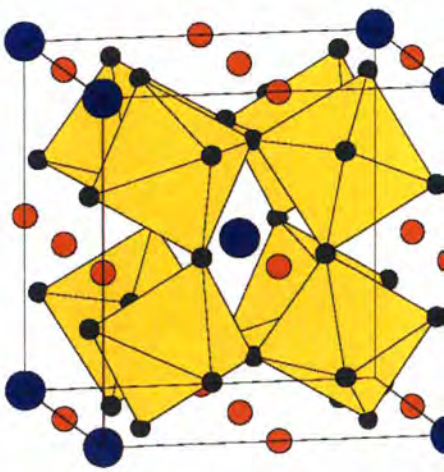

Figure 1: Schematic representation of the unit cell of the high temperature cubic phase of $CaMn_7O_{12}$. The Ca,Mn and O ions are shown as blue, red and grey circles, respectively. The MnO_6 octahedra of the 6 oxygen ions around each Mn ion are shown in yellow.

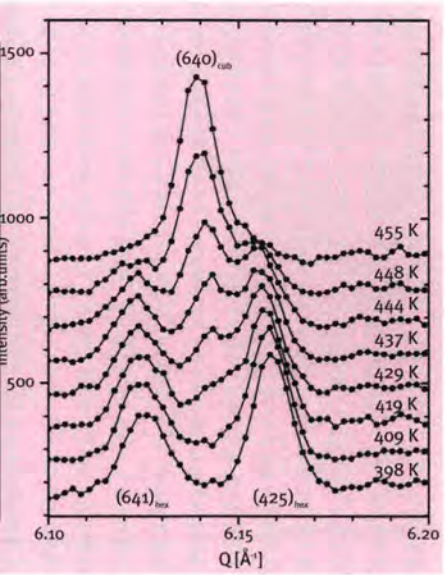

Figure 2: Representative parts of the neutron powder diffraction patterns of $CaMn_7O_{12}$ measured at the phase separation temperatures. Solid circles represent measured data, and the lines are shown to guide the eye. Q is the length of the scattering vector $Q=(4\ \pi/\lambda)\ \sin\theta$, where the scattering angle is 2θ. The patterns measured at different temperatures are vertically shifted for clarity.

the structural properties of the low temperature phase start to change when it becomes a minority phase.

The concentration of the high temperature phase (figure 3a) as well as the unit cell volumes (figure 3b) and the value of the pseudocubic angle (figure 3c), determined on either warming or cooling, are slightly different which shows that the transition is of first order with a hysteresis of a few degrees Kelvin. The present studies clearly show that the electronic properties of the Mn ions in both phases are different. It can be concluded that in $CaMn_7O_{12}$ it is more favourable to maintain large clusters of the high temperature phase growing in a matrix of low temperature phase, rather than to continuously change from one to the other structure.

Acknowledgements

This work was supported by the European Community Marie Curie Fellowship performed at ILL by one of us (RP) under contract HPMF-CT-2000-01002. It was partially supported by the Committee for Scientific Research (Poland).

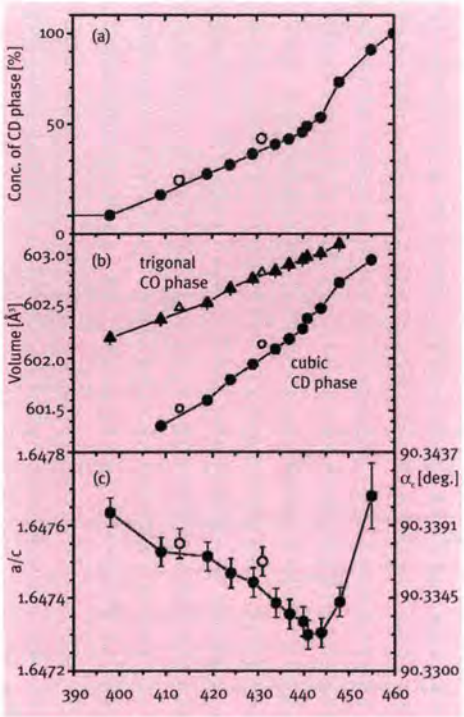

Figure 3: Temperature dependence of (a) the high temperature phase concentration, and (b) the normalized unit cell volumes of the trigonal low temperature phase (triangles) and the cubic high temperature phase (circles). The values of the pseudocubic angle are shown in (c). The full symbols show values measured with warming between the temperature steps, the open symbols were measured with cooling.

REFERENCES

[1] M. Uehara, S. Mori, C.H. Chen and S.-W. Cheong, Nature 399 (1999) 560
[2] R. Przeniosło, I. Sosnowska, E. Suard, A. Hewat and A.N. Fitch, J. Phys. Condens. Matter 14 (2002) 5747
[3] I.O. Troyanchuk and A.N. Chobot Crystallography Reports 42 (1997) 983

Discrimination between $L2_1$ and DO_3 structures in metallic alloys

J. I. Pérez-Landazábal, V. Recarte and C. Gómez-Polo (Public University of Navarra, Pamplona)
J. Campo (ILL)

Powder neutron diffraction and Rietveld analysis in texture free samples allow us to distinguish in a simple way between different possible crystallographic structures. This procedure is applied to two different alloy systems of high technological interest, the high temperature phase of Cu-Al-Ni shape memory alloys and the FeCoSiBCuNb nanocrystalline system. In both cases, the discrimination between DO_3 and $L2_1$ structures has allowed to determine the actual crystalline phases that control the basic characteristics of these systems.

DO_3 and $L2_1$ are two similar cubic structures with the same space group. Both structures can be described by four f_i, i=1 to 4 interpenetrating face centred cubic sublattices. In the DO_3 structure there are only two different occupancy probabilities, one for the f_1 sublattice and the other for the $f_{2,3,4}$ sublattices respectively (see figure 1a). In contrast, the $L2_1$ structure shows three different occupancies for the sublattices f_1, f_2 and $f_{3,4}$ respectively (see figure 1b). Neutron powder diffraction is a powerful technique to distinguish these structures by means of the Rietveld method. This technique has been applied to Cu-Al-Ni shape memory alloys (SMA) (24-27 at% Al and 3-6 at%Ni) and nanocrystalline $Fe_{73.5-x}Co_xSi_{13.5}B_9Cu_1Nb_3$ magnetic alloys (NMA). These are two alloy systems of very different technological interest [1,2] which present phases associated to this kind of order. In both cases, it is not possible to distinguish between both structures by X-ray diffraction since the atoms involved in the ordered phases (Cu - Ni and Fe - Co) have almost the same x-ray atomic structure factors.

The type of order of the high temperature phase controls the characteristics of the martensitic transformation in Cu-Al-Ni SMA. On the other hand, the order of the crystalline precipitates in nanocrystalline $Fe_{73.5-x}Co_xSi_{13.5}B_9Cu_1Nb_3$ alloys determines the macroscopic magnetic properties of the alloy. In both cases, the discrimination between both DO_3 and $L2_1$ ordering is required in order to understand the mechanisms involved in the behaviour of these alloys. Neutron powder diffraction (D20 for SMA and D1B for NMA) measurements have been performed at room temperature in a

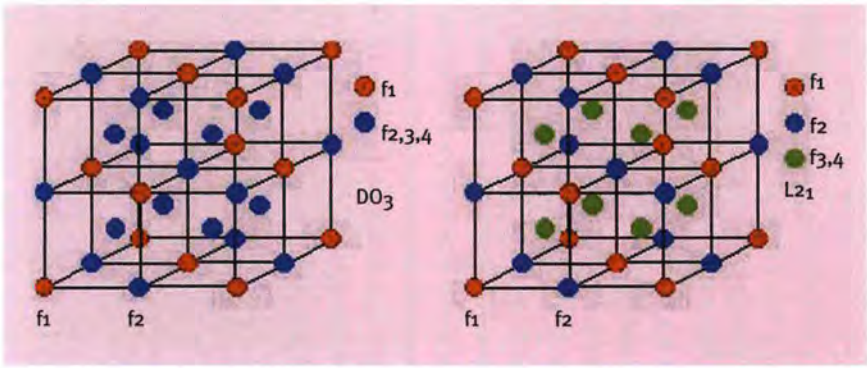

Figure 1. DO_3 and $L2_1$ crystallographic structures.

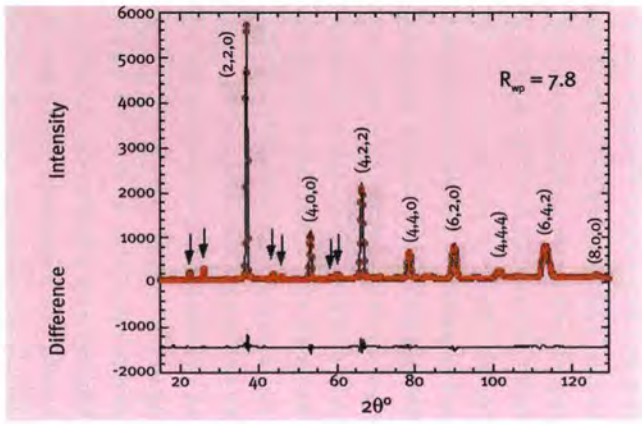

Figure 2. Experimentally measured neutron diffraction pattern (empty dots), the fitted pattern (full line) assuming an $L2_1$ structure, and the difference between the measured and calculated profiles (bottom of the diagram). Polycrystalline samples obtained from powder after Hot Isostatic Pressing are texture free thus forming ideal powders for diffraction studies.

Cu-27.4 Al-3.6 Ni at.% ordered alloy and in two $Fe_{73.5-x}Co_xSi_{13.5}B_9Cu_1Nb_3$ ($x = 0$ and 45) alloys.

Figure 2 shows the powder diffraction pattern corresponding to the SMA (empty dots), the Rietveld fitting, assuming a $L2_1$ crystallographic structure and the standard differences between both measured and calculated profiles (solid line at the bottom of the diagram). The experimental spectrum was also fitted to a DO_3 structure in order to compare with the $L2_1$ order. The occurrence of the DO_3 or $L2_1$ structures can be distinguished through the relative intensity of the smallest superlattice diffraction peaks (indicated by arrows in figure 2). As figure 3 shows, the best fit is obtained assuming an $L2_1$ structure where the Ni atoms are located on the $f_{3,4}$ sublattices as nearest neighbours to Al atoms [3]. The type of order changes the nature of the martensitic phase and the characteristic transformation temperatures.

On the other hand, figure 4 shows the room temperature neutron diffraction patterns for nanocrystalline $Fe_{73.5-x}Co_xSi_{13.5}B_9Cu_1Nb_3$ alloys with $x = 0$ (a) and $x = 45$ (b). Firstly, the Fe-based sample ($x = 0$) is characterised by the precipitation of Fe_3Si with the DO_3 superstructure as shown in figure 4a. The inclusion of Co atoms changes the structure of the precipitated crystalline phase to an $L2_1$ structure (figure 4b), where the Co atoms are located on the $f_{3,4}$ sublattices as nearest neighbours to Si atoms. Again, the difference between the DO_3 and $L2_1$ phases is directly reflected in the relative intensities of the (111) and (200) superlattice reflections (see figures 4a and 4b). The inclusion of Co atoms in these positions increases the magnetic moment of the precipitated crystalline phase with respect to the Fe base sample, and drastically changes the high temperature behaviour of the alloy [4]. In summary, the difference in the neutron scattering factors for Ni-Cu and Fe-Co atoms promotes differences in reflection intensities depending on the kind of order (DO_3 or $L2_1$). The analysis of neutron powder diffraction patterns by the Rietveld method allows us to elucidate the actual order in the crystalline phases that determine the macroscopic behaviour of these alloys.

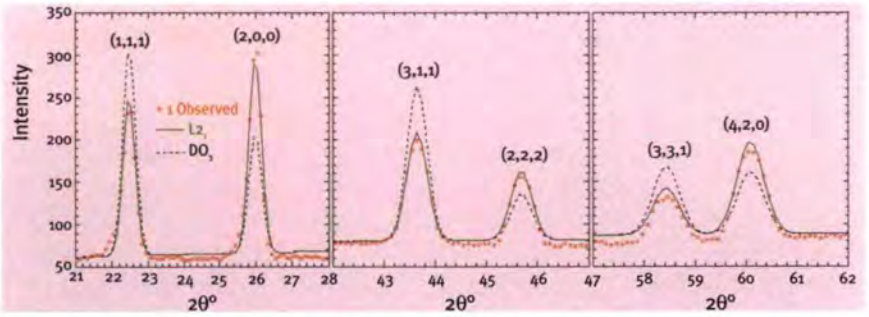

Figure 3. Experimental measured data (empty dots), the fitted pattern assuming an $L2_1$ structure (full line) or a DO_3 structure (dashed line).

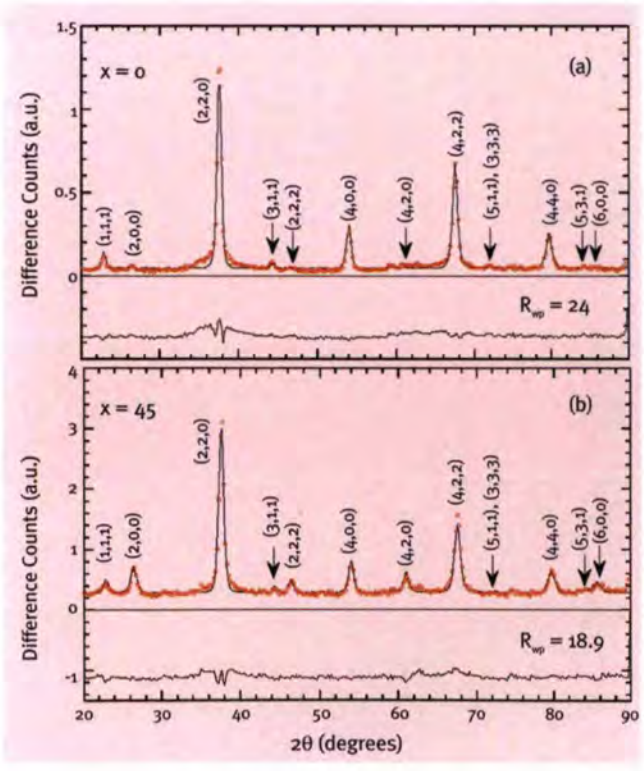

Figure 4. Room temperature neutron diffraction patterns for nanocrystalline $Fe_{73.5-x}Co_xSi_{13.5}B_9Cu_1Nb_3$ samples for (a) $x = 0$ and (b) $x = 45$. The solid line represents the Rietveld refinement. The standard difference between the measured and calculated profiles is shown at the bottom of the diagram. Randomly oriented nanocrystals precipitated in an amorphous matrix are texture free.

Acknowledgement

This work has been supported by the Spanish "Ministerio de Ciencia y Tecnología".

REFERENCES

[1] M.V. Ghandhi and B.S. Thompson, Smart Materials and Structures, Chapman and Hall, London, UK, (1992)

[2] G. Herzer, J. Magn. Magn. Mater. 112 (1992) 258

[3] J.I. Pérez-Landazábal, V. Recarte, R.B. Pérez-Sáez, M.L. Nó, J. Campo, J. San Juan, Appl. Phys. Lett., 81(10) (2002) 1794

[4] C. Gómez-Polo, J.I. Pérez-Landazábal, V. Recarte, J. Campo, P. Marín, M. López, A. Hernando, M. Vázquez, Phys. Rev. B 66 (2002) 12401

No stress!

Supriyo Ganguly – Department of Materials Engineering. Oxford – studying residual stresses in Welded Aircraft Structures.

Diana Sanchez and José Antonio Alonso (Instituto de Ciencia de Materiales de Madrid, C.S.I.C.) during their experiment on D20.

Thomas Ferger (left) and Andreas Hillenbach, two motivated young men working in the tomography area.

Penetration power is our strength! (Thilo Pirling, inspecting the whirlpool option for the new strain imager, SALSA).

John Stride, College 7 Secretary

Materials science

The study of composition and structure on the properties of materials is one definition of materials science. An interdisciplinary science, it combines aspects of physics, chemistry, metallurgy and engineering to understand real-world problems of real-world materials. The broad range of neutron scattering techniques available at the ILL, yields a range of information in this diverse subject area and many of the experiments have a close bearing on industry and engineering.

Since the discovery of high temperature superconductivity (HTSC) in cuprate systems almost 20 years ago, neutron scattering has contributed much to the understanding of the effect. The ILL has maintained its position at the forefront of this research, which is demonstrated by two contributions to this year's annual report. The first, follows the recent discovery that the standard laboratory chemical MgB_2 displays SC up to ~40 K. The high availability and low cost of this material make every day SC devices more feasible – albeit below –230°C! Its structural simplicity also makes it an ideal model for more fundamental studies into HTSC. Schober *et al* have shown that SC decreases with increasing Al-doping, which they rationalise as being due to a break- down of the Born-Oppenheimer approximation. In essence, the HTSC of MgB_2 is due to the high frequency vibrations of the boron atoms, observed here in the densities of states measured on IN6. The second example of cutting-edge HTSC research at ILL is that of Mesot *et al*. The phase diagram of type-II superconductors is well understood with a vortex lattice (VL) present between two critical fields at any given temperature up to T_c. The VL is effectively the confinement of the magnetic field leaking into the superconductor and forms a hexagonal lattice in isotropic systems. By performing SANS measurements in applied fields on a single crystal of $La_{2-x}Sr_xCuO_{4+\delta}$, $x = 0.17$, on D22, Mesot *et al* found that the VL undergoes a phase change into a square lattice at relatively low fields. This field-induced transition implies anisotropic coupling of the VL, although at this stage they are unable to ascertain its exact nature.

The observation, a little over 10 years ago, of low-temperature magnetic phases in doped fullerenes prompted research efforts to understand the mechanisms behind the magnetic exchange interactions. Despite many attempts, no magnetic structure determination has been achieved for any of the alkali-metal salts studied to date. Using D20, Prassides *et al* have managed to obtain the first magnetic structure of a C_{60} salt, Eu_6C_{60}. The system orders ferromagnetically in a *bcc* lattice, with the moment on each Eu being close to the free ion value for Eu^{2+}, invalidating reports of mixed Eu-valency. In addition, the short Eu-C distances suggest that FM exchange is mediated by interactions between the Eu^{2+} 4*f* electrons and the C_{60} π orbitals.

The drive toward higher density storage media has focussed attention on magnetic nanoparticles. Dewhurst *et al* have used the SANS technique on D11 to study self-assembled FePt nanoparticles. These are deposited onto Si substrates layer-by-layer and then be annealed at elevated temperatures to obtain highly anisotropic magnetic phases. By studying samples covering a range of annealing conditions, they found that at temperatures >500°C, the particles cluster into larger agglomerates. Hence, for applications requiring monodisperse, magnetically anisotropic nanoparticles, very careful attention must be paid to the annealing conditions.

Another method of material preparation which is of great industrial relevance is Shot Peening, which hardens surfaces by inducing residual compressive forces below the surface. Surface hardness is of prime importance for mechanical components which undergo high operational cyclic loads, such as fan blades in aero-engines. A new technique in this area is Laser Shock Peening (LSP), which induces stresses much deeper into the material, rendering the surface less susceptible to cracking. In a study very much of interest to us all, Evans *et al* have performed residual strain measurements on D1A into the application of LSP in the production of fan blades. In essence this was a study of a processing problem: which of two production methods provides the best commercial option? The two methods were found to result in equivalent degrees of surface hardening – fan blade safety to you and I – making the cheaper (and faster) of the two methods advantageous.

In an ingenious experiment, Bellissent *et al* were able to peer at deeply undercooled metallic liquids of several pure transition metals. This experiment required beads of the liquid metal to be magnetically suspended to prevent nucleation at container walls. The high count rate available on D20, made it possible to produce and measure these metastable states *in situ*. An icosahedral short-range order was found to be present in all of the undercooled melts, independent of the material or the structure of the solid phase. This had been previously postulated, on purely topological grounds.

Finally, Cuello *et al* have used chemical isomerism to look for topological effects on the intermediate-range ordering, i.e. next nearest neighbours and beyond, in glass forming propanol. Using D4, they have shown a scaling behaviour in 1- and 2-propanol and ethanol, indicating that intermediate-range ordering can be understood by the packing of spherical moieties based upon the molecules.

The range of materials science research at the ILL is broad, making full use of the wide suite of available ILL instruments to investigate the diverse structural, magnetic and dynamic properties of materials. This selection of articles is a small glimpse of the materials-related research currently being performed at the ILL.

Laser Shock Peening
for aerospace Ti-6Al-4V alloy: a residual stress study

A.D. Evans and G. Bruno
(ILL and University of Manchester)
A. King and P.J. Withers
(University of Manchester)
T. Pirling (ILL)

In aircraft flight, the large cyclic or fluctuation stresses that are generated, place great demands on specific aerospace component. These cyclic stresses, so called fatigue, are usually highest at the materials surface. Over long periods or time, these stresses can cause cracks to initiate and propagate from the surface of the material. Surface hardening is therefore a favourable procedure to improve reliability of engineering components. The conventional method of hardening surfaces is Shot Peening, which places the surface under compression down to several hundred micrometers. A very new technique is Laser Shock Peening which generates compressive stresses much deeper into the material, which will hinder crack growth for a longer period. It is very important to the manufacturer to know precisely the range, location and magnitude of the stresses generated by the process. This is important to evaluate the reliability, and helps to optimise the manufacturing process.

Laser Shock Peening (LSP) is a relatively new surface treatment for metallic materials to induce residual compressive stress fields in the near surface regions of engineering components. These stress fields can greatly improve the resistance of the material to crack initiation and propagation when the material is loaded in a cyclic way, or fatigued. Laser Shock Peening is capable of producing compressive residual stresses to a much greater depth than the conventionally used technique of shot peening. The technique involves the production of mechanical shock waves through the expansion of confined plasma. The area of the critical component that needs to be Laser Shock Peened is coated by an overlaying sacrificial material that is absorbing to laser radiation, commonly black paint or tape. Overlaying this layer is usually water, which is transparent to laser radiation but can act as a confinement medium for the plasma. The plasma is formed by the irradiation of the sacrificial layer by a pulse of a high power laser, vaporising the sacrificial material and partially ionising the vapour to a plasma. The plasma expands but is confined by the layer of water, hence the expansion causes a mechanical shock wave to be driven into the component. The pressure of the shock wave is greater than the yield strength of the material under shock conditions, plastically deforming the material to a depth where the pressure is no longer higher than the yield strength. The undeformed material attempts to restore the original shape of the surface, causing in-plane compressive residual stress fields to be set up in the near surface region of the component (see figure 2).

Laser Shock Peening has been used on the root sections of Ti-6Al-4V aerospace components to improve their fatigue performance. To insure a uniform stress state over a surface, Laser Peening spots must be overlaid; hence a pattern of spots is generated. Two patterns were studied and are shown in figure 3. Since these patterns are applied to curved shaped components, a change of the vertical position requires a time consuming alteration of the angle of laser. This is undesirable,

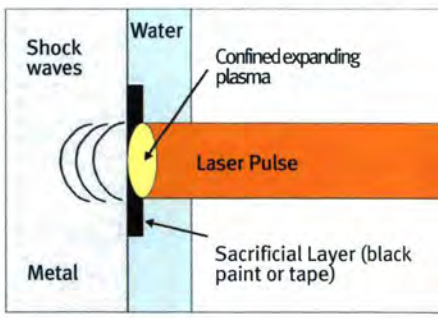

Figures 2 and 3: Schematic of the Laser Shock Peening process and two Laser Shock Peening patterns studied.

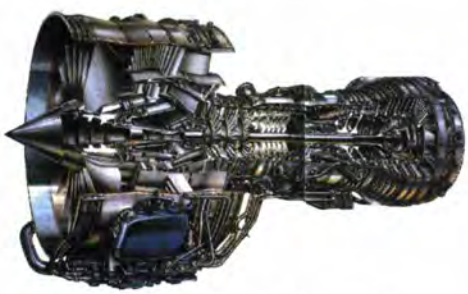

Figure 1: Aeroplane turbine engine.

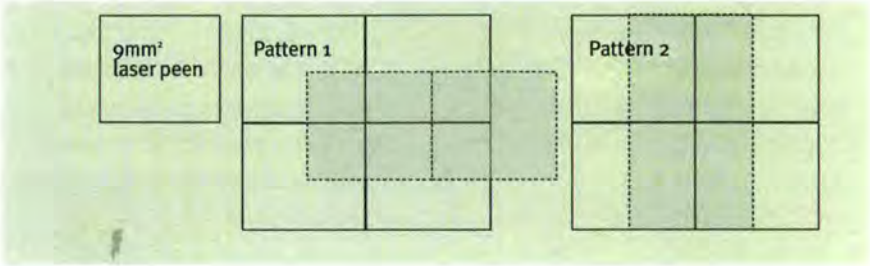

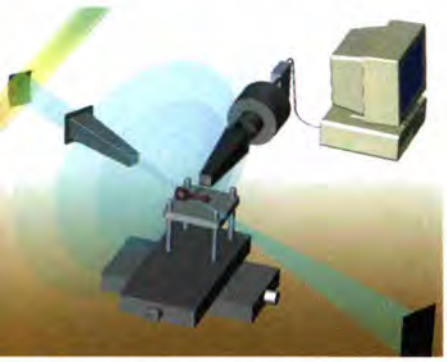

Figure 4: Schematic of experimental arrangement of collimators.

hence pattern 2 which requires a third less changes to the vertical position would be the preferable pattern to use. But the stress state must be the same as for pattern 1 before it is valid to safely use this pattern.

The residual strains were determined in a Ti-6Al-4V plate mockup which had been Laser Shock Peened with the two peening patterns adjacent to each other in the central region of one side of the plate. Residual strain profiles as a function of depth in three perpendicular directions were measured (two in-plane directions parallel to the plates surface and the out of plane direction, normal to the plates surface) in both the peening patterns. The measurements have been performed using the strain scanning option of the D1A powder diffractometer. Since stresses very close to the surface are to be measured, the instrument must provide very high lateral resolution. This is possible at the D1A-diffractometer using two radial collimators for the gauge volume definition. The advantages of this set-up are the very precise definition of the gauge dimensions and the very low surface error [1,2]. This enabled us to perform measurements down to 25 µm to the surface. The scattering geometry was of 84° (scattering angle) giving a relatively square gauge volume suitable for high spatially resolved strain scanning.

The strain was measured through the whole thickness of the plate, in addition the peak width was determined which is only possible with the setup of a secondary collimator as found on D1A. Figure 5 shows how the peak width increases towards the surface which indicates that this region is plastically deformed. This shows how compressive residual stresses are introduced by Laser shock peening. Stress was then calculated for the two peening patterns using stress and moment balance criteria to correct for d0, the unstrained lattice parameter (figure 5).

The neutron diffraction data was correlated to X-ray diffraction measurements made at the very suface using laboratory X-rays at the University of Manchester. The increased peak width indicates the plastically deformed region. Where compressive stresses are introduced they are very similar and exhibit the same distinctive characteristics. This means that either peening pattern can be applied for manufacturing. Their characteristics are: firstly, the maximum compressive residual stress of approximately –800MPa occurs at the surface and the material remains in compression to approximately 1 mm in depth which is approximately 10 times deeper than can be achieved with the conventional technique of shot peening. The deeper compressive stresses mean that longer cracks can be retarded from growing, hence improving the resistance to fatigue cracking of the material. Secondly, the maximum tensile residual stress of 200MPa is located 2 mm beneath the surface, which is very important to stress engineers, since this may be a location of subsurface cracking if the residual stress plus applied stress is greater than the strength of the material at this location.

The measurements show that the neutron strain scanning method is capable of providing stress profiles non-destructively with high lateral resolution. Additionally the measuring geometry around 90° is advantageous for many applications. In conclusion, it can be remarked that Laser Shock Peening is an effective technique to generate favourable compressive residual stresses in the near surface region of Ti-6Al-4V alloys. These stresses are expected to improve the materials resistance to fatigue cracking, allowing longer operating lifetimes of Laser Shock Peened components. In addition, the stress state within pattern 1 is almost identical to pattern 2 which validates the use of pattern 2 for Laser Shock Peen components. This will allow parts to be manufactured faster and hence at lower cost to the manufacturer. And the air passenger should feel safer at the same time.

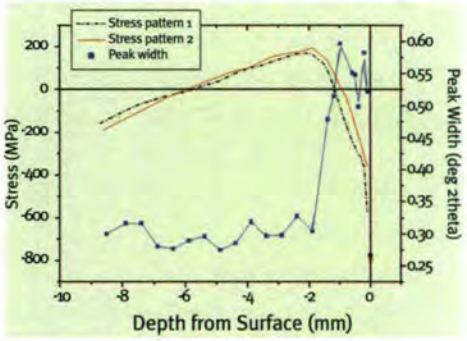

Figure 5: The residual stress in one in-plane direction is plotted against position beneath the materials surface for both peening patterns. The neutron data is shown as a solid line and can be perfectly extrapolated to the surface X-ray diffraction measurements. The peak width as a function of depth shows that where the residual stress is compressive at the surface, the peak width is the highest corresponding to plastic deformation of the material. The error in the stress determination is from +/- 25MPa in the bulk to +/- 50MPa near the surface.

REFERENCES

[1] C.S. Montross, T. Wei, L. Ye, G. Clark, Y.M. Mai, 'Laser shock processing and its effects on microstructure and properties of metal alloys : a review', International Journal of Fatigue, Volume 24, Issue 10 (2002) 1021-1036

[2] T. Pirling, Neutron strain scanning at interfaces: Optimised beam optics to reduce the surface effect; Materials Science Forum, 347-349 (2000) 206-211

[3] T. Pirling, A new high precision strain scanner at the ILL, Materials Science Forum Vols. 321-324 (2000) 206-211

Chemical details
in the microscopic structure and dynamics of glasses

G.J. Cuello, M.A. González (ILL)
C. Talón (Universidad Autónoma de Madrid)
F.J. Bermejo (Univ. Basque Country and Consejo Superior de Investigaciones Científicas, Madrid)
C. Cabrillo (Consejo Superior de Investigaciones Científicas, Madrid)

We have studied the effects of a minor chemical-isomeric modification on the microscopic structure and low-frequency dynamics of glassy propanol. Our results show that intermolecular orientational correlations explain the observed changes in the dynamics and also play a prominent role on the short-range structure of these glasses. In contrast, the intermediate range order in these materials is revealed as a purely geometric effect, accountable in terms of packing of effectively spherical entities.

The low-temperature properties of glasses and disordered materials constitute the most clear-cut evidence of universal behaviour in disordered matter. Tunnelling motions of particles between energetically close potential minima separated by a potential well, account for the specific heat at temperatures below 1 K. The description of the experimental observations is still confined within the realm of phenomenology, exception made of a few cases such as the mixed alkali-halide crystals, where the tunnelling entities are amenable to a fully microscopic treatment. For moderately low temperatures ($1 < T/K < 10–20$) the dynamics of disordered matter is pictured as governed by the same entities that coherently tunnel below 1 K. But above this temperature range, they are subjected to strong scattering mechanisms destroying coherence and leading to thermally activated relaxation. Such regime then persists up to temperatures comparable to those where liquid-flow effects start to be prominent, that is, the glass → liquid transition. Reasons hampering progress in describing theoretically the experimental results are the complex chemical details of many of the materials employed as test-bench for these studies. This leads to difficulties in clarifying the nature of atomic motions, i.e., in determining whether they arise from the internal dynamics of glass-particles or from interactions between intra- and intermolecular-modes, such as is known to happen in complex organic or strong glasses.

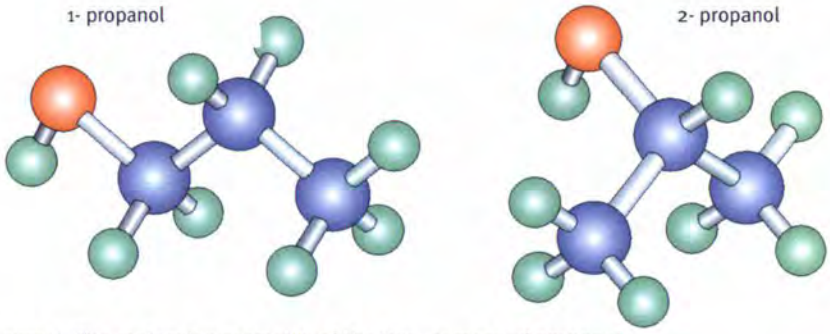

Figure 1: The molecular geometry of the two isomers of propanol.

Here we deal with a relatively simple system where we can vary the strength of inter- and intra-molecular interactions by means of a subtle chemical change. The material, propyl alcohol, presents two isomers referred to as 1-(1P) and 2-propanol (2P), which differ by the location of the OH group (figure 1). This chemical isomerism, rather than altering properties such as the number of molecular internal degrees of freedom, van der Waals volumes or electric dipole moments to any significant extent, leads to a change in the overall molecular "shape". In turn, this change is translated into rather different thermal [1], structural [2] and transport [3] properties of both compounds. It is worth pointing out that there is a shift in the melting points of the crystals from 148 K (1P) to 185 K (2P), and in the glass-transition temperatures from 98 K (1P) to 115 K (2P). With regard to the structure, we have employed such chemical difference to get a deeper insight of the nature of intermediate-range-order in amorphous matter. That is, to study the existence of spatial regularities at distances significantly beyond those separating nearest neighbours, where order results as a consequence of chemical and topological details of the particles forming the glass. By means of neutron diffraction experiments (D4-ILL) we have obtained the static structure factors for both isomers in their glassy

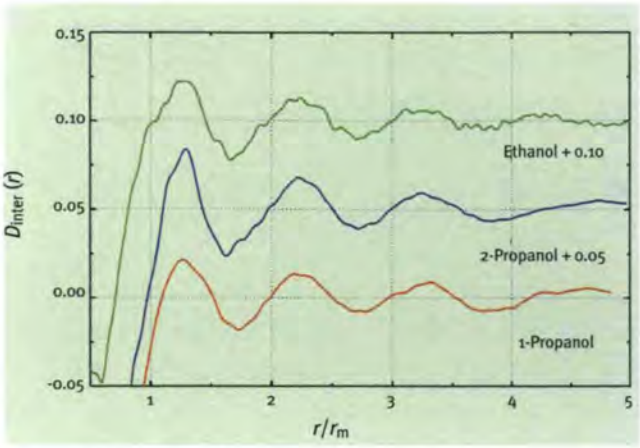

Figure 2: Intermolecular pair correlation functions.

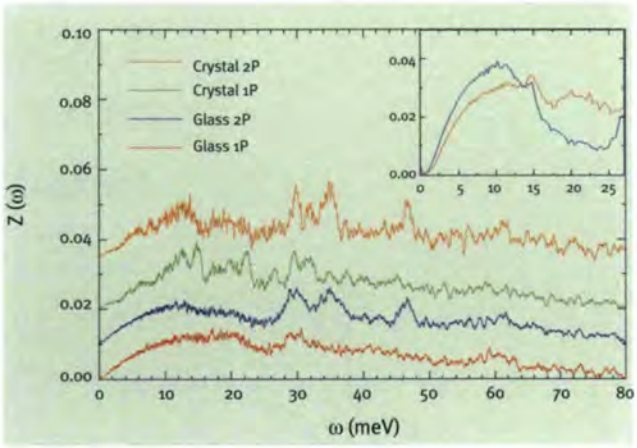

Figure 3: Densities of states (normalised to unity up to $\omega_{max} = 80$ meV) as obtained from QENS data and from IN6 data (inset and arbitrary normalisation).

and crystalline states. The first diffraction peak in $S(Q)$ of both glasses appears at $Q_p = 1.56$ Å^{-1} and 1.52 Å^{-1}, respectively. Its inverse $2\pi/Q_p$ closely matches the period of the broad oscillations in the respective total static pair correlation functions $D(r)$, providing direct evidence linking the first diffraction peak to the presence of intermediate range order. We have related the position of the first diffraction peak with the structure factor for molecular centres-of-mass - which plays a fundamental role in liquid state theory - by carrying out a scaling of distances for both isomers as well as for a smaller alcohol: ethanol. Dividing by the molecular diameter of each alcohol, taken as the position of the first intermolecular peak in $D(r)$, we remove the effects of short-range order and density. The obtained results are plotted in figure 2, showing that the intermolecular parts of the radial distribution function of the three alcohols are fully in phase. An evaluation of the strength of molecular orientational correlation was carried out by means of computer simulations. These simulations reproduce reasonably well the experimental $S(Q)$ and they allow us to study the orientational correlation functions that are not experimentally accessible, showing that orientational effects are enhanced in 2P compared to 1P. In contrast, they are far shorter-ranged if compared to packing effects that extend up to distances 3–4 times longer than orientational correlations.

Quasi- and inelastic scattering measurements (IN6-ILL, QENS-IPNS) provide a microscopic illustration to specific heat measurements and also allow us to establish a clear separation between frequency regions dominated by internal modes with those of purely intermolecular origin. The low-frequency data ($E < 10$ meV) reveal how the vibrational density of states, $Z(\omega)$, for 2P rises stronger with frequency than that for 1P, both showing a noticeable excess of low frequency modes compared to their parent crystals (figure 3). This feature relates well with their differences in the specific heat. Above 15 meV all the observed features in the experimental $Z(\omega)$'s arise as a consequence of the interaction between external (lattice) and internal (molecular) modes, the latter being the dominant contributor to the dynamics for frequencies above 25 meV relevant features is aided by the difference seen for both isomers and is also assisted by results from our simulations as well as by comparison of the frequency distributions of glasses and crystals [4]. As a result, some prominent features appearing in $Z(\omega)$ could be ascribed to CH_3 reorientation and motions of the OH moieties.

The main features of the interaction potential govern geometric arrangements involving nearest neighbours. However, our results show that changes in ordering patterns induced by isomeric effect are far from trivial. For larger distances, intermediate range order is finally understood as a purely geometric effect, accountable in terms of spherical entities. On the other hand, our dynamical results show that intermolecular orientational dynamic correlations are the most likely candidates to explain different behaviours on the dynamics of a glassy material. Finally, the assessment of their intermolecular origin solves a long-lasting controversy concerning the microscopic nature of the lowest frequency relaxation in these materials.

REFERENCES

[1] C. Talón et al., J. Non-Cryst. Solids 287 (2001) 266
[2] C. Talón et al., PRL 88 (2002) 115506
[3] F.J. Bermejo et al., to be published (2003)
[4] C. Talón et al., accepted in Chem. Phys. (2003)

Icosahedral short-range order in deeply undercooled metallic melts

T. Schenk, D. Holland-Moritz, D.M. Herlach (DLR, Köln)
V. Simonet (Laboratoire Louis Néel, Grenoble)
R. Bellissent (CEA, Grenoble)
T. Hansen (ILL)

Since the pioneering work of Turnbull [1] it has been well established that metallic liquids can be deeply undercooled below their freezing temperature provided heterogeneous nucleation on container walls is avoided. Undercooling by as much as 20% of the melting temperature, T_L, was observed for many different metals [2], indicating correspondingly high activation barriers for crystallisation. Frank [3] postulated the existence of icosahedral short-range order (ISRO) in the melt, which could explain the high solidification barriers. Experimental evidence of icosahedral SRO in the stable liquid state ($T > T_L$) and in deeply undercooled melts of pure metallic elements, is obtained here using thermal neutron scattering in combination with the electromagnetic levitation technique. The icosahedral SRO is shown to occur in the bulk metallic melt, independent of the nature of the system investigated. It increases with the degree of undercooling.

Icosahedral clusters, consisting of compact arrangements of 13 atoms, have an energy 8.4% smaller than that of clusters with dense-packed fcc or hcp structures and the same number of atoms [3]. This result holds for atomic interactions deriving from a Lennard-Jones potential. Very recent experiments using synchrotron radiation on liquid Pb at $T > T_L$, produced evidence of fivefold icosahedral symmetry in Pb clusters adsorbed onto a Si substrate [4]. This synchrotron technique is only sensitive to SRO present close to the Si surface and does not allow to probe either the bulk melt or the undercooled melt. Such measurements are however essential for studying the nucleation of the solid phase from the parent liquid state. Therefore, a neutron scattering structural study - using the combination of a new levitation device and the high throughput diffractometer D20 - has been performed at temperatures above and below the bulk melting temperature, for several pure transition metals. The metallic elements were chosen such that they form bcc (Zr), fcc (Ni) or both (Fe) structures in the solid state, in order to test the influence of the crystalline solid structure on the SRO in the liquid. Electromagnetic levitation was applied to undercool liquids for extended periods of time, as required for diffraction experiments. The levitation method produces a freely suspended liquid drop, about a centimetre in size, which can be deeply undercooled since heterogeneous nucleation on container walls can thus be avoided. In spite of the limited lifetime of the metastable undercooled state, we were able to obtain accurate diffraction diagrams on deeply undercooled melts. The structure factors for the different melts were measured at several temperatures above T_L in the stable regime and below T_L in the deeply undercooled regime: $\Delta T = T_L - T = 140$ K for Fe and 290 K for Ni and Zr [5]. This high degree of relative undercooling ($\Delta T / T_L \approx 17\%$ in the case of Ni) should allow one to access the structural changes occurring in the liquid. The experimental S(Q) curves are presented in figure 1. A shoulder on the right-hand side of the second oscillation is obser-

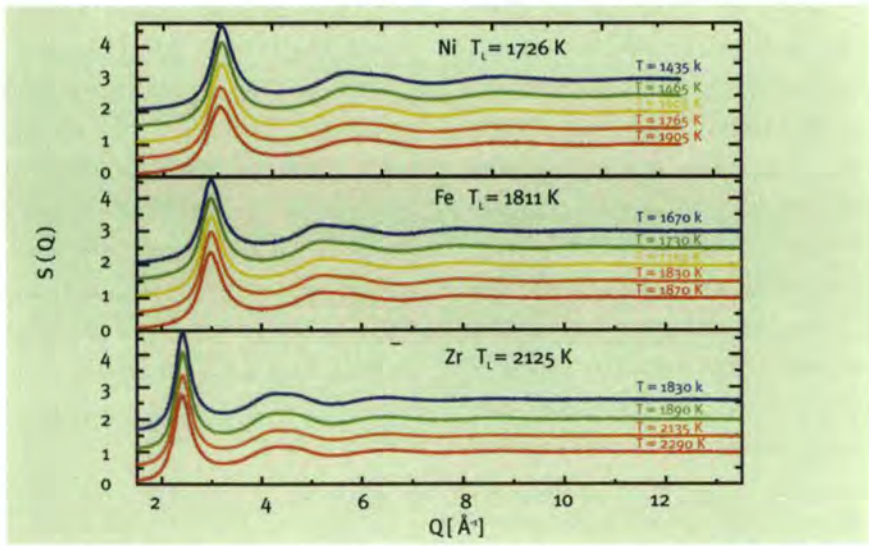

Figure 1: Structure factors of liquid transition metal above the melting point and in the undercooled state.

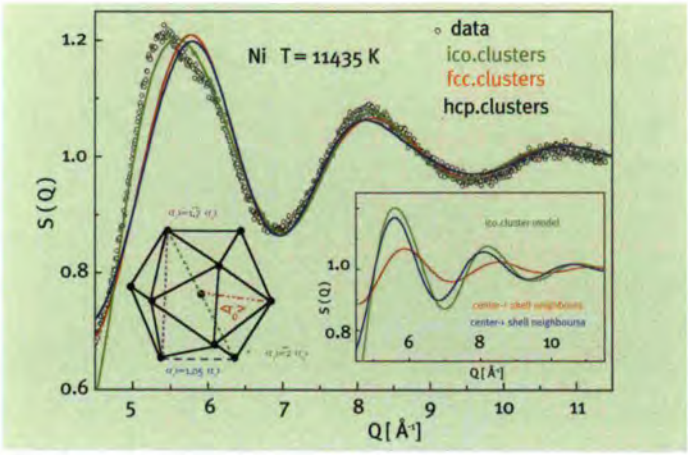

Figure 2: Cluster model for the high Q part of the undercooled Ni structure factor.

ved on all curves. This is the first time such a clear shoulder is observed in structure factors of monoatomic liquids. It has been identified as a signature of ISRO, based on the theoretical work of Sachdev and Nelson [6]. The same feature has been recently evidenced in quasicrystal-forming alloy melts [7].

To obtain further information concerning the SRO in the melt, the high Q part of S(Q) was compared to the calculated structure factor of isolated clusters. The simulation method is described in detail in [7]. Only two fitting variables are required to model the relevant cluster geometries: bcc, fcc, hcp and icosahedral (ico): the shortest mean intracluster atomic distance, $<r_0>$, and its mean thermal fluctuation amplitude $<\delta r_0^2>$, which determines the Debye-Waller factor, $\exp(-<\delta r_0^2>/3)$. All larger mean intracluster distances, $<r_i>$, and their thermal amplitudes $<\delta r_i^2>$ can then be computed. A third parameter in the simulation is the concentration of cluster atoms in the liquid. Note that the large Q part of S(Q) is determined by the SRO only, the contribution from larger interatomic distances being damped by thermal motions. The results for Ni in the undercooled regime at T = 1435 K are presented in figure 2 together with the measured S(Q) at large Q. If a bcc-, fcc- or hcp-like cluster structure is assumed, neither the position nor the shape of the second oscillation of S(Q) are reproduced, whereas for the icosahedral cluster a significantly better agreement is achieved. This can be understood by examining the individual contributions to S(Q) of each interatomic distance within these clusters [cf. the right inset in figure 2]. Let r_0 and r_1 be the nearest neighbour distances from center to shell and on the shell, respectively, for a given cluster. These two distances differ by about 5% for an icosahedron [cf. the left inset in figure 2], while being identical in fcc and hcp clusters. As the contributions from nearest neighbour distances dominate the total simulation, the calculated S(Q) can better reproduce the large oscillation at about 5.5 $Å^{-1}$ (figure 2) and the presence of a characteristic shoulder on the right-hand side of this oscillation (observed as an asymmetry in the calculated curve). The better fit obtained with the icosahedral cluster gives evidence for the presence of ISRO in all monoatomic liquids.

The SRO of Ni, Zr, and Fe metallic melts was investigated by neutron scattering in a large temperature range including the deeply undercooled metastable state. From the simulation of the measured structure factor, ISRO is evidenced in all these bulk metallic liquids independently of the structure of the nucleating solid phases at all studied temperatures. The ISRO becomes more pronounced with decreasing T. The present work provides an unambiguous experimental proof of the early conjecture of Frank [3], originally based on arguments of topological ordering only.

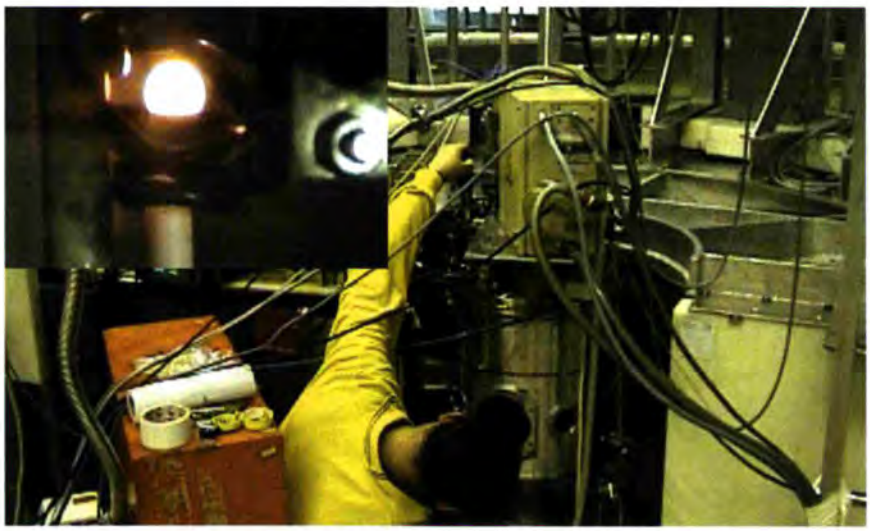

Photo 1: Levitation furnace set-up on D20. Inset shows up the liquid droplet.

REFERENCES

[1] D. Turnbull, J. Appl. Phys. 21 (1950) 1022
[2] D. Holland-Moritz, D. M. Herlach and K. Urban, Phys. Rev. Lett. 71 (1993) 1196
[3] F. C. Frank, Proc. R. Soc. London A 21, (1952) 43
[4] H. Reichert, O. Klein, H. Dosch, M. Denk, V. Honkimaki, T. Lippmann and G. Reiter, Nature (London) 408 (2000) 839
[5] T. Schenk, D. Holland-Moritz, V. Simonet, R. Bellissent and D. M. Herlach, Phys.Rev. Lett. 89 (2002) 075507
[6] S. Sachdev and D. R. Nelson, Phys. Rev. Lett. 53 (1984) 1947
[7] V. Simonet, F. Hippert, M. Audier and R. Bellissent, Phys. Rev. B 65 (2002) 024203

Magnetic structure of Eu_6C_{60}: a molecular magnetic material based on C_{60}

I. Margiolaki and K. Prassides
(University of Sussex)
S. Margadonna
(University of Cambridge)
T. Hansen (ILL)
K. Ishii and H. Suematsu
(University of Tokyo)

The powder neutron diffraction technique was used for the direct observation of magnetic scattering below a Curie temperature of ~14 K in the fullerene-based molecular ferromagnet, Eu_6C_{60}. Europium is in the divalent state with a magnetic moment of 7.1(3) μ_B per atom and the configurational symmetry of the magnetic structure is body-centred cubic. Close contacts between Eu^{2+} and neighbouring C_{60} units provide the signature of orbital hybridisation, which can account for the conducting and magnetic properties of the material.

A remarkable discovery in fullerene chemistry has been the reaction of C_{60} with the strong organic donor TDAE to afford a ferromagnetic solid, $(TDAE)C_{60}$ with a Curie temperature, T_c = 16 K. Antiferromagnetic ground states have been encountered in various fulleride salts, including the polymers RbC_{60} and $Na_2Rb_{0.3}Cs_{0.7}C_{60}$, and the ammoniated salt, $(NH_3)K_3C_{60}$. Despite efforts, no magnetic structure determination has been possible for any of these systems, as no magnetic Bragg scattering has been observed in neutron diffraction experiments, presumably related to the small magnetic moment per C_{60} and the details of the C_{60} magnetic form factor. On the other hand, potentially interesting magnetic molecular materials may be also formed when the metal dopants in fulleride salts carry a magnetic moment. Good candidates are rare-earth fullerides in which the lanthanide ions occupy the interstitial space between the C_{60} units in the solid state and magnetic correlations involving the unpaired 4*f* electrons could develop either through direct exchange interactions between the lanthanide 5*d*-4*f* orbitals or through π-*f* interactions modulated by C_{60}. Such an example has been recently provided by work on the phase diagram of Eu-C_{60}, which led to the isolation of the cubic fulleride, Eu_6C_{60}. This displays a transition to a ferromagnetic state near 14 K, which is accompanied by a very large negative magnetoresistance [1].

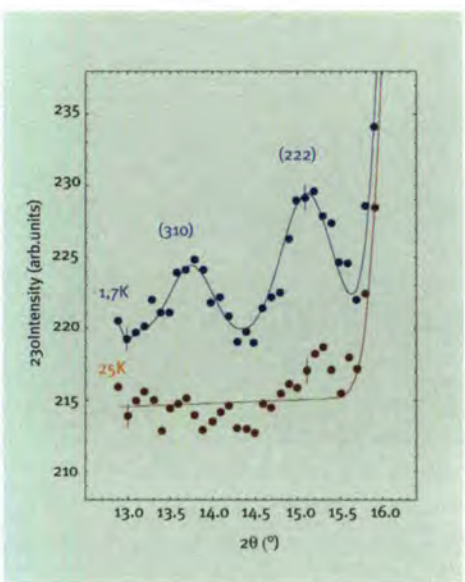

Figure 1: Selected region of the normalised powder neutron diffraction profiles (λ = 0.808 Å) of Eu_6C_{60} at 1.7 and 25 K showing the appearance of additional reflections below the Curie temperature.

In order to search for scattered intensity of magnetic origin, which provides the unambiguous signature of long-range magnetic order and allows the determination of the spin arrangement, powder neutron diffraction measurements below T_c are necessary. However, natural Eu has an extremely high absorption cross section, σ_a (4530 barns at λ = 1.798 Å) for neutrons, making such measurements challenging and possible only under optimised experimental conditions [2]. As σ_a is strongly wavelength dependent and shows a minimum at λ = 0.72 Å, powder neutron diffraction data above (25 K) and below (1.7 K) T_c were collected (22-hour runs) on D20 at λ = 0.808 Å. At this wavelength, the linear absorption coefficient, m of Eu_6C_{60} is 0.948 mm^{-1}. The sample (0.43 g) was in a double-walled vanadium cylinder (5 cm height, 4.5 cm outer diameter, 0.5 mm annular thickness) with a calculated transmission, $T = \exp(-\mu x)$ of 0.39. Inspection of the 1.7 K diffraction profile revealed significant increase in the intensities of selected nuclear peaks and the presence of additional reflections of magnetic origin not present at 25 K. The latter could be indexed on the basis of the chemical unit cell (*e.g.* as (310) and (222) in figure 1), implying that the magnetic and chemical unit cells coincide (magnetic propagation vector, κ = (000)), as expected for a ferromagnetic material. In addition, as all reflections obey *bcc* extinction rules at 1.7 K, the configurational symmetry of the magnetic structure of Eu_6C_{60} is bcc [3].

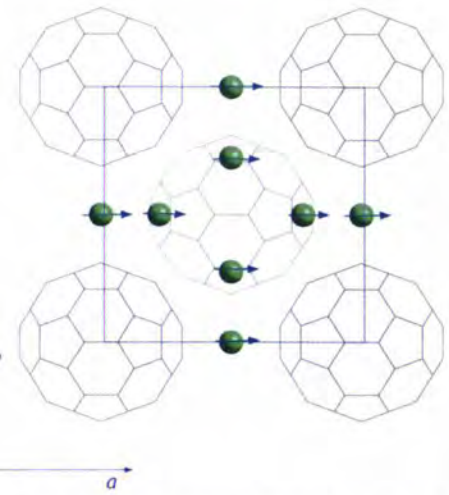

Figure 2: Unit-cell basal plane projection of the crystal and magnetic structure of body-centred cubic Eu_6C_{60} (a = 10.926 Å). The moment directions are arbitrarily drawn parallel to the a axis.

Given the paucity of magnetic reflections and the superposition of nuclear and magnetic scattering, the neutron diffraction profile at 25 K was first examined in order to obtain a starting model for the chemical structure below T_c. Rietveld analysis was initiated with a model obtained from synchrotron X-ray diffraction data collected on BM16 at the ESRF. The fit improved significantly when the geometry of the C_{60} units was relaxed and the carbon positions refined. Rietveld refinement of the neutron diffraction data at 1.7 K was performed with a two-phase model to account for the chemical and magnetic structures. The former was described with the structural model obtained at 25 K, while for the latter, the magnetic moments of the twelve Eu sites in the unit cell were aligned in the same direction. We note that for a cubic ferromagnet, the spin direction cannot be deduced for randomly oriented domains, as the same magnetic intensities result for any spin direction with respect to the crystallographic axes. The refinement proceeded smoothly resulting in a refined magnetic moment per Eu atom, $\mu_{eff} = 7.1(3)\ \mu_B$.

Several points arising from the present work are of particular interest. Figure 2 shows a perspective view of the bcc crystal and magnetic structure of Eu_6C_{60}. As the free-ion value of the magnetic moment of Eu^{2+} ($^8S_{7/2}$) is 7.94 μ_B and Eu^{3+} is non-magnetic ($^7F_0$), the magnetic moment observed at the Eu sites leads to the unambiguous conclusion that Eu is present in the divalent state in Eu_6C_{60}. This is in agreement with field-dependent magnetisation measurements at 2 K and contrasts with earlier reports of the presence of sample-dependent Eu mixed valency ($Eu^{2+}/Eu^{3+} \approx 1$ to 4). Concerning the origin of the ferromagnetic exchange interactions between Eu^{2+}, we note that the closest Eu^{2+}-Eu^{2+} distance in Eu_6C_{60} is 3.885 Å, considerably smaller than that in the antiferromagnetic graphite intercalate EuC_6 (~4.3 Å) but straddling those in ferromagnetic EuO and EuC_2 (~3.6-4.1 Å). In the latter, the FM interaction between Eu^{2+} ions is through direct exchange of nearest neighbour $5d$-$4f$ unpaired electrons and T_c scales with the Eu^{2+}-Eu^{2+} distance. However, in Eu_6C_{60}, each Eu^{2+} ion coordinates to two hexagonal and two pentagonal faces of neighbouring C_{60} anions and displays short Eu-C contacts: 2.88 and 2.90 Å to hexagon C(3) and pentagon C(1) atoms, respectively (figure 3). These are only marginally larger than the sum of the ionic radius of Eu^{2+} (1.12 Å) and the van der Waals radius of C (1.70 Å) and are suggestive of hybridisation between the $5d$ and $6s$ orbitals of Eu and the t_{1g} orbitals of C_{60}, in analogy with the isostructural and isoelectronic, Ba_6C_{60} and Sr_6C_{60}. Such orbital mixing implies that the ferromagnetic exchange interactions between the $4f$ electrons are modulated by the $\pi(C_{60})$ orbitals and provides a natural explanation for the conducting and giant magnetoresistive behaviour of Eu_6C_{60}. Namely, in the absence of hybridisation, the formal valence of C_{60} would be -12 and both the LUMO t_{1u} and the (LUMO+1) t_{1g} derived bands would be completely full, giving rise to insulating behaviour and very weak interactions between charge carriers and localised magnetic moments.

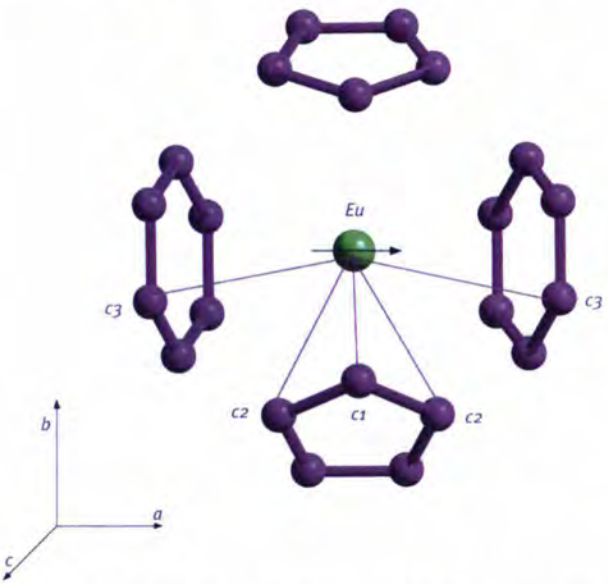

Figure 3: Coordination of Eu^{2+} and near-neighbour Eu^{2+}-C contacts in Eu_6C_{60}.

REFERENCES

[1] K. Ishii, A. Fujiwara, H. Suematsu and Y. Kubozono, Phys. Rev. B 65 (2002) 134431
[2] H. Kohlmann, F. Gingl, T. Hansen and K. Yvon, Angew. Chem. 38 (1999) 2029
[3] I. Margiolaki, S. Margadonna, K. Prassides, T. Hansen, K. Ishii and H. Suematsu, J. Am. Chem. Soc. 124 (2002) 11288

FePt magnetic nanoparticles: *a SANS study of agglomeration effects*

T. Thomson
(IBM - Almaden Research Center)
S.L. Lee, C.J. Oates
(University of St. Andrews)
C.D. Dewhurst (ILL)
F.Y. Ogrin (University of Exeter)
S. Sun
(IBM - T.J.Watson Research Center)

Nanoparticles offer exciting possibilities to study fundamental physics and create new technologies in catalysis, sensors, biology and medicine, and data storage. In particular self-assembled FePt magnetic nanoparticles offer the potential to store data at areal densities > 1 Tbit/in^2. This potential arises from the high anisotropy ($L1_0$) phase of approximately equi-atomic FePt, that allows particles of ~20 Å diameter to be thermally stable at room temperature. However, in order to create the $L1_0$ phase of FePt it is necessary to anneal at temperatures in excess of 500 °C, typically for times of 30 minutes [1]. This gives rise to a number of thermally activated processes including the desired phase transformation, oxidation and particle agglomeration. In this study we use small-angle neutron scattering (SANS) to obtain information on agglomeration as a function of annealing conditions and show that for all the conditions significant clustering occurs. Complementary magnetisation measurements demonstrate that a significant fraction of the particles are superparamagnetic indicating the complete $L1_0$ ordering is not achieved. However coercivities of up to 13 kOe at room temperature were readily obtained, demonstrating that self-assembled nanoparticles do indeed offer significant potential as recording media.

FePt nanoparticles were prepared using a solution chemistry approach and deposited onto double-sided Si substrates using the polymer mediated, layer-by-layer technique described previously [2]. This resulted in films consisting of 3 layers of 40 Å $Fe_{58}Pt_{42}$ self-assembled particles, as shown for similar films in figure 1. The polymer-mediated approach results in nanoparticles with an extremely narrow size distribution, typically σ/mean < 5 %, and a well defined periodicity. The as-deposited films were annealed under a range of temperatures (580 to 800 °C) and times (2 to 120 minutes). Magnetisation measurements as a function of temperature were completed for all films. A subset of the annealed films were investigated using the D11 diffractometer with a neutron wavelength of λ = 4.5 Å. The neutrons were collimated to give a beam diameter of 16 mm. Data were collected at three detector positions in order to scan a q range of 0.012 – 0.3 Å-1. The small volume of material meant that it was necessary to stack a number of samples to increase signal to noise ratio. However, significant counting times were required to obtain statistically meaningful data.

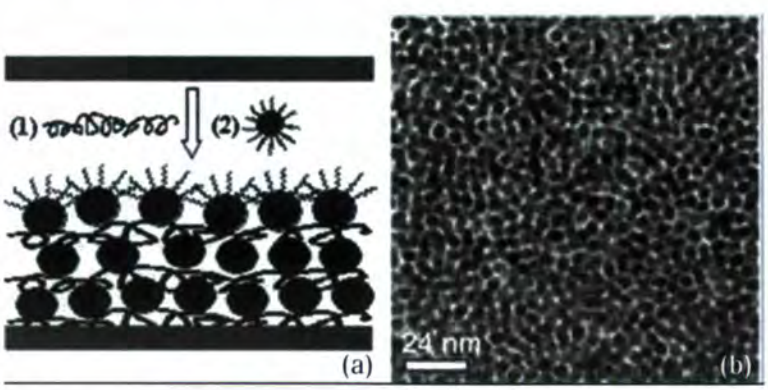

Figure 1: (a) Illustration of polymer-mediated self-assembly of nanoparticles, (1) is the polymer and (2) is the surfactant coated particle. (b) TEM bright field image of 60 Å $Fe_{50}Pt_{50}$ nanoparticles showing that as-deposited the particles have a very narrow size distribution, typically s/mean < 5 % for this process, and that the particles have a well defined separation [2].

Figure 2 shows diffraction images for an as-deposited sample. The coherent diffraction ring is immediately apparent, demonstrating the regularity of the as-deposited nanoparticle films as previously shown using electron microscopy [1]. Integrating round the detector gives an interparticle distance of 65 Å with a distribution σ = 12 Å. This diffraction ring was absent for all of the annealed samples over the q-range measured (q = 0.012 - 0.3 Å^{-1})

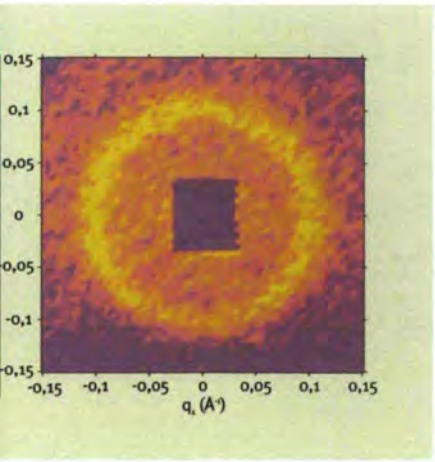

Figure 2: Diffraction image measured at room temperature for as-deposited $Fe_{58}Pt_{42}$ nanoparticles with a diameter of 40 Å and a separation of 65 Å.

indicating that annealing disrupted the inter-particle ordering. To estimate particle sizes from the SANS data it was necessary to compare the measured data with simulations. A number of models based on the hard sphere, Percus Yevick approximation were produced and compared to the experimental data. Given that the nanoparticle films are known to consist initially of 40 Å particles with a 65 Å centre-to-centre spacing, a polydisperse model of interacting particles with a Schultz-gamma distribution of sizes described by Griffith *et al.* [3] was adopted. However, the salient features of the data were reproduced for a number of different models giving confidence that the results obtained did not depend on the details of the model used.

Figure 3 shows SANS data, simulations of the data and the particle/cluster size implied by the simulation. The SANS data indicate that significant agglomeration occurs for all three samples. Using the median particle diameter to characterise the distribution, the particle/cluster size increases from 40 Å for the as-deposited film to 62 Å for the film annealed at 580 °C for 30 minutes and to 160 Å for the 650 °C / 5 minutes film. In the case of the 700 °C / 5 minutes film the median size appears to increase rather dramatically, giving a median cluster diameter of 660 Å. The details of this large increase in size for the 700 °C / 5 minutes film remain to be fully explained. Complementary magnetic measurements show that the temperature dependence of coercivity is significantly less for this sample which also suggests a large increase in volume as thermally activated magnetisation reversal will be less significant.

SANS data shows that a high degree of inter-particle ordering is achieved when $Fe_{58}Pt_{42}$ nanoparticles, with as-deposited diameters of 40 Å, are deposited onto Si substrates in an organic binder. Subsequent annealing at temperatures greater than 500 °C, necessary for the FePt to form the high magnetic anisotropy $L1_0$ phase, results in the particles forming clusters, the size of which increases with annealing temperature.

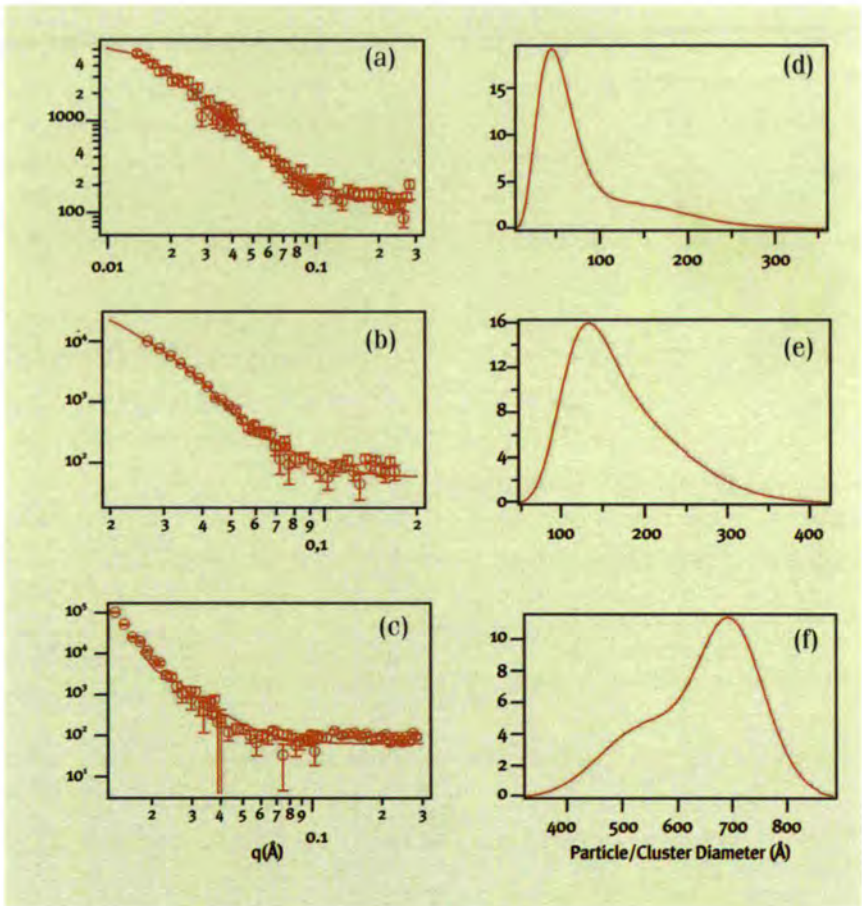

Figure 3: SANS data with simulation (solid line) for three FePt nanoparticle films annealed at (a) 580 °C / 30 minutes, (b) 650 °C / 5 minutes and (c) 700 °C / 5 minutes. All measurements were carried out at room temperature (d-f) particle size distributions obtained from simulation of the SANS data using the hard sphere, polydisperse interacting model of Griffith et al. [3].

REFERENCES

[1] S. Sun, C.B. Murray, D. Weller, L. Folks, A. Moser, Science 287 (2000) 1989
[2] S. Sun, S. Anders, H.F. Hamann, J-U. Thiele, J.E.E. Baglin, T. Thomson, E.E. Fullerton, C.B. Murray, B.D. Terris, J. Am. Chem. Soc. 124 (2002) 2884
[3] W.L. Griffith, R. Triolo, A.L. Compere, Phys. Rev. A 35 (1987) 2200

Field-induced transition *from hexagonal to square vortex lattice in $La_{1.83}Sr_{0.17}CuO_{4+\delta}$*

R. Gilardi and J. Mesot
(LNS, ETH Zurich & PSI, Villigen)
A.J. Drew, U. Divakar and S.L. Lee
(University of St. Andrews)
E.M. Forgan
(University of Birmingham)
C. D. Dewhurst and R. Cubitt (ILL)

Cuprate superconductors are still a matter of great scientific interest, both from the theoretical and experimental point of view. Although $La_{2-x}Sr_xCuO_{4+\delta}$ (LSCO) belongs to the family of the first high-temperature superconductor to be discovered, the microscopic observation of the vortex lattice in LSCO has to date remained remarkably elusive. Recently we performed small-angle neutron scattering experiments that revealed the first clear evidence for a vortex lattice structure in LSCO (x=0.17) [1]. Moreover we were able to observe a field-induced crossover from hexagonal to square symmetry, which is indicative of the coupling of the vortex lattice to a source of anisotropy, such as the one provided by the d-wave superconducting gap.

The magnetic phase diagram of type-II superconductors (see figure 1) can be divided in three main regions: Meissner phase, mixed phase and normal phase. In the Meissner phase, below the lower critical field $H_{c1}(T)$, magnetic flux is completely excluded from the superconductor, whereas above the upper critical field $H_{c2}(T)$ the normal state is recovered and magnetic field is homogeneously distributed over the sample bulk. In the mixed phase between, $H_{c1}(T)$ and $H_{c2}(T)$, magnetic flux can penetrate the superconductor in the form of quantized magnetic vortices that interact and create a vortex lattice (VL). These vortices consist of magnetic flux lines of radius ξ (the coherence length) surrounded a zone of radius λ (the penetration depth) where supercurrents screen the external field.

Knowing that the magnetic field is confined to flux lines each carrying one flux quantum Φ_0 and arranged in a lattice, the symmetry of the VL is found by minimising the free energy. The result of these calculations for isotropic systems shows that the hexagonal VL rather than the square VL is stabilised [2]. In high-temperature superconductors the situation is complicated because of thermal fluctuations and anisotropy effects [3]. At high temperatures vortices are thermally activated and the VL can melt into a liquid phase above $H_m(T)$ (see figure 1). On the other hand, a sufficiently large degree of anisotropy can affect the symmetry of the VL. Our small-angle neutron scattering investigations of the VL in LSCO have been performed both on the D22 and SANS-I (PSI, CH) instruments. The sample was a slightly overdoped LSCO single crystal (x = 0.17, T_c = 37 K), grown with the TSFZ method, by the group of Prof. Oda at Hokkaido University (Japan). The structure of LSCO at low temperature is orthorhombic with the c-axis perpendicular to the CuO_2 planes. In our notation the {1,1} direction is along the Cu-O-Cu bonds. For most of the measurements the c-axis was oriented along the magnetic field direction (applied horizontally parallel to the incident neutron beam).

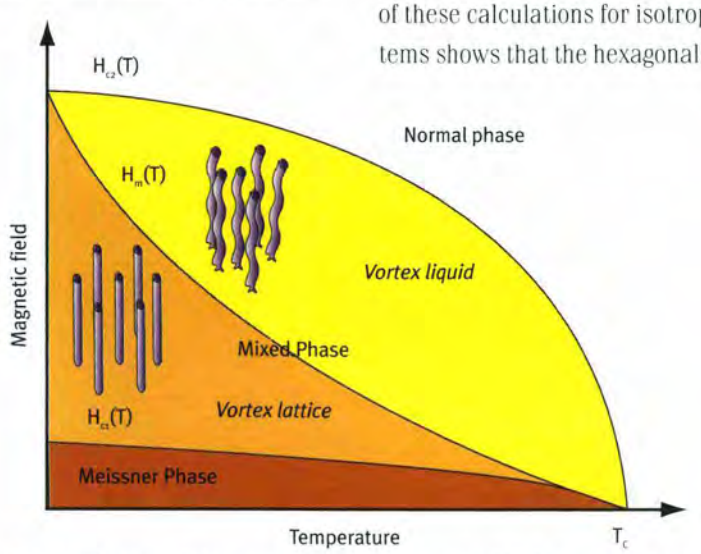

Figure 1: Schematic view of the magnetic phase diagram of high-temperature superconductors.

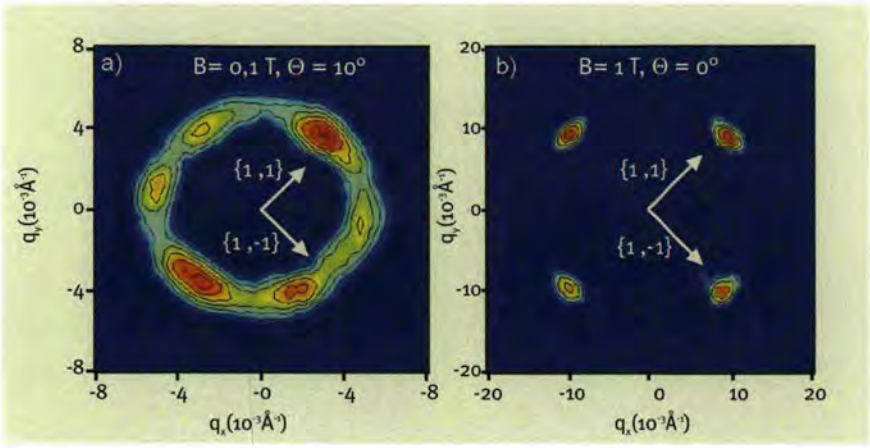

Figure 2: Diffraction pattern obtained on D22 at a) B = 0.1 T applied 10 degrees out of the c-axis and b) B = 1 T applied parallel to the c-axis.

Figure 2 shows diffraction patterns obtained on D22 at T = 1.5 K after subtraction of a background taken at T = 40 K (>T_c).

At B = 0.1 T, when the field is applied along the c-axis, one observes a ring-like distribution of intensity, which is consistent with the superposition of four hexagonal domains oriented along the crystalline axes {1,0}, {0,1}, {1,1} and {1,-1}. In order to lift the degeneracy of the vortex lattice, we rotated the c-axis 10 degrees away from the field direction. As a result a hexagonal pattern emerges, as shown in figure 2a.

At B = 1 T the intensity is concentrated in four bright spots oriented along the {1,1} and {1,-1} directions (see figure 2b). Even rotating the c-axis 30 degrees out of the field direction retains this four-fold coordination. The VL is only slightly distorted to a rhomboid, as expected for superconductors with uniaxial anisotropy. The experimental evidence thus indicates a field-induced crossover from a hexagonal VL at low fields to an intrinsic square VL at higher fields.

In order to quantify this field-induced transition, we analysed our data in two alternative ways (see figure 3). The relationship between the magnitude q of the fundamental wavevector of the VL and the applied magnetic field B depends on a structure dependent quantity $\sigma = \left(\frac{2\pi}{q}\right)^2 \frac{B}{\Phi_0}$, where σ is equal to 0.866 for a hexagonal VL and 1.0 for a square one. For fields larger than B = 0.4 T the values of σ are as expected for a square VL, whereas at lower fields they are consistent with that of a hexagonal VL. We also monitored the intensity ratio in sectors (± 15 degrees) containing the {1,0} and {1,1} directions for fields applied parallel to the c-axis. Indeed the intensity ratio decreases steadily from 1 at B = 0.1 T to about 0.2 above B = 0.4 T and then remains constant.

Our experimental results therefore indicate that, in slightly overdoped LSCO, an intrinsic square vortex lattice (oriented along the Cu-O-Cu bonds) exists at fields larger than 0.4 Tesla. Similar effects have been reported in $YBa_2Cu_3O_7$ (T_c ~ 90 K), but at much higher magnetic fields [4,5]. One should notice however that in $YBa_2Cu_3O_7$ the square VL is oriented at 45° from the Cu-O-Cu bonds. An intrinsic fourfold symmetry is indicative of the coupling of the VL to some source of anisotropy. Square VL resulting from the anisotropic (d-wave) nature of the superconducting gap via the increasing importance of the anisotropic vortex cores at high fields have been theoretically predicted [6,7]. In principle other sources of anisotropy, such as those involving Fermi surface/velocity anisotropies [8], dynamical stripes or charge-density waves, could lead to the formation of a square vortex lattice. It remains a challenge to corroborate detailed small-angle neutron scattering measurements with other microscopic data in order to explain the origin of this exotic vortex behaviour.

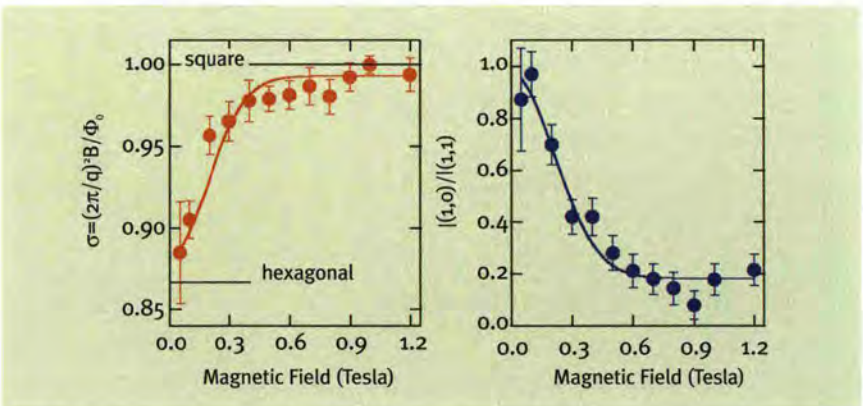

Figure 3: Two alternative ways of quantifying the field-induced transition from hexagonal to square vortex lattice (see text).

REFERENCES

[1] R. Gilardi et al., Phys. Rev. Lett. 88 (2002) 217003
[2] W.H. Kleiner et al., Phys. Rev. 133 (1963) A1226
[3] G. Blatter et al., Rev. Mod. Phys. 66 (1994) 1125
[4] B. Keimer et al., Phys. Rev. Lett. 73 (1994) 3459
[5] E.M. Forgan et al., submitted to Phys. Rev. Lett.
[6] A.J. Berlinsky et al., Phys. Rev. Lett. 75 (1995) 2200
[7] M. Ichioka et al., Phys. Rev. B 59 (1999) 8902
[8] N. Nakai et al., cond-mat/0205245 (2002)

Unravelling *superconductivity in MgB_2*

H. Schober (ILL)
B. Renker and R. Heid (INFP, Forschungszentrum Karlsruhe)

Superconductivity is still one of the major puzzles of solid state physics. While BCS theory provides a basic understanding in terms of electron pairing the intrinsic properties of superconducting materials remain difficult to predict. This holds in particularly for the high-temperature oxide superconductors where even the attraction mechanism responsible for the pairing remains elusive. The recently discovered superconductor MgB_2 with a T_c of about 40 K [1] offers a different picture. It has a sufficiently simple structure to be accessible to modern ab-initio calculations [2]. These provide us with a good understanding of both the electronic band structure and the phonon spectrum. Neutron spectroscopy constitutes an important check on the validity of these calculations, confirming strong electron-phonon coupling for only a subset of vibrational modes [3]. Using the band structure results it is possible to predict T_c based on the anisotropic Eliashberg equation [4].

In MgB_2 layers of boron atoms arranged in a honeycomb lattice are separated by Mg spacers (see figure 1). The material is known since more than 50 years and can be bought of the shelf for a couple of Euros. Like in the case of fullerenes the high T_c of about 40 K discovered in MgB_2 came as a big surprise. A tremendous rush of both theoretical and experimental work followed the first publication. Our current understanding allows us to draw a rather complete picture of the physics responsible for superconductivity in MgB_2. The electron pairing in MgB_2 is phonon mediated. The coupling varies appreciably depending on the state of the electron [2]. This leads in particular to two well-separated gaps in the electronic excitation spectrum [4]. Only selected phonons participate in the coupling process. These phonons, however, show a very strong coupling.

It is possible to gain insight into the electron-phonon coupling by investigating the evolution of phonon spectra in the mixed $Al_xMg_{(1-x)}B_2$ system [3]. In pure MgB_2 the Mg ions donate two electrons to the boron sheets, which, therefore, should be isoelectronic to graphite. In graphite three of four valence electrons are bound in σ-orbitals lying within the plane. The forth electron is placed in a non-bonding π-orbital which sticks out of the plane. σ- and π-orbitals equally exist in MgB_2.

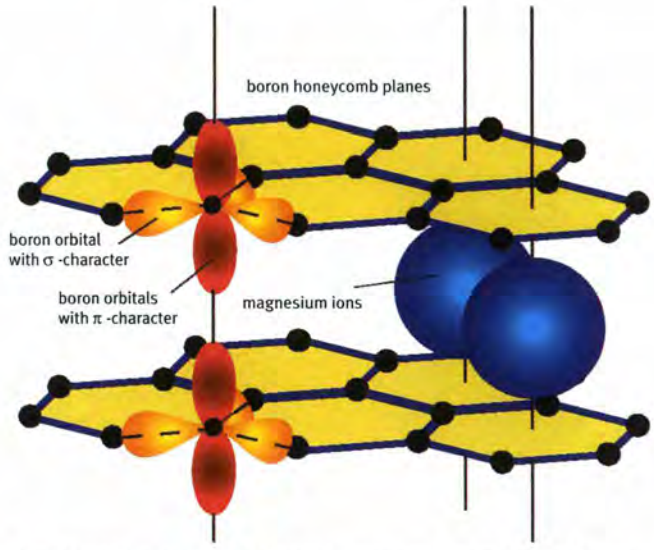

Figure 1: Schematic picture of MgB_2. Boron planes are separated by Mg spacers. The atomic orbitals leading to σ- (inplane) and π- (out-of-plane) bonding are indicated.

However, as band structure calculations show, the positive attraction exerted onto the electrons by the Mg ions transfers about 10 % of the electrons from the σ- into the π-orbitals. We are thus confronted with hole-doped metallic boron planes. By gradually replacing Mg with Al, we pump electrons into the sheets while hardly altering the chemical structure. Experimentally we observe that superconductivity becomes weaker and finally completely disappears at high Al levels [5].

In figure 2 we show how the phonon spectrum reacts to Al doping. The densities of state have been obtained in upscattering on isotopically pure samples using the instrument IN6. We immediately realise that the spectra depend strongly on the presence of Al

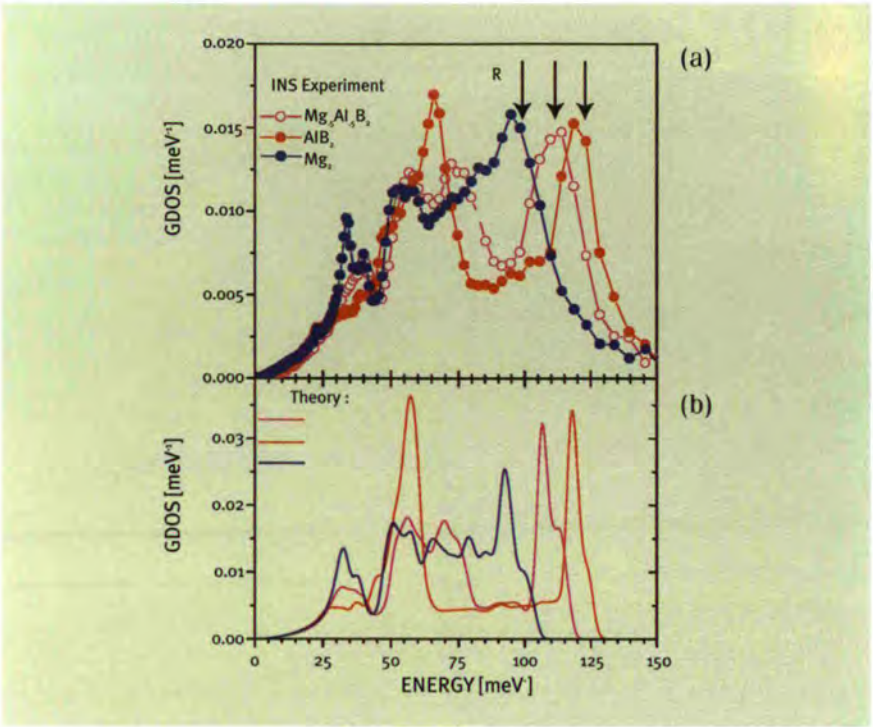

Figure 2: Phonon densities of states as a function of Al-doping. Experimental results obtained on IN6 (a) are compared with theoretical calculations (b). R indicates position of Raman modes.

in particular at higher energies where exclusively the lighter Boron ions vibrate. The comparison with the theoretical calculations for the pure systems MgB_2 and AlB_2 is excellent. The calculations allow us to identify the character of the modes contributing to the experimentally observed shifts. It turns out that the boron modes with propagtion vectors along the hexagonal stacking axis and displacement patterns in the boron planes (see figure 3) react radically to the doping. This is a strong indication for pronounced electron-phonon coupling of these modes. In so-called adiabatic systems vibrational frequencies can be predicted knowing the potential E({R}) which indicates how the electronic energy E changes as a function of the ionic coordinates {R}. In MgB_2 the particular set of boron vibrations mentionned above is no longer compatible with this simple description. The movement of the boron ions strongly redistributes electrons among bands heavily distorted around the Fermi-level (see figure 3). In other words the phonons not only influence the total energy of the electronic system but pump electrons from one state into another in a synchronized way. Adding electrons to the system and thus filling the σ-holes strongly influences this pumping process and thus the phonon frequencies. Electrons and phonons can no longer be viewed as separate entities; i.e. they are strongly coupled.

Modern ab-initio calculations are capable of reproducing the electron-phonon coupling for the ordered end members MgB_2 and AlB_2. For the intermediate systems experimental data as presented here are the only source of information. The strong coupling is certainly the deeper reason for the high T_c in MgB_2. It is equally essential that the frequencies of the phonons contributing to the coupling are high. However, the high frequencies are fortunately due to the light mass of the boron ion and not to strong restoring forces. AlB_2 has far higher vibrational frequencies but, according to the calculations, lower electron-phonon coupling. It still should be a superconductor according to basic theory, which it is not. So putting all the parts of the puzzle together is still a challenge, even in MgB_2.

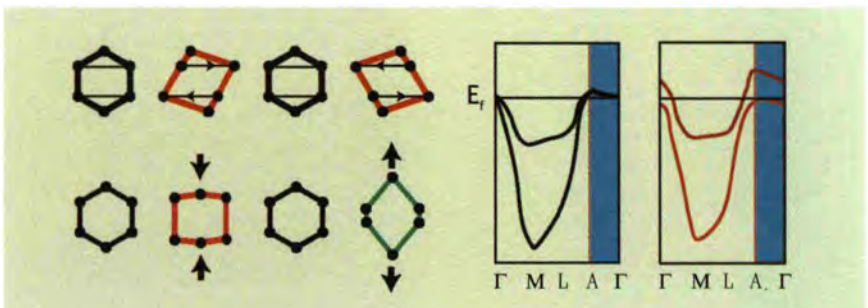

Figure 3: Schematic presentation of two vibrational patterns involving stretching of σ-bonds in the boron planes. The deformation of the hexagons during the vibrations leads to a strong modification of the σ-band structure as indicated to the right. Electrons are pumped to different states via the vibration leading to strong electron-phonon coupling.

REFERENCES

[1] J. Nagamatsu et al., Nature (London) 410 (2001) 63
[2] J.M. An and W.E. Pickett, Phys. Rev. Lett. 86 (2001) 4366, Kortus et al., Phys. Rev. Lett. 86 (2001) 4656, Bohnen et al., Phys. Rev. Lett. 86 (2001) 5771
[3] B. Renker et al. Phys. Rev. Lett. 88 (2002) 67001
[4] H.J. Choi et al. Nature (London) 418 (2002) 758
[5] J.S. Slusky et al., Nature (London) 410 (2001) 343

Pointing the way in biology

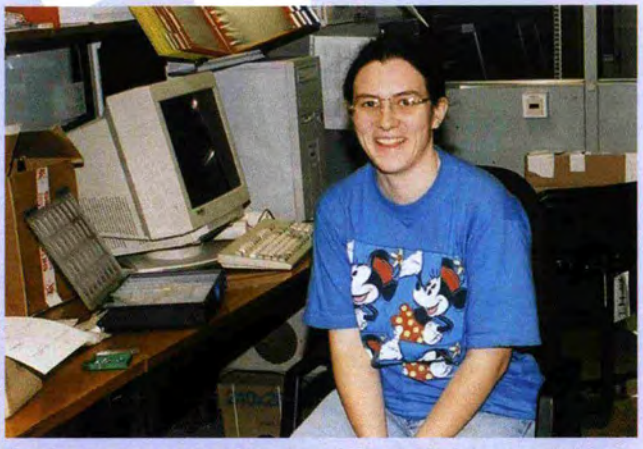

Aurelie Vandeneynde (IBS, Grenoble) during her experiment on IN13.

Marité Cardenas, Lund University (Sweden) during a talk on the adsorption of DNA and DNA-CTAB complexes at hydrophilic and hydrophobic silica surfaces.

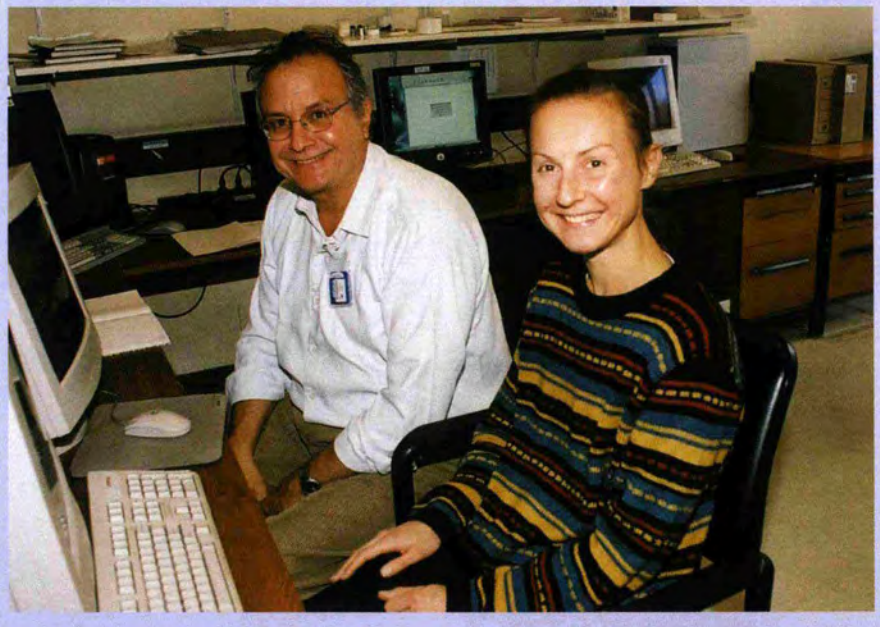

Joe Zaccai and Isabelle Grillo analysing their data on the small angle scattering instrument D22.

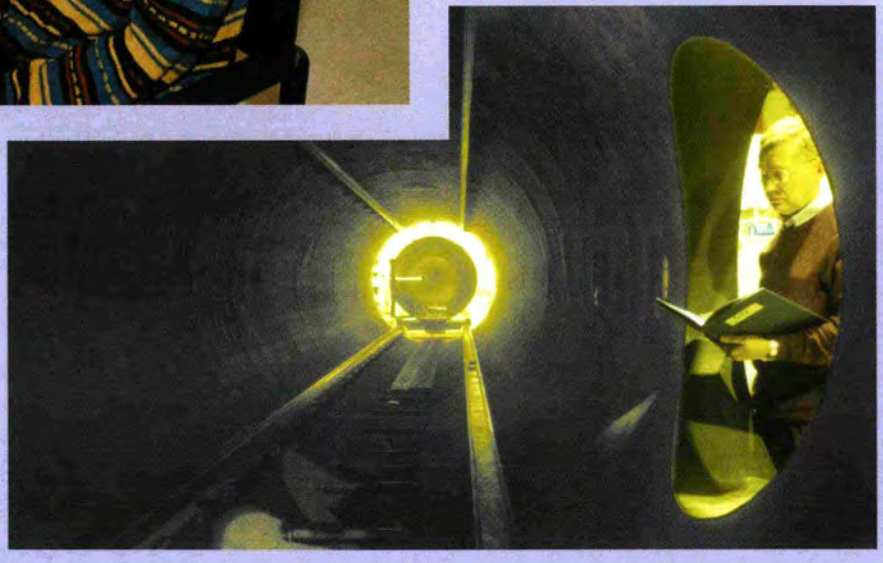

Roland May, checking the vacuum tube of the D22 detector.

Roland P. May, College 8 Secretary
http://www.ill.fr/Colleges/C8/

Biology

The Biology College at the ILL traditionally has been dealing with the structures of biological macromolecules in solution and in crystals, as well as with their dynamics. In the last years, work on the borderline between "soft condensed matter" and biological structures has been added to the topics that are being peer-reviewed by Subcommittee 8 (Biology). Artificial membranes, for instance, often do not have exactly the compositions found in vivo, but research on them will ultimately provide information that is valuable for understanding "real" biological systems. A similar argument holds for crystallographic or inelastic investigations of compounds of biological macromolecules (e.g. oligopeptides, i.e. short chains of amino acids). Studies of the interactions of nucleic acids and lipids (fats) are relevant for developing vectors for the introduction of genes into ill cells.

Nearly all of the work done with neutrons in biology is based on the particular properties of the naturally abundant hydrogen and its heavy isotope deuterium. In terms of its neutron scattering amplitude, deuterium behaves much like the two other biologically most frequent nuclei, carbon and oxygen, whereas normal hydrogen is "exotic", with an amplitude about half the size of deuterium, but negative. Contrary to X-rays, neutrons can "see" hydrogens, because of this smaller, but still relevant amplitude, whereas the X-ray amplitude is proportional to the charge of a given atom.

At low resolution, it is the contrast that one can create by replacing deuterium for hydrogen either in the solvent or in the macromolecules themselves. The former "contrast variation" allows one to distinguish between components of macromolecules that differ in their specific hydrogen content. This is the case for proteins, sugars, lipids, and nucleic acids. In a virus, for example, the protein hull becomes "invisible" for neutrons at 40 % D_2O in the aqueous solvent, while the nucleic-acid core vanishes around 70 % D_2O. The latter "specific deuteration" allows one even to highlight parts in a molecule that are of naturally identical composition, e.g. single amino acids in a protein, or a single protein in a large complex like the ribosome, the organelle that translates the genetic code to proteins.

Two of this year's highlight reports are using the techniques described above, a study of collagen in human bone (Aspden et al.), and a study of the location of two proteins in a double-stranded RNA virus (Ikonen et al.).

Neutron-crystallographic studies aiming at revealing the location of hydrogen atoms that are crucial for reaction mechanisms are increasing in number and in the volume of biological beam-time allocation at the ILL. So are investigations of the dynamics of molecules, where one must not only count experiments performed on ILL-owned instruments, but also such on the Franco-Italian CRG instrument IN13.

At present, about every eighth instrument day at the ILL is devoted to experiments in the field of Life Sciences. Although, evidently, neutrons are not the main tool for investigations in this area, they can answer questions that cannot be solved by other techniques, as indicated in the above examples.

The ILL has decided to further strengthen its support for biological research by co-founding the Partnership for Structural Biology (PSB), an initiative to create a Centre of Excellence for Structural Biology at Grenoble, together with the ESRF, the EMBL and the IBS. A milestone for the PSB was the signature of the international agreement for the Partnership on 15 November. The Biological Deuteration Laboratory, one of the corner-pillars of this scientific collaboration, has completed its first year of activity; two gene products have been successfully expressed in deuteriated form and used in diffraction and scattering experiments: aldose reductase (A. Podjarny *et al.*), and plasmid DNA (J. Lawrence *et al.*). An account of the progress of the Deuteration Laboratory can be found on page 62 of the Annual Report.

Collagen in human bone, *a small-angle scattering study*

R. M. Aspden and J.M.S. Skakle
(University of Aberdeen)
G. Fragneto (ILL)

Bone forms the skeleton on which depends our ability to stand, walk, and perform all the amazing things we can do with our bodies. However, in the elderly, alterations in the bone can lead to serious problems: loss of bone in osteoporosis results in bone fragility and a rising tide of fractures; proliferation of undermineralised bone in osteoarthritis indicates problems with metabolism and cell behaviour. The protein collagen and the mineral apatite are the main constituents of bone and changes in either of these can lead to loss of mechanical integrity. However, studying the structure of collagen in the presence of mineral is difficult. Hence the need for neutrons.

Bone can be described as a naturally occurring fibre-reinforced ceramic. It is formed as a cartilaginous precursor, in which fibres of collagen provide reinforcing to a gel-like matrix. This becomes impregnated with calcium phosphate mineral, in the form of small, poorly-crystalline apatite crystals, which considerably increases the strength and stiffness of the material. Bone is found in two main forms: cortical and cancellous (or trabecular). Cortical bone is dense and compact and makes up about 80 % of the mass of the skeleton. It forms the outer shell of most bones. Cancellous bone has an open spongy texture and hence is lighter but less stiff and strong. It is found primarily at the ends of long bones and in the interior of short bones such as spinal vertebrae. The X-ray of a hip in figure 1 shows the difference in density between the two types of bone: cortical shows up as bright white, cancellous as darker, in which the open structure can just be seen.

Collagen is a triple-helical molecule, about 300 nm long and 1.5 nm diameter. It assembles into fibres with a relatively disordered side-to-side packing of molecules but a regular axial structure with a repeat distance of about 67 nm. These structures can grow up to nearly 1 mm wide and of unknown length though commonly they are 10 -100 mm across.

Mineralization of the cartilaginous matrix alters the packing of the collagen molecules but presents a challenge to the measurement of that packing. In non-mineralised tissue, X-ray methods for studying collagen are well established. But, for fully mineralised bone, these are only possible with thin sections (~100 μm) of cortical bone because of the strong scattering by the mineral itself. It is, however, cancellous bone which is biologically the more important because of its more rapid turnover and its role in diseases as outlined above.

Neutron diffraction would, therefore, seem the technique of choice for the study of intact bone. It has been used previously to study soft tissues and demineralized bone, and also for the study of bovine cortical bone. This latter study showed a reduction in the lateral packing of collagen as the bone was dehydrated, and it was this we used as a starting point for our own study, in which for the first time we have recorded neutron diffraction patterns from collagen in human cancellous bone.

Figure 1: X-ray of the hip region, showing the location and relative densities of cancellous and cortical bone.

The lateral spacing to be studied occurs at a Q value of ~0.5 $Å^{-1}$. At D16, the detector that we used covered a ~9° 2θ range which corresponds, at λ=4.54 Å, to a range of 0.4 $Å^{-1}$ in Q and thus data could be collected with the detector stationary. In addition, D16 had just been equipped with a humidity chamber, which ensured that samples could be kept fully hydrated. The chamber also allowed a degree of temperature control; for this study, data sets were collected at 293±2 K. The preparation of samples is described

elsewhere [1]. We studied cortical bone first, for comparison with published data [2], followed by measurement of a number of cancellous bone samples, both osteoporotic and osteoarthritic.

The measurement of the peak position was the most crucial part of the data analysis. We used the instrumental background subtraction facility in LAMP [3] and then used a Loess function to model the peak shape. The first derivative then gave the peak position. By adjusting the fitting parameters, slight variations in the chosen function also allowed an estimate of the error. In cortical bone the peak is well defined (figure 2) and the lateral spacing was lower for the dehydrated bone, as reported elsewhere [2]. However, the actual values (12.30(2) Å for hydrated and 11.91(4) Å for dehydrated) differed from those previously reported; this can be accounted for by differences in the method of peak fitting and in the level of dehydration [1].

Figure 3 shows patterns obtained from cancellous bone, which are not so well-defined as those for cortical bone. The main difference arises from the lower density of cancellous bone, but there may also be an influence of extra disorder, as it is possible that the longitudinal alignment of collagen fibres is less in cancellous bone. The peak positions were established using the same method as for the cortical bone and with a similar level of accuracy. Average values were 12.53(9) Å for osteoarthritic and 12.33(25) Å for osteoporotic bone. The number of samples in this initial study was not enough for statistical comparisons to be made between the two groups, but we found the spread of values to be greater for osteoporotic than for osteoarthritic bone. In future studies, we will analyse a greater number of samples so as to provide a true comparison, and also will investigate the effects of controlled dehydration. These data will be compared with analyses of composition and mechanical properties.

In summary, we have demonstrated that not only is neutron diffraction a feasible technique for the study of collagen within intact human bone, but that the data produced is of high enough quality to merit a more detailed analysis.

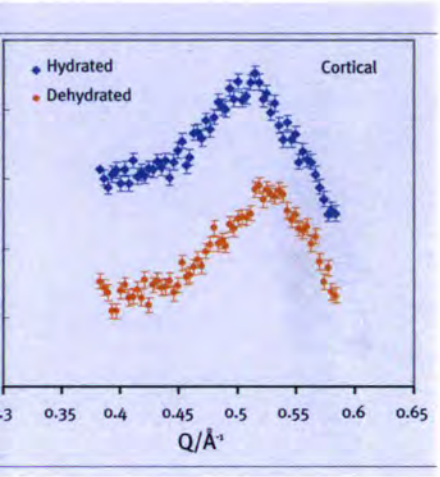

Figure 2: Neutron diffraction patterns recorded from cortical human bone, showing comparison between hydrated and dehydrated bone.

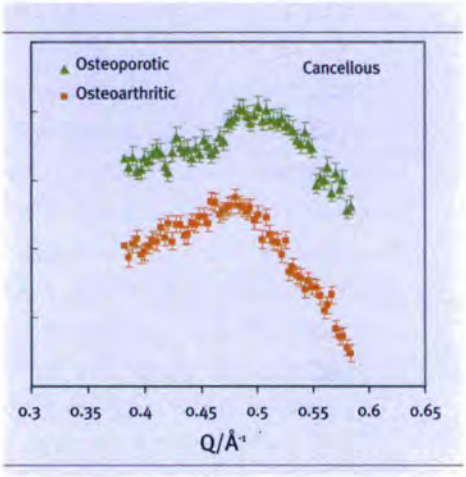

Figure 3: Neutron diffraction patterns recorded from cancellous human bone. One example from each disease group (osteoarthritic, osteoporotic) is given.

REFERENCES

[1] J.M.S. Skakle and R.M. Aspden, J. Appl. Cryst. 35 (2002) 506
[2] L.C. Bonar, S. Lees and H.A. Mook, J. Mol. Biol. 181 (1985) 265
[3] D. Richard, M. Ferrand and G.J. Kearley, http://www.ill.fr/data_treat/lamp/front.html

Localisation of the *polymerase within a dsRNA virus assembly*

T.P. Ikonen, D. Kainov, R.E. Serimaa and R. Tuma (University of Helsinki)
P. Timmins (ILL)

The polymerase core of double-stranded (ds) RNA virus provides the molecular machinery for RNA packaging and replication. Procapsid of bacteriophage ϕ6 constitutes a well-studied model of such RNA-processing machine. Due to their low abundance minor procapsid constituents, P2 (RNA polymerase) and P7 (packaging factor), have not been localised. We have applied small-angle neutron scattering (SANS) and contrast variation in order to localise the two proteins. Radial positions of labelled proteins were obtained and modelled within the electron density of the procapsid. P2 monomers reside at each five-fold vertex just under the RNA packaging complex. P7 was detected at distance of 160 Å from the procapsid center indicating localisation on the inner surface of the procapsid.

Because dsRNA genomes cannot be replicated by the host replication machinery dsRNA, dsRNA viruses must carry their own polymerase. Therefore, most dsRNA viruses employ similar architecture, a polymerase complex (also called a core), for sequestering the genome from the cellular environment and for effective replication of the genome [1]. The polymerase complex constitutes the innermost component of the mature virion and it is formed from multiple copies of a small number of virally encoded structural protein and enzymes. Typical lifecycle of a dsRNA virus is exemplified in figure 1 using bacteriophage ϕ6, a model organism for studying assembly and replication of other dsRNA viruses.

ϕ6 is a triple-layered icosahedral phage infecting *Pseudomonas syringae* [2]. The polymerase complex is composed of four protein species (copy number in parentheses), P1 (120), P2 (12), P4

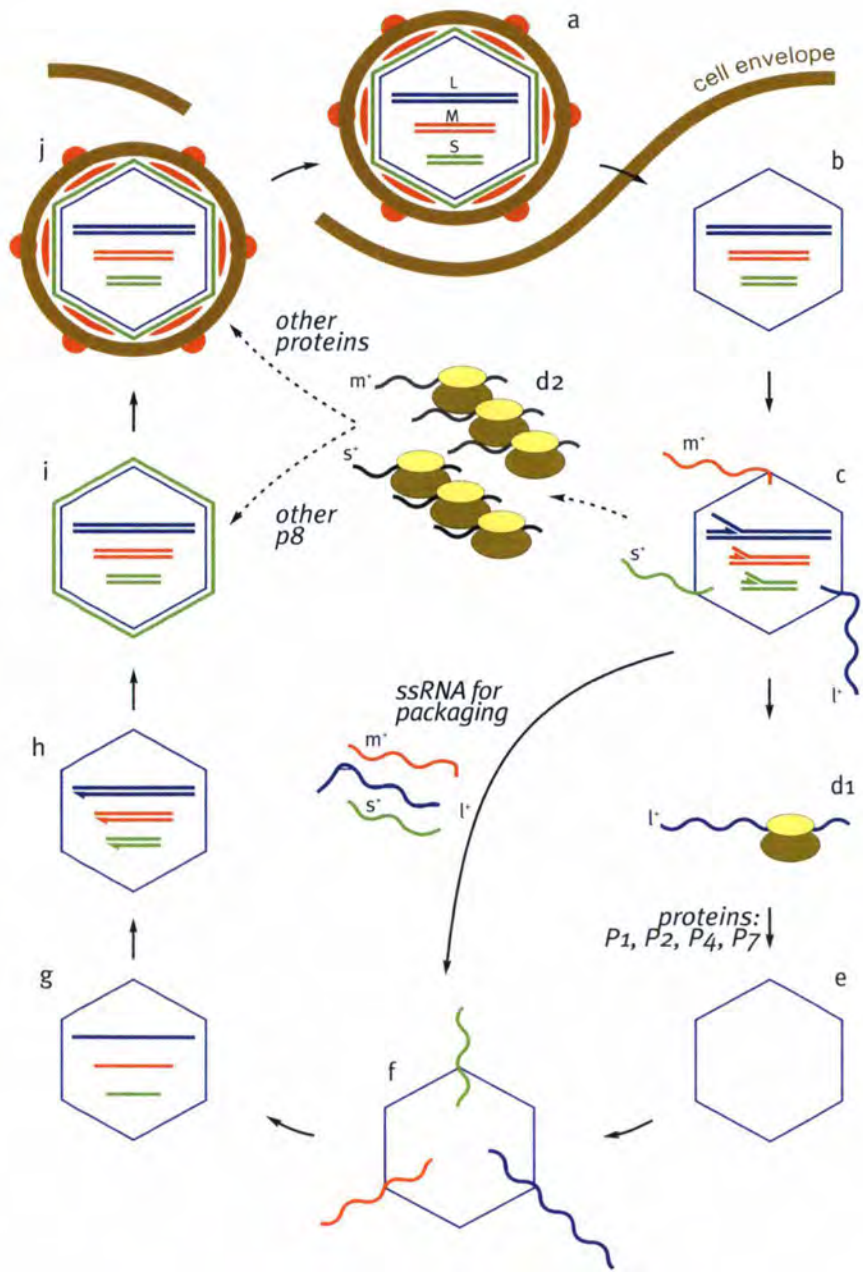

Figure 1: Life cycle of bacteriophage ϕ6. The virion, containing 3 dsRNA segments S (small), M (medium), L (large) attaches to the host cell (a) and the polymerase complex penetrates the host membranes and loses both the envelope and the nucleocapsid coat (b). The polymerase complex is activated and produces transcript mRNA (c) which are subsequently translated into viral proteins (d1-d2). An empty polymerase complex (procapsid, PC) is self-assembled from proteins P1, P2, P4 and P7 (e). The icosahedral procapsid specifically packages the three single stranded RNA molecules s^+, m^+, and l^+ (f). The packaged ssRNA (g) is replicated by viral RNA polymerase P2 into the double stranded form inside the polymerase complex (h). The polymerase complex is coated by a shell of protein P8 to form a nucleocapsid (i), which is subsequently enveloped and mature virions (j) leave the cell by lysis.

(72) and P7 (60) together with three dsRNA segments. P1 forms a dodecahedral framework of the complex (a $T = 1$ lattice, triangulated with dimers). Each five-fold vertex contains a P4 hexamer, which is the packaging ATPase [3].

It is assumed that one P2 monomer (the RNA-dependent RNA polymerase) is present at each five-fold vertex of PC. Similarly, the stoichiometry of P7 (30 dimers) indicates that one dimer is associated with each of the two-fold symmetry positions. In neither case the localisation has been confirmed experimentally. The intrinsically low contrast of proteins within assemblies and the breakdown of strict icosahedral symmetry within the procapsid made it difficult to localise P2 and P7 by electron microscopy (EM).

In order to circumvent the shortcomings of electron microscopy (EM) in localising minor capsid components, we have resorted to small-angle neutron scattering (SANS) and contrast variation to determine the position of P2 and P7. Selective deuterium labelling has been facilitated by the ϕ6 *in vitro* assembly system [4]. The neutron scattering experiments were performed at the high flux beamline D22 of ILL. Three sets of procapsid samples were measured, unlabelled (PC), PC containing deuterated P2 (designated PC-P2-*d*) or P7 (designated PC-P7-*d*), respectively (figure 2).

The deuterated sub-units were modelled as a collection of spheres. Based on the crystallographic structure of P2 [5] and stoichiometric considerations one P2 (modelled as a sphere of 30 Å radius) was positioned on each of the twelve icosahedral 5-fold axes. The parameter of the model was the distance of the sub-units from the center of the procapsid. The 60 P7 sub-units were modelled as 30 dimers, each dimer consisting of a linear string of 10 beads (string length 200 Å, bead diameter 10 Å) with the string axes perpendicular to the 2-fold symmetry axes; i.e. P7 dimers were positioned along the dodecahedral edges of the P1 framework. The fitted parameter was the distance of the string center from the procapsid center.

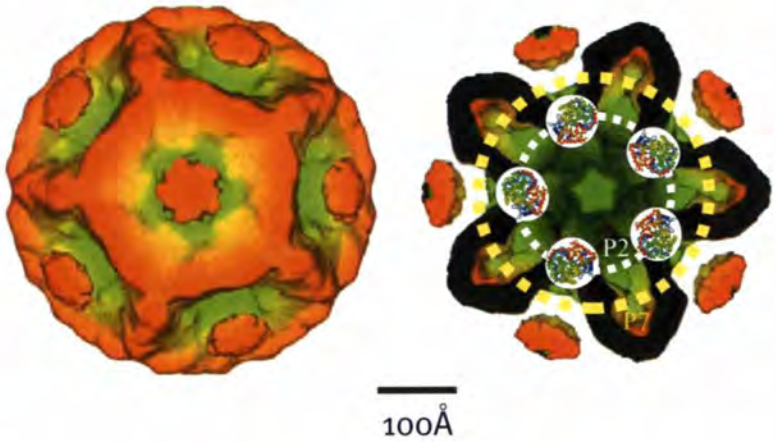

Figure 2: Model of P2 and P7 location. Left: Surface representation of the procapsid electron densities [3]. Right: Vertices shown in a cross-section through the procapsid EM density with radial positions of P2 and P7 indicated by the white and yellow circles, respectively. Using the SANS constraints five P2 atomic models were placed within the EM electron densities under the five-fold vertices in the cross-section.

The scattering from unlabelled procapsid gives a smeared shell model whose parameters are in very good agreement with the procapsid radius determined by cryo-EM (diameter 460 Å) [3]. The fit of the P2 model to the data collected from the procapsids with deuterated P2 also showed good correspondence. The distance of P2 from the procapsid center was 110 Å. A sphere of radius 110 Å intersects the EM densities on the inner surface of the procapsid at positions just under the five-fold vertex (figure 2). Thus, the most likely position of P2 is under the five-fold vertex in contact with the P1 framework and in close proximity to the packaging machinery (e.g. P4 hexamer). A similar arrangement has been seen within the rotavirus core [6] and inferred from the low-resolution X-ray models of BTV [7]. This indicates that the position of the polymerase machinery is conserved across a wide range of dsRNA virus species and is dictated by similar genomic organisation and replication mode.

The P7 model yielded an average radial distance of 160 Å, but rather noisy data makes this estimate less reliable. Nevertheless, the present estimate of radial position indicates that P7 might be located inside the particle at a site that is distal to the replication and packaging machinery. P7 may act as an internal stabilising clamp of the dodecahedral framework as recently suggested [4].

These studies demonstrate the unique ability of neutron small-angle scattering combined with deuterium labelling to locate *in situ* the presence of specific sub-units within a multi-protein complex.

REFERENCES

[1] D.H. Bamford, Curr. Biol., 10 (2000) R558
[2] M.M. Poranen, M.J. Pirttimaa and D.H. Bamford, Bacteriophage phi6, in Viral genome packaging, C. Catalano, Editor, 2002, Landes Bioscience
[3] F. de Haas et al., J. Mol. Biol. 294 (1999) 357
[4] M.M. Poranen et al., Cell, 7 (2001) 845
[5] S.J. Butcher et al., Nature, 410 (2001) 235
[6] B.V. Prasad et al., Nature, 382 (1996) 471
[7] P. Gouet et al., Cell, 97 (1999) 481

In vivo deuteration *of proteins and DNA*

M. Härtlein, T. Forsyth and P. Timmins (ILL)
D. Myles (EMBL)

The ILL/EMBL Biological Deuteration Laboratory is now up and running. There has been a steady expansion of facilities and P2 level laboratory space is currently being constructed. A major UK based EPSRC award for projects that will exploit this facility will start in February 2003, strongly complementing an existing EU RTD award. Two major user projects have been completed and others are in the pipeline. In addition, a healthy in-house program is under way as well as preparations to join the Partnership for Structural Biology (PSB).

Deuterated plasmid DNA for gene therapy studies

L. Kudisova, J. Lawrence, (King's College, London)
M. Härtlein, T. Forsyth, V. Laux-Lesourd, I. Parrot (ILL)

Tremendous opportunities exist to use genes to tackle diseases hitherto untreatable by traditional lines of drug therapy. In the case of acquired diseases like AIDS, the goal is to deliver a gene which makes a protein which either kills the invading organism, or alternatively triggers the body's natural defence system to destroy it. For inherited diseases such as cystic fibrosis, the idea is that a gene will be introduced to diseased patients' cells to enable the production of a protein that is defective or absent, so that the patients are returned to good health. For the present, however, such treatments amount to little more than wishful thinking because we do not yet have any effective method(s) of gene delivery. Early efforts to deliver genes to a patient's cells by packaging them inside viruses have proved disappointing. Much of the more recent work has focussed on the use of gene delivery vehicles prepared by mixing the gene of interest with cationic vesicles - *ie* sub-microscopic spherical particles prepared from positively charged lipids.

Central to the success of a gene delivery vehicle is an understanding of the interaction of the vesicles with the added gene, and of their behaviour when they encounter the body's cells. For example, whether the complex collapses upon encountering a membrane or remains intact is vitally important in determining whether the gene enters the target cell. Surprisingly, however, there have been virtually no studies concerned with looking either at the detailed structures of the gene-vesicle complexes, or with their subsequent interaction with cell membranes.

Researchers in the Pharmacy Department at King's College together with colleagues at the ILL and Keele University have embarked on a programme of research to address these questions, using neutron scattering techniques coupled with contrast variation (that is, the technique of 'highlighting' specific components of the system of interest by selective deuteration). Small angle neutron scattering, on D22, has been

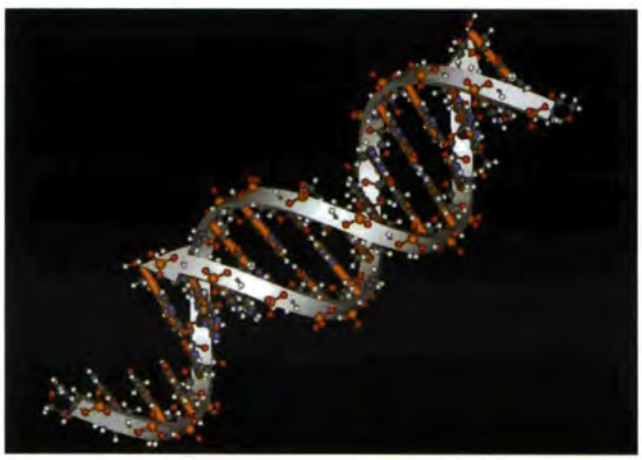

Figure 1: Double-helical DNA.

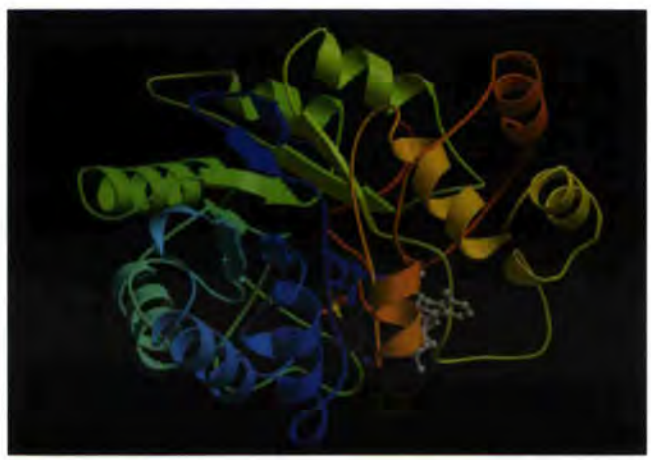

Figure 2: X-ray crystal structure of Human Aldose Reductase.

successfully used to examine the interaction between genes and cationic vesicles as well as providing information about the overall size and shape of the gene delivery vehicles. Neutron specular reflection studies on D17 have been used to see whether the gene delivery vehicles adsorb and collapse at the cell surface, or whether they remain intact at the surface allowing their gene payload to be delivered into the cell. This is the first time such studies have been undertaken. Central to the success of these is the opportunity to use both hydrogenous and deuterated forms of DNA in our study. In October 2002 Leila Kudisova and Jayne Lawrence from King's College visited the facility to produce and purify (per)deuterated plasmid DNA. A protocol for fermentation and large-scale purification of DNA developed in the Deuteration Lab was used to produce mg quantities of DNA. This material will be used to increase contrast in the vesicle/DNA binding studies.

Deuterated Human Aldose reductase: A target for drug design.

I. Hazemann, A. Podjarny (Strasbourg)
M. Härtlein (ILL),
D. Myles, M.Th. Dauvergne (EMBL-Grenoble)

Diabetes is a chronic disease affecting as many as 150 million people worldwide. People with diabetes are unable to use the glucose from their food which then accumulates in the bloodstream, where it can damage the heart, kidneys, eyes and nerves. Left untreated, diabetes can develop devasting complications that lead to disability and death. Enzymes involved in the development of the disease are therefore leading targets for drug design in the pharmaceutical industry.

Human Aldose Reductase is important because it reduces D-glucose into D-sorbitol and is believed to be involved in degenerative complications of diabetes. The catalytic reaction involves a hydride transfer from the C4 atom in the nicotinamide ring of the coenzyme NADPH and a proton donation from the enzyme. Due to its medical interest, numerous X-ray, site-directed mutagenesis and modelling studies of AR have been carried out. Current high resolution (0.66A) X-ray structures have determined the protonation state of the catalytically important residues, as well as of inhibitor binding and of the solvent structure, but the H-atom signal is weak, and the protonation state is clearly seen only for the most ordered atoms. Neutron diffraction experiments on LADI should now help determine the fine detail of the interatomic interactions between the chemically important hydrogen atoms of the protein and potential drugs.

In January 2002 Isabelle Hazemann from the protein crystallography group of Alberto Podjarny (IGBMC, Strasbourg) spent two weeks at ILL growing deuterated cells for the expression of the Aldose Reductase in its fully (per)deuterated form. The experiment was an unqualified success, with high cell density growth in only 1.5 litres of deuterated minimal media producing ~100mg of labelled protein. The D-labelled protein is now being crystallised for neutron crystallography studies on LADI. The ability to locate the hydrogen atoms of interest and thus define the protonation states of many side chains including the active site groups should help in the design of better drugs.

The Deuteration Laboratory as part of the Partnership in Structural Biology (PSB) Programme

On November 15th, ILL signed a Memorandum of Understanding with the ESRF, EMBL and the Institut de Biologie Structurale establishing the Partnership for Structural Biology. This project to create a centre of excellence will be marked by the construction of a new building providing laboratories for cloning, gene expression and purification of biological macromolecules and will also have specialised rooms for the operation of, for example, fermentors. With completion expected in 2004 the present Deuteration Laboratory will expand into this building which will be constructed alongside the present ILL20/EMBL.

The provision of isotopically labelled and deuterated macromolecules will greatly enhance both the quality and quantity of experiments that can be done using neutron scattering at ILL and NMR at IBS, and in many cases will make feasible new and more sophisticated experiments than can presently be performed. More information can be obtained at http://psb.esrf.fr/

Members of the ILL user community may apply to use the Deuteration Facility through a peer review process. The facility, under the direction of Dr Michael Härtlein (ILL) with the technical support of Benoit Gallet (ILL), functions in much the same way as an ILL instrument. (for further details see: http://www.ill.fr/pages/science/User/UProposals.htm#anchordeut)

Small is beautiful

The Scientific Council in April discussed in detail the scientific case for the horizontal reflectometer (proposed by Bob Thomas, Adrian Rennie, Robert Cubitt and Giovanna Fragneto, here in the photo) and agreed that the construction of this instrument would have a major impact on the study of free liquid surfaces and interfaces in biology and soft condensed matter.

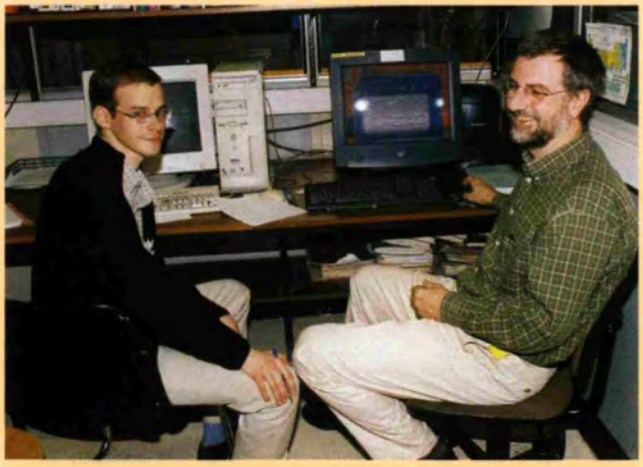

Cedric Lorthioir and Angel Alegria from San Sebastian, doing their experiment on miscible polymer blends.

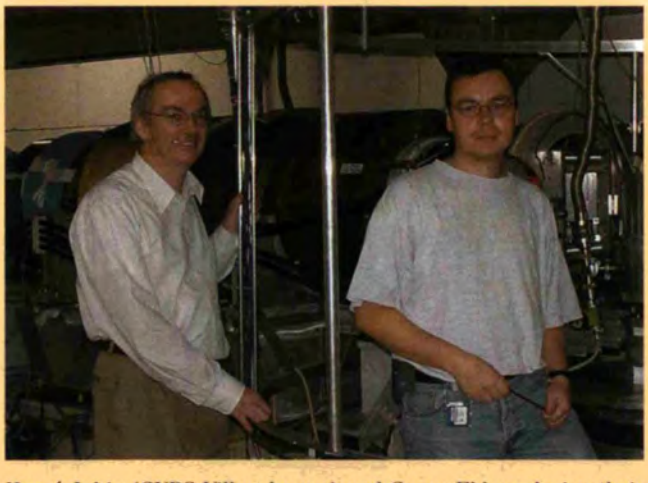

Hervé Jobic (CNRS-Villeurbanne) and Georg Ehlers during their experiment on the spin-echo machine IN11.

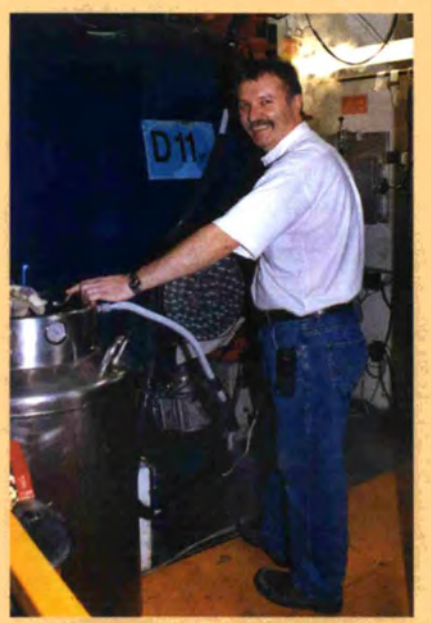

David Bowyer preparing a cryostat on D11.

Isabelle Grillo, College 9 Secretary
http:/www.ill.fr/colleges/c9/

Soft matter

Egyptians knew how to filter muddy water, Chinese were able to prepare stable inks. This empirical knowledge has crossed the centuries and gave rise to the field of research called "soft condensed matter", that investigates physical properties and structural characteristics of polymer melts or in solution, assemblies of surfactant molecules or colloidal suspensions. All these particles or aggregates have at least one dimension in the range of a few Å up to thousands of Å and may have a long-range order resulting from the fine and sensitive balance between attractive and repulsive molecular forces. Temperature, concentration and ionic strength are the main parameters governing the structures.

Mechanical, optical, rheological properties of the sample are often closely related to the size, shape and structure of the objects. With the possibility of solvent or molecular labelling, neutron technique remains a unique, non-destructive and powerful tool to explore heterogeneities in matter as well as molecular dynamics.

Around 15 instruments at the ILL are used to investigate static and dynamics features in soft condensed matter. The two small-angle scattering spectrometers (D11 and D22) covered a broad Q-range from $5x10^{-4}$ to 0.7 $Å^{-1}$ that can be extended up to 2 $Å^{-1}$ using D16. Compositions, thickness and fluctuation of interfaces are studied on D17. In parallel, transport properties, molecular motions, and dynamics of molecules are investigated on time-of-flight (IN5, IN6), backscattering (IN10, IN13, IN16) and spin-echo (IN11, IN15) spectrometers.

Progress and innovation in soft condensed matter are closely related to the development of sophisticated sample environments. Magnet, furnace, cryostat, rheometer, stopped-flow apparatus or osmotic box are regularly mounted on the instrument and the scientific users invest time to develop there own setups, as for example a polymer extruder machine specially designed for D22.

New trends also include a rise in bio-inspired problems: surfactant bilayers are viewed as models for biologic membranes, associations between proteins and polyelectrolytes offer a simplified picture for combinations in cells and knowledge in polymer science helps to understand the structure of natural fibers.

Mesoscopic (1 nm - 1µm) structures and textures are major questions in industrial processes. The highlights presented this year demonstrate the importance of neutron scattering for applied research. Model systems are used to put in evidence general rheo-behaviour related to the structure and orientation of aggregates (Förster et al.); oil lubrication is depicted within the motion of molecules (Wolff et al.) and polymer chain constraint is followed during the extrusion process (Bent et al.). Soft condensed matter is a multidisciplinary work, covering various domains of research from biology to material nanotechnology. The new ideas and technical developments combined with the always-improved instruments insure a bright future for neutron experiments.

A molecular description of extrusion

J.F. Bent, L.R. Hutchings and R.W. Richards (University of Durham)
T. Gough (University of Bradford)
I. Grillo (ILL)

Small-angle neutron scattering has been used to determine the molecular conformation of two monodisperse polystyrene melts in Poiseuille flow through a slot die. This provides a direct molecular description of a simplified extrusion process. Maximum chain deformation is seen at the die entry and this increases with flow rate but decays as the chains traverse the slot die. The deformation of the chains in the direction of melt flow relative to their unperturbed dimensions is independent of polymer molecular weight. However, the relaxation of deformation on passage through the die is molecular weight dependant and directly related to the longest relaxation time of the polymer. The consequence of this is observed at the slot die exit where the chain conformation responds to the change from contraction to expansional flow of the bulk melt.

Understanding and controlling the rheological properties of polymer melts is of huge importance in polymer processing [1] and has stimulated a multidisciplinary collaboration between UK academics and industrial partner [2]. The melt flow and mechanical properties of well defined polyethylene and polystyrene samples have been studied to test molecular models that are extensions of the Doi-Edwards tube model [3]. These numerical models consider the conformation of a single polymer chain as it travels through a stress field. The small-angle neutron scattering experiments, described herein provide the first, direct, molecular test of these theories [4].

For these experiments we developed apparatus to re-circulate polymer melt through a flow contraction by forcing the melt through a slot die, see figure 1. Details of the flow cell are given elsewhere [5] but in summary: it consists of a gear pump, flow channels and a melt reservoir to provide steady, pressure driven flow in an inert atmosphere over a range of flow rates. The experiments were conducted on D22 where the highest flux of neutrons is available. Data collection times were as short as possible in order to avoid sample degradation. The neutron path length was 10 mm, this large dimension being necessary to minimise contributions from wall effects. Consequently, the polymer melt was a matrix of deuterated polymer 'doped' with hydrogenous polymer of identical molecular weight. Beam dimensions of 5x1 mm were used to measure the scattering as the melt (at 200 °C) flowed into, through and out of the die.

Figure 1 shows the isotropic scattering from the flowing melt upstream of the die, this is identical to that from a thin plaque (1mm) of the same material. The radii of gyration, obtained by fitting the data with the Debye function, are equal and the same as that for a quiescent melt of the same molecular weight [6]. This is an important result

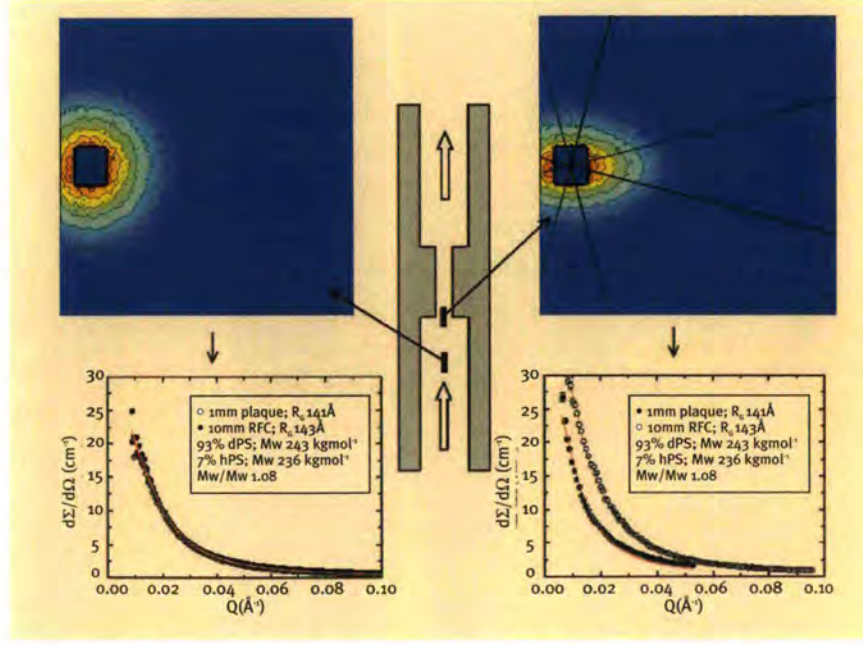

Figure 1: Whole chain scattering during polymer melt flow through a slot die.

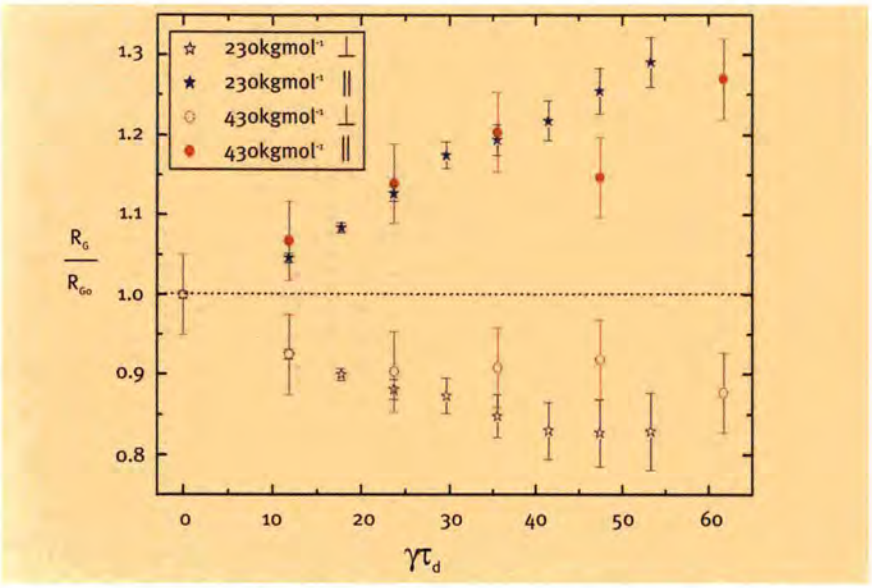

Figure 2: Polymer chain deformation at the slot die entry for increasing flow rates.

because it demonstrates that the scattering through the thick flow channel is not compromised by multiple scattering. Figure 1 also shows the oblate scattering from the flowing melt at the die entry. This is the first direct observation of chain deformation as bulk flow contracts. We have quantified this by fitting radial averages of the scattering, taken over sectors parallel and perpendicular to the direction of flow, with approximations of the Debye function (using Zimm and Kratky plots). However, this is not our final analysis, because the accuracy of the fits deteriorates as the chains deform from a Gaussian distribution with increasing flow rate. Further analysis is ongoing, using the models referred to above to generate contour plots of the scattering. Our analysis highlights the increase in chain deformation with flow rate, moreover, the relative deformation is comparable in samples with very different molecular weights. This is shown in figure 2, where the ratio of the deformed radius of gyration to its quiescent value is plotted against the product of the shear rate and the reptation time [7]. This result is in good qualitative agreement with the molecular models, which are being improved with the aid of this data.

However, our most dramatic observation is the response of the chain as it flows through the contraction. The chains are unperturbed upstream of the die, but then experience maximum deformation at the die entrance. This relates directly to a maximum in the principle stress difference, as measured for the same material and the same geometry using stress birefringence. The chain deformation then decays as it flows through the die. This rate of decay is dependant on the polymer molecular weight, see figure 3. At the die exit, where the magnitude of the orthogonal stress vectors is inverted, the deformation of the high molecular weight chains decreases significantly whilst the deformation of low molecular weight chains inverts in response to the change from contraction to expansional flow. Ultimately, the chains relax to their unperturbed, isotropic dimensions downstream from the die exit. This is the first molecular description of a model polymer during melt flow.

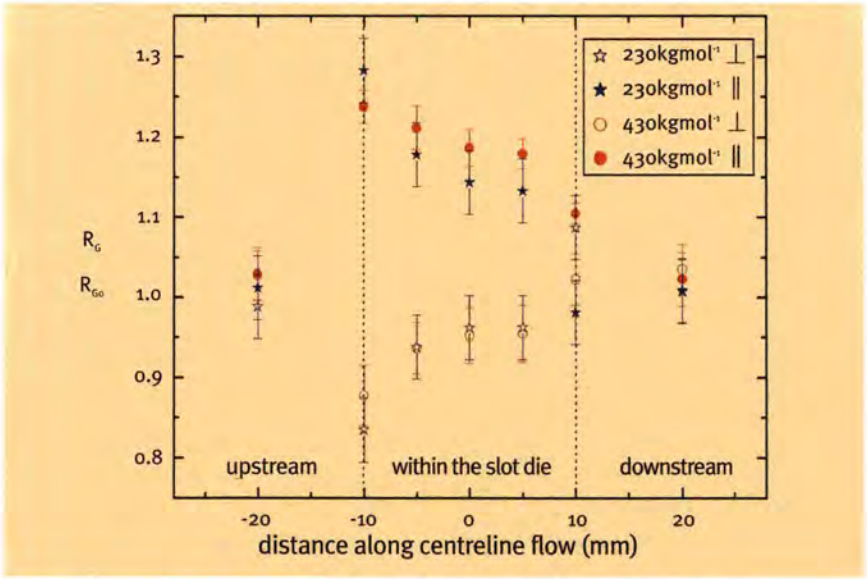

Figure 3: Polymer chain deformation during fast melt flow through the slot die.

REFERENCES

[1] H.J.M. Hanley, Curr. Opin. Colloid Interface Sci. 2 (1997) 635
[2] http://irc.leeds.ac.uk/mupp/
[3] M. Doi and S.F. Edwards, The theory of polymer dynamics. Oxford University Press (1986)
[4] A.E. Likhtman, T.C.B. McLeish, Macromolecules 35 №16 (2002) 6332
S.T. Milner, T.C.B. McLeish, A.E. Likhtman, J. Rheol. 45 №2 (2001) 539
A.E. Likhtman, S.T. Milner, T.C.B. McLeish, Phys. Rev. Lett. 85 №21 (2000) 4550
[5] J.F. Bent, T. Gough, L.R. Hutchings, R.W. Richards and I. Grillo, Rev. Sci. Inst. (in progress)
[6] J.P. Cotton, D. Decker, H. Benoit, B. Farnoux, J. Higgins, G. Janninck, R. Ober, C. Picto and J. des Cloizeaux, Macromolecules 7 №6 (1974) 863
[7] P.G. de Gennes, Scaling concepts in modern physics, Cornell University Press (1979)

Dynamics of lubricants: *anisotropy of diffusion in a liquid and surface slip under shear*

M. Wolff and A. Magerl
(University of Erlangen-Nürnberg)
H. Zabel (Ruhr University, Bochum)
M. Gonzales and B. Frick (ILL)

Lubrication is an old but nevertheless barely understood phenomenon in physics. The large incoherent scattering cross section of hydrogen makes neutrons a very sensitive tool for an investigation of dynamics in liquids. Special shear devices have been constructed, adapted for studies on high resolution inelastic spectrometers and reflectometers. On IN16 surface slip has been found for the macroscopic velocity distribution of a motor oil. In addition, within the same measurement the microscopic diffusion has been observed to become anisotropic under shear.

The well known painting from a grotto at El-Berhed (dated about 1880 B. C.) shows that already the Egyptians used olive oil as a lubricant to make the transport of heavy loads easier. Significant progress has been made since then but many questions relating to lubrication remain unsolved up to now and in particular a fundamental understanding of lubrication on an atomic scale is still in its infancy. Considering the large penetration power of neutrons for engineering materials and the dominant incoherent scattering cross section of hydrogen contained in most liquid lubricants, neutrons appear as an excellent tool to investigate the dynamics of liquids under conditions relevant for applications.

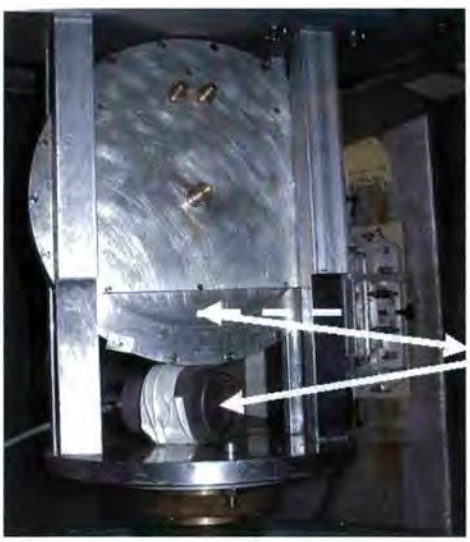

Figure 1: Shear device for quasielastic and inelastic neutron scattering studies mounted on IN10 (The white arrows mark the neutron path, the dashed line is before the sample and the solid line represents neutron beams from sample to analyser and back to detector).

To bring about such investigations with neutron backscattering a special plate-plate shear device has been developed. Figure 1 shows this cell mounted on IN10. A standard viton radial shaft packing is used to seal the liquid compartment. It allows shear rates of up to 5000 1/s for a minimum disc spacing of 0.3 mm to reduce multiple scattering. Neutrons from the monochromator (white dashed arrow) are scattered by the sample. After backreflection by the analyser they are counted in the detector underneath the shear device. To achieve high energy resolution the detector has to be close to the neutron window of the shear device.

Figure 2 shows spectra from an experiment on IN16: for the empty shear device (where the discs had been covered with a strong scatterer-sticky tape to make them visible) (a-d) and for a commercial motor oil ANTAR (e-h) in transmission and reflection geometry either with and without shear (e-h). Two spectra (a-b) with the shear device stationary and spectrum (c) with the shear device rotating in reflection geometry (momentum transfer Q perpendicular to the flow) show a similar line width of 1.2 μeV. These spectra are used to determine the resolution of the experimental set-up. Inelastic Doppler scattered neutrons become visible in a fourth spectrum (d) which was taken in transmission geometry (momentum transfer parallel to the flow) with one disc rotating. The width of this peak is slightly broadened because it averages the velocities of the driving disc over the finite beam size. The position at 8.5 μeV represents directly the velocity of the disc being v_m = 1.8 m/s. The different intensities originate from a different coverage of the discs by sticky tape and have no further implications. The spectra for the ANTAR oil (e-h) have been fitted by appropriate scattering laws. Without shear in both geometries a similar Lorentzian line width of about 4.1 μeV is found prooving an isotropic diffusion. Under shear the line broadens clearly in reflection geometry to 5.2 μeV showing an acceleration of diffusion. In transmission geometry the spectrum is dominated by the inelastic scattering from the flowing liquid. This contribution to the scattering law is appropriately described by a velocity distribution with a surface slip of 0.15 v_m and 0.3 v_m at the stationary and at the moving disc, respectively. This asym-

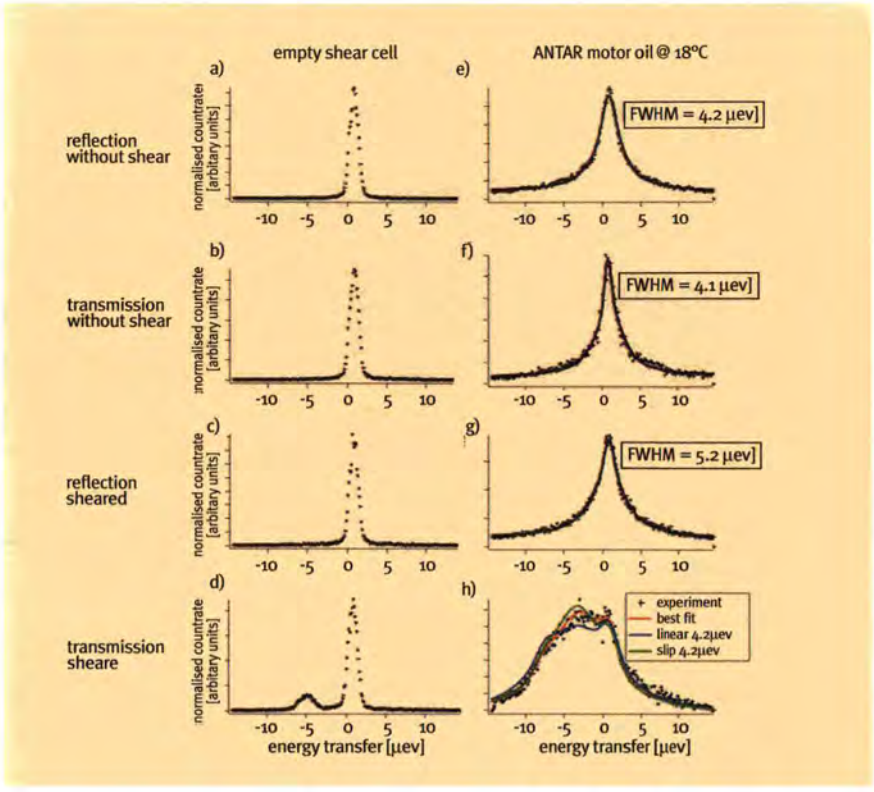

Figure 2: Backscattering spectra obtained at IN16 (ILL). The left side shows spectra of the empty cell with the aluminium discs covered with tape to make them visible. The right side (e-h) shows data for a sample of the commercial motor oil ANTAR at 18°C. In addition to the information about diffusion processes from quasielastic scattering also inelastic scattering representing the macroscopic flow profile is visible.

metry of slip is probably due to a slight dynamic unbalance at the rotating disc. A fit of the quasi elastic contribution results in a line width of 4.2 µeV quite similar to the line width without shear. This result shows that diffusion becomes anisotropic under shear.

Figure 3 shows calculations considering contributions to the scattering from (i) the molecular diffusion by a Lorentzian line convoluted with an assumed Gaussian instrumental resolution function (ii) a velocity distribution function for the inelastic part of the spectrum and (iii) corrections for the relaxed Q-resolution of IN16 and the smearing of velocities due to different disc radii. The x-axis represent the energy transfer in units of the inelastic peak position from the rotating disc and the y-axis represent the quasielastic line width for the internal diffusion in the same units. The different colours represent the difference in the scattering patterns which is shown as the local percentage value. The upper panel shows the difference in the energy spectrum between a linear velocity distribution (upper right) from the fixed to the moving surface and a velocity distribution with a surface slip (bottom right) of 50% at each boundary (this is equivalent to a liquid layer with no internal shear gradient). For statistics with error bars smaller than 10% a distinction between the two scenarios is possible if the quasielastic line width is not larger than the energy value of the inelastic peak position. The lower panel shows the difference of a linear velocity distribution with a quasielastic line width of 1 (in units of the inelastic peak position) and a distribution with surface slip and quasielastic line widths between 0 and 2. It follows that the line widths can be determined from experimental data with an estimated error of 10%.

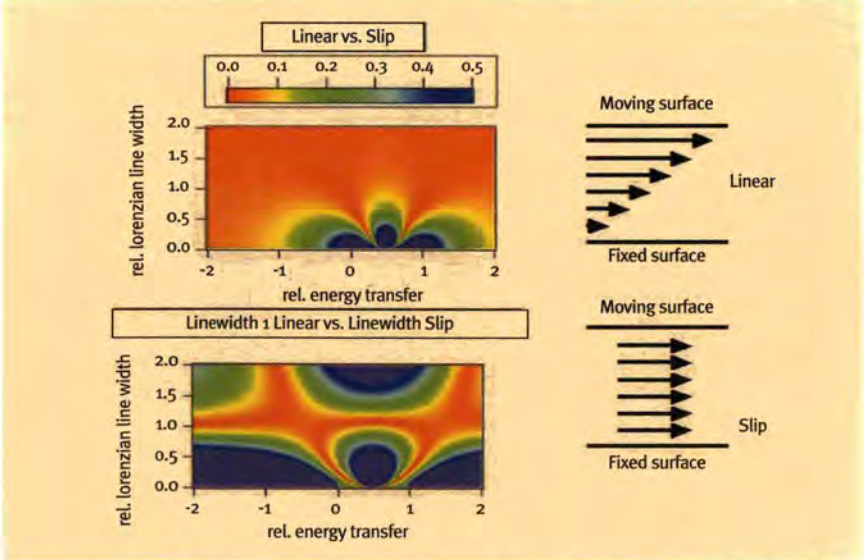

Figure 3: Contour maps of the difference in intensity distributions between simulated quasielastic spectra. Details are given in the text.

In summary, we have shown that high resolution neutron spectroscopy is an excellent tool to observe simultaneously the macroscopic flow and the microscopic diffusion of lubricants occurring on time and length scales which differ by many orders of magnitude. Such measurements are well suited to contribute to an understanding of lubrication on a molecular level.

Acknowledgement

This study was financially supported by the DFG project Ma 801/4 and ZA 161/17.

Shear thinning *and orientation of wormlike micelles*

S. Förster and M. Konrad
(University of Hamburg)
P. Lindner (ILL)

Small-angle neutron scattering experiments under shear flow (Rheo-SANS) were used at the newly developed set-up at D11 to follow the structural changes of solutions undergoing shear-thinning. In the experiments solutions of wormlike micelles were used that exhibit pronounced shear-thinning over a wide range of shear rates. The experiments show that shear-thinning is directly related to shear-orientation of the micelles. The data allowed a detailed analysis of the orientational distribution of the micelles as a function of shear rate and revealed characteristic features of the molecular orientation process.

Many fluids such as polymer and surfactant solutions display complicated rheological properties. The viscosity may decrease with increasing shear rate ("shear thinning") or increase ("shear thickening") [1,2]. Many industrial processes are concerned with these properties, for example in paints, lubricants, drag reducers, personal care products, and in many fluids that have to be pumped and/or extruded at some point of their processing. Despite their technical significance, the molecular origin of this complex rheological behaviour is quite poorly understood. To explain these phenomena, it is important to determine the particle motion, structure and orientation as well as the large-scale mechanical properties simultaneously in an experiment.

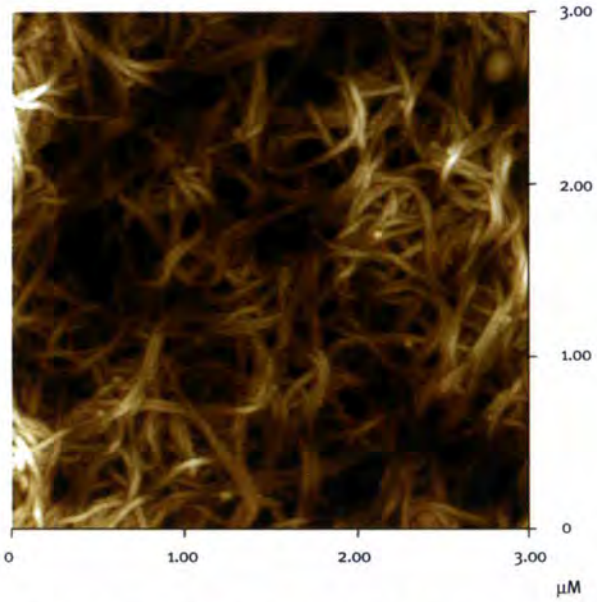

Figure 1: AFM-image of wormlike block copolymer micelles used in the experiment.

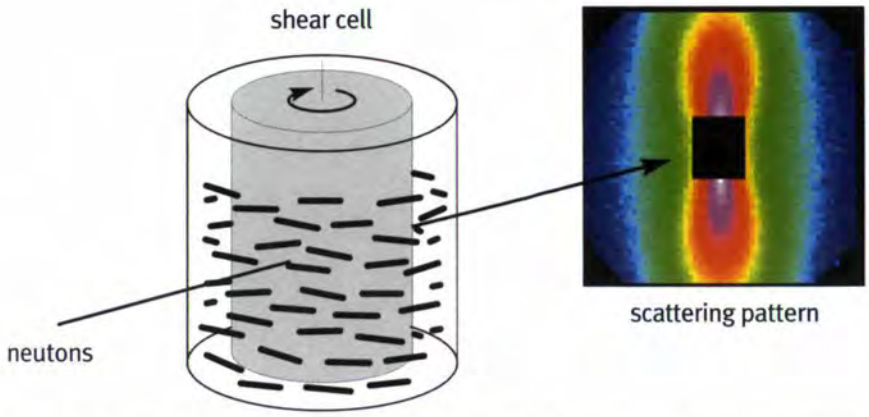

Figure 2: Shear orientation of micelles in a shear cell with the corresponding SANS-pattern.

The penetration of neutrons through both solution and flow cell allows the investigation of changes in particle structure and orientation during shear. In the newly developed rheo-SANS set-up at D11 scattering patterns can be measured while the solution is sheared in a Bottlin CVO rheometer that allows simultaneous measurement of the shear viscosity. In these experiments solutions of wormlike block copolymer micelles were used

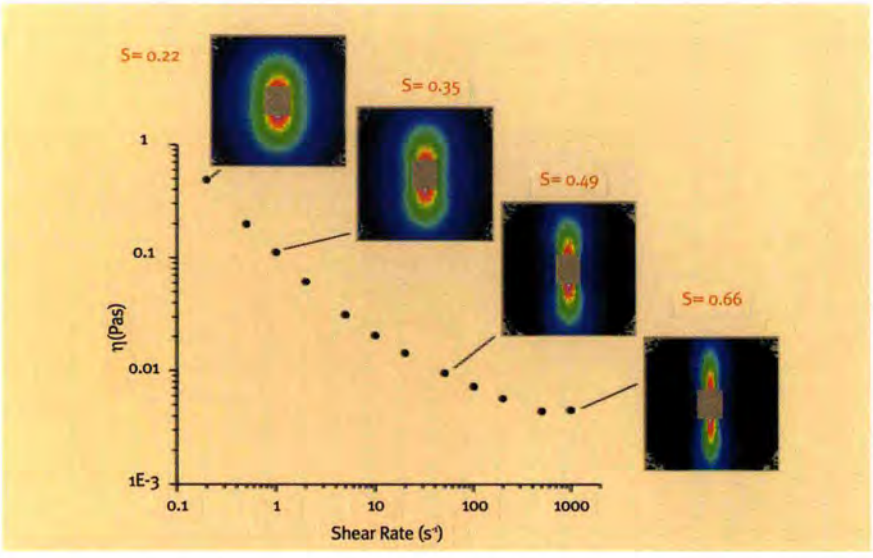

Figure 3: Decrease of the shear viscosity η with increasing shear rate ("shear thinning") together with the simultaneously measured SANS-patterns.

having diameters of the order of 10 nm and lengths of several mm (see figure 1). The micelles orient in the direction of shear which leads to a characteristic anisotropic scattering pattern as shown in figure 2.

The decrease of the viscosity with increasing shear rate ("shear-thinning") is shown in figure 3 for a 10% w/w solution. The shear viscosity decreases by a factor of 100 thereby developing a pronounced anisotropy of the scattering pattern. The scattering patterns can be quantitatively analysed by taking into account the form factor of cylindrical micelles with an Onsager-type orientational distribution, from which the order parameter S can be calculated [3]. The order parameters at various shear rates are also shown in figure 3.

The relation between shear viscosity and order parameter reveals important features of the molecular orientation processes. As seen in figure 4 for all solutions investigated, irrespective of micellar thickness and concentration, there are two characteristic regimes (two different slopes) that relate to different ordering mechanisms. They are identified as the alignment of either single micelles or whole nematic domains by the external shear force.

Rheo-SANS is a powerful technique that can be used to obtain a detailed molecular picture of the structural changes of complex fluids under shear. As is shown in the present study, the shear-thinning behaviour of wormlike micelles can be directly related to shear orientation. A quantitative data analysis is possible allowing the orientational distribution of the micelles to be obtained. Despite the complexity of such systems, there appears to be a simple relation between shear viscosity and orientation. This enables a better prediction of rheological properties for many technically relevant fluids.

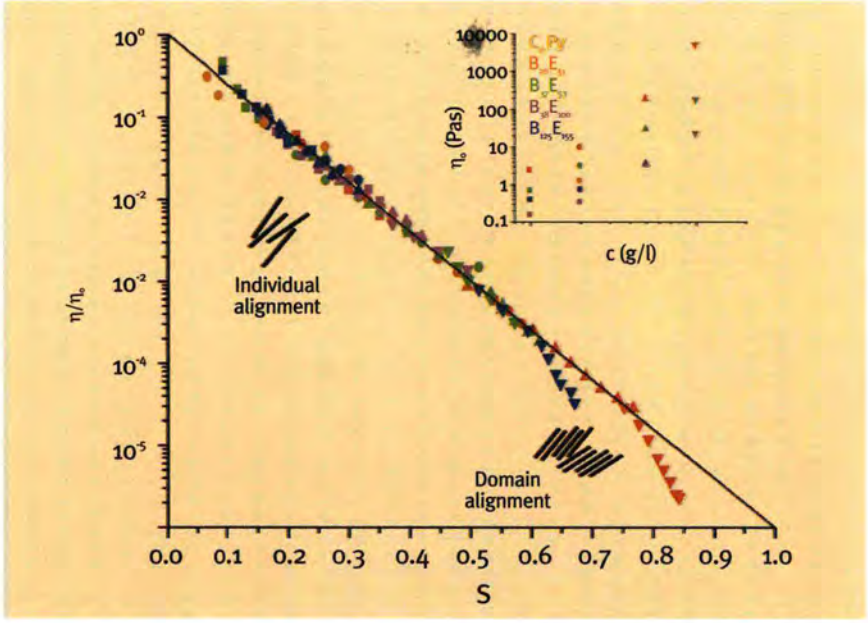

Figure 4: Relation between shear viscosity h and order parameter S for various micellar solutions. The data indicate two characteristic orientation mechanisms.

REFERENCES

[1] H. Thurn, J. Kalus and H. Hoffmann, J. Chem. Phys. 80 (1984) 3440
[2] M.E. Cates, J.S. Candau, J. Phys.: Condens. Matter 2 (1990) 6869
[3] S. Förster, M. Konrad, P. Lindner, in preparation

Back to fundamentals

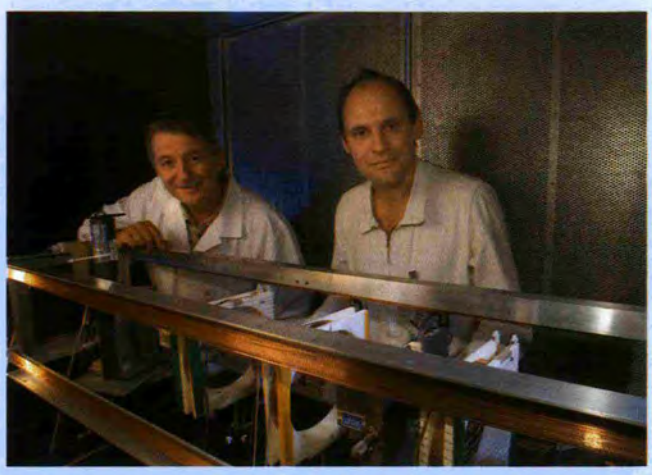

Peter Geltenbort (left) and Thomas Brenner verifying the alignment of the Very Cold Neutron Spin Interferometer (VCNSI) at the PF2/VCN beam position.

The set-up used by Valery Nesvizhevsky and his team for the detection of quantised states of neutrons in the gravitational field of the earth.

Hans Börner on the high precision angle interferometers of the spectrometer GAMS5.

Torsten Soldner preparing the cold polarized beam PF1 for an experiment.

Gary Simpson, College 3 Secretary

Fundamental and nuclear physics

The nuclear and particle physics group members investigate an extremely broad range of physical phenomena, including atomic, nuclear and particle physics. Experiments span a huge range in energy, from 10^{-19} eV to 0.1 GeV, and involve all four fundamental forces (strong, weak, electromagnetic and gravitational). A distinctive feature of some of the experiments requires that the whole instrument is reconfigured. The nuclear and particle physics group manage to perform quality experiments in fundamental areas of physics, at a fraction of the cost of experiments at other nuclear and particle physics labs. The experimental techniques used in this group are completely different to any others used at the ILL.

The Lohengrin (PN1) mass separator provides beams of exotic radioactive ions for studies of the structure of the nucleus and for experiments on the fission process. The installation of an array of borrowed germanium detectors at the focal point of the Lohengrin fission-fragment spectrometer took place this year. This will allow the structure of exotic neutron-rich nuclei to be investigated by gamma-ray spectroscopy. The detectors were borrowed from the Anglo-French Eurogam loan pool. Several new isomeric states were found in the region around the exotic doubly-magic neutron-rich nucleus ^{132}Sn. These states, and information from the states below the isomer allows the nuclear shell model to be tested. Nuclear shell-gaps are expected to be reduced in very neutron-rich regions.

The ultra-high resolution GAMS spectrometers (PN3) very accurately measure the energy of gamma-rays emitted by the nucleus during neutron-capture reactions. This allows the structure of nuclei in the target to be probed. The stability of the GAMS5 spectrometer (already the world's most precise gamma-ray spectrometer) has been improved this year and the uncertainties introduced into an experiment are now as low as 10^{-7}. Recent test measurements have shown that lifetimes of excited nuclear states can be determined by measuring the Doppler broadening of gamma rays following beta decay.

The PF1 cold-neutron facility gives users an intense beam of cold neutrons. Highlights this year include the development of techniques to polarize neutrons. A polarization of 99.6 %, and a spin-flip efficiency of 99.9 %, was achieved. It is believed that these results can be further improved upon. Production of highly polarized cold neutron beams allows considerable improvements to be made in the study of neutron beta-decay, and will help to improve the precision in determining neutron-decay asymmetry coefficients.

The PF2 ultra-cold-neutron facility produces several beams for use in fundamental physics problems, which are mainly focussed in searching for effects beyond the "Standard Model" in particle physics, which are known to exist. Some of these experiments include measurements of the neutron lifetime and measurements of the electric-dipole moment (EDM) of the neutron. The later experiment is one of the most precise experiments in all of science, with the limit of the size of the neutron EDM now known to be less than 6×10^{-26} e.cm. The measured lower limit of the neutron EDM can show that some particle physics theories are invalid.

Trine - a new limit *on time reversal violation in neutron decay*

T. Soldner (ILL)
L. Beck (LMU München)
C. Plonka, K. Schreckenbach, O. Zimmer (TU München)

The *D* coefficient in the free neutron decay was measured with unprecedented precision. This puts a new limit to a possible violation of time reversal invariance in neutron beta decay.

Whereas in daily life the direction of time is defined by thermodynamics – coffee is only becoming colder – most fundamental interactions are invariant under time reversal T. This holds for gravitational, electromagnetic and strong interaction. For weak interaction, however, a tiny violation of T invariance was observed in 1998. It is connected via the CPT theorem to a violation of CP, the combination of charge conjugation C (exchange of particles and antiparticles) and parity P (inversion of space), which was discovered earlier.

The tiny CP and T violations as well as the "maximal" violations of C and P found in weak interaction are implemented in the Standard Model of particle physics, but the deeper origin of these violations is not yet understood. Furthermore, the observed excess of matter over antimatter in the universe ("baryon asymmetry") requires an even stronger CP violation. Theories are wanted that both explain us the Standard Model and open new channels for CP violation.

To examine these theories, new CP or T violating processes have been chased in various systems. Using neutrons, two ways are exploited: The quest for the electric dipole moment (EDM) and the pursuit of time reversal violating correlations between the decay particles such as the triple correlation *D* we have measured. These two approaches are complementary: Whereas the neutron EDM is established as a working horse in this field, the observation of a T violating effect in the decay has a more direct theoretical interpretation and is more sensitive to some models like leptoquarks which appear in grand unified theories [1]. One should note, however, that in the decay a T violating signal is simulated by interactions between the decay products. But this can be completely neglected at the present experimental precision.

The free neutron decays with a lifetime of 885.7(8) s [2] into proton, electron and antineutrino:

$$n \rightarrow p + e + \bar{\nu}. \quad (1)$$

	Year	Reactor	Events [10^6]	Signal/ Background	D [10^{-3}]
[4]	1976	ILL	6	4	-1.1±1.7
[5]	1978	IAE	2.5	2.2	2.2±3.0
[6]	2000	NIST	15	2.5	-0.6±1.2±0.5
Trine	2000	ILL	30 (13.5 used)	23	-0.31±0.78±0.47

Table 1: Comparison of the latest *D* measurements.

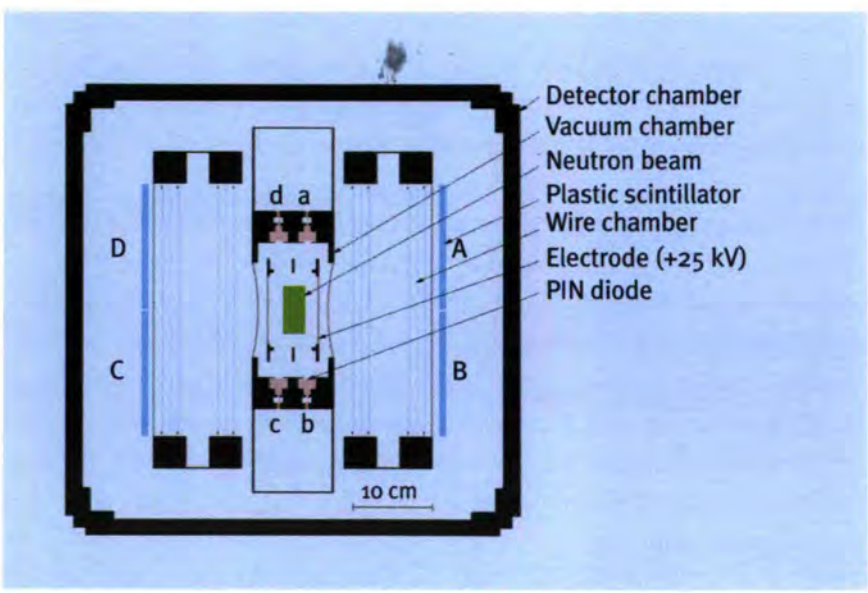

Figure 1 : Cross section of the Trine detector. The neutron polarization is perpendicular to the plane of the drawing and inverted every three seconds. The electrode accelerates and focuses the proton prior to detection in a PIN diode. The full detector consists of 64 PIN diodes in 16 planes (see figure 2).

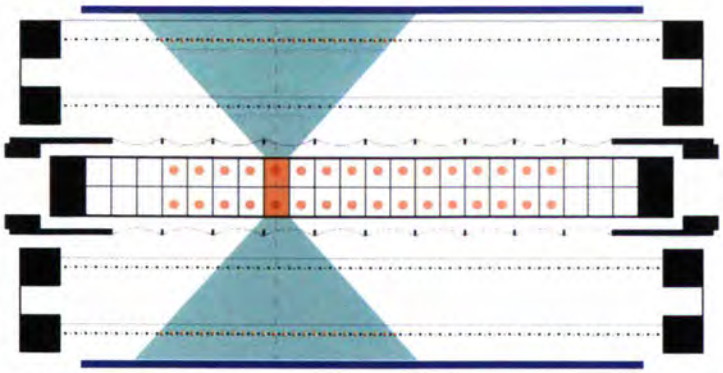

Figure 2 : Top view of the detector. Using the wire chamber signal, the electron detector can be restricted to an area symmetric to the PIN diode hit. This suppresses the influence of the A and B coefficients.

For polarized neutrons, the correlation between the decay products is described by in total 5 coefficients, a (electron-antineutrino-correlation), b (Fierz interference term), A (beta asymmetry), B (antineutrino asymmetry), and D [3]:

$$dW \alpha 1 + a\frac{\mathbf{p}_e\mathbf{p}_\nu}{E_eE_\nu} + b\frac{m_e}{E_e} + \frac{\langle\boldsymbol{\sigma}_n\rangle}{\sigma_n}\left(A\frac{\mathbf{p}_e}{E_e} + B\frac{\mathbf{p}_\nu}{E_\nu} + D\frac{\mathbf{p}_e\times\mathbf{p}_\nu}{E_eE_\nu}\right). \quad (2)$$

Under T, the neutron spin $\boldsymbol{\sigma}_n$ and the momenta $\mathbf{p}_i$ of electron e and antineutrino ν change their sign, resulting in a change of sign of the triple product $\boldsymbol{\sigma}_n(\mathbf{p}_e\times\mathbf{p}_\nu)$. $D \neq 0$ would therefore indicate T violation. Beta and antineutrino asymmetry are related to P violation and well understood within the Standard Model; the associated coefficients A = -0.1162(13) and B = 0.983(4) are large compared to the present experimental world average for $D = -0.6(1.0)\cdot10^{-3}$ [2] which is still compatible with 0.

A precise measurement of D faces three principal difficulties: 1) a huge number of decays has to be detected to obtain sufficient statistical precision, 2) the detection of the decay proton (needed to trace the undetectable antineutrino) is particularly difficult due to its low energy (maximal 750 eV), and 3) the influence of the coefficients A and B has to be suppressed carefully to avoid systematic errors.

The particular features of the Trine detector (figure 1) are its high segmentation, the efficient proton detection by special PIN diodes, and the use of multi wire proportional chambers for background suppression and systematic tests (figure 2). The data analysis bases primarily on the electron-proton time-of-flight spectra (figure 3) for both neutron spin directions, which are measured simultaneously for each of the 4x64 detector combinations. The properties of the detector were studied experimentally and by Monte Carlo simulations. Our preliminary result is $D=(-3.1\pm7.8^{stat}\pm4.7^{syst})\cdot10^{-4}$. The systematic error originates from an asymmetric beam profile caused by the polarizer and detector inhomogeneities in combination with the limited precision for the alignment of the neutron polarization. The latest D measurements are compared in Table 1.

In the next step, we will improve statistical sensitivity and systematics of our set-up. A measurement with an enlarged detector and an improved neutron beam (instrument PF1b with 4 times higher flux and a new homogeneous polarizer) is scheduled for 2003.

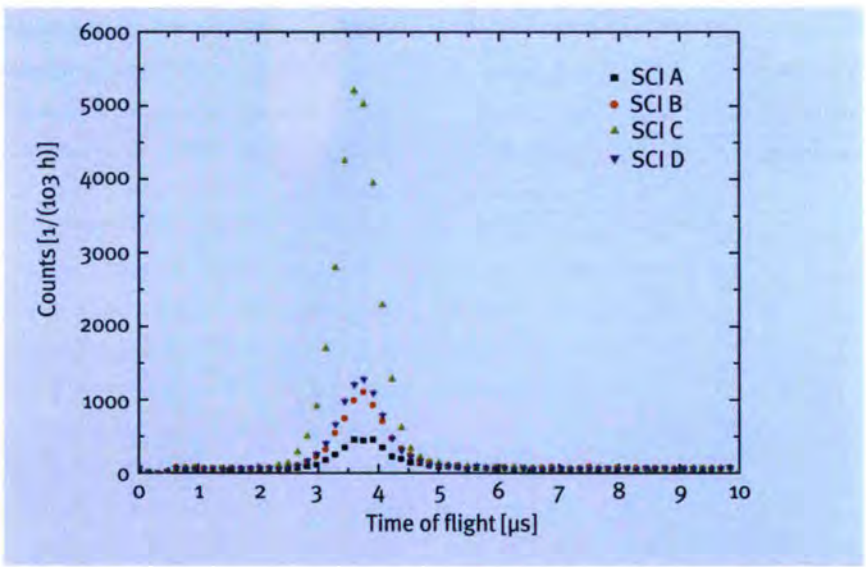

Figure 3 : Time-of-flight spectra (electron: start, proton: stop) for one PIN diode (row a) and the 4 scintillators. The different count rates are caused by kinematics that prefers large angles between electron and proton. The coincidence count rate of the full Trine detector at PF1 was 10 s^{-1}.

REFERENCES

[1] P. Herczeg, Prog. Part. Nucl. Phys. 46 (2001) 413
[2] K. Hagiwara et al. (Particle Data Group), Phys. Rev. D 66 (2002) 010001
[3] J.D. Jackson et al., Phys. Rev. 106 (1957) 517
[4] R.I. Steinberg et al., Phys. Rev. D 13 (1976) 2469
[5] B.G. Erozolimskii et al., Sov. J. Nucl. Phys. 28 (1978) 48
[6] L.J. Lising et al., Phys. Rev. C 62 (2000) 055501

Quantum states *of neutrons set limits for non-Newtonian interaction*

H. Abele (University of Heidelberg)
A. Westphal (Desy, Hamburg)

Quantum states in the Earth's gravitational field can be observed, when ultracold neutrons fall under gravity. In an experiment at the Institut Laue-Langevin in Grenoble, neutrons are reflected and trapped in a gravitational cavity above a horizontal mirror. The quantum states probe Newtonian gravity on the micrometer scale and we place limits for gravity-like forces in the range between 1 µm and 10 µm.

Quantum physics is a fascinating but subtle subject. The subtlety of the quantum system described here arises from the fact, that gravity appears very weak in our universe. Quantum theory and gravitation affect each other, and, when neutrons become ultra-cold, the fall experiment of Galileo Galilei shows quantum aspects of the subtle gravity force in the sense that neutrons do not fall continuously. We find them on different levels, when they come close to a reflecting mirror for neutrons [1]. Of course, such bound states with discrete energy levels are expected when the gravitational potential is larger than the energy of the particle. Here, the quantum states have pico-eV energy, a value that is smaller by many orders of magnitude compared with an electromagnetically bound electron in a hydrogen atom, opening the way to a new technique for gravity experiments, for neutron optics, neutron detection and measurements of fundamental properties.
A side-effect of this experiment is its sensitivity for gravity-like forces at length scales below 10 µm. In light of recent theoretical developments in higher dimensional field theory [2,3], gauge fields can mediate forces that are 10^6 to 10^{12} times stronger than gravity at submillimeter distances, exactly in the interesting range of this experiment and might give a signal in an improved set-up.

The idea of observing quantum effects occurring when ultracold neutrons are stored on a plane was discussed long ago by V.I. Lushikov and I.A. Frank [4]. An in some aspects similar experiment was discussed by H. Wallis et al. [5] in the context of trapping atoms in a gravitational cavity. A neutron mirror makes use of the strong interaction between nuclei and an ultracold neutron, resulting in an effective repulsive force: neutrons propagate in condensed matter in a way similar to the propagation of light but with a neutron refractive index less than unity. Thus, let's consider the surface of matter as constituting a potential step of height V. Neutrons with transversal energy $E < V$ will be totally reflected. Ultra-cold neutrons (UCN) are neutrons that, in contrast to faster neutrons, are retro-reflected from surfaces at all angles of incidence. When the surface roughness of the mirror is small enough, the UCN reflection is specular. Neutron mirrors are interesting because they can be used to store neutrons, to focus neutrons, or to build a Fabry Perot interferometer for neutron de Broglie waves.

A possible deviation from the inverse square law for gravity has been discussed in the past few years. A new effective interaction coexisting with gravity would modify the Newtonian potential. On the assumption that the form of the non-Newtonian potential is given by the Yukawa expression, for masses m_i and m_j and distance r the modified Newtonian potential V(r) is having the form

$$V(r) = -G\frac{m_i \cdot m_j}{r}\left(1 + \alpha \cdot e^{-r/\lambda}\right)$$

where λ is the Yukawa distance over which the corresponding force acts and α is a strength factor in comparison with Newtonian gravity. G is the gravitational constant. For a neutron, the gravitational force of the mass m_E of the entire earth with radius R_E lead to a free fall acceleration

$$g = \frac{Gm_E}{R_E^2} = \frac{4\pi \cdot G\rho R_E^3}{3R_E^2} = \frac{4}{3}\pi G\rho R_E$$

When a neutron approaches the mirror, the mass of this extended source might modify g, when strong non-Newtonian forces are present. For small neutron distances z from the mirror, say several micrometers, we consider the mirror as an infinite half-space with mass density ρ. The additional non-Newtonian acceleration g' as a function of distance z is given by

$$g'(z,\lambda) = 2\pi \cdot \rho\alpha\lambda G \cdot e^{-z/\lambda}$$

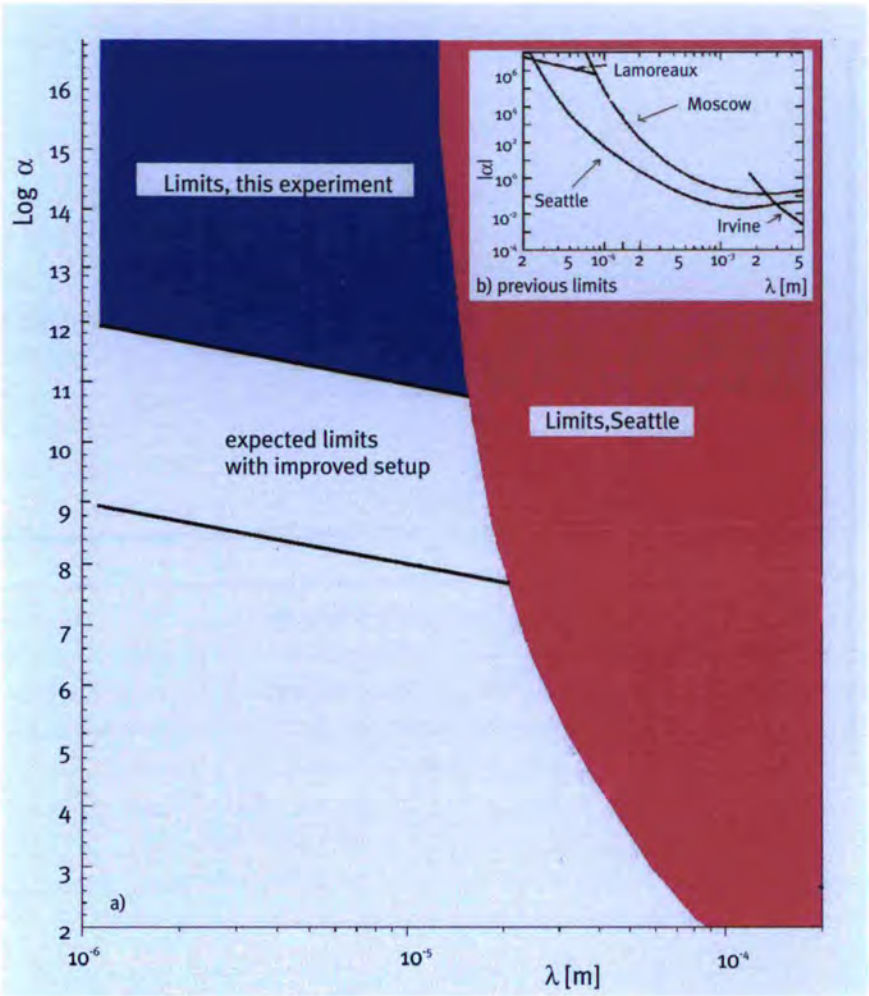

Figure 1: Limits for non-Newtonian gravity: Strength α vs. Yukawa length scale λ
a) Experiments with neutrons place limits for |α| in the range 1 μm < l < 10 μm.
b) Constraints from previous experiments [9-12] are adapted from [12].

As a consequence, the ratio is

$$\frac{g'}{g}(z,\lambda) = \frac{3}{2}\,\alpha\cdot\frac{\lambda}{R_E}\cdot e^{-z/\lambda}$$

For $z = \lambda = 10$ μm and $\alpha = 1$, the ratio g'/g is about 10^{-12}. Figure 1a shows the present status of an experimental search for gravity-like forces below 10 μm. The results of a fit of a modified Newtonian potential to the measured data yields predictions for 90% confidence level exclusion bounds on α and λ. These limits from neutron mirror experiments are the best known in the range 1 μm < λ < 3 μm and exclude for the first time gravity-like short-ranged forces at 1 μm with strength $\alpha > 10^{12}$ and at 10 μm with strength $\alpha > 10^{11}$ (figure 1a). Previous constraints [9-12] on both α and λ are shown in insert b.

One of the great challenges today is to unify the known fundamental forces in one theory. A consistent theory of gravity and quantum mechanics is still missing. A promising attempt are superstring theories in which a deviation from the 1/r Newtonian potential is introduced for small distances. In the language of high energy particle physics, the Planck scale, the scale where gravity and other forces are comparable, has been brought to the TeV scale, the scale of the Standard Model of particle physics. At the expected sensitivity, a number of gravity-like phenomena emerge. For example, a hypothetical gauge field can naturally have miniscule gauge coupling $g_4 \sim 10^{-16}$ for 1 TeV, independent of the number of extra dimensions [3]. If these gauge fields couple to a neutron with mass m_n, the ratio of the repulsive force mediated by this gauge field to the gravitational attraction is [3]

$$\frac{F_{gauge}}{F_{grav}} \sim \frac{g_4^2}{Gm_n^2} \sim 10^6\left(\frac{g_4}{10^{-16}}\right)^2$$

With $g_4 = 10^{-16}$ as a lower bound, these gauge fields can result in repulsive forces of billion or triillion times stronger than gravity at micrometer distances. This is exactly in the range which becomes accessible with these new experiments.

REFERENCES

[1] V. Nesvizhevsky et al., Nature 415 (2002) 297
[2] N. Arkani-Hamed, S. Dimpoulos, G. Dvali, Phys. Lett. B 429 (1998) 263
[3] N. Arkani-Hamed, S. Dimpoulos, G. Dvali, Phys. Rev. D 59 086004 (1999)
[4] V.I. Luschikov and A.I. Frank, JETP Lett. 28 (1978) 559
[5] H. Wallis et al., Appl. Phys. B 54 (1992) 407
[6] C.G. Aminoff, A.M. Steane, P. Bouyer, P. Desbiolles, J. Dalibard, and Cohen-Tannoudji, Phys. Rev. Lett. 71 (1993) 3083
[7] M.A. Kasevich, D.S. Weiss, and S. Chu, Opt. Commun. 15 (1990) 607
[8] T.M. Roach et al., Phy. Rev. Lett. 75 (1995) 629
[9] S. Lamoreaux, Phy. Rev. Lett. 78 (1997) 5
[10] J.K. Hoskins et al., Phys. Rev. D 32 (1985) 3084
[11] V.P Mitrofanov and O.I. Ponomareva, Sov. Phys. JETP 67 (1988) 1963
[12] C.D. Hoyle et al., Phys. Rev. Lett. 86 (2001) 1418

Vaporisation of ultracold *neutrons from a trap*

E.V. Lychagin, A.Yu. Muzychka, G.V. Nekhaev, A.V. Strelkov (JINR, Dubna)
D.G. Kartashov (NINP, Pisa)
V.V. Nesvizhevsky (ILL)

In 1997 we reported on the observation of an additional loss channel of ultracold neutrons (UCN), where the losses could be associated to an increase in the UCN energy ("heating") by ~10^{-7}eV, with a probability of $10^{-7} - 10^{-5}$ per collision of a neutron with a surface. We have now studied this process in detail and found that i) preceding outgasing of samples at 500-600 K leads to an increase of the "heating" probability by at least a factor of 100 on a surface of stainless steel and by a factor of 10 on a copper surface, ii) extremely intensive UCN "heating" is observed for diamond nanoparticles powder, iii) no "heating" is observed on a clean nanoparticle-free mono-crystalline sapphire surface. These findings and the comparison to theoretical expectations allow to relate this phenomenon of "heating" to inelastic scattering of UCNs by the thermal motion of nanoparticles, weakly bound to the surface. This has major consequences for storage of UCNs in material traps and opens very interesting perspectives in other fields of physics.

One of the most attractive features of ultracold neutrons (UCN) is that they can be stored in traps. The typical energy of UCNs is ~10^{-7}eV and they are totally reflected from a surface when their energy is lower than the Fermi-potential barrier of the surface material. However, so-called anomalous losses of trapped UCNs have been a puzzle for many years. To understand the loss mechanisms is very important because UCNs stored in traps are used in many experiments in fundamental physics. In particular for the loss mechanism described here (see also [1-3]), a UCN is lost if its energy exceeds the Fermi potential of the trap material (because it can then penetrate into/through the wall of the trap). This process is similar to the well-known vaporisation of molecules from the surface of a liquid. For this reason, such neutrons are called "vaporised UCN" (VUCN, see figure 1).

In order to investigate the origin of VUCNs, we constructed a big gravitational spectrometer. This spectrometer can simultaneously detect stored UCN and formed VUCN with broader energy range (50-150 neV) with higher efficiency (50%) than before. The spectrometer volume can be heated up to 600 K or cooled down to 80 K. Details of the spectrometer are described elsewhere [4]. It allows to shape the spectral distribution of neutrons by placing an absorber at a given height in the spectrometer, so that neutrons cannot jump over a well-defined gravitational barrier. Figure 2 shows the typical time dependence of the detector count rate with various samples. When filling the spectrometer, neutrons with energies higher than the gravitational barrier can penetrate into the detector. Then, after closing the input valve, these neutrons are rapidly eliminated by the absorber and the detector count rate decreases steeply. After this "cleaning process" the absorber is lifted upwards and this enables that VUCN - neutrons which have changed their energy due to interaction with the surfaces of samples and/or spectrometer walls - can survive and be counted in the detector. Therefore, the detector count rate rises until equilibrium is reached. Finally, the absorber is moved back down again, and the detector count rate falls down to the background value.

For the first time, the integral VUCN spectrum was measured with an accuracy sufficient to calculate the differential spectrum. We have established that the probability of this «heating» of UCNs depends on details of the preparation of, for instance, stainless steel samples. Indeed, preceding heating of samples at a temperature of 500-600 K increased the probability of "heating" of UCN by a factor of ~100! Independent measure-

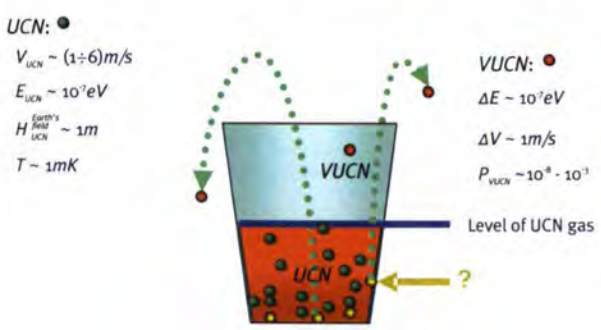

Figure 1: Illustration of losses of UCN from a trap via VUCN production. The typical parameters of UCN (velocity, energy, rising height in the gravitational field, temperature) and VUCN production (change in energy, in velocity, the probability) are shown on the picture.

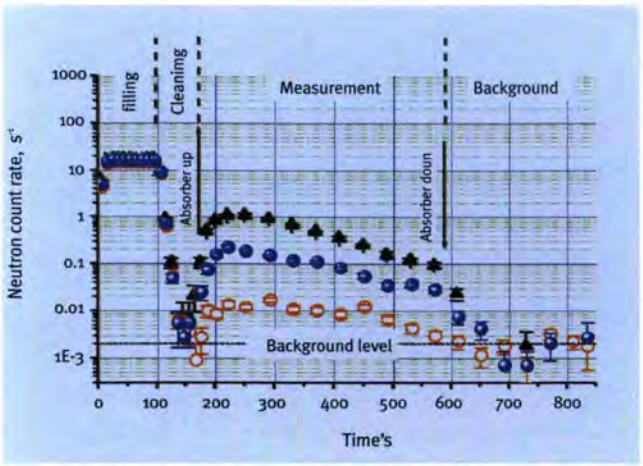

Figure 2: Neutron count rate for different samples: measurements (o) on surface of empty copper spectrometer, (•) with stainless steel samples, and (Δ) with diamond nanoparticles powder. The dashed line shows the background level.

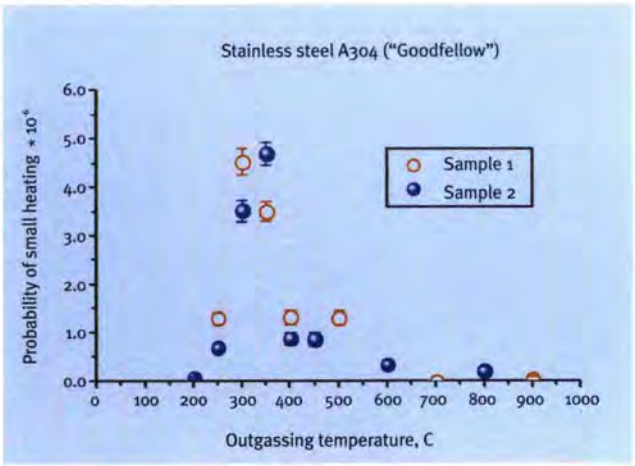

Figure 3: Probability of the small heating of UCN as a function of the outgasing temperature for two stainless steel samples.

ments with identical samples indicate that this result is well reproducible (see figure 3). Measurements with an atomic-force microscope showed that the nanostructure of stainless steel surfaces experience a strong change (formation of nanoparticles) just at those temperatures. A similar abrupt increase in the probability of heating (by a factor of ~10) after heat treatment was also observed for the interaction of UCN with a copper surface. It should be noted that baking of traps and samples up to these temperatures is the routine preparatory procedure in UCN storage experiments.

We concluded that acceleration of UCN by the thermal motion of nanoparticles which are weakly bound to a surface, could be the most probable cause of this kind of heating of UCN [5]. To verify this hypothesis, we deposited a powder (~1 cm^3) of diamond nanoparticles with a mean size of ~5 nm (Ultradiamond-90) on an area of ~150 cm^2 on the copper bottom surface of the spectrometer. In this case, the VUCN flux increased strongly (see figure 2), and the probability of VUCN production became as high as ~10^{-3} per collision. In contrast to the observation of a high VUCN flux from the nanoparticles powder, this heating effect was not observed when using a surface of a sapphire single crystal. Here the probability of heating was determined to be < 10^{-8} per collision. In this case, also the scanning atomic force microscope could not observe any trace of nanoparticles on this surface. These findings are in line with our interpretation that this "heating" of UCN, interacting with a surface, is caused by their acceleration in collisions with very small solid particles. The observed small changes in energy of UCNs during their collisions with surfaces are important for the storage of UCNs in traps. It provides that UCN spectra are generally "spoiled" by an admixture of VUCN. Those cannot be removed by any spectral shaping method when using common materials for trap walls, such as solid surfaces and liquid fomblin oil. This mechanism can lead to a significant increase in the loss probability of UCNs from traps and can induce systematic errors in precision experiments. Therefore an analysis of many experiments on UCN storage is not reliable if the VUCN production rate is/was not controlled. The probability of this process is usually 10^{-7}-10^{-5} per collision. However, as we know now, the preparation of surfaces allows to influence the probability of VUCN production to both, higher and lower ranges, respectively. The description of interaction of neutrons with nanoparticles is not limited to the UCN storage experiments. This phenomenon provides also a new sensitive method to study their motions on a surface. Small energy changes with a probability as low as 10^{-9}-10^{-8} per collision can be measured. Only moving (weakly bound) nanoparticles contribute to the measurable values. They are most effective if their size corresponds approximately to the neutron wavelength. Additionally, the present results are important for the possibility of the production of a high-density UCN source, based on a completely new physical principle: The thermalisation of very cold neutrons by ultracold nanoparticles.

REFERENCES

[1] V.V. Nesvizhevsky, A.V. Strelkov, P. Geltenbort, and P.S. Yaidjiev, ILL Annual Report (1997); European Journal of Applied Physics 6 (1999) 151; Physics of Atomic Nuclei 62 (1999) 776; A.V. Strelkov, V.V. Nesvizhevsky, P. Geltenbort et al., Nuclear Instruments and Methods in Physics Research A 440 (2000) 695

[2] E.V. Lychagin, A.Yu. Muzychka, V.V. Nesvizhevsky, G.V. Nekhaev, R.R. Tal'daev, and A.V. Strelkov, Physics of Atomic Nuclei 63(4) (2000) 548

[3] E.V. Lychagin, A.Yu. Muzychka, V.V. Nesvizhevsky, G.V. Nekhaev, R.R. Tal'daev, A.V. Strelkov, and V.N. Shvetsov, JINR Preprint R3-2001-49; Surface: Roentgen, Neutron and Synchrotron Investigations, 7 (2002) 81

[4] E.V. Lychagin, D.G. Kartashov, A.Yu. Muzychka, V.V. Nesvizhevsky, G.V. Nekhaev, and A.V. Strelkov, Physics of Atomic Nuclei 65(11) (2002) 1

[5] V.V. Nesvizhevsky, Physics of Atomic Nuclei 65(3) (2002) 400

Simulating is stimulating

From the left: Helmut Schober, Markus Pohlmann and Karin Schmalzl enjoying the lunch break during one of the ILL Users Forum.

Jean-Francois Perrin (left) and Fabien Pinet (both from the Informatics Service, SI) with a cluster of PC's recently installed at ILL.

Francesco Albergamo setting up his isotherm adsorption system.

Some ILL simulators and members of the Computing for Science group.

Mark Johnson,
Leader of Computing for Science
http:/www.ill.fr/computing/club.html
Efim Kats, Leader of Theory Group
http:/www.ill.fr/colleges/c2/
theorycollegehome.html

Modelling and theory

David Mermin said recently that "theoretical physics was done by physicists who lacked the skill to do real experiments". This statement is partially true but in the "Modelling and Theory" chapter the collected papers are devoted to problems investigated by experimentation combined with numerical and theoretical studies. The physical problems posed in these contributions are far too complicated to be solved analytically. Insight on a microscopic level can be obtained using numerical modelling techniques, such as molecular dynamics (MD) simulations, but the underlying physics can be extracted from experimental and numerical data by carefully constructed models based on the minimal set of "ingredients" required to capture the observed physical effects. Numerical simulations, that can be manipulated more easily than real experiments, can be used to guide theoreticians towards the correct ingredients and reasonable parameters.

In the work on discotics by Kearley et al., two quasielastic signals were measured and identified from MD simulations with motions parallel and perpendicalar to molecular chains, whereas, originally, they were expected to originate from the motion of different groups on the same molecule. Modelling the lattice dynamics in methane-ice clathrates (Baumert *et al.*), based on simplified, rigid water molecules, reveals the phonon dispersion curves associated with guest-host coupling as seen experimentally in the vibrational density of states. Similar dispersion relations are obtained from a model of beads in coupled spheres. Parameter-free (first principles), numerical methods are used to analyse the molecular vibrations in Kevlar, a model β-sheet compound (Plazanet *et al.*). Since the initial solid state structure is the only input in the normal mode calculation, agreement between measured and calculated spectra shows the validity of the initial structure. Vibrational spectroscopy is used as a probe of local structure.

The paper by Currat et al., devoted to composite, incommensurate crystals, illustrates the minimal model approach. Fundamental questions concerning the nature of elementary excitations in these systems are still open. In previous work all excitations were studied collectively using many phenomenological parameters. In this paper the authors restrict themselves to robust and experimentally testable features of the excitation spectra related to dissipative coupling between subsystems, surprisingly a mechanism overlooked previously. Similarly Jackeli presents a minimal model devoted to spin wave theory of so-called metallic double perovskites, a class of materials with rich potential for applications. For a theory with such simple physical input, the Jackeli model shows remarkably good agreement with existing experimental data and, based on the model, new predictions certainly contain more than a grain of physical truth.

Stabilising self-assembled *discotic molecular electronics*

G.J. Kearley, F.M. Mulder (IRI, Delft)
S.J. Picken, P.H.J. Kouwer (Univ. of Delft)
J.A. Stride (ILL)

Discotic materials are molecules with planar, disc-like poly-aromatic cores that can self-assemble into "molecular wires". Highly anisotropic charge transfer along the wires arises when there is sufficient intermolecular overlap of the π-orbitals of the molecular cores. These materials have potential applications in molecular electronics, field-effect transistors and recently, with record quantum efficiencies, in photovoltaics [1]. Nevertheless, there is still an order of magnitude difference between the conductivities measured on microscopic and more macroscopic scales, the latter being much smaller [2]. Our aim is to account for this "missing" conductivity, the suspicion being that it arises from a loss of correlation within the columns due to thermal motion of the discs. This problem, plus the role that the tails and of charge-transfer inserts, makes a good study for quasielastic neutron scattering (QENS).

Discotic materials often have mesomorphic properties depending on the nature of the hydrocarbon chains that are attached as "tails" to the aromatic cores. In addition to a crystalline phase they often display intermediate liquid crystalline phases prior to melting to the isotropic liquid (figure 1). The liquid crystalline phases appear to have the best conductivity, whereas the crystalline phase results in unwanted tilting of the cores. Recently, it has been shown that the liquid crystalline columnar hexagonal phases can be stabilised, and tilting of the discs reduced, by adding electron acceptor molecules such as TNF (2,4,7 trinitrofluoren-9-one). This extends the range in which efficient charge transfer occurs down to room temperature (figure 2).

Figure 1: Liquid crystalline phases with increasing molecular order. In order of decreasing temperature: a) Nematic discotic, b) nematic columnar, c) columnar hexagonal.

The first part of our QENS study was of HAT6, which is about the simplest discotic system to form liquid crystalline columnar phases (figure 3).

Ideally, the important core motion could be studied by deuteration of the tails, but this deuteration is difficult. Therefore, we used a more indirect route: deuteration the 6 core-hydrogens and then subtraction of this spectrum from that of the fully protonated material. The quasielastic spectra revealed motion on two timescales within the range of IN6: 0.2 and 7 picoseconds. However, whilst the intensity of the slower component decreases on core-deuteration, it is too intense to arise only from the core hydrogens, which constitute only 10% of the total. In such complex systems there is motion on almost every timescale and the only reasonable route to understanding the origin of the two motions observed on IN6 is via a molecular dynamics simulation. A rather simple model (for such a complex system) consisting of a column of 4 discotic molecules (578 atoms) was constructed from which it quickly became clear that the two observed motions are whole-molecule displacements parallel and perpendicular to the column axis.

The more rapid motion corresponds to a sliding of the discs relative to each

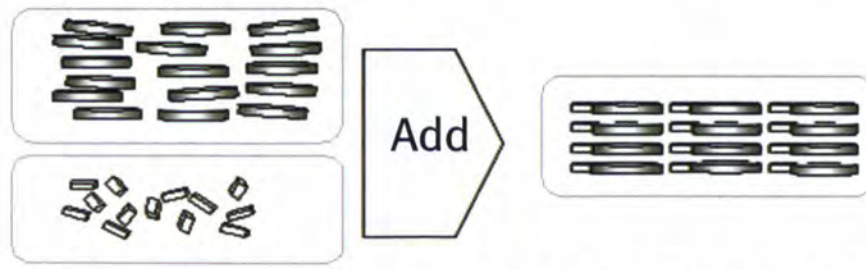

Figure 2: Indicated on the right is the proposed structure in the liquid crystalline columnar phase of the donor-acceptor complex of triphenylene and TNF.

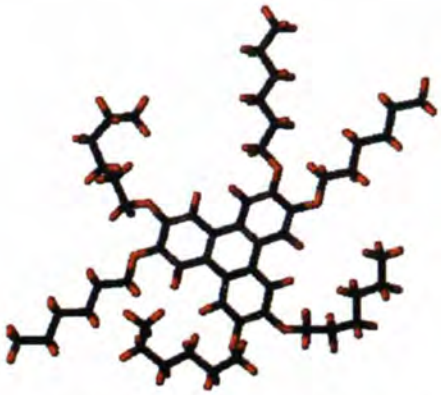

Figure 3: HAT 6 or hexakis(n-hexyloxy) triphenylene.

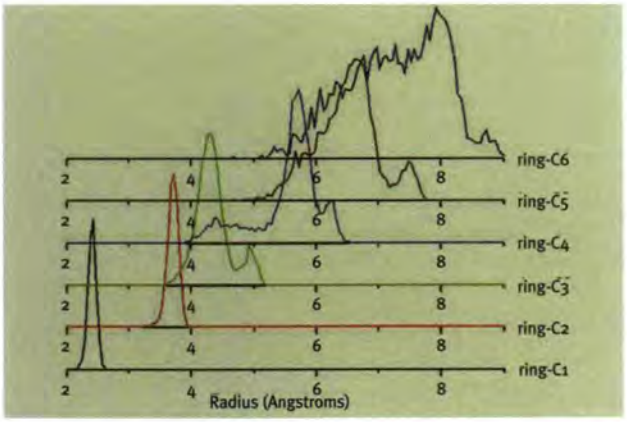

Figure 4: Radial correlations between the indicated tail C atoms with the corner of the HAT6 core it is connected to.

other whilst the slower motion corresponds to a tilting of the discs out of their formal molecular plane. Interestingly, on the picosecond timescale the motions of the tails and the cores are strongly correlated, the original concept of distinct core and tail motion being found to be incorrect. This is shown in the radial correlation function between a core carbon atom and successive carbon atoms along the alkyl chain (figure 4). It is also interesting to note that the core-core and tail-tail interactions play an almost equal role in determining the dynamics of the disc. In fact, there is some "entanglement" between tails of successive discs, and consequently, only very limited partial rotation of the discs was seen even on the 1 nanosecond timescale.

In the second part of the study we investigated HMT which has the same triphenylene core as HAT6, but has the simplest possible, $-OCH_3$, tails that are easy to deuterate (figure 5). Again, motion on two timescales was found, but perhaps surprisingly, in this simpler system the signal for the slower motion disappears on deuteration of the methyl tails. A molecular dynamics simulation of 4 HMT discs also shows clearly that the slower motion seen on IN6 is associated with torsion of the whole methyl group (including the carbon) around the O-core bond.

The measured core motion is about twice as fast as in HAT6, reflecting the slowing down effect of the longer tails. However, on addition of the TNF the charge-transfer complex is formed and the signal from the slow motion becomes too slow to measure on IN6. The faster core-motion slows by more than a factor of 2, to a timescale similar to that of HAT6. The molecular dynamics simulation for HMT with the charge-transfer complex has yet to be done, but it is seems likely that the motion parallel to the column has become too slow to measure, and that the sliding of the discs slows down to the value obtained with the much longer tails of HAT6.

One particularly interesting aspect of HAT6 is that just above the melting point in the isotropic liquid phase the measured quasi-elastic signal is not liquid-like, even though all Bragg-peaks are absent. The measured quasi-elastic spectra are similar to those of the columnar phase, though somewhat broader. What does this mean? It transpires that our MD simulation using a single column of 4 discotic molecules agrees better with these "liquid" spectra than with the columnar liquid crystalline phase. The lack of column-column interactions and the limited size of our model seem to provide a good representation of disc-disc interactions that persist into the 'isotropic liquid' phase. This is a correlation over a limited distance and limited time, as evidenced by the lack of Bragg-peaks, and should not be regarded as "chunks of column" floating around in the liquid. This study demonstrates that a combination computer modelling and neutron scattering data, can lead to a complete picture of molecular dynamics in complex systems. These motions often have direct bearing on bulk material properties - in this case, the interplay between cores and tails provides a direct insight into increasing core rigidity and hence conductivity along the molecular wires. This is particularly important as the loss of intra-column correlations due thermal agitation of discs acts to decrease overlap of core π-orbitals and becomes increasingly critical as the column length increases when moving into the bulk.

Figure 5: Hexamethylene-tetramine.

REFERENCES

[1] L. Schmidt-Mende et al., Science 293 (2001) 1119
[2] A.M. van de Craats et al., Adv. Mater. 8 (1996) 823

Lattice dynamics
and guest-host coupling in clathrate hydrates

J. Baumert
(ILL and University of Kiel)
C. Gutt (University of Dortmund)
M.R. Johnson and W. Press (ILL)
J.S. Tse (NRC)

Clathrate hydrates are a special class of inclusion compounds, in which small hydrophobic guest molecules or atoms are trapped in cages formed by an ice-like host lattice of water molecules. In recent years large deposits of natural gas hydrates (e.g. methane hydrate) have been discovered on the ocean sea floors, and are considered as a potential future energy resource, but also for their possible contribution to the greenhouse effect [1].
In the case of gas hydrates the guest-host interaction is weaker than the bond strength of the cage structure. Nevertheless it is this hydrophobic interaction, which stabilises the ice framework and is thought to be responsible for a coupling between the low frequency vibrations of the guests and the vibrations of the host lattice. These interactions between the guest molecules or atoms and the water network make gas hydrates a model system for the study of hydrophobic interactions, relevant for a fundamental understanding of the water and repulsive water-guest potentials.

Most common gas hydrates occur in one of the following crystal structures: cubic structure type I or cubic structure type II. Structure type I hydrates consist of 2 small spherical cages and 6 large ellipsoidal cages (figure 1), whereas the structure type II is formed of 16 small and 8 large cages, of which both are nearly symmetrical. As both structure types contain 80% of hydrogen bonded water molecules, many properties resemble those of ordinary ice I_h. This, however, is not true for the thermal conductivity k, which is unusually low and displays a temperature dependence similar to that of glasses [2], despite the crystalline character of the gas hydrates. At least two different qualitative models have been proposed to explain the unusual thermal conductivity: (i) the large unit cell is leading to a limited phonon mean free path [3], and (ii) a coupling between the guest and host vibrations in the low frequency region leads to effective phonon scattering [4].
In the case of clathrate hydrates, the structure consists of an open framework structure with encaged atoms/molecules. Recently the guest-host coupling was confirmed experimentally in inelastic incoherent neutron scattering experiments on structure type I xenon hydrate [5,6]. Due to the

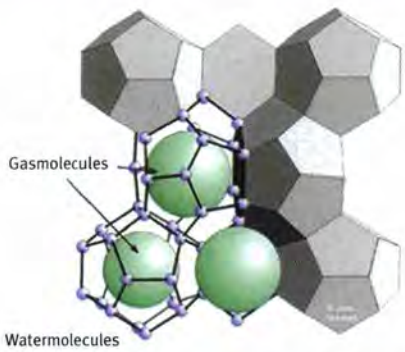

Figure 1: The schematic of a structure type I hydrate (GEOMAR – Kiel).

importance of this study we have included methane hydrate and the structure type II argon and krypton hydrates in our studies. The nominal stoichiometry of the samples was $CD_4 5.75H_2O$, $Kr 5.67H_2O$, and $Ar 5.67H_2O$.
Figure 2 shows the spectra of argon and krypton hydrate and of ice Ih as recorded on the cold neutron time-of-flight instrument IN6 at T=100 k for a neutron energy gain of 0 to 15 meV. For argon and krypton hydrate the peaks at around 7 meV and 11 meV may be attributed, in analogy to Ice I_h, to the transverse acoustic phonons near the zone boundary and their fold-back towards the zone centre, respectively. Of particular interest are, in the case of the hydrate spectra, the peaks below 5 meV, which are absent in the spectra of ice I_h. These lines show indirectly the coupling between the guest and host vibrations: As the incoherent scattering cross section of the water host lattice exceeds that of the guest molecules or atoms by more than two orders of magnitude, the scattered signal arises from the vibrations of the hydrogen atoms, displaying only the density of states of the water molecules. Furthermore it is known that the guest atoms in the cages behave like low frequency Einstein oscillators. As structure II is formed by 2 types of spherical cages of different size, the guest atoms in the small cage vibrate with the highest frequency (around 4.5 meV) whereas the large cage leads to a lower frequency (around 3 meV). The coupling of the guest atom vibrations to

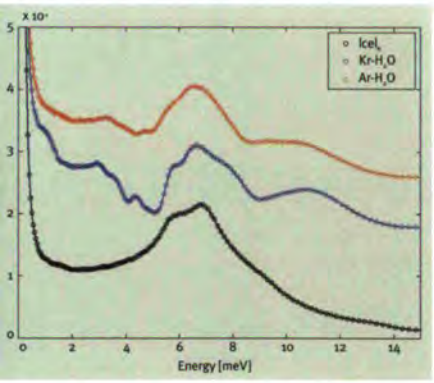

Figure 2: IINS spectra of Ar- and Kr-hydrate together with ordinary ice as reference. The spectra were recorded at T=100 K on the cold neutron time-of-flight instrument IN6. The low frequency excitations in the hydrate spectra at around 3 and 4 meV are attributed to the localized guest vibrations, which are coupled to the host lattice modes.

the surrounding cages causes cage oscillations with the same frequency, making them visible in the neutron spectra.

In the case of structure type I, the large cage has an ellipsoidal shape. While the guests in the small cage still vibrate with the highest frequency, the ellipsoidal shape of the large cage leads

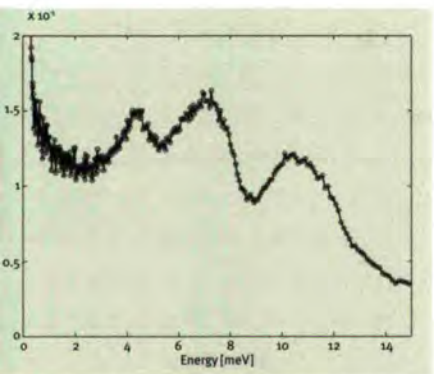

Figure 3: IINS spectrum of CD_4-H_2O hydrate measured on Focus (PSI). Only one guest excitation is observable at around 4 meV as the other two overlap with the host lattice peaks at 7 and 11 meV.

to 2 distinct lower vibrational frequencies. In the case of xenon hydrate the corresponding 3 low frequency excitations could be observed [6]. In figure 3 the spectrum of CD_4 hydrate is displayed for T=100 K and neutron energy gain between 0 and 15 meV. In order to understand the presence of only one low frequency guest mode in the case of methane hydrate, we additionally calculated the density of states (DOS) using lattice dynamical (LD) simulations. The LD calculations were performed with periodic boundary conditions on one proton disordered unit cell containing 46 water and 8 methane molecules. The resulting DOS is displayed in figure 4. The calculated frequencies of the guest modes are shifted towards lower frequencies with respect to the measured frequencies by about 20%. This points towards an underestimation of the repulsive methane-water potentials in the present calculation. The calculated DOS of the host framework is nevertheless in good agreement with the experiment. Additionally, the calculations show that there are 3 localised guest vibrations, though 2 of them coincide with the excitations arising from the host lattice.

The coupling, which can also be observed in the calculated DOS, is originating from an avoided crossing between acoustic (host)-lattice phonons and localised guest modes of the same symmetry. This avoided crossing leads to

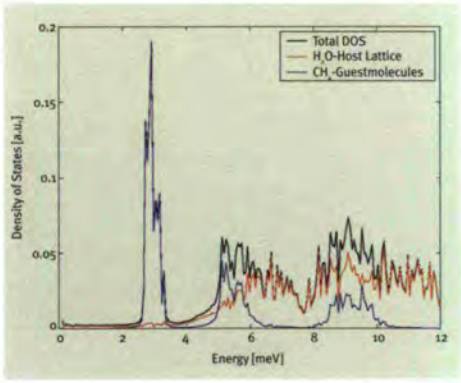

Figure 4: Calculated density of states of methane hydrate. The partial density of states of the host lattice reflects to a small degree the DOS of the methane guest molecules. This contribution can then be observed in the IINS spectra.

a mixing of the eigenvectors of the guest and host modes, which can then be observed in the IINS spectra. For the argon and krypton hydrate, as the equilibrium position of the guest atoms in the large cage is not well defined, molecular dynamics simulations should be used to calculate density of states.

In conclusion, we could confirm the guest-host coupling for structure II hydrates. For methane hydrate we identified with the help of lattice dynamical calculations the coupling mechanism. The standard empirical potentials for water reproduce well the dynamical properties of the host lattice. However, the repulsive interaction between the guest molecules and the water lattice is underestimated by the combination of the water-methane potentials, pointing towards the importance of these interactions for the guest-host coupling.

REFERENCES

[1] E.D. Sloan, Jr., Clathrate Hydrates of Natural Gases (Marcel Deccer, Inc., New York, 1998) 534
[2] R.G. Ross, P. Andersson, and G. Bäckström, Nature (London) 311 (1981) 322
[3] M.W.C. Dharma-Wardana, J. Phys. Chem. 87 (1983) 4185
[4] J.S. Tse and M.A. White, J. Phys. Chem. 92 (1988) 5006
[5] J.S. Tse, V.P. Shpakov, V.R. Belosludov, F. Trouw, Y.P. Handa, and W. Press, Europhys. Lett. 54 (2001) 354
[6] C. Gutt, J. Baumert, W. Press, J.S. Tse, and S. Janssen, J. Chem. Phys. 116 (2002) 3795

Vibrational spectroscopy *of oriented Kevlar fibres, a model β-sheet compound*

M. Plazanet, M. Johnson, T. Forsyth, A. Ivanov, J. Stride (ILL)
K. Gardner (Dupont, USA)

The commercial fibre Kevlar is a polymer composed of para-phenylene terepthalamide monomer units. Peptide linkages in and between the monomer units allow hydrogen bonding between polymer chains and the formation of β-sheets, more familiar in the secondary structure of proteins. Infrared absorption spectroscopy is used empirically in peptide and protein conformational analysis. INS allows the structure-dynamics relation to be quantified. The vibrational modes of oriented fibres of Kevlar have been measured on IN1. Solid state, quantum chemistry calculations allow a reliable assignment of the modes and are used to investigate the dependence of the modes on the inter-sheet packing in the solid state structure.

The frequencies and polarization vectors of molecular vibrations depend sensitively on all, local interatomic interactions. In organic solids, in the absence of charged molecular groups, these interactions typically have a range of 5-6 Å. For an isolated oscillator of mass m, the frequency ω of excitation is given directly by the force constant k (i.e. $\omega = (k/m)^{1/2}$). In a multi-atom system the vibration frequency is given by the gradient of the potential energy surface which depends on the sum of all such contributions e.g. $E = \Sigma k(l-l_0)^2$, where l_0 describes the equilibrium geometry of an isolated oscillator. Thus, if the force constants k are known, the relative atomic positions l can be deduced from the vibrational excitations. The critical input in quantifying the structure/dynamics (atomic positions/vibration frequencies) relation is the force constants and these are obtained most reliably from quantum chemistry calculations. By combining density functional theory (DFT)-based, quantum chemistry methods and periodic boundary conditions, as in the VASP code [1], complex solids described by a box containing hundreds of atoms, can be treated. In practice, vibrational spectra are calculated for a range of solid state structures, by using DFT calculations to generate the dynamical matrix, which on diagonalisation gives the vibrational eigenfrequencies and eigenvectors [2,3]. For inelastic neutron scattering (INS) spectra, this information is sufficient to calculate the whole spectral profile. Comparison between measured and calculated spectra enables the most likely solid state structure to be identified. INS is therefore useful for local structure determination in amorphous or partially crystalline samples, for example polymers, where diffraction data is limited.

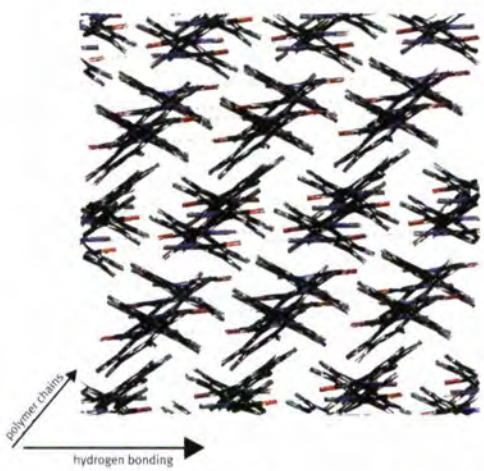

Figure 1: The crystal structure of Kevlar [1].

Kevlar, poly(p-phenylene terepthalamide), is a fibre, produced commercially by Dupont, that is well-known for its high strength and related applications, for example in bullet proof vests. The physical strength of the fibres is determined by the structure at a molecular level. Figure 1 shows the structure obtained from the original, fibre diffraction experiments [4]. Pep-

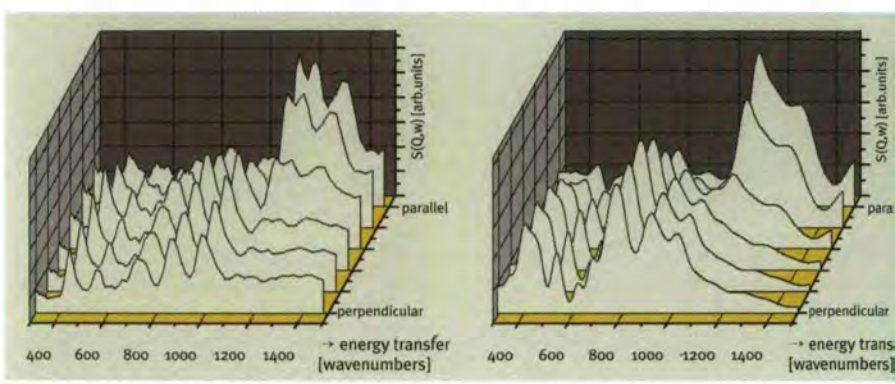

Figure 2 :(a) Spectra measured on IN1, and (b) calculated from structure [1].

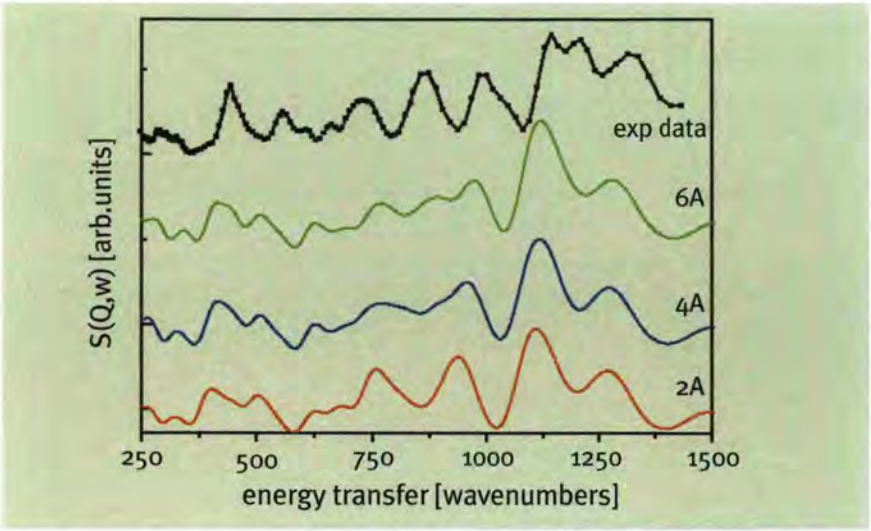

Figure 3: Sum spectra calculated as function of translation between sheets along the fibre axis from 2 to 6 Å.

tide linkages allow hydrogen bonding between polymer chains and thus the formation of parallel β-sheets, which along with α-helices constitute the main secondary structural elements of proteins. Vibrational spectroscopy, in particular infra-red absorption, is commonly used for poly-peptide and protein conformational analysis, based on empirical correlations of the amide-I (amide C=O stretch at ~1600 cm^{-1} ~200 meV) band profile with known structural units [5]. A recent application of this approach is the identification of β-sheet formation in different proteins, responsible for Alzheimer's and prion diseases. In the case of Kevlar, the structural question is more subtle, new fibre diffraction data from partially deuterated samples suggesting a relative translation in the direction of the polymer axis between sheets of about half a monomer unit compared to the original structure.

The Kevlar sample was wound onto a thin, flat aluminium plate so that the fibres were in the scattering plane and the fibre axis could be oriented with respect to momentum transfer (Q) vector. Spectra measured at 10K for orientations ranging continuously from parallel to perpendicular to the incident beam are shown in figure 2(a). Scattered intensity is highest at energy transfers corresponding to modes polarized parallel to the Q vector and lowest when the polarization vectors are perpendicular to Q.

Each calculated spectrum shown in figure 2(b) is an average of spectra for a mono-crystal rotated about the fibre axis, followed by a single rotation about a perpendicular axis, corresponding to the sample orientation. The resolution function of IN1 has been included in the calculated spectra, although the sample-dependent background, which increases with energy transfer, and sample geometry effects have not. The overall agreement between measured and calculated spectra is good, including the intensity variation of modes with sample orientation. The modes at ~1200 cm^{-1} (~150 meV) that vary most strongly in intensity involve rocking of the phenyl C-H bonds, which are polarized along the fibre axis.

However, comparing the sum of the measured spectra with the sum of the calculated spectra reveals the systematic overestimate in intensity of the lowest frequency peak in the 600 - 1100 cm^{-1} (~75 - 140 meV) range and small errors in peak positions. Figure 3 shows calculated sum spectra for different initial structures, varying the relative alignment along the chain direction from 2 to 6 Å. Although vibrational modes are expected to be dominated by intra-sheet interactions, they are quite sensitive to interactions between sheets. The spectrum corresponding to inter-sheet translations of 6 Å along the fibre axis shows the clearest formation of the principal peaks in the 600 - 1100 cm^{-1} (~ 75 - 140 meV) range and the best agreement in terms of peaks positions with the experimental data. This structure deviates significantly from the original structure but agrees with the analysis of the new fibre diffraction data.

In conclusion, the analysis of the vibrations of Kevlar demonstrates the use of INS and solid state DFT methods for investigating β-sheets, showing how local structural information can be obtained in partially crystalline materials.

REFERENCES

[1] http://cms.mpi.univie.ac.at/vasp & http://www.ill.fr/Computing/club.html
[2] http://wolf.ifj.edu.pl/phonon & http://www.ill.fr/Computing/club.html
[3] M. Plazanet, N. Fukushima and M.R. Johnson, Chem. Phys. 280 (2002) 53
[4] Polymer Letters 11 (1973) 333
[5] B. R. Cowen and R. M. Hochstrasser, Infra-red spectroscopy of biomolecules, Wiley-Liss; Chichester U.K. (1996) 107

Sound modes
in composite incommensurate crystals

R. Currat, E. Kats, I. Luk'yanchuk
(ILL)

We propose a simple phenomenological model describing composite crystals, constructed from two parallel sets of periodic inter-penetrating chains. In the harmonic approximation and neglecting thermal fluctuations we find the eigenmodes of the system. It is shown that at high frequencies there are two longitudinal sound modes with standard attenuation, while in the low frequency region there is one propagating sound mode and an over-damped phason mode. The crossover between these two regions is analysed numerically and the dynamical structure factor is calculated.

Among the various types of incommensurate systems one of the simplest kind (the so-called composite one dimensional crystal) is constructed from two sets of regular interpenetrating incommensurate chains. The recurrent interest for these systems is related mainly to the experimental activity on several classes of intergrowth compounds which can be viewed as good physical realizations of the 1d composite crystal. There is a considerable literature (mainly theoretical but not only) discussing eigenmodes and related properties of composite systems (see e.g. the review article [1] and references therein, and the more recent papers quoted in [2], [3], [4]). Although a number of sophisticated calculations have been published over the last 20 years there is still a clear need for a simple (but yet non-trivial) theoretical model with predictions which can be directly tested experimentally. The most interesting aspect of the physics of composites is the dynamics of their sublattices. In order to formulate the problem, let us consider first two inter-penetrating atomic chains with periods a and b and with no coupling between them. Then, two independent sets of incommensurate (in q-space) phonon branches with dispersions $\omega_a(q)=c_a a^{-1}|\sin qa|$ and $\omega_b(q)=c_b b^{-1}|\sin qb|$ should be observed (figure 1). What happens with them, when the inter-chain interaction is properly taken into account? Different types of coupling are responsible for different effects.

The elastic coupling results in the renormalisation of the sound velocities. It leads to repulsion of the crossing branches with formation of intermediate gaps. The umklapp intersection of branches occurs however for any q since, because of the period incommensurability, the condition $\omega_a(Nq)\approx\omega_b(Mq)$ can always be satisfied when the integers N, M are chosen properly. Hence a rich hierarchical set of gaps in phonon spectra is expected (see e.g. [3]). Some general features related to the longitudinal sliding mode, and breaking of analyticity due to static elastic couplings in the 1d double-chain model were reported in [3].

The electrostatic coupling takes place when the chains a and b are oppositely charged. It leads to nonlocal renormalisation of the phonon selfenergy, nontrivial retardation effects, and to the plasmon gap formation.

The dynamical dissipative coupling originates from the internal friction between the chains described by a friction parameter γ.

The scattered intensity is proportional to the dynamical structure factor $S(\mathbf{q},\omega)$, where $\hbar\omega$ is the energy trans-

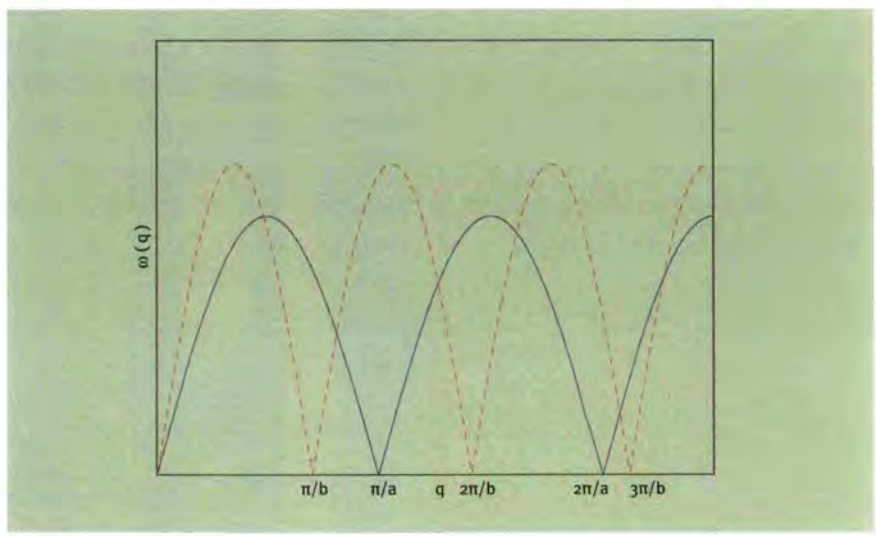

Figure 1: Phonon spectra of two uncoupled incommensurate chains a and b.

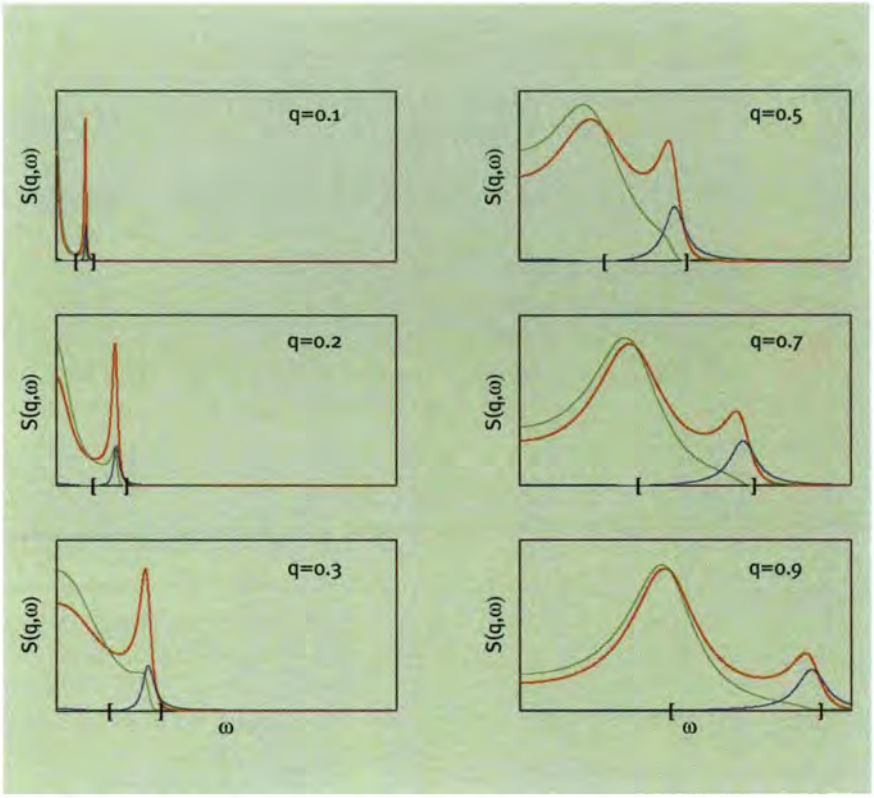

Figure 2: The dynamical structure factor of 1d composite systems. Red lines correspond to S(q,ω), green and blue lines correspond to $S(Q_a^m + q,\omega)$ and $S(Q_b^m + q,\omega)$, respectively; q is measured in γ units. Ticks: "[" and "]" corresponds to $c_a q$ and $c_b q$.

fer, and $\hbar q$ is the momentum transfer. The results of the calculations of S(q,ω) for different values of ω scanning the structure factor at a fixed value of q are shown in figure 2. The picture presented above leads to the following qualitative predictions:

- The maximum in S(q,ω) due to the lower frequency sublattice phonon disappears below a certain wave-vector.
- Both S(q,ω) and S(nπ/a+q,ω), S(mπ/b+q,ω) have asymmetric profiles with "antiresonance" points where they vanish (as in the case of the Fano resonance, when the interference between a discrete state and a continuum gives rise to characteristically asymmetric peaks in excitation spectra);
- Although S(nπ/a+q,ω), S(mπ/b+q,ω) correspond to "decoupled" a and b sublattice phonons, they show traces of mixing because of the umklapp process;
- At low q we always have a double peak structure with a central mode and a propagating sound peak.

Thus we show that at high frequencies there are two longitudinal sound modes with (in this simplified model) wave vector independent attenuation, while in the low frequency region there is one propagating sound mode and an overdamped phason mode. The dynamical structure factor has a specific line shape resembling the Fano resonance. We anticipate that these effects will be observable, and that understanding the physical mechanism leading to the dissipative coupling between the sublattice will be essential to model the behaviour of the composite materials. In spite of the current research activity in the field of composite crystals, there are still few experimental results to which model predictions can be compared, and the experimental situation still remains very open. To a large extent, this is due to the difficulty in identifying suitable model systems and in growing single-crystal specimens of appropriate size and quality for light and neutron scattering experiments. We hope that this work (see also [5]) stimulates further efforts in this field.

REFERENCES

[1] R. Currat, T. Janssen, Solid State Physics, 41 (1988) 201
[2] O. Radulescu, T. Janssen, J. Phys. 1, 30 (1997) 4199
[3] O. Radulescu, T. Janssen, J. Phys. B, 60 (1977) 12737
[4] D. Schmicker, S. van Smaalen, J. Mod. Phys. B, 10 (1996) 2049
[5] R. Currat, E.I. Kats, I. Lukýanchuk, Eur. Phys. Journal B, 26 (2002) 339

Spin wave theory
of metallic double perovskites

G. Jackeli (ILL)

Ordered double perovskite oxides such as Sr_2FeMoO_6 and Sr_2FeReO_6 have recently attracted intense interest for their possible applications to magnetotransport devices. These compounds are metallic ferrimagnets with half-metallic electronic structure and with fairly high magnetic transition temperatures. We have recently formulated a theory of carrier-induced ferrimagnetism in these compounds. We have derived the dispersion law of the spin waves and analysed quantum corrections to linear theory. We have found that quantum effects are strongly enhanced in systems with higher carrier density (such as in the Re compounds) and can cause nontrivial modification of the semi-classical magnon dispersion law. The effect can be investigated by inelastic neutron scattering experiments. We have also analysed the electron density dependence of a ground state magnetic structure and predicted layered antiferromagnetic ordering at high carrier density.

The recent discovery of the room temperature magnetoresistance in double perovskite compounds [1] has generated intense interest in these materials because of their potential applications to magnetotransport devices as well as their rich and challenging physical properties. With regard to the former aspect, metallic ferrimagnetic (FiM) compounds such as Sr_2FeMoO_6 and Sr_2FeReO_6 are of particular recent interest, because both have high magnetic transition temperature ($T_c = 420$, and 400 K, respectively) and their electronic structure has been suggested to be half-metallic. We have recently taken a step towards a theoretical understanding for the magnetism in these compounds [2]. We have proposed a minimal microscopic model, which allows for consistent analytical analysis. We have constructed a spin wave theory of metallic ferrimagnetic compounds and discussed in detail the basic features of the spin excitation spectrum. Here we give a brief account of the outcome of the proposed theory. We first shortly describe basic particularities of double perovskites. We then provide a qualitative picture of the origin of ferrimagnetism and, finally, we discuss the essential aspects of microscopic theory and the results based on it.

In the double perovskite structure *Fe* and *Mo/Re* ions form two face centered cubic sublattices and each pair of nearest-neighbor lattice sites is occupied by two different ions. In the ionic picture, *Fe* is in the 3+ valence state and has five d-electrons, which are strongly coupled by Hund's rule in the high spin state $S = 5/2$ and are localised. The *Mo* ion is in 5+ valence state and has one t_{2g} electron in the 4d-shell. (The *Re* based systems have one more charge carrier per formula unit.) Only this extra electron can move to neighbouring sites and form a band. Moreover, in the classical picture, only an electron with spin down (with respect to the local *Fe* moment) can hop to an iron site. The spin up electron is not able to move at all, because at each *Fe* site the spin up states are already all occupied, so the Pauli principle forbids such motion. Thus, it is the exclusion principle, which couples the itinerant spins and the local moments and this coupling is kinematical in origin. This contrasts with the case of double-exchange systems, in which the intra-atomic Hund's rule is responsible for the coupling between the two subsystems. The common feature of these two magnets is the stabilisation of the ferromagnetic (FM) arrangement of local spins due to the reduction of kinetic energy. In the case considered here, the kinetic energy of itinerant electrons is minimised when the local moments are parallel to each other and antiparallel to the itinerant spins. This is the origin of the carrier-induced FiM ordering.

To provide a quantitative description of the above discussed physical picture we have proposed a model Hamiltonian. In the Hamiltonian we have retained only low energy charge excitations in the system, which correspond to the transitions from ($Fe\ d^5$, $B\ d^0$) to ($Fe\ d^5$, $B\ d^{n-1}$) configurations, where B stands for *Mo/Re* ion. The *Fe* ions have been treated as localized spins $S = 5/2$ and extra electrons from nonmagnetic *Mo/Re* ions as itinerant degrees of freedom. In order to respect Pauli exclusion principle and to project out unphysical state with total local spin $S = 3$, we have introduced an infinite local antiferromagnetic (AFM) coupling between core and itinerant spins. We recall that for six electrons in a d-shell the maxi-

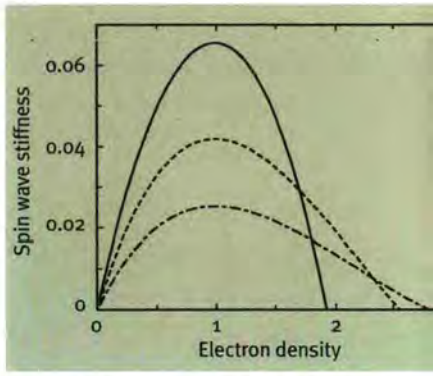

Figure 1: Spin wave stiffness (in units of $t = 1$) versus carrier density, for different values of the charge transfer gap Δ ($\Delta = 0$, 4, and 8, solid, dashed and dotted-dashed lines, respectively).

mum allowed total spin is $S = 2$.
Since the value of the core spin is relatively large ($S = 5/2$) we have used the $1/S$ expansion to study the spin dynamics of the ferrimagnetic metallic state. We found that there are two branches of spin excitations, similarly to the case of localised ferrimagnets. They describe, respectively, a gapless Goldstone mode and a gapped optical mode. In addition to these two modes, there exists a Stoner continuum in the metallic systems. The dispersion law of the gapless branch at the quasi-classical level is Heisenberg-like, corresponding to a Heisenberg ferromagnet with nearest- (J_1) and next-nearest-neighbour (J_2) exchange energies. We have analysed the electron density dependence of the exchange

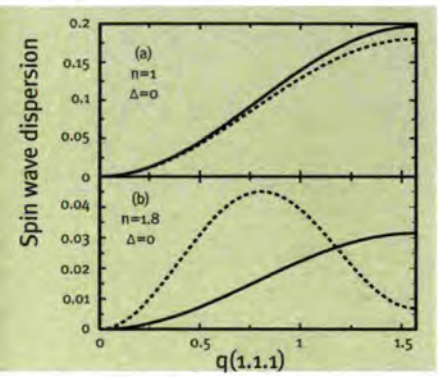

Figure 2: Spin wave spectrum in the $(1,1,1)$ direction (in units of $t = 1$) versus momentum. Solid and dashed lines represent the magnon dispersion law in the harmonic approximation and with quantum corrections included, respectively.

energies and of the spin stiffness. Figure 1 shows the carrier density n dependence of the spin stiffness $D = 16S(J_1+J_2)$, in units of the electron transfer integral $t = 1$, for different values of the charge transfer gap Δ. We note that the compound $Sr_2FeMo(Re)O_6$ corresponds to the case $n = 1(2)$. At a fixed density the stiffness scales with the carrier bandwidth: $D \sim t$ (for $t > \Delta$) and $D \sim t^2/\Delta$ (for $t < \Delta$). As a function of density, the spin stiffness exhibits a strong nonmonotonic behaviour. It shows a maximum at optimal filling $n_{opt} \sim 1$ and then drops to zero at some critical density n_{cr}. This agrees with the density dependence of Tc obtained in Ref. [3].
We now discuss quantum corrections to the linear theory discussed above. These corrections are governed by fermionic excitations and are thus different from those in insulating magnets. The quantum corrections generate two main effects in the magnon spectrum: (i) they give rise to spin wave damping in the ground state, and (ii) they modify the semi-classical dispersion law of magnons. Figure 2 shows the semi-classical (solid line) and renormalised (with quantum corrections included) (dashed line) dispersion of magnons for carrier densities $n = 1$, figure 2(a), and $n = 1.8$, figure 2(b). In the case of optimal carrier density $n = 1$, the quantum effects do not practically alter the semi-classical dispersion. However, for a higher carrier density the quantum effects become strongly pronounced. They cause a stiffening of the long-wavelength excitations and a softening of the zone boundary magnons. This is clearly seen in figure 2 (b). Based on our analysis, we suggest that Sr_2FeReO_6, which has two charge carriers per formula unit, is most suitable, among the presently available compounds, for experimental studies of quantum effects in the spin wave spectrum.
We have mentioned above that there is a critical carrier density n_{cr} at which the spin wave stiffness vanishes (figure 1). This indicates that there exists another type of magnetic ordering which competes with the FiM order and becomes favourable as n approaches n_{cr}. We have identified the symmetry of the new magnetic order and found that it corresponds to the layered antiferromagnetic arrangement of local moments (so called AFM-II ordering). This state consists of [111] FM planes, which are coupled antiferromagnetically. The above discussed zone-boundary magnon softening can be thus interpreted as a precursor effect associated with the proximity of layered magnetic ordering. In figure 3 (left panel) we show a 2D cut of the AFM-II magnetic structure. In this state the charge carriers are confined within the 1D FM stripes. It appears that for carrier densities $n > n_{cr}$, electrons can gain more kinetic energy in the AFM-II state than in the FiM one, and the former becomes favourable.
Finally, in figure 3 (right panel) we present the proposed qualitative phase diagram of double perovskites. The dashed curve in this figure denotes the second order phase boundary between paramagnetic and magnetically ordered states. The FiM phase is stable for carrier densities $n < n_{cr}$ and there is a first order phase transition to the AFM-II phase upon increasing the density. The first order phase boundary [see solid line in figure 3 (left panel)] is terminated by the bicritical point.

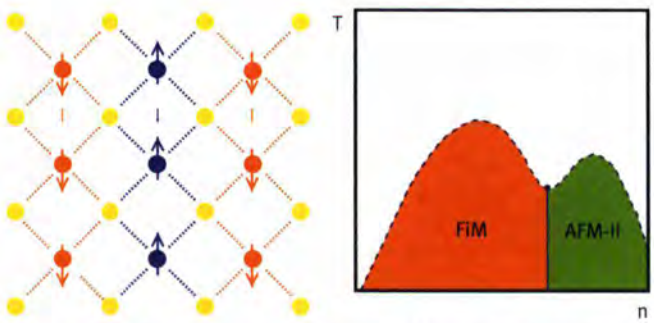

Figure 3: Left panel: Two dimensional sketch of the AFM-II structure. Large (small) arrows denote the core (itinerant) spins. Red (blue) dashed lines indicate the allowed path for spin up (down) electrons, and filled yellow circles stand for nonmagnetic ions; Right panel: proposed qualitative phase diagram in the (T, n) plane.

REFERENCES

[1] K.-I. Kobayashi et al., Nature (London) 395 (1998) 677
[2] G. Jackeli cond-mat/0208586 (submitted to Phys. Rev. Lett. September 2002)
[3] A. Chattopadhyay and A. J. Millis, Phys. Rev. B 64 (2001) 024424

FaME38 at ILL-ESRF

P. J. Webster, A. M. Dale,
D. J. Hughes, H. Sitepu
and B. Malard
(University of Salford)

FaME38 is the new Facility for Materials Engineering that has been set up jointly by ILL-ESRF, with start-up funding from an EPSRC grant, to provide extra support for European Engineers to enable them to make the best use of neutron and synchrotron X-ray beam facilities. The FaME38 team began work on-site in April 2002 and the FaME38 laboratory was officially opened for users in November.

Engineering research at the ILL

The early days

Materials engineering research has been carried out at the ILL for many years. The principal activity has been neutron strain scanning which started in the early 1980's [1-3] on D1A. The first measurements used crudely cut holes in cadmium sheet to define neutron beams a few millimetres square. Scanning the sample involved manually moving it on a calibrated slide through the 'gauge volume'. Iterative single peak fitting, to determine accurate peak positions from which the strain is determined, took of the order of hours. Gradually beam-defining systems were refined, automated XYZ translators were introduced and computer peak fitting routines enabled data to be processed in minutes. These facilities were then combined into a 'Salford-Imperial Engineering Package' that was made available to all users. In the mid-1980s strain scanning was also started on D20. The angular resolution was lower, but was sufficient for many applications and it was 10 times faster than for D1A. By 1991 D1A was probably the world's highest resolution strain scanner; one of the few capable of measuring through surfaces, and D20 was the world's fastest, used for multi-point internal medium resolution area scanning. It was perhaps ironic that in 1991 the ILL reactor had to be shut down for four years – because of fatigue cracks that had propagated as a result of tensile residual stress fields caused by welding – at a time when it was being used to measure welding-related stresses.

The 1990s – the decade of international development and collaboration

In March 1991 most of the then small, scattered, neutron stress measurement community convened in Oxford for a week long Advanced Research Workshop sponsored by NATO [4]. The workshop stimulated collaboration, accelerated development, and an active international community was formed. In 1995 VAMAS, the Versailles Project on Advanced Materials and Standards approved the formation of a new Technical Working Area 20, (TWA20), 'Measurement of Residual Stress [5]. Its remit was to establish the scientific base for, and to deliver, the first international draft standard for the non-destructive measurement of residual stress by neutron diffraction. It held its inaugural meeting at the ILL in January 1996. As well as representatives of the ILL, participants included most major worldwide neutron sources and leading researchers. Subsequent meetings were held at approximately 8-monthly intervals at the other participating neutron facilities. European members obtained EU funding for the parallel RESTAND project, which involved close collaboration with industrial partners. An accepted standard is a prerequisite for wider industrial and engineering adoption of any new technique.

The new millennium – establishment and exploitation

An ISO/VAMAS TTA 'Polycrystalline materials – Determination of residual stress by neutron diffraction' was delivered in 2001 as a precursor to a full international standard. In 2001 the joint VAMAS/RESTAND draft standard was delivered and adopted by ISO as a pre-standard 'Technology Trends Assessment', TTA [6]. It is now in the process of being converted into the format of a full international and European standard. The existence of the TTA makes it possible for engineers now to adopt neutron strain scanning as an approved reliable technique. However, for the technique to become routinely used, neutron facilities must have instruments and must adopt practices that meet the ISO/VAMAS TTA pre-standard and that are also cost-effective and user-friendly to engineers.

FaME38

FaME38 is the new Facility for Materials Engineering that has been set up jointly by ILL-ESRF to provide extra resources and support for European Engineers to enable them to make the best use of neutron and synchrotron X-ray beam facilities. The 40-month start-up phase of the project is funded by a UK EPSRC grant that is administered through the University of Salford on behalf of seven collaborating institutions, the universities of Manchester, Oxford and Loughborough, the Open University, Imperial College and the Rutherford Appleton Laboratory. Matching on-site support is provided by ILL-ESRF. The FaME38 team began work on-site in April 2002 and thea FaME38 laboratory was opened for users in November.

The FaME38 team: Left to right: Husin Sitepu, Benoît Malard, Darren Hughes, Anne Dale and Peter Webster.

The basic philosophy of FaME38 is that ILL and ESRF are very well equipped to support the broad range of science for which they were founded but have not been similarly resourced to provide the extra and specialised support that is required by engineers to perform engineering research. Until now most 'engineering' research at the facilities has been done by applied scientists, rather than by engineers. Typically they have found that the equipment and software available was not optimised for engineering measurements, particularly for users with limited scientific background. For example, a substantial proportion of allocated beam-time has been wasted spent positioning complex-shaped components on the beam-line in preparation for strain scanning measurements. It is intended that this will now be done off-line, prior to an experiment, and to much higher levels of precision.

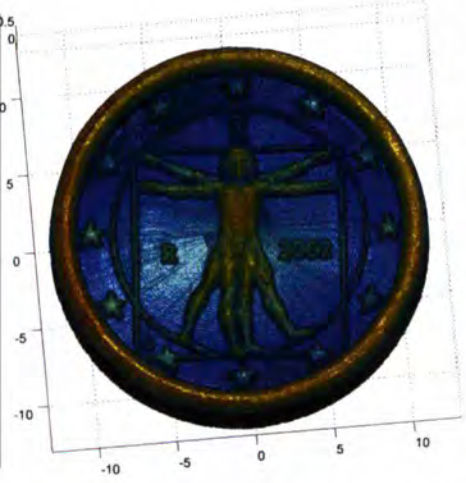

Image of an Italian 1 Euro coin generated from a 120,000 point scan using the FaME38 co-ordinate measuring machine (1 mm diameter touch probe, accuracy ± 2 microns, speed 1,500 points/min).

The FaME38 'Technical Centre' will provide engineering users with a 'Technical Centre' with a metrology laboratory equipped with a co-ordinate measuring machine to determine complex and distorted component shapes, together with a simulator to optimise scans off-line before starting measurements on the beam-line. Its materials laboratory will have micro-structural characterisation and static and dynamic thermo-mechanical loading equipment. Its 'Knowledge and Training Centre' will provide technical and scientific know-how. Users will be helped to draft proposals, to plan and prepare experiments off-line, and be assisted with data collection, on-line processing and analysis. FaME38 will provide a focus and user facility for European engineers wishing to make use of Central Facilities. Its focus will be on developing strain scanning facilities at ILL-ESRF but is likely also to stimulate and will support the engineering use of SANS, SAXS, radiography and tomography.

The Opening Ceremony: Michael Harloe, Vice-Chancellor of Salford University cuts the chain opening the FaME38 laboratory – and the way to the champagne reception.

FaME38 Opening Ceremony and Forum

The official opening ceremony for FaME38, took place on 26 November 2002. It was attended by members of the ILL Scientific Council, representatives of the ESRF and engineers and scientists from member countries from across Europe. The guests were welcomed in speeches given on behalf of the ILL by Director Colin Carlile and for the ESRF by Director General Bill Stirling. Mme Geneviève Fioraso, Maire-Adjointe de Grenoble, represented the City and the Département de l'Isère, from which FaME38 takes the '38' part of its name. The basic philosophy and resources of FaME38 were described by the project manager Peter Webster who predicted that efficiency gains would lead to beam-time cost reductions of the order of 100 and that strain scanners for engineers would become as common as body scanners in medicine. The Vice-Chancellor of Salford University, Michael Harloe, gave his address on behalf of the UK-based collaborators and spoke of the close connections that they had with the ILL and ESRF. He referred to some famous Salford-born individuals including, appropriately for the occasion, James Prescott Joule, whose name is now used for the SI unit of Energy, and the industrial landscape painter L.S. Lowry, some of whose prints can be seen on the walls of FaME38. He then 'opened' the laboratory by cutting a chain using a large pair of industrial shears. The opening was followed by a demonstration of equipment and a display of posters from materials engineering users of ILL-ESRF. In the evening a dinner was held at the Château de la Commanderie. The following day a FaME38 Technical Forum was held for engineers and scientists involved with the project. The facility is now open to users, in particular to all academic and industrial engineers with interests in stress measurement.

REFERENCES

[1] A. J. Allen, C. Andreani, M. T. Hutchings and C. G. Windsor, 'Measurement of internal stress within bulk materials using neutron diffraction', NDT International 14 249-254 (1981)

[2] L. Pintschovius, V. Jung, E. Macherauch and O. Vohringer, 'Residual stress measurements by means of neutron diffraction', Mater. Sci. Eng. 61 43-50 (1983)

[3] A. Stacey, H. J. MacGillivray, G. A. Webster, P. J. Webster and K. R. A. Ziebeck, 'Measurement of residual stresses by neutron diffraction', J. Strain Analysis 20 93-100 (1985)

[4] M. T. Hutchings and A. D. Krawitz (Editors) 'Measurement of residual and applied stress using neutron diffraction', Kluwer Academic Publishers, Series E: Applied Sciences – Vol. 216 (1992)

[5] G. A. Webster 'TWA20 Measurement of residual stress', VAMAS Bulletin No. 20, 6-8, July 1996

[6] 'Polycrystalline materials – Determination of residual stresses by neutron diffraction', ISO/TTA 3:2001

Teams teaming up

The projects and techniques division (DPT) organised an **open day** on Monday, 16 December for ILL staff. Visits to the different services were guided by the DPT staff itself.

Giuliana Manzin revealing the magic of the Microstrip detector.

Barbara Standke on a guided tour in the vacuum Lab by Claude Yoccoz (left) and Jean Gangi (right).

David Jullien guides a tour in the Optics Lab.

In all weathers the ILL guardians keep an eye on all comings and goings on to site. From the left: Jean Paul Basset, Lionel Richard, Bernard Gremillet and Anthony Chudeau.

MILLENNIUM PROGRAMME & TECHNICAL DEVELOPMENTS.

The arrival of the New Year brought the ILL's Millennium Programme to its third birthday. Progress on this major initiative for the renewal of ILL's instruments and infrastructure continues to be rapid, with numerous instruments already boasting considerable improvement. We have also been bringing to a successful conclusion the ILL's previous programme for the upgrade of six instruments and a ballistic guide (five instruments on ILL's own budget and one with funding from Spain).

We can now concentrate therefore on the Millennium Programme which currently has ten instrument projects underway. VIVALDI, the single-crystal image-plate-detector diffractometer, was the first to be completed and we are optimistic that two or three more instrument projects will be finished in 2003, thus ensuring that there will be no let-up in instrument upgrade and the development of components.

These achievements have stretched our human resources to a maximum

Energy at the moment is being devoted to the modernisation of the infrastructure, and to the replacement of the H22 and H1/H2 guides in particular, projects which will extend over several years. At the same time we have opened to users the Facility for Mechanical Engineering (FaME38, see page 92), a partnership with the ESRF receiving significant external funding from the UK's EPSRC, and have secured the purchase and delivery of a 15T-cryomagnet, an important breakthrough for our sample environment facilities. Finally, over 50% of the ancient vacuum pumps have been replaced by modern dry pumps and turbo molecular pumps.

In December a series of talks and guided tours was organised as part of the "DPT Day" in order to explain the activities of the Division. There was a very positive response to this event.

These achievements have stretched our human resources to a maximum, but we are satisfied with the progress. There remain areas where firmer project guidance may be necessary. A more detailed view of the progress so far is given below.

Werner Press

The ILL Millennium Programme: couldn't be without it![1]

W. Press (ILL)

The new chopper system for the **IN5 time-of-flight instrument** finally arrived at the ILL in the autumn - just in time to have it installed on the instrument and tested with neutrons. The intensity gains promise well for the future (figure 1).

The **IN8 triple-axis spectrometer** came on line during the last reactor cycle and is providing much-improved neutron intensity and excellent results. With some additional shielding the initial radiological problems have been dealt with.

The **D3 diffractometer** is establishing itself as the home of polarization development. Amongst other improvements on D3 in 2002, progress on the new version of Cryopad deserves mention. Unfortunately, the diffractometer will not be operational in 2003, given the work to be carried out on the exchange of the hot source beam tubes.

Work on IN20, the **polarization analysis triple-axis spectrometer**, has continued, with the installation of the secondary spectrometer. Detector intensity has further increased by about a factor of 5. At the same time background conditions have been improved.

On the **small-angle scattering** instrument D22, the fast-read-out electronics of the new two-dimensional **detector** have improved, with the high count rate of at least 2 MHz now achievable. We will have to be patient, however, as the reliability of the 1m-long linear position-sensitive detectors is still in need of additional testing. We nevertheless expect the camera (consisting of 128 of these linear detectors) to be ready - as planned - this year. If other instruments (D11, D2, IN5, etc.) are to benefit from this development, appropriate budgets will have to be found.

Figure 1: Installation of one of the IN5 double choppers: with very small gaps between chopper disks and guides - this is precision work.

A completely new **instrument for strain analysis** (Univ. Manchester/ILL) is on its way, complete with a name-change from Strain Imager to **SALSA** (Strain Analyser for **L**arge- and **S**mall-scale engineering **A**pplications). In 2002 both the construction of the primary instrument – casemate and guides – and the design of the hexapod-based sample area progressed considerably (see article p. 98). The latter is a rather challenging project aiming to position and orient samples of up to several hundred kilograms with a high degree of accuracy (range of 10 µm). Design work is being performed by the Swiss company OHE with the assistance of a robotics institute.

The **new facility for mechanical engineering (FaME38)** – planned as an interface between engineers and scattering techniques – is closely linked to the SALSA project. FaME38 was started in spring 2002 in collaboration with the University of Salford, to work with both neutron (ILL) and synchrotron radiation (ESRF). Standard laboratory devices and advanced software are being made available to users, aiming at a more efficient use of instruments and improving engineers' access to neutron and X-ray scattering technology (see also p. 92).

Another example of a project with a strong EPSRC-based budget is the **large-unit-cell powder diffractometer D19**, built jointly by the University of Durham and the ILL. In 2002, the detector arran-

1 - With thanks to EIROforum.

gement was decided, and work started on 3 large 2D-detectors (*bidim26*, already successfully used on D16) and a new large solid-angle banana-type detector. The first *bidim26* is expected in spring 2003, together with one segment (= 1/8) of the new banana.

As regards D2, **the high-resolution powder diffractometer**, the detector housing and collimators have been delivered. With the mounting of new position-sensitive detectors a new secondary instrument has been assembled. The instrument responsibles are now impatiently waiting for neutrons. There is additional good news concerning external funding and collaboration with the Universities of Oxford and Cambridge.

After successful new experiments with short-lived isotopes, performed despite difficulties with the sample transport trolley, it is now planned that the instrument used for the **detection of exotic neutron-rich nuclei** (a modification of the Lohengrin fission fragment spectrometer) will carry a combination of plain Ge-detectors purchased by the ILL and detectors on loan from external institutions.

A great deal of effort has been devoted to the replacement of the **neutron guides**; they have already gained in reliability and intensity. The outsourced manufacture of the H22 thermal guides is proceeding according to schedule. The specifications for the H1/H2 guide are well-advanced and work on its replacement, including the exchange of the H1/H2 beam tube, is getting underway. An assessment is also being made on the possibility of replacing the aluminium in replacement of a selection of the **beam tubes** with zircaloy, which offers much longer lifetimes.

Following the installation of a new velocity selector, the **D11 small-angle scattering instrument** is to benefit from improved collimator sections (also see article p. 102). This work will be complete by about May of this year. We are aiming to provide D11 with a new fast small-angle detector in the future, like the one on D22.

It had been planned, for 2002, that an order would be launched for a **14.9 T-cryomagnet**. In fact, in a happy combination of circumstances, an Oxford Instruments cryomagnet could be delivered shortly after the order, and was tested soon after at the ILL. To host this long-awaited extension to the ILL's sample environment, modifications to the triple-axis instruments are now being made, in order to avoid any damage to the coils of the magnet from the forces generated. It is hoped that the first successful experiments can be started on IN14 when the reactor starts up in 2003 (figure 2).

The notions "**quality**" and "**unified process**" are now frequently heard at the ILL, reflecting the launch of intense

Figure 2: Force measurements on IN14 with the cryomagnet cooled down.

work on a new approach to instrument control. The instrument computers are also being replaced independently of this.

Finally, the new "**TYREX**" compressor for polarized ^{3}He has reached completion and is performing brilliantly: the production rate has increased by a factor of almost 10 in comparison to the first compressor (figure 3).

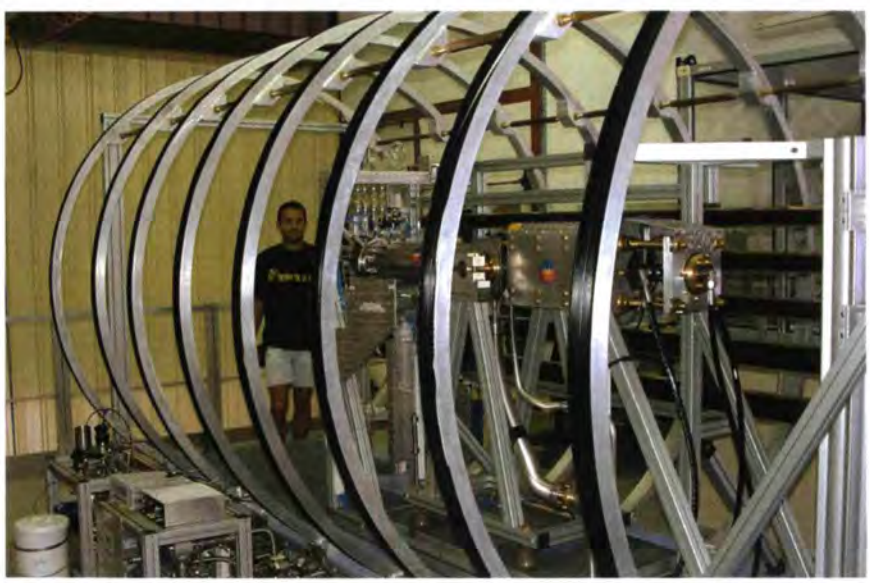

Figure 3: TYREX, which is not really a dinosaur, can now supply polarized ^{3}He much more rapidly (in the photo, David Jullien).

A parallel robot
for the Strain Imager (SALSA)

S. Rowe (ILL)

Traditionally, standard translation and rotation tables or goniometers have been used for sample positioning in various configurations, in order to generate the required degrees of freedom for the end-actuator. This serial system suffers from two primary problems. Each unit is required to support not only the load of the sample, but also the load of all the units above it. Both absolute accuracy and repeatability errors generated by each unit, are passed on in succession. Generally, these limitations do not present a problem for standard powder diffraction experiments, but may be crucial for residual stress analysis, where the highest positioning precision of big samples is required. However, other architectures do exist and the most interesting looks to be the parallel closed-loop mechanism, more commonly known as a parallel robot (figure 1 is an example).

Parallel mechanisms have several advantages. Depending on the exact configuration the load can often be purely axial, and is always distributed through the legs. The structures have a high degree of inherent rigidity, and as any errors generated in the legs are averaged, these mechanisms tend to be more accurate. Furthermore, the speed of displacement is often greater as the motors are generally positioned on the fixed base.

Figure 1: Stewart platform with a repeatability in X, Y and Z better than 5µm, and a load capacity of 20 kN.
(Courtesy of European Molecular Biology Laboratories, Hamburg)

On the other hand, calculation of the available workspace can be difficult and generally results in quite a complex shaped volume (figure 2). Within this workspace forbidden areas can exist, known as singularities. These are particular positions where the end actuator will either lose its rigidity entirely and hence fall over, or the forces in the legs will increase to infinity and result in breaking part of the robot or locking up. Finally, due to the complex mathematical relationship between the leg length and the position of the end effect, control has been a problem in the past. Modern computer systems have eliminated this disadvantage.

Historically, the design and manufacture of parallel robots have remained within the domain of academia or high-tech companies, who have had a need for a solution to unique problems, such as aircraft simulation. However, as a result of lower cost and high-speed computing availability (easing the control of such mechanisms), industry has started to make in-roads into areas traditionally restricted to standard mechanism configurations, such as high- precision placement required for silicon chip manufacture. This higher volume market means that a number of systems are now commercially available.

It is the variable actuator length Stewart platforms (also known as Hexapods or Gough platform after the original designer) that have had the highest degree of exposure. They now represent the top end of the market both in degrees of freedom (offering 6) and in terms of cost. They are marketed by such companies as Physik Instrumente [1] offering the M-850, Micos [2] building the PAROS (figure 3) and others, who offer

Figure 2: Stewart platform showing two possible work volumes, within the complex and total volume available.
(Courtesy of William Hutt, Manchester University-ILL)

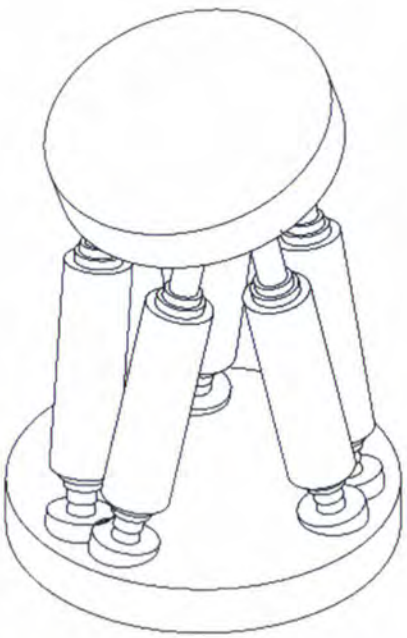

Figure 3: Stewart platform showing tilt of the top plate.

machines capable of positioning loads in excess of 50 kg to a resolution better than 2µm and 5µrad.

The majority of requirements will often not need the full six degrees of freedom offered by the above machines, and unfortunately it is this market that is currently under-developed. The large number of possible combinations of degrees of freedom has meant that unless a specific application exists, little has actually been constructed beyond theoretical models, although a number of interesting smaller units are available from such companies as New Focus [3].

Figure 4: CAD 3D image of the proposed Stewart platform being developed for the ILL. *(Courtesy of OHE)*

What is the ILL's position regarding parallel robots? The ILL is constructing a neutron Strain Imager as part of the Millennium Programme and in collaboration with the University of Manchester (partly funded by an EPSRC grant). Its sample positioning system will consist of a full six degrees of freedom Stewart platform, capable of positioning loads up to 500 kg to better than 50µm. The initial configuration was designed jointly by the ILL and INRIA Sophia-Antipolis. This is now in the process of being turned into a detailed 3D model by OHE [4] (see figure 4). The basic features will be six hydraulically driven actuators, each with a stroke of 470 mm and a working pressure of up to 160 bar. A linear transducer with a resolution of 0.1 µm will be positioned within each cylinder and used to determine the leg length. Control will be via a controller-board with a 500 MHz CPU with a cycle-time of 4 kHz. These actuators will be fixed to the top and bottom plates using universal joints. The speed of operation and workspace will be restricted, with two or three possible configurations within the total volume available. These will hopefully be singularity free, although until the final configuration is realised it is not possible to calculate whether this will be the case. If not, then position restrictions will be incorporated into the driver software.

What is the future? There is no danger of the disappearance of traditional serial robots - their simplicity of control and use will always safeguard their place in the market. But certainly the Strain Imager Stewart platform represents a leading edge technology with regard to load capacity and positioning precision. In general, the advantages provided by parallel type architectures will ensure an increase in their use.

Figure 5: Stewart platform. *(Courtesy of Micos)*

REFERENCES

[1] Physik Instrumente (PI) GmbH & Co, D-76337 Waldbronn, Germany
[2] Micos, D-79224 Umkirch, Germany
[3] New Focus, San Jose CA 95138, USA
[4] OHE, Ebikon, CH-6030 Switzerland

A new copper *monochromator for D20*

P. Courtois, M. Berneron, A. Escoffier, B. Hamelin, R. Hehn, E. Hetzler, C. Menthonnex and B. Mestrallet (ILL)

Starting from copper crystals of high quality grown at the ILL, a new Cu(200) doubly focussing monochromator in transmission geometry has been built for the diffractometer D20. Installed in June 2002, it provides a gain in intensity of more than 50 % at the sample position as compared to the old set-up. We present here the procedure used in the production of this new copper monochromator.

The growth of high quality copper crystals is well established at the ILL and large crystals (diameter 75 mm and length 300 mm) with a uniform intrinsic mosaicity distribution in the range of 1 to 5 minutes can be easily produced (figure 1). Thanks to this, very efficient doubly focussing neutron copper monochromators can be constructed at the ILL. Roughly speaking, the vertical focussing leads to a substantial increase in the neutron flux, whereas the horizontal focussing directly affects the resolution of the instruments.

Besides the growth of large single crystals, the main difficulty involved in the production of a copper monochromator for neutrons is the use of crystals with a well controlled and often anisotropic mosaicity. In order to obtain reasonable reflected intensities, the crystal mosaicity in the diffracting plane (horizontal mosaicity) has to match the incoming beam divergence (which is generally rather large as compared to the mosaic spread of the as-grown crystal). Moreover, the mosaicity in one direction perpendicular to the diffracting plane (vertical mosaicity) should be as small as possible in order to permit efficient vertical focussing of the beam onto the sample.

The "onion peel" method developed at the ILL - consisting of stacking thin wafers of copper crystals - is a well adapted technique for producing copper crystals with anisotropic mosaicity [1]. Unfortunately, in the case of D20, this

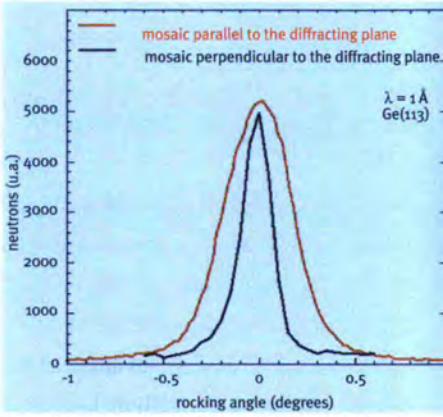

Figure 3: Typical neutron rocking curves for a Cu(200) single crystal plate used for the new D20 monochromator (Measurements performed on T13A at 1 Å using a perfect Ge(113) monochromator).

Figure 1: Hard X-ray diffraction image and peak profile obtained from a copper single crystal of high quality grown at ILL.

Figure 2: The new D20 copper monochromator.

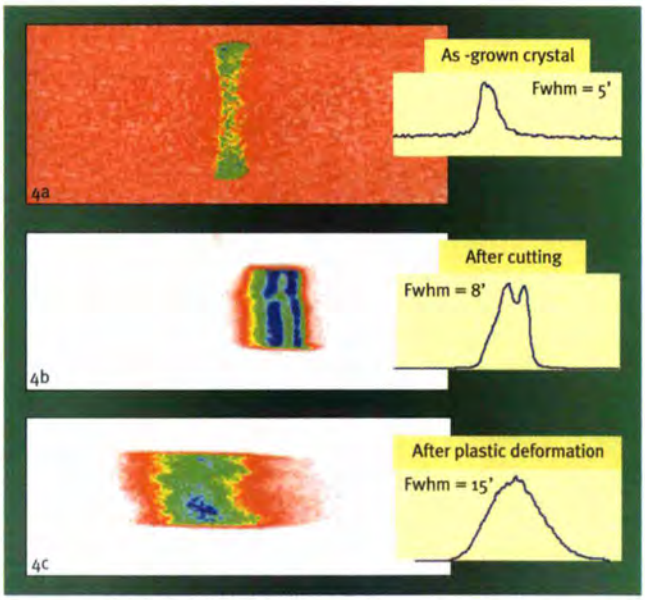

Figure 4: Hard X-ray diffraction images and peak profiles obtained from Cu(200) copper single crystals showing the evolution of the horizontal mosaic distribution. Figure 4a: the as-grown crystal; figure 4b: the crystal after cutting; figure 4c: the crystal after plastic deformation.

method could not be applied because it was not possible to cut the long copper wafers (length 75 mm and thickness about 1.5 mm) by electro-erosion without inducing dramatic changes in the mosaic structure of the crystal. This was one of the main reasons why we used plastic deformation at high temperature instead in order to obtain single crystal plates with the required scattering properties.

The new D20 copper monochromator was built to improve the neutron flux onto the sample at a wavelength of 1.36 Å [2]. It is a doubly fixed focussing Cu(200) monochromator in transmission geometry (see figure 2). It consists of a column of 13 curved copper crystal plates (75*22*6.5 mm^3) characterised by a horizontal neutron mosaic spread ($fwhm_{//}$) of 0.35° and an anisotropy factor ratio $fwhm_{//} / fwhm_{\perp} = 2$ (figure 3). The crystal thickness and the horizontal mosaic spread have been optimised for a wavelength of 1.36 Å.

The starting material was a large copper single crystal with an intrinsic mosaicity of 5 minutes which was cut by spark electro-erosion into the above-mentioned plates (figure 4a). The direction of cutting was parallel to the Cu(220) crystal planes in order to obtain plates with the Cu(200) crystal planes perpendicular to their surfaces as required for D20. Detailed studies using hard X-ray diffraction have shown that the quality of the Cu(200) planes is affected by the electro-erosion process. As shown in figure 4b, after cutting, we observed that the horizontal mosaicity has a double peak structure and its distribution is quite inhomogeneous. This effect is not well understood at present, but it is certainly due to complex thermo-mechanical deformations induced along the (200) planes during the spark electro-erosion cutting. Moreover, the change in the microstructure probably depends on the amount of dislocations present in the as-grown crystal. This important feature has been taken as an advantage in order to construct the D20 copper monochromator. Indeed, the vertical mosaicity being unchanged, it directly gave rise to an anisotropy in the mosaic distribution!

The real difficulty was therefore to improve the neutron scattering properties of the crystal plates with regard to their homogeneity and mosaic spread after the cutting process. This difficulty was overcome by plastic deformation at high temperature, even though previous studies have shown that it is difficult to produce a controlled and reproducible mosaic spread in this way. [3]. However, by applying a well adapted pressure perpendicular to the surface of the copper crystal plates at high temperature, we both successfully increased the mosaic spread up to the desired value for D20 and widely improved its uniformity (see figure 3 and figure 4c). In addition, through careful positioning in the hot-pressed furnace, it was possible to produce a mosaic distribution which is fairly homogeneous throughout the length of the crystal (figure 5a). Thirteen single crystal plates were prepared in a reproducible way using the plastic deformation technique developed at the ILL for the D20 project.

To bring about the horizontal focussing, with the aim of improving the peak shapes on D20, we decided to curve the copper crystal plates with a radius of curvature R = 7m corresponding to an optimum for the diffractometer at 1.36 Å. The curvature was reached without affecting the quality of the crystals

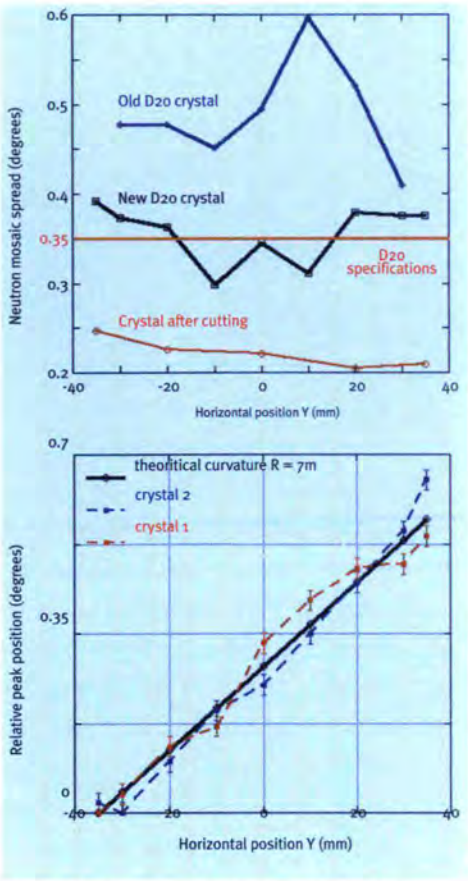

Figure 5: Neutron mosaic distribution of a typical crystal (figure 5a) and the relative peak positions (figure 5b) as a function of the horizontal position on the crystal (y = 0 denoting the centre of the crystal plate).

by using very smooth plastic deformations applied with an anvil having a special shape (figure 5b).

Afterwards, we glued each crystal plate on a special Cu support, which, apart from the central one, had been machined by electro-erosion to an angle corresponding to the vertical focussing, i.e. 0.7°, 1.4°, 2.1°, 2.8°, 3.5°, 4.2° respectively (figure 2). Finally, the crystal plates were oriented in both directions by neutron diffraction, with an accuracy of 0.02°.

The new monochromator was installed on D20 in June 2002, providing a gain factor of more than 50 % at the sample position as compared to the old set-up.

REFERENCES

[1] B. Hamelin, ILL Annual Report (1966) 80
[2] T.C. Hansen et al., Proc. ILL Millennium Symposium Symposium 2001, 276
[3] A.K. Freund, ORNL Report N8 CONF-760601-P2 (1976) 1143

Renewal
of the D11 collimation after 30 years

P. Lindner (ILL)

In a first step of the D11 renewal project, the selector area and the guide sections between 20.5 m and 40.5 m away from the sample position have been completely refurbished during the winter shutdown 2001/ 2002. The Dornier velocity selector has been displaced close to the entrance of the collimation section at 40.5 m. By replacing the two separated guides in front of the selector by a single Ni-guide, the air gaps and the number of windows in this area have been reduced, resulting in a 30% gain of neutron flux at the collimation entrance, after the selector.

The 30 year old neutron guides have been exchanged during this first intervention against new glass guides (1 m length each) and a new computer controlled translation mechanism between the selector and the 20.5 m position. Two additional collimation distances at 28 m and 34 m have been introduced, allowing for optimised flux conditions for low Q experiments at detector distances between 20 m and the maximum distance of 36.7 m.
It is now possible to perform SANS experiments at a distance slightly smaller (36 m) than the maximum distance, but with a collimation setting of 34 m (instead of 40.5 m so far): moving the apparent source by 6.5 m closer to the sample yields a 45% flux increase (which for some experiments compensates the loss of 2 data points due to a slightly larger masking of the central beam stop region).

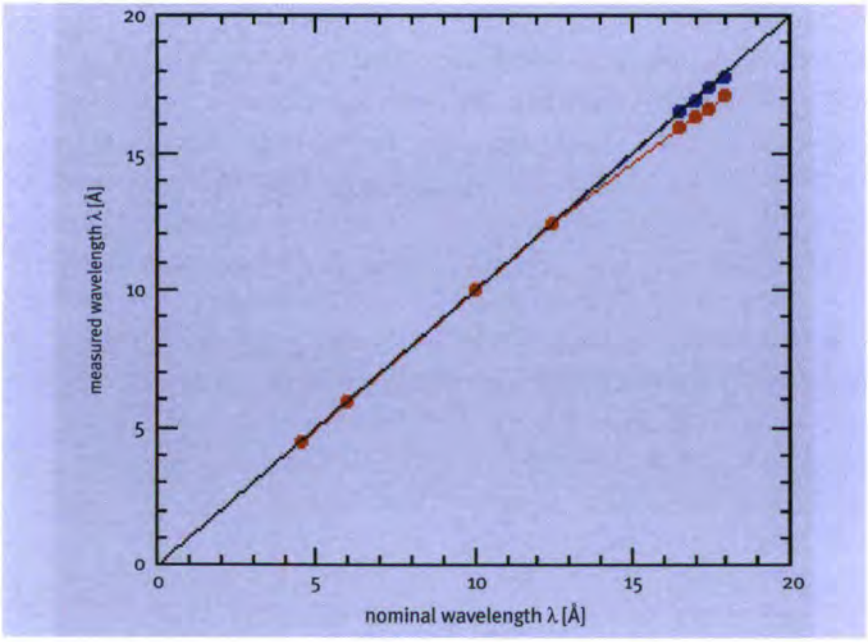

Figure 1: TOF wavelength calibration at D11. Drawn line: standard conditions (collimation 10.5 m). Red circles: standard aperture (20.5 m) 35 x 55 mm and collimation distance 40.5 m. Blue circles: asymmetric aperture (20.5 m) 35 x 78 mm and collimation distance 40.5.

The project continues during the winter shut-down 2002/2003 with the renewal of the neutron guides and their translation mechanism between the 20.5 m and the sample position and the introduction of a new collimation distance at 1.5 m.

Another aspect of the ongoing D11 renewal is the installation of diaphragm changers with variable apertures of rectangular and circular shapes at distances of 20.5 m, 10.5 m, 5.5 m and at the new 1.5 m collimation distance (to be installed during the winter shutdown 2002/ 2003). The rectangular standard apertures used up to date with their size of 55 x 35 mm are slightly larger than the neutron guides (50 x 30 mm). For long wavelength neutrons and at large detector and collimation distances a significant part of the beam is cut off in the collimation housing due the distinct parabolic neutron flight path.

In summer/autumn 2002, the prototype of a new asymmetric diaphragm with an extended vertical opening (35 x 78 mm) has been tested at the 20.5 m collimation position of D11. For the maximum detector distance 36.7 m and a collimation of 40.5 m, we measured a flux increase by a factor of ≈ 3 for a wavelength $\lambda = 16.5$ Å and ≈ 10 for a wavelength $\lambda = 18$ Å.
Furthermore, the partial masking of the beam by the old standard diaphragm changes the neutron wavelength for ultra-low Q experiments. This effect has been confirmed with

time-of-flight (TOF) calibration measurements by comparing the old standard diaphragm with the new asymmetric diaphragm at the 20.5 m position (figure 1). For the new asymmetric diaphragm (35 x 78 mm) at the 20.5 m position (full circles in figure 1), the measured wavelength is in much better agreement with the standard TOF calibration (drawn line in figure 1).

The improved conditions for ultra-low Q experiments at D11 are illustrated in the following example.
Electro-rheological fluids [1] (usually made of apolar oils into which colloidal particles are dispersed) respond to an applied electrical field by switching from a disordered fluid-like structure to an ordered structure with a solid-like response. They are mainly used as hydraulic actuators in micro-devices. More research on these fluids is performed in order to use them as electro-optical devices, e.g. sensors, ruptors, switches, narrow-band filters and wave guides. When an electrical field is applied, the particles (having a different electrical polarizability than the dispersion medium) are polarized and become small electrical dipoles. Above a certain field threshold, these dipoles attract each other and assemble into chains that are aligned along the field direction. These chains extend across the whole fluid and block its flow, thus giving rise to the electro-rheological effect.

In December 2002, a SANS experiment was performed at D11 by Persello et al. (Experiment n° 9-10-651) in order to determine the structures of the chains in such an electro-rheological fluid. The experimenters wanted to measure the mean inter-particle distance as a function of the applied alternating electrical field, and in this way observe the competition between the field-induced attraction and the inter-particle repulsion. However, these distances are at the very end of the usual range of small-angle neutron scattering experiments. Only with the new asymmetric diaphragm at the 20.5 m collimation distance and the flux gain obtained with this recent improvement in the D11 collimation system, it has become possible to use very long neutron wavelengths (up to 18 Å) and the maximum sample-to-detector distance of 36.7 m, hence giving access to low momentum transfers down to $Q = 5 \times 10\text{-}4$ Å^{-1}. Under these conditions, a remarkable diffraction pattern has been found (figure 2): at high fields, a one-dimensional set of diffraction spots is obtained, located in the direction of chain alignment. The horizontal spacing of these diffraction spots yields the average inter-particle distance, which is found to vary with the electrical field. From the extension of the spots in perpendicular direction, we can determine the cross-section of the (thin) chains, and find out whether they are single-stranded or multi-stranded. When the field is switched off, the scattering pattern immediately reverts to the azimuthally isotropic pattern of isolated spherical particles, indicating that the effects are fully reversible down to the particle scale.

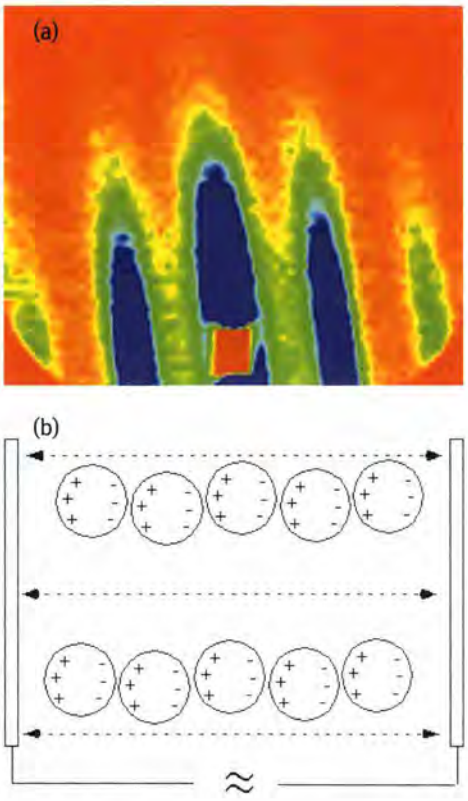

Figure 2: Electro-rheological fluid (spherical silica particles of diameter 460 nm dispersed in methylcyclohexanole, volume fraction 10%) in an alternating electrical field of 3.75kV/cm.
a) SANS at D11: λ = 16.5 Å, sample-to-detector-distance: 36.7 m, asymmetric collimation diaphragm at 20.5 m;
b) Real space picture of the chain alignment in the alternating electrical field (snap shot).

REFERENCES
[1] J. Persello, B. Cabane, C. Gehin, J.P. Boisvert, A. Guyard, G. Bossis, ILL experiment n° 9-10-651

Towards a perfectly *polarized neutron beam*

A. Petoukhov, T. Soldner, V. Nesvizhevsky and M. Kreuz (ILL)
M. Dehn (University of Mainz)
M. Brehm (University of Heidelberg)

We propose a new method of double super-mirror polarizers in crossed geometry for neutron beam polarization. With such a geometry, it is possible to reach a beam polarization of 99.60(5) % without any significant spatial and wavelength dependence between 3 and 10 Å.

Many experiments in particle physics with cold neutrons require both a high degree of neutron polarization and its precise measurement. High neutron polarization is crucial for measurements of electron and anti-neutrino asymmetry in neutron beta decay. Improvements of these experiments are particularly important to test the unitarity of the Cabibbo-Kobayashi-Maskawa matrix and to search for right-handed currents. The next generation of these experiments requires the beam polarization to be known to better than 0.1 %. Other types of experiments require a neutron beam with a very homogeneous and wavelength independent polarization, with variation of less than 10^{-3} (the absolute value is less important here). Examples are spin-rotation experiments that search for parity or time reversal violation in the passage of polarized neutrons through matter.

Presently, super mirror (SM) polarizers [1] are the most powerful tool to polarize a white neutron beam. They exploit the strong spin dependence of the neutron reflectivity on magnetised SM. Using this technique, a polarized neutron beam with an intensity of $3 \cdot 10^8$n/cm^{2}s and an average polarization of 98% is available at the instrument PF1B at the ILL. However, the variation of the polarization in the beam due to wavelength and position can be as high as 20% and 3%, respectively (see figure 2). This strong variation limits the application of SM polarizers in spin-rotation experiments since a change of position or orientation of the sample changes the effective neutron polarization.

In polarization analysis, only the convolution of polarizing and analysing power can be determined. Therefore, for an absolute measurement of the beam polarization - as required by neutron beta decay experiments - the analysing power has to be known independently. This is not possible with SM analysers but can be solved using opaque ^{3}He spin filters [2]. This technique provides 100% analysing power and is not angle and spatial dependent. It can therefore be used to average over the neutron beam (with several practical problems like corrections for windows, the time dependence of ^{3}He polarization, etc.). However, it is limited to a narrow wavelength range by a very low and wavelength-dependent transmission of less than 10^{-3}. Moreover, for an inhomogeneous beam, even the correct average polarization may differ from the average seen from the experimental set-up.

A perfectly polarized neutron beam should therefore be homogeneous on the level of the attempted experimental precision. Today, this can be obtained neither with a single SM nor with a ^{3}He polarizer.

We propose to use double SM polarizers in crossed geometry (figure 1). This geometry is particularly important since the angular acceptance of one device is independent of the angular acceptance of the other. Therefore, both devices are independent. This allows us to predict the properties of the combined polarizers (polarization P_{12} and transmission T_{12}) from the properties of the single devices (P_i and T_i):

$$P_{12} = \frac{P_1 + P_2}{1 + P_1 P_2} \approx 1 - \frac{1}{2}(1 - P_1)(1 - P_2)$$

and $T_{12} = T_1 T_2$.

Using typical SM polarizer properties ($P_i \approx 98\%$), we predict a very high polarization ($P_{12} > 99.9\%$) for a wide wavelength range and an angular variation of less then 10^{-3}. The intensity

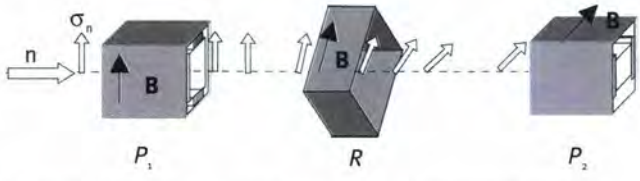

Figure 1: Scheme of double SM polarizer in crossed geometry.

should only drop to about 50% of the single device ($T_i \approx 50\%$ for the "good" spin component).

For the experimental test at PF1B the following set-up was used: the polarized beam was created by double SM polarizers in crossed geometry, followed by a radio frequency flipper (f=50 kHz) and a current sheet flipper. The beam was analysed by either a single SM analyser, double SM analysers in crossed geometry, or a polarized ^{3}He spin filter. A time-of-flight set-up allowed us a wavelength-resolved analysis. All SMs were adjusted to maximum transmission. To cover the wavelength range between 3 and 10 Å, different ^{3}He cells and pressures were used.

In figure 3b the performances of the two spin flippers are compared. The efficiency of the radio frequency flipper was 99.93(1)%, averaged between 2 and 15 Å (only statistical error given). Figure 2a (2b) compares the wavelength (angular) dependence of the product AP of polarization and analysing power for the single and the crossed analyser. Both dependences are suppressed strongly for the crossed analyser. Figure 3a compares the AP products for the crossed analyser and the ^{3}He spin-filters. The values 99.01(5)% and 99.60(5)% differ significantly. We explain this by a depolarization in the SM analyser and attribute the difference between 99.60(5)% and 100% to a depolarization in the SM polarizer itself. A depolarization during the polarization transport can be excluded since we use the same configuration and change only the analyser. Moreover, any depolarization due to a non-adiabatic transport in the magnetic field should be wavelength-dependent. This was not observed within the obtained precision of 10^{-3}.

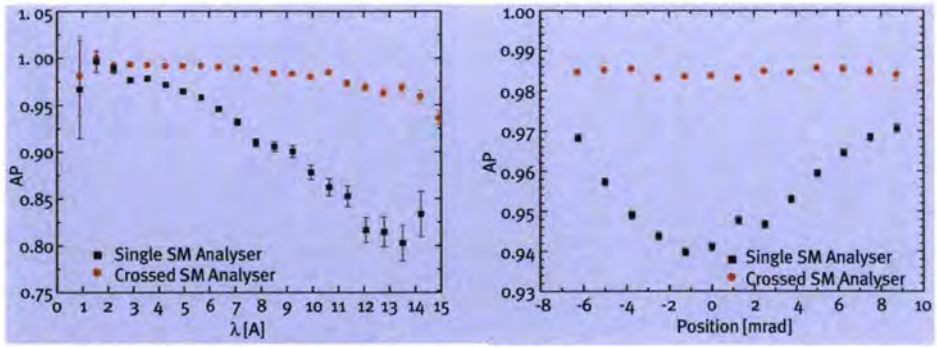

Figure 2: Comparison of single analyser and double SM analyser in crossed geometry. a) wavelength dependence, b) angular dependence.

To check the depolarization, we reduced the magnetic field in the SM housing from 35 mT to 20 mT in both, polarizer and analyser. The AP product dropped by 1%.

We conclude: 1) For absolute measurements of correlations in neutron beta decay and for spin-rotation experiments, double SM polarizers in crossed geometry should be used to polarize the beam. With this set-up, an average polarization of more than 99.5%, without any significant spatial and wavelength dependence, can be obtained for a cold-neutron beam. The neutron flux is only reduced by about 50% compared to a single SM polarizer. 2) For such a perfect beam the polarization can be measured with a precision of better than 0.1% using ^{3}He spin filters. 3) A spin flip efficiency of more than 99.9% can be reached with a radio frequency spin flipper.

We hope that the absolute value of polarization can be increased in the near future using higher SM housing magnetic fields.

Acknowledgements

We thank H. Humblot, D. Jullien, and F. Tasset for providing us with polarized ^{3}He cells, M. Thomas for optimising the magnetic housing for the ^{3}He cells, R. Gähler for providing us with his nice new SM polarizers, and D. Berruyer for preparing many components of the installation.

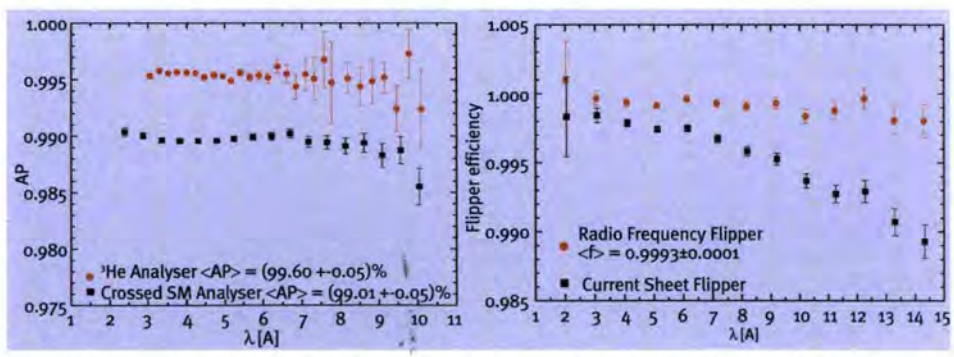

Figure 3: Comparison of a) double SM analyser in crossed geometry and ^{3}He spin filters, b) radio frequency and current sheet spin flipper.

REFERENCES

[1] O. Schärpf, N. Stüsser, NIM A 284 (1989) 208. O. Schärpf, Physica B 156/157 (1989) 639
[2] O. Zimmer, Phys. Lett. B 461 (1999) 307. O. Zimmer, T.M. Müller, P. Hautle, W. Heil, and H. Humblot, Phys. Lett. B 455 (1999) 62

TYREX, a new polarized ^{3}He filling station for Neutron Spin Filters

F. Tasset, K. Andersen, R. Chung, H. Humblot and D. Jullien (ILL)
L.P Regnault (CEA-Grenoble)

The ILL production capacity of polarized ^{3}He has been increased by an order of magnitude with the advent of the new TYREX machine in 2002. Up to four ILL instruments can now be provided with fresh spin-filter cells every day. Simultaneously, the polarization in the spin-filter cell has been increased and now exceeds 60%. We expect to reach 65-70% polarization by the end of 2003.

Polarized ^{3}He gas has now been routinely produced at the ILL for the last 5 years. The gas is processed in a central facility using Metastable Exchange Optical Pumping (MEOP), which is presently the most effective route for high-spin polarization. This method only works in a discharge at low gas pressure and a polarization preserving mechanical compressor is therefore needed to inflate cells to the appropriate pressure. Neutron Spin Filter cells are then detached from the filling station and delivered at remote beam lines (RMEOP) where they can operate in appropriate magnetic containers before being replaced typically once a day. The technique is not trivial but owing to developments at various places, in particular ENS-Paris, the University of Mainz and the ILL, considerable progress has been made during the last decade. RMEOP now appears more and more as a generic neutron polarization analysis method capable of high-quality measurements, specialised for short wavelengths and large solid angle coverage on thermal-to-cold neutron instruments. The ILL is playing a key role, featuring modern IR light sources, a state-of-the art mechanical compressor, cells with various shapes and silicon windows and magnetostatic cavities at selected spectrometers.

A new kind of laser has been introduced, which represents a leap forward for MEOP. Infra-red fiber lasers, a product of the telecommunications industry, have now replaced the LNA crystal solid state lasers introduced 10 years ago at ENS-Paris. Following preliminary tests at Mainz and Jülich, such a 2 W Yb-doped fiber laser was acquired 2 years ago at the ILL. As these lasers are now fully optimised for Helium pumping, it has been decided to acquire four units of 4 W this year, representing an optimally flexible solution for TYREX and its 5 optical pumping cells.

Several years of exploitation for the COW prototype delivered by the University of Mainz have led to the independent design at the ILL of a much improved polarization preserving compressor, which makes up the heart of the new TYREX filling station.

Made of non-magnetic Titanium alloy, the compression unit features a single 5.2 litre stroke volume with a very small 0.15 cm^3 dead-volume. The high purity of the ^{3}He gas is maintained by using

Tyrex main characteristics (November 2002)

Magnetic Guide Field
9 coils, 2 m diameter;
B = 8 Gauss, $\Delta B/B < 10^{-4}$/cm in 1.3 m^3.

Light source
Infrared Yb-fiber laser (All-fiber V-Groove Tech. from Keopsys SA);
Optimised for Helium gas 2^3S_1-2^3P transition (1083 nm, 2 GHz bandwidth);
Individual fiber optics, adjustable telescopes, polarizing beam splitters, end-mirrors;
Power: 8 W (two 4 W units);
Planned (Spring 2003): five 4 W units.

^{3}He Polarization in Low Pressure Stage
Metastability Exchange Optical Pumping (MEOP) in a weak RF discharge at 0.9 mbar;
5 interconnected Pyrex cylinders 6-8 cm diameter, 2.3 m length and 37 liter total volume;
Spin Polarization (668 nm fluorescence monitoring): 65 %;
Relaxation time (without discharge): 25';
Sustainable flux (8 W): 1.3 bar.liter/hour (58 mmole/hour).

Volumetric Unit data
Powerful hydraulic actuator under closed-loop computer control ;
Velocity: 30 cm/sec, final position within 3 µm precision;
Polarization Preserving Piston and chamber: Titanium alloy, 11 cm diameter and 55 cm stroke;
Total displacement: 5200 cm^3, Dead volume: 0.15 cm^3;
Relaxation time for polarization T1 ~ 1 hour at 200 mbar in 300 cm^3;
Insignificant Gas contamination after 8 hours closed-cycle operation with LN_2 trap & vacuum guards.

Intermediate Pressure Storage Buffer
Uncoated Quartz glass: 2.5 liter;
Typical inflation rate: 10 mbar/minute;
T1 relaxation time ~ 45 hours at 200 mbar.

High Pressure In-Out ports
2 independent in/out ports;
Pressure: up to 6 bar;
Spin Polarization: > 60 %.

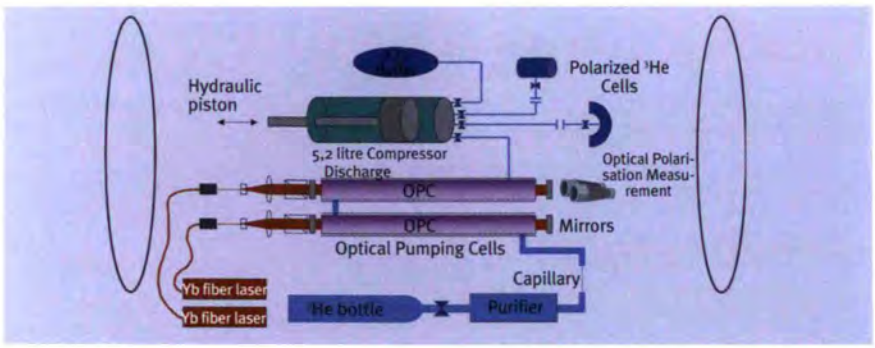

Figure 1: Schematic of TYREX.

double quad-rings and vacuum guards, designed into a comprehensive vacuum network throughout the compressor head, in parallel with the main channels devoted to gas transportation.

The piston is actuated by a powerful hydraulic system, giving a highly satisfactory dynamical performance to the system, which is designed to process two cells in parallel. All the electronic control values, sensors and gauges are accessible via a high-speed digital interface (National Instruments). A Labview program with a friendly graphical user interface controls the hydraulic power system, the piston, the compressor head and all the ^{3}He-gas circuit.

TYREX has been entirely designed, built and assembled at the ILL in 3 years. High-pressure polarization was tested in July and the machine commissioned in September 2002. First neutron measurements made at PF1B in July confirmed the value of polarization obtained with the fluorescence light from the low-pressure discharge. In September, with 8 W of light available, the end-product polarization reached a reproducible 60 %, allowing to deliver several cells successfully for a scheduled experiment at the EVA reflectometer.

We believe that the imminent installation of the 4 laser units from Keopsys will allow us to reach 65 % as was originally foreseen in the TYREX project. The use of a high resolution position detector makes the hydraulic actuator capable of a positioning precision of 3 µm. This means that the piston chamber can be operated reversibly, taking a precise amount of gas at high pressure in the Spin Filter cell to expand and be recycled in the optical pumping stage in order to refresh its polarization. Very encouraging tests have been made, opening the possibility of operating our system in a Closed Cycle mode of operation, as could be desired in future applications.

Acknowledgements

We acknowledge important scientific and technical help from Y. Gibert, E. Lelièvre-Berna, A. Petoukhov and M. Thomas. We also thank ILL services and CEA-Grenoble for their valuable assistance. This project, mainly funded by a 3-year grant from EPSRC, benefited also from the ENPI Access-RTD Network (EC-HPRI-CT-1999-50016) coordinated by ILL.

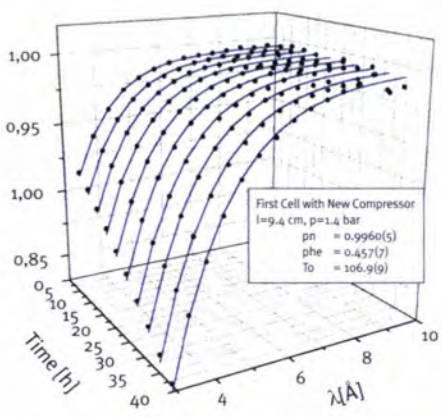

Figure 2: Early check of Helium-3 polarization from TYREX with a TOF neutron measurement on PF1B (Courtesy A. Petoukhov & T. Soldner).

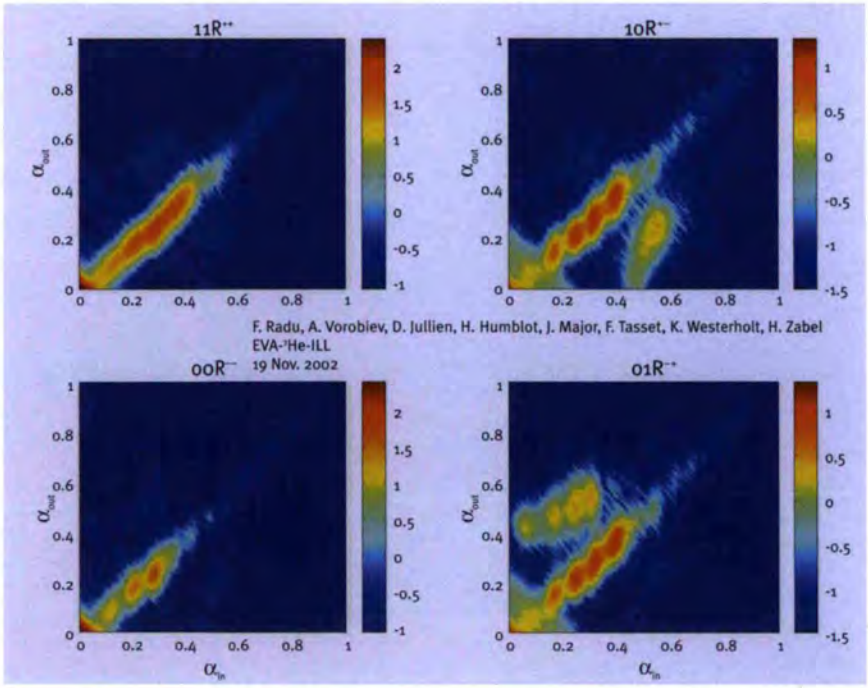

Figure 3: November 2002: Resolving off-specular spin-flip scattering on EVA with a ^{3}He-NSF from TYREX (Courtesy F. Radu & A. Vorobiev).

Large solid-angle *polarization analysis using a ^{3}He spin filter on a multidetector spectrometer*

J.R. Stewart, K.H. Andersen, H. Humblot, C. Ritter and T. Roberts (ILL)
R. Cywinski (University of Leeds)
W. Heil (University of Mainz)

The advent of the polarized ^{3}He spin-filter has made it possible to polarize neutrons efficiently in the hot and thermal neutron energy ranges, and to analyse neutron polarization over a large solid angle. ^{3}He spin-filters have been employed with great success for over 5 years at the ILL on the hot neutron instruments D3 and IN1, as well as on the thermal triple-axis spectrometer IN20. However, the simultaneous application of large solid-angle polarization analysis coverage and thermal neutron energies, for which the ^{3}He spin filter is so supremely well-suited, has, up till now, not been achieved. We present here the first large-solid angle polarization measurement using a ^{3}He spin-filter at thermal neutron energies.

Experiments with polarized neutrons:

- are essential for the accurate determination of absolute neutron cross-sections;
- provide the ability to unambiguously and simultaneously determine the individual nuclear, spin-incoherent and magnetic scattering cross-sections;
- provide the means of performing ultra-high resolution inelastic neutron spectroscopy;
- are invaluable in the determination of magnetic structures and form-factors.

Polarized neutron experiments are often limited by their inherently low counting rates, and by severe restrictions in the ranges of energy and momentum transfer available. These restrictions can be partially addressed by brute-force. For example, the D7 diffuse scattering spectrometer employs over 6000 individual supermirrors on a multidetector in order to provide a wide momentum transfer range [1], but the energy transfer range of these supermirrors is extremely narrow, with the supermirror devices being virtually opaque to neutrons of energies larger than 10 meV. ^{3}He spin filters, however, make it possible to analyse neutron polarization over a wide Q-range and energy range simultaneously [2], thus enabling wide-angle polarization analysis in the thermal and hot neutron energy regimes.

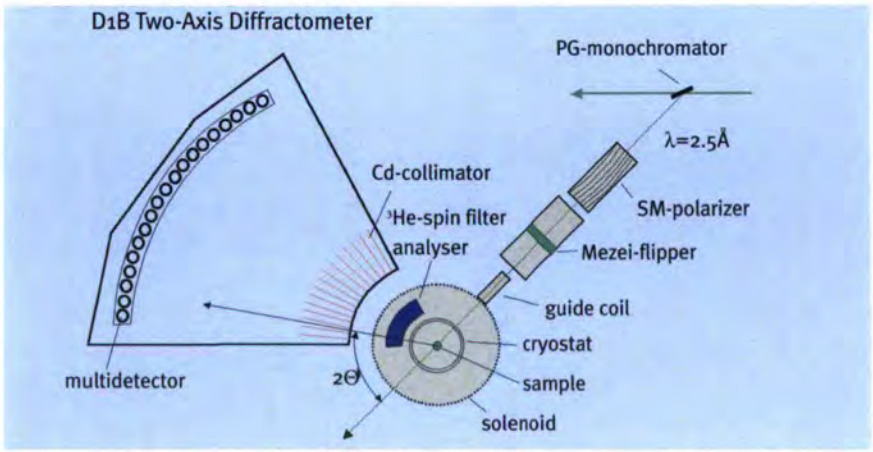

Figure1: A schematic view of the set-up of the D1B spectrometer equipped for polarization analysis using a ^{3}He spin filter. The beam is polarized by a supermirror Schärpf-type bender. The ^{3}He spin-filter is positioned close to the sample in the scattered beam.

Figure2: The ^{3}He spin filter used in this measurement, produced at the ILL by W. Heil and H. Humblot. The horizontal coverage of the cell is 90°, and the height of the cell is 70 mm. The cell contained 2.7 bar of ^{3}He during the measurement.

In order to demonstrate the effectiveness of ^{3}He spin-filters for neutron polarization analysis at thermal neutron energies, over a wide solid angle, we have performed a neutron polarization analysis study of a magnetic amorphous metal, Y_6ErNi_3 on the D1B diffractometer at the ILL [3]. This sample was cho-

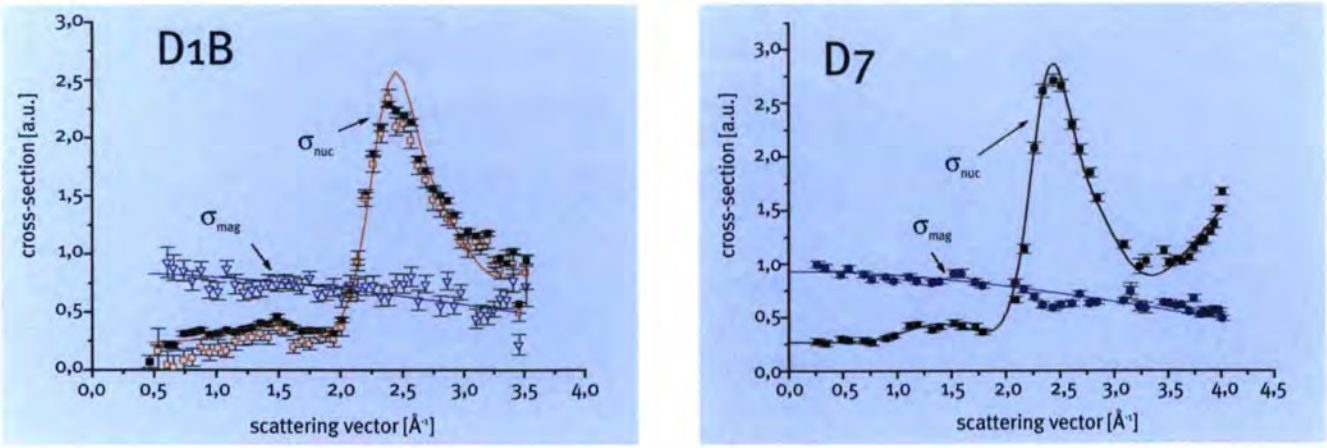

Figure3: Comparison of the nuclear and magnetic scattering cross-sections measured on D1B with a ^{3}He spin filter and on D7 with a multidetector containing 6000 individual supermirrors. The data taken on each spectrometer are qualitatively identical, showing that the ^{3}He spin-filter provided a clean separation of the magnetic and nuclear cross-sections.

sen since it had previously been studied on the D7 spectrometer, enabling a quantitative comparison of the results obtained. The instrument set-up employed is shown in figure 1, and the wide angle ^{3}He spin-filter used in the measurement is shown in figure 2. Measurements of a standard quartz sample showed that the initial polarization of the ^{3}He nuclei was 52%, giving a neutron analysing power of 87%. The quality of the filter and the homogeneity of the magnetic guide field assembly around the spin filter led to a ^{3}He nuclear spin-relaxation time of 92 h – which was ample to allow the experiment to proceed for an entire 2 day period.

The separated spectra – nuclear and magnetic – obtained during this experiment are shown in figure 3, along with the same spectra obtained using the D7 spectrometer. The D1B data are heavily binned to reduce the number of points to approximately the same as the D7 data. It is immediately apparent that both the D1B and D7 data set are qualitatively identical, with a typical glass-like structure factor exhibited in the nuclear spectrum, and a flat magnetic scattering cross-section. The solid line through the magnetic spectra is the squared Er^{3+} magnetic form-factor. The line through the nuclear spectra measured on D7 is a fit to a series of four Gaussian peaks. This fit is then superimposed on the D1B nuclear spectrum to give the red line in the figure. Since the spectra taken on each instrument are identical it is clear that the ^{3}He spin filter has provided a clean separation of the magnetic and nuclear structure factors over a wide solid angle at thermal neutron energies.

This is an extremely encouraging result since the D1B spectrometer suffered from an extremely high background, and also a low incident beam polarization coming from the supermirror bender polarizer. Looking again at figure 3, the solid black symbols in the D1B spectrum represent the extracted nuclear cross-section without a background subtraction having been performed. We see that the statistical error bars are much reduced here, demonstrating that the background on D1B was a significant fraction of the measured signal. This is not the case on D7, where great care has been taken over many years, to ensure that minimal background contamination is present. Therefore, given an optimal low background instrument, with a high incident beam polarization, we can confidently expect that the performance of the ^{3}He spin filters will easily surpass that of supermirror benders, in the thermal energy range. This is especially true since the level of ^{3}He nuclear polarization now routinely attains values as high as 65%, giving a greatly increased analysing power.

A working group has recently been set up at the ILL to finalise the design of the proposed PASTIS instrument, which will be the first at the ILL to make dedicated use of a wide angle ^{3}He spin-analyser, almost identical to the one used in this study, and allowing for the first time, polarization analysis experiments on a multidetector spectrometer at thermal neutron energies. This instrument will have broad application in the fields of

- itinerant magnetism – (high-energy zero-point spin-fluctuations);
- phonon-magnon coupling studies;
- amorphous magnetism (where a wide Q and ω range is generally required);
- disordered molecular systems [4] (oxygen, non-simple liquids, nanotubes), and many others.

REFERENCES

[1] O. Schärpf and H. Capellmann, Phys. Stat. Sol. A135 (1993) 359
[2] D.J. Goosens and L.D. Cussen, Nucl. Inst. Meth. Phys. Res. A 481 (2002) 475
[3] W. Heil, K.H. Andersen, R. Cywinski et al., Nucl. Inst. Meth. Phys. Res. A 485 (2002) 551
[4] M. Garcia-Hernandez, F.J. Mompean, O. Schärpf, et al., Phys. Rev. B 59 (1999) 958

Holographic imaging *of single atoms using thermal neutrons*

L. Cser and Gy. Török
(CRISP Budapest)
G. Krexner (University of Wien)
B. Farago (ILL)
I. Sharkov
(State University of St. Petersburg)

As an alternative to X-rays and electrons, a recent paper [1] proposed the use of thermal neutrons with wavelengths close to interatomic distances in condensed matter to obtain holographic images on an atomic scale. Two experimental methods were considered which either put the radiation source inside and the detector outside the object or vice versa. The second approach, called the inside-detector concept, requires strongly neutron-absorbing isotopes acting as point-like detectors in the sample. In the present work we demonstrate for the first time the feasibility of this technique by recording a holographic image of lead nuclei in a Pb(Cd) single crystal.

The idea of holographic imaging has been conceived by Denis Gabor already more than half a century ago [2]. However, it was successfully applied only more than two decades later as one of the striking consequences of the development of laser technology. For a long time, holography was restricted to essentially the wavelength range of visible light with its inherent limitations as to the resolution obtainable in recording a hologram. A serious effort to extend holographic techniques to shorter wavelengths allowing for better resolution, was only made after the pioneering work of A. Szöke [3] proposing the use of photoelectrons and X-rays. Holographic imaging techniques are based on the recording of the interference pattern of two coherent waves emitted by the same source. The first wave that reaches the detector directly, serves as the reference wave. The second one is scattered by the object of interest and subsequently interferes with the reference wave.

For thermal neutrons the inside-detector concept is realised as follows: A well-collimated neutron beam, i.e. a plane wave, propagates in a single- crystal sample containing a small amount of strongly neutron-absorbing atoms. The neutron wave reaches these "detector" nuclei either directly, without any scattering (thus serving as the reference beam), or after scattering from other nuclei in the sample (object beam). The intensity distribution of neutron radiation inside the crystal and, in particular, at the sites of the detector nuclei, results from the interference between these two waves. Because the sample is a single crystal, the object beam will strongly depend on the orientation of the sample with respect to the incoming beam direction. The absorption of neutrons gives rise to the emission of (usually) γ-radiation. The intensity of this γ-radiation is directly proportional to the intensity of the neutron wave field at the position of the detector nuclei. If recorded as a function of the sample orientation, relative to the direction of the incident neutron beam, this intensity pattern yields a hologram [1].

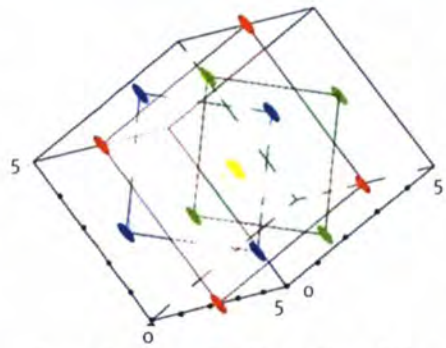

Figure 1: Schematic illustration of the arrangement of the lead atoms surrounding a Cd atom (yellow spot) as first neighbours in the FCC structure. The orientation and positions of the spots are equivalent to those in figure 2. The FCC cubic lattice, however, is tilted with respect to the Z-axis of the diffractometer according to the angles given in the text. The grid marks are given in Ångstroems.

In the present work a spherically shaped single crystal of $Pb_{0.9974}Cd_{0.0026}$ with a diameter of about 7 mm was used as the sample. In the case of Cd the absorption cross section for thermal neutrons is more than four orders of magnitude larger than for Pb so that the Cd atoms act as highly efficient detectors. The phase diagram [4] shows that the crystal structure of the alloy is face-centered cubic (*fcc*) as for pure lead. The quality of the single crystal was checked at the Laboratoire Léon Brillouin (Saclay, France) before the experiment, and a mosaicity of about 1.5° was found. The lattice parameter is a = 4.935 Å [4]. The Cd atoms are randomly distributed on regular lattice sites. In an *fcc* lattice every atom has 12 nearest neighbours and, since the Cd concentration is very low, usually all lattice sites surrounding any one Cd atom are occupied by Pb atoms. The lead nuclei play the role of the object while the cadmium nuclei serve as point-like detectors inside the sample. Figure 1 shows the arrangement of the first neighbourhood of the Cd atom in such a lattice.

The experiment was carried out at the ILL, on the D9 four-circle diffractometer. The sample was mounted on the cradle of the diffractometer in such a way that the plane of the cradle was parallel to the incident beam. The sample was rotated about the angle χ through a range of 45° and about the angle φ through a range of 354°. The angular step-width was 3° for both rotations leading to a mesh of 16x119 = 1904 pixels. Neutrons with a wavelength of $\lambda = 0.8397$ Å were used. The prompt γ-rays emitted by the Cd nuclei were detected using two scintillation detectors (one 3"x 3" NaI(Tl) and one 2"x 2" BGO). The detectors were shielded by lead and with polymer foil containing ^{6}Li. The signal-to-noise ratio was slightly above 25.

In order to decrease the influence of slow variations of the incident beam intensity the measuring time for one pixel was limited to 30 seconds. During the course of the experiment 14 cycles were completed resulting in typically 2.5×10^7 counts in one pixel for the BGO and 1.5×10^7 counts for the NaI(Tl) detector.

For reconstructing the object, computer-generated spherical waves were applied to the recorded hologram, i.e. convolution of converging s-waves with the data matrix of the scanned (χ,φ) surface was carried out. The pattern obtained by this procedure gives the restored holographic picture. More details on data processing and noise filtering are given in ref. [6]. Figure 2 shows the 12 led atoms around a given cadmium atom on the surface of a sphere. From the radius of this sphere the lattice parameter of the Pb(Cd) crystal was derived. The value of 4.93 Å obtained from the holographic data is in very good agreement with the above-mentioned value. The orientation of the crystal lattice was reconstructed from the hologram by suitably rotating the z- and y-axes. Comparison with the model calculation showed the [001] direction of the lead crystal to have a declination angle from the z-axis of the diffractometer of $\theta = -59 \pm 3°$ and the initial value of the rotation around the φ-axis to be $\varphi_0 = 21 \pm 3°$. Without removing the crystal, D9 was used again in its original 4-circle diffractometer mode and the orientation matrix of the crystal was determined. This gave the values of $\theta = -60.3°$ and $\varphi_0 = 20.3°$ in excellent agreement with the holographic data, thereby demonstrating the power and reliability of the technique.

We emphasise that, due to the nuclear interaction of neutrons, these distances reflect the positions of neighbouring nuclei in contrast to the case of X-rays where interatomic distances are defined by the interaction with the widely distributed electronic shell.

To our knowledge, this work is the first in which the internal-detector concept was successfully realised for neutron holography and the object was restored without making use of any *a priori* knowledge about the orientation of the sample. Thus, the feasibility of the concepts of atomic resolution neutron holography proposed in [1] is now proven. The special properties of the nuclear scattering process of neutrons, like its isotopic sensitivity and its dependence on the magnetic moment, will substantially enlarge the field of investigation opened up by this novel technique of which we briefly mention just two examples: First, as already discussed in more detail [5], the internal-source concept is applicable to the investigation of a wide variety of hydrogen-containing compounds, both anorganic and organic. Second, by using polarized neutron beams, both the internal-source and the internal-detector concepts, may be extremely useful and flexible tools for studying the local magnetic structure of magnetic materials. There are at least two fundamental differences compared to traditional diffraction techniques. On the one hand, holography is a full reconstitution without the known phase information loss of diffraction. As such it might appear as challenging, but the signal-to-noise ratio at present is much less favourable than in standard techniques. On the other hand, it can reconstitute only the neighbourhood of the "detector" atom, but this it can do without ambiguity. In this sense it becomes a local probe.

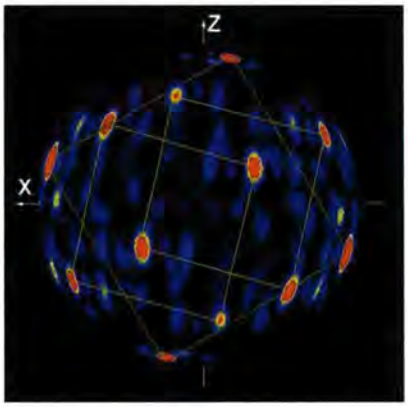

Figure 2: The spots representing the positions of the twelve Pb atoms forming the first neighbours of the Cd nucleus are displayed on the surface of a sphere of radius 3.49 Å = $a/\sqrt{2}$, a being the lattice parameter. The X-axis is the incident beam direction, the Z-axis is the z direction in the system of coordinates of the D9 diffractometer.

Acknowledgements

The authors acknowledge the intellectual contribution and technical assistance of J. Allibon, J. Archer, M. Kocsis, J. Laugier, Ch. Ling, A. Pastor, M. Prem, Yu. Tolmachev, and G. Vaspál.

REFERENCES

[1] L. Cser, G. Krexner and Gy. Török, Europhys.Lett. 54, (2001) 747
[2] D. Gabor, Nature 161, (1948) 777
[3] A. Szöke, in Short Wavelength Coherent Radiation: Generation and Applications, edited by D.T. Attwood and J. Baker, AIP Conference Proceedings No 147 (American Institute of Physics, New York) 1986
[4] J. Dutkiewicz, Z. Moser and W. Zakulsky, Bulletin of Alloy Phase Diagrams 9 (1988) 694
[5] L. Cser, G. Krexner and Gy. Török, Appl.Phys. A 74 [Suppl.] S215-S217 (2002)
[6] L. Cser, Gy. Török, G. Krexner, I. Sharkov, B. Farago, Phys. Rev. Lett. 89, 175504 (2002)

Interferromagnetic *measurement of the longitudinal coherence-function for cold neutrons*

C. Pruner, R.A. Rupp, M. Fally and H. Dachraoui (University of Vienna)
R. Mazzucco, J. Zipfel and R.P. May (ILL)

During the last twenty years various interferometric experiments with thermal and very cold neutrons were performed. While interferometers for thermal neutrons are usually based on the dynamical diffraction from perfect silicon crystals [1], interferometers for very cold neutrons utilise artificial gratings made by sputter- or photolithography-techniques [2]. With our new interferometer we open up interferometric techniques for the cold neutron wavelength range. The interferometer consists of three holographically generated density gratings of deuterated polymethylmethacrylat (d-PMMA) which are arranged in triple-Laue geometry. We present the first direct measurement of the longitudinal coherence-function and - as a by-product - an estimation of the longitudinal coherence length of a cold neutron beam.

Experiments employing cold neutrons in materials science generally provide information about the intensity and the direction of the scattered or diffracted beams which are determined by the coherence properties of the neutron beam and the scatterer. For an exact analysis and interpretation of the experimental data it is necessary to have detailed knowledge about the coherence properties of the wavefield. Interferometric measurements give direct experimental access to the complete coherence function of the wavefield, the amplitude and the relative phase of the transmitted and the scattered beam.

This fact opens new possibilities not only in fundamental but also in applied physics.

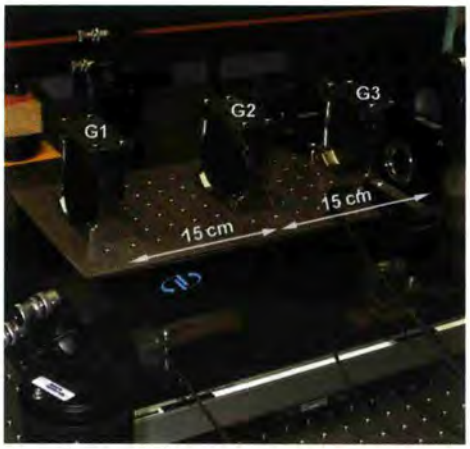

Figure 1: Photograph of the interferometer in our laboratory in Vienna after recording the gratings.

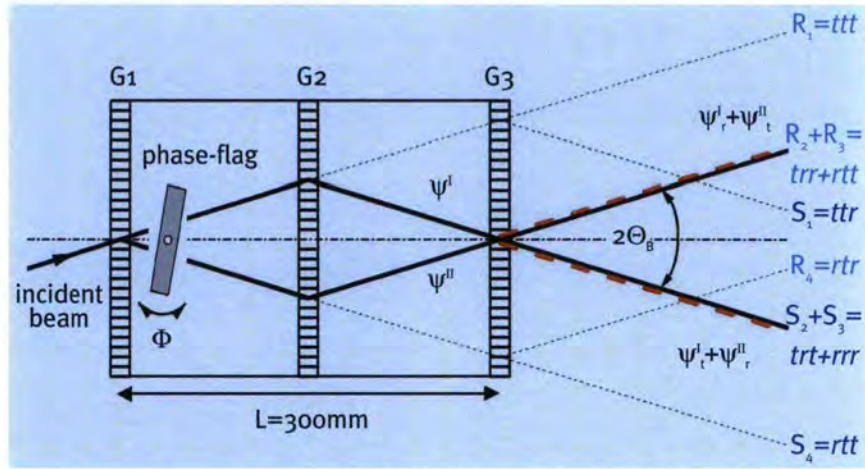

Figure 2: Sketch of the interferometer for cold neutrons based on holographically generated density gratings in d-PMMA.

To generate the gratings we are employing the photo-neutron refractive effect of deuterated polymethylmethacrylat doped with a photosensitizer [3-5]. A standard holographic two-wave mixing set-up was used to induce refractive-index changes for neutrons. As the number density of the polymer and the monomer differs, an irradiation of the samples with a sinuousidal light-interference pattern leads to density changes which act as gratings. This process is enabled by a decomposition of the photosensitive component into free radicals which start a polymerisation process in the bright region.

Advantages of this technique are that the grating spacing can be varied between 180 nm and several µm, that the magnitude of higher diffraction orders and their diffraction efficiency can be tuned by the exposure, intensity and thickness of the samples.

The interferometer consists of three gratings which are arranged in the symmetric triple-Laue geometry (figu-

re 2) [6]. The incident beam is split at each grating, resulting in a total of 8 rays (R_1-R_4 and S_1-S_4) behind the third grating. Only two pairs (R_2+R_3 and S_2+S_3) contribute to interference. After the third grating we obtain a coherent superposition of the wavefunctions $\Psi^{I}+\Psi^{II}$. To record an interferogram a phase-flag of sapphire was inserted in both beam-paths between the first and second grating. A subsequent rotation Φ of the sapphire around an axis perpendicular to the plane of incidence generates a phase-difference between the beams and results in correlated intensity modulations behind the third grating. Those intensity changes were monitored on the detector matrix.

The observed decay of the interference fringes with increasing phase-difference gives direct experimental access to the absolute value of the normalised coherence function via the visibility

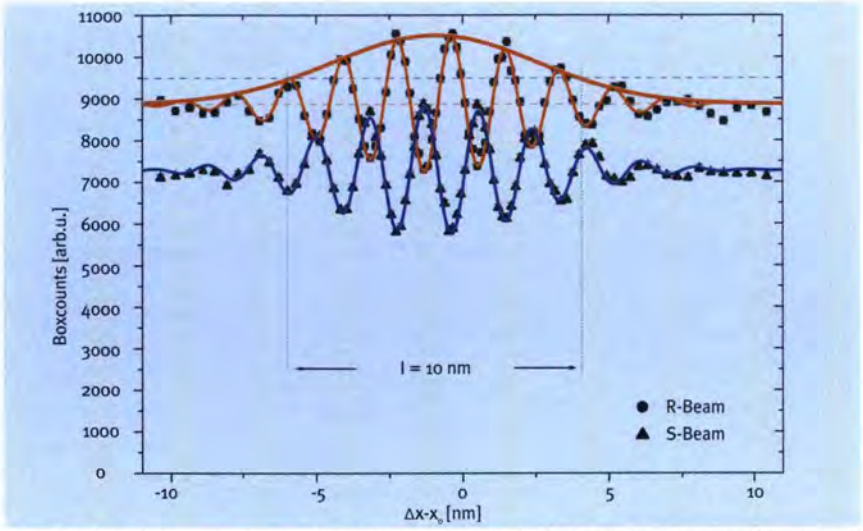

Figure 3: Interferogram obtained by rotating a 4.1 mm thick phase-flag from sapphire around an axis perpendicular to the plane of incidence. The decay of the visibility reflects the coherence function. The solid line represents a fit to a Gaussian decay function.

[7,8], and as a by-product to the coherence length l_c. The cross-correlation or van Cittert-Zernike theorem gives an interrelation between the coherence function and the spectral distribution of the neutron beam via a Fourier transform. For a mean neutron wavelength of $\lambda = 2.0$ nm and a spectral distribution of $\Delta\lambda/\lambda = 10\%$ we obtained a coherence length of $l_c = 10.3 \pm 0.5$ nm. The maximum visibility of the inference fringes is 21%. Those measurements were performed at the SANS instrument D22 at the ILL.

REFERENCES

[1] H. Rauch, W. Treimer and U. Bonse, Phys. Lett. A47 (1974) 369
[2] M. Gruber, K. Eder, A. Zeilinger, R. Gähler and W. Mampe, Phys. Lett. A 140 (1989) 363
[3] R.A. Rupp, J. Hehmann, R. Matull, Phys. Rev. Lett. 64 (1990) 301
[4] H. Havermeyer, C. Pruner, R.A. Rupp, D.W. Schubert, E. Krätzig, Appl. Phys. B 72 (2000) 201
[5] M. Fally, Appl. Phys. B 75 (2002) 405
[6] U. Schellhorn, R.A. Rupp, S. Breer, R.P. May, Physica B 234-236 (1997) 1068
[7] H. Rauch, S.A. Werner, "Neutron Interferometry", Clarendon Press, Oxford 2000
[8] H. Rauch, H. Wöhlwitsch, H. Kaiser, R. Clothier, S.A. Werner, Phys. Rev. A53 (1996) 902

A novel multiplexing *three-axis spectrometer*

N. Grach, F. Demmel (ILL)
H.M. Ronnow (CEA Grenoble)

There is an increasing demand to map out the energy momentum space also for single crystalline materials. One idea is to extend the range of scattering angles of a three-axis spectrometer. This opens up the possibility to investigate large volumes in the Q-ω space from small single crystals simultaneously. A novel multiplexing secondary spectrometer for the thermal three-axis spectrometer (TAS) IN3 has been installed and tested. The entire 2D dispersion manifold in the bc plane of the spin-Peierls compound $CuGeO_3$ has been measured.

The classical TAS has reached the possible limits in the last years by applying focussing techniques. Vertical and horizontal focussing monochromators and analysers with large dimensions have been developed as far as possible to get the highest flux at the sample position and in the detector. These achievements come along with degraded resolution in momentum space. Energy resolution is unaffected by choosing appropriate geometries. All these developments increased the flux, but the principle of operation for the TAS remained: a scan in the reciprocal space step by step. There is now an increasing demand for scanning a large range in Q-ω space to get a global overview of the excitation spectrum, often called "mapping". This method has proved to be successful, in particular when applied to low dimensional systems. A further demand can be to get more constraints on dispersion-calculations, hence being able to determine many-parameter Hamiltonians or to distinguish between different models.

While the use of time-of-flight spectrometers for this purpose is quite obvious here, similar/comparable possibilities based on TAS are demonstrated.

The angular range was enlarged at the FRM in Garching by the multi analyser detector arrangement (MAD) [1]. The design is a monochromatic defocussing arrangement, which means all analyser crystals reflect the same energy in their own detector (see figure 1). The secondary spectrometer is now equipped with 32 Cu(200) analysers, each one about 75 mm high. All analysers are arranged on a circle with radius 1031 mm and aligned to the same final energy of 31 meV. The analysers are separated by 1 degree and therefore the set-up covers now an angle range of 31 degrees. Each analyser is followed by its own ^{3}He counter with an active length of about 100 mm. All channels are separated by collimators. The MAD secondary spectrometer is now at the ILL, on loan from TU München and installed at the three-

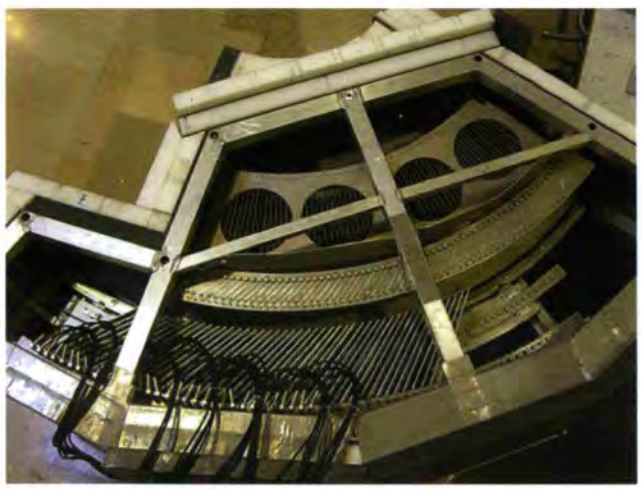

Figure. 1: Top view of the detector box. The row of Helium detectors is at the bottom of the picture. The aluminium bank, housing the analyser crystals, is installed between the two collimator systems.

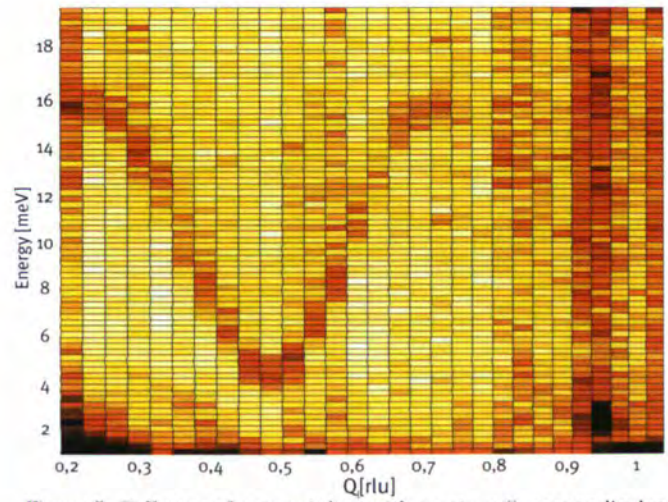

Figure 2: Q_i E map of a scan taken with a set-up Q_i perpendicular to k_i. The Q_i axis shows the different detector channels whilst the energy transfer was scanned.

axis spectrometer IN3. Due to the curvature of the neutron guide higher orders of neutrons are absent in the range of incident energies.

The operation of such a multi analyser set-up is more complicated, due to the enhancement of scattering angles the TAS loses a part of flexibility scanning in Q-ω space. But for low dimensional systems, like 1D or 2D magnetic excitations, there exists an advantageous set-up for the sample crystal, by which one can measure a large part of a spin wave dispersion in one scan. The necessary condition is that the sensitive reciprocal axis is aligned perpendicular to the incoming wave vector ki. Changing the incoming energy results in a constant Q-scan for all detectors along this direction. There exist further scan possibilities, which can be quite helpful with this set-up. By rotating the sample crystal, one can map in a plane of the reciprocal space at a certain energy transfer. Therefore cuts in the Q-ω space with a predefined energy transfer are possible. The ability to make these constant energy cuts and focus the intensity in a small region of energy transfer is a reminiscent feature of the flexibility of the TAS.

To benchmark the set-up we have chosen the spin 1/2 quasi one-dimensional Heisenberg antiferromagnet $CuGeO_3$, which is an interesting system with low value of spin and hence weakly scattering to challenge the box. At a temperature $T_{sp} = 14$ K, this system undergoes a spin Peierls transition to a chain of coupled dimers [e.g. 2]. Due to the low dimensionality of the spin system it is an ideal candidate to test the proposed different scan geometries.

A 15x5x7 mm^3 single crystal of $CuGeO_3$ was mounted in a Helium flow cryostat and aligned with (0,k,l) in the scattering plane. The temperature was 2 K throughout the experiment. The secondary spectrometer was fixed to a minimum scattering angle of 6° for the detector channel nearest to the primary beam. The scans have been performed by varying the incoming energy up to an energy transfer of 20 meV. To map out the whole dispersion surface the sample orientation was changed by 10 degrees for different scans. Nine different sample orientations have been recorded in this way and for some orientations we have made several scans to get better statistics. Each scan point was measured on average for 7 min. One scan over the magnetic excitations with a step size of 0.25 meV needed about 11 hours. A total of more than 20 000 pixels in the momentum energy space have been recorded. Figure 2 shows the results of the scan with the constant Q set-up. Clearly visible is the magnon dispersion with the gap at $Q_l = 0.5$.

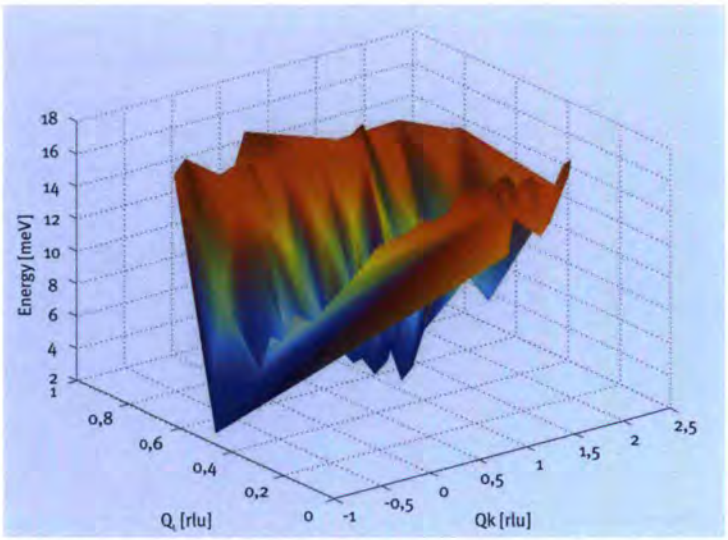

Figure 3: The 2D dispersion of $CuGeO_3$ in the bc plane is shown derived from 140 analysed inelastic peaks.

From the measured data sets about 140 excitation peaks could be fitted. From these we derived the full 2D representation of the dispersion in the bc plane of $CuGeO_3$ (figure 3).

Whether our data set can now be used to differentiate between different competing theories for the dispersion in the main direction is now under investigation. Keeping in mind that the data were obtained at the IN3 beam-line with an incident flux of a factor 100 less compared to the newly upgraded IN8, and that the box in future will be able to host twice the number of detectors, one can imagine what a powerful tool a multi analyser set-up can be.

REFERENCES

[1] F. Demmel, A. Fleischmann, W. Gläser, NIMA 416 (1998) 115

[2] L.P. Regnault, M. Ain, B. Hennion, G. Dhalenne, A. Revcolevschi, Phys Rev B 53 (1996) 5579

Combination of neutron *spin-echo with resonance spin-echo using longitudinal magnetic field geometry*

W. Häussler, G. Ehlers (ILL)
U. Schmidt
(University of Heidelberg)
F. Mezei (HMI Berlin)

We report on a recent Neutron Spin-Echo (NSE) experiment which was performed in order to examine a new experimental realisation of the Neutron Resonance Spin-Echo (NRSE) technique. Previously built NRSE spectrometers use transversal magnetic fields, making it impossible to correct for field integral inhomogeneity caused by the beam divergence. For the first time, we have built a NRSE set-up with longitudinal field geometry, which does not have this disadvantage. In order to test this new approach, we combined one spectrometer arm of IN11 (NSE set-up) with a new longitudinal NRSE set-up in the other arm. This experiment demonstrates how NRSE can be realised in longitudinal field geometry and sheds light on the differences to previous NRSE realisations. As main achievement, we could correct the effect of beam divergence by means of standard Fresnel coils.

In Neutron Spin-Echo (NSE) [1,2] neutrons accumulate spin phase in magnetic fields before and after the sample. The measured quantity is the final scattered beam polarization, which contains information about the sample dynamics (the intermediate scattering function $S(Q,t)$). This method is limited by the inhomogeneities of the magnetic field B. They cause spin phase differences of individual neutrons and, therefore, influence the scattered beam polarization even in the absence of sample dynamics. The Neutron Resonance Spin-Echo (NRSE) [3,4] technique can overcome this limitation by reducing the dimensions of the field. In NRSE on either spectrometer arm the magnetic field of a long NSE coil (figure 1, left) is replaced by a pair of two relatively short NRSE coils and a guide field in between (figure 1, right). The NRSE coils produce

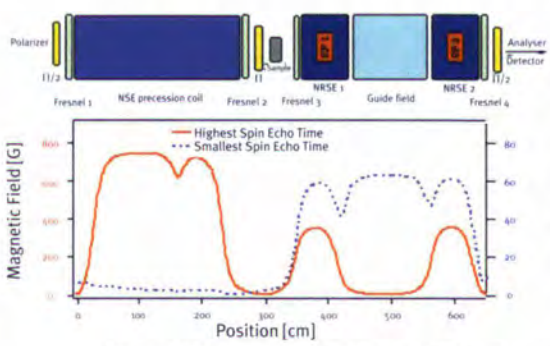

Figure 1: The experimental set-up (top) and the profile of the longitudinal static magnetic field created by all solenoids (bottom).

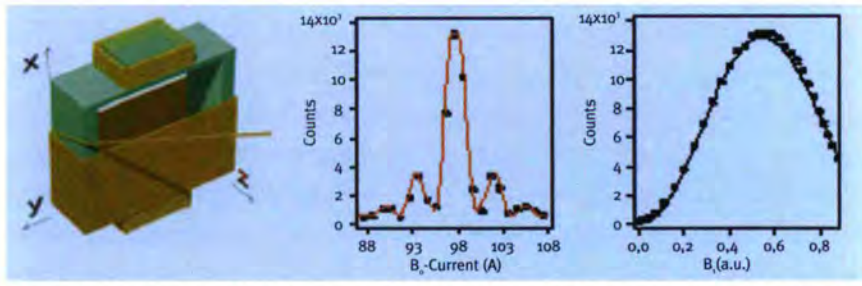

Figure 2: The design of the RF-coil (left). The coil is cuboid-shaped, while at both ends, additional correction coils are added. The appropriate functioning of the RF coil together with the B_0-coils is demonstrated by B_0- and B_1-resonance scans (center and right).

a static magnetic field B_0 and additionally, a radio frequency (RF) field perpendicular to B_0. Neutrons entering the first NRSE coil undergo a resonant π-flip as they precess with Larmor frequency $\omega_L \sim B_0$ and perform Rabi-oscillations in the RF field. The guide field in between the NRSE coils avoids uncontrolled changes of the spin phase. In the second NRSE coil, again a resonant π-flip takes place. The dynamic resolution in NRSE depends on B_0 and on the distance between the NRSE coil centers d, but *not* on the length of an individual NRSE coil. This is the main advantage of NRSE compared to conventional NSE, where the resolution depends on the field integral $\int B \cdot ds$ (s parameterises the neutron trajectory) suffering from field inhomogeneities. A measure of the Spin-Echo resolution is the spin-echo time τ. In NSE, $\tau_{NSE} \sim \lambda^3 \cdot \int B \cdot ds$ with λ being the neutron wavelength. However, in NRSE, $\tau_{NRSE} \sim \lambda^3 \cdot 2B_0 \cdot s$. The NRSE arm provides the same spin-echo time as a NSE arm of field strength $2B_0$ (and of the same length).

The spin-echo times reached in earlier built NRSE spectrometers [5,6] are limited to about 10 ns, mainly because the individual neutron flight paths accepted by the diaphragms differ in length. Neu-

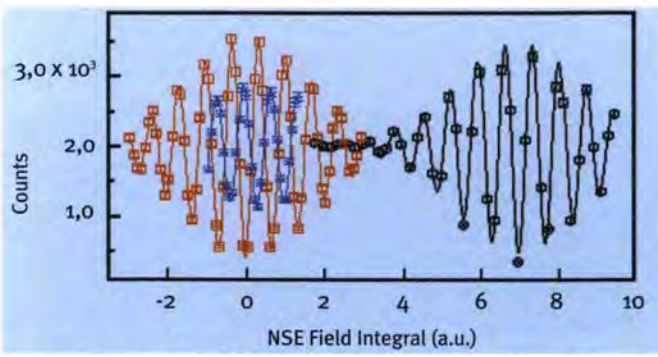

Figure 3: The first NSE-NRSE spin-echo group measured in the direct beam (circles). Spin-echo groups measured in elastically scattered intensity (triangles: Fresnel coils off, squares: Fresnel coils on). The mean wavelength was 5.5 Å, the wavelength spread was 16.4 % (FWHM).

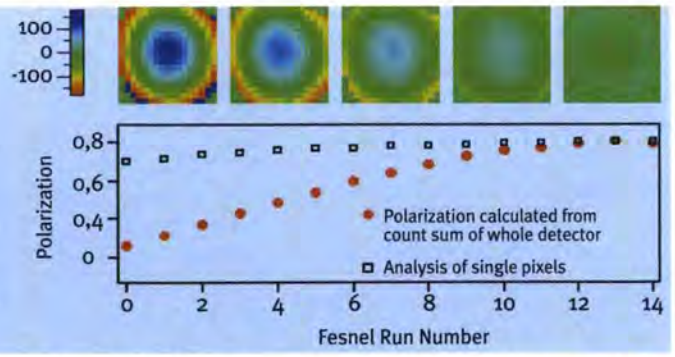

Figure 4: The phase of spin-echo groups measured in each detector pixel, dependent on the fresnel coil current (top). The polarization depends strongly on the tuning of the fresnel coils (bottom). Every three polarization values belong to one phase image.

trons traversing the NRSE arm not parallel, but at an angle to the axis of symmetry, stay longer between the NRSE coils accumulating more phase ("divergence problem"). This fact deteriorates the resolution, because NRSE (equally as NSE) is based on the condition that neutrons of the same wavelength accumulate the same spin phase. All earlier NRSE instruments used NRSE coils with B_0 directed perpendicularly to the flight path of the neutrons, making it practically impossible to correct for the divergence problem.

We have built and tested a completely new NRSE set-up with longitudinal B_0 field. Fresnel coils established in conventional NSE spectrometers in order to correct for field integral inhomogeneities can be used to overcome the divergence problem, however, they can only be used if the static precession field is parallel to the flight path of the neutrons.

In order to test the proper operation of the new NRSE set-up, we combined one NRSE spectrometer arm with one NSE spectrometer arm of the instrument IN11. The whole arrangement represents a NSE-NRSE spin-echo spectrometer shown in figure 1, together with the shape of the static magnetic fields B and B_0 for two adjustments with different spin echo time. At high spin-echo time the static magnetic field needed in the NRSE coils is smaller by about a factor 2, as discussed above.

Figure 2 depicts the design of the RF coil (left) which is needed for the resonant π-flip. The field integral inhomogeneity inside the coil was reduced to 4 % by correction loops. This is sufficient to reach a resonant π-flip for all neutrons of the beam (center and right). Divergence effects are negligible because of the shortness of the coil.

In figure 3, spin-echo curves at high spin-echo time (τ = 4.6 ns, only limited by the maximum current of the NRSE power supply) are shown. The first spin-echo group measured in the direct beam is shown on the right hand side of the figure (black curve). Using a standard elastic scatterer, the polarization is found to decrease as expected, if the field integral homogeneity is not corrected by Fresnel coils (blue curve). All fit functions shown in figure 3 are a cosine function convoluted with a Gaussian.

In order to achieve spin-echo curves with high amplitude again (figure 3, red curve), the magnetic fields produced by the Fresnel coils have to be optimised. The position of the Fresnel coils was fixed as shown in figure 1. The effect of the Fresnel coils is demonstrated in figure 4, where the phase of the spin-echo curve at each detector pixel is analysed. The current in all Fresnel coils was tuned linearly in 15 steps from zero to the optimum current. With Fresnel coils switched off, the phase between the center pixel and off-center pixels varies strongly (more than 2π), while the phase pattern is very smooth for the optimum Fresnel tuning (phase differences reduced by factor 10). Only on a more sensitive scale, remaining deviations of the phase in different pixels can be recognised. These deviations remain because position and radial current density of the used standard Fresnel coils were not optimised. In future, Fresnel coils especially optimised for NRSE will be used and we expect that the resolution of the NRSE set-up can be further improved.

In conclusion, we demonstrated by means of a test experiment, that NRSE with longitudinal field geometry is a promising new method in order to perform Neutron Spin-Echo investigations. First spin-echo measurements were performed, and the appropriate function of Fresnel coils in order to optimise the resolution of the NRSE set-up was tested.

REFERENCES

[1] F. Mezei, Z. Phys. 255 (1972) 146
[2] F. Mezei (ed.), Neutron Spin Echo (Springer, Heidelberg, 1980)
[3] R. Gähler, R. Golub, Z. Phys. B 65 (1987) 269. R. Golub, R. Gähler, Phys. Lett. A 123 (1987) 43
[4] D. Dubbers, P. El-Muzeini, M. Kessler, J. Last, Nucl. Instr. and Meth. A 275 (1989) 294
[5] U. Schmidt, S. Biche, W. Häussler, D. Dubbers, Physica B 234-236 (1997) 1133
[6] T. Keller, R. Golub, F. Mezei, R. Gähler, Physica B 241-243 (1998) 101

Comings and goings

At the end of November 2002, Walter Kaiser – Head of the Service Mécanique des Aires Experimentales – left the ILL after 31 years. Walter brought to a success all his far-reaching tasks with sagacity and reliability. We wish him well for the future. In the picture, Walter (left) at his farewell pot with Frédéric Descamps.

Cheers then! From the left, Francis Tasset, Laurent Brayer, Hervé Guyon, Steve Jenkins and Michel Mollier.

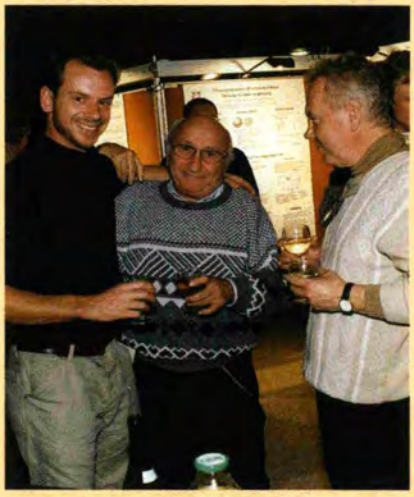

Bob Cubitt, André Gabriel and Peter Timmins during the REFILL workshop.

Ultra cold neutrons at the ILL...

WORKSHOPS.

Scientific meetings hosted by the ILL during 2002

UK User meeting - 10-11 January

Workshop in honour of Jane Brown - 8 March

Simulation of Neutron Spectrometers using Monte Carlo packages (SINS-II) - 20-22 March
Emmanuel Farhi and Ron Ghosh (ILL).

6th Bombannes European Summer School on Scattering Methods Applied to Soft Condensed Matter - 26 May - 1 June
Peter Lindner (ILL), Thomas Zemb (CEA Saclay), Otto Glatter (U Graz), Jan Skov Pedersen (U Aarhus) and Peter Schurtenberger (U Fribourg).

Satellite meeting IUCr 2002: Neutron and Synchrotron X-rays - 1-3 August
Alan Hewat (ILL) and Ake Kvick (ESRF).

Bridging the gap in molecular science - 26-28 September
Mark Johnson (ILL), Don Kearley (TU-Delft), Peter Trommsdorff (UJF Grenoble) and Marie Plazanet (ILL).

Neutron Reflection: Progress in the study of interfaces (REFILL) - 24-26 October
Robert Cubitt, Giovanna Fragneto and Ron Ghosh (ILL).

Workshop in honour of Anton Heidemann - 28 November
Bernhard Frick and Werner Press (ILL).

Workshop on the perspectives in Single Crystal Neutron Spectroscopy (SCNS) - 12-14 December
A. Hiess (ILL).

UK Neutron Users' meeting

Blessed with three days of continuous sunshine 120 neutron scatterers from the UK assembled in Grenoble for the first time for their annual user meeting on 10-11 January. With contributions from more than 30 of our own staff the meeting went off with a real zing.

The poster session - with over 60 posters - attracted interest not only from the scientists, and we congratulate Ingrid Parrot, one of the ILL thesis students, on winning the poster prize.

Thanks to all those from all sections of the ILL who helped to make the meeting a real success, from the security staff, electricians, hostesses and SCO, to Thilo Pirling and Wolfgang Schmidt who provided the musical entertainment at the dinner - and of course to all those who made scientific presentations and contributions in the various sessions.

The UK neutron scatterers assembled at the ILL for their Users' Meeting.

Jane Brown: a celebration of the prizes awarded for her outstanding scientific career

Jane Brown's outstanding contribution to the field of neutron scattering, especially in the area of spin polarization phenomena in scattering processes, was recently recognised by two prestigious awards: the 2001 European Neutron Scattering Association Walter Hälg Prize and the 2002 Institute of Physics Guthrie Medal and Prize.

In honour of her achievements, and to celebrate Jane's birthday as well, the ILL management organised a Colloquium on 8 March, in the Chadwick amphitheatre. The presence of a select international audience gave further proof of the world-wide interest in Jane's key contribution to Physics Research.

As Bruce Forsyth pointed out with humour, in his speech during the morning session, Jane's life can be split in three different periods:

- BC (Before Cambridge) 1932-1951, Scotland, where Jane was born and educated;

Jane during the Colloquium organised in her honour.

- DC (During Cambridge) 1951-1974, and her stay at the Newnham College and Cavendish Laboratory;
- AC (After Cambridge) 1974, Grenoble and the ILL, where she is presently running an extremely active research programme, although formally retired in 1995.

Jane has made a significant impact upon our understanding of the fundamental magnetic properties of materials through her contributions to both the development and exploitation of polarized neutron diffraction and advanced spherical neutron polarimetry techniques for the precise determination of complex magnetic structures and spin density distributions. When she arrived at ILL she tackled ferromagnets, weak ferromagnetism and antiferromagnetism. Her work covered a wide range of subjects, from a study of VO_2 to Rare-earth elements like Pr and Nd. Jane also studied systems such as URh_3 and UGe_3, molecular compounds such as Tanol suberate and diamagnetism in graphite. She used one-dimensional polarization analysis (UPA) on the three-axis spectrometer with the polarization analysis techniques of the period - D5 - in order to separate magnetic from nuclear scattering. She has also helped to develop a novel 3D polarization analysis (SNP), which measures the rotation of the neutron polarization vector, offering more direct observa-

tion of the complex magnetic interaction vector. In the last few years Jane often used the Cryopad technique to determine complicated magnetic structures. Jane also has played a key role in developing and establishing a computational framework: for example, one of Jane's unwavering interests during her career was the coherent development of the CCSL library, which now features 470 subroutines and 40 programs. She was also deeply involved in the software development for D3 and Cryopad, and she demonstrated the powerful use of CCSL to interpret measurements based on new concepts.

Jane is undoubtedly very well known to the European neutron scattering community and appreciated by all her collaborators. The workshop was extremely successful, and many of Jane's good colleagues attended, as well as her old Cambridge friends, all contributing to the lively spirit of the occasion. Jane herself confessed that she was relieved to have survived all those honours and she kindly thanked the organisers and all participants.

Remembering the good old days!
From the left: Francis Tasset, Jane and Prof. L. Alte da Veiga, (Coimbra University).

Simulation of Neutron Spectrometers, using Monte Carlo packages (SINS-II)

The Simulation of Neutron Spectrometers (SINS) Workshop, sponsored by the European Neutron Round Table and the ILL, was held on 20-22 March. Twenty-four participants from external laboratories joined the ILL/ESRF simulators and developers to share recent advances and comparisons.

There were updates on the two principal European packages. McStas, originally developed at Risø and now strongly supported at the ILL, was presented by Kim Lefmann (Risø) and Emmanuel Farhi (ILL). Geza Zsigmond (HMI) and his collaborators presented features from the most recent version of VITESS. Luke Daemon presented a new treatment of Neutron Polarization within the LANSCE package NISP. This elegantly avoids numerical instability through simplistic brute-force treatment of neutron spin precession.

All three packages are in regular use by the groups developing new instruments for the American SNS centre. Their presentations carefully compared results, which cross-validated all three packages. As each has its strengths, these groups often use more than one for different aspects of the beam-line design. Materials and cross-section database utilities (Sanchez de Rio - XOP/NOP) were also helping designers of optical components.

Recent results from other participants showed off the range of instruments which could be improved by redesign. A number of projects were presented for upgrading the ILL inelastic spectrometers (IN5, IN16), resulting in considerable flux gains at the sample. New instruments at the ILL and the Munich FRM2 reactor were presented.

During the informal demonstration sessions the developers had to bear some criticism on installation problems, but these problems are becoming rarer. The sessions offered an opportunity for the three different approaches to be compared.

Although initial beam-line design appears now to be treated very consistently between the packages, there is increasing interest in developing sample (and environment) scattering models to complete experiment simulation. Further details can be found on the conference web site http://www.ill.fr/tas/mcstas/workshop0203.html.

SINS-II Group Photo.

6th European Summer School on Scattering Methods Applied to Soft Condensed Matter

Based on the positive experience with 5 previous events (1990, 1992, 1996, 1998 and 2000), this year's "Bombannes" school was held from 26 May to 1 June, again at the vacation centre "Les Bruyères" in the pine tree forest between Lake Hourtin and the Atlantic Ocean in Carcan-Maubuisson, France.

The School brought together 14 teachers and 38 post-graduate and post-doctoral students with 15 different nationalities. The maximum of the age distribution of the students was 27 years.

Scattering methods, using neutron, X-ray or light sources, are key techniques to study structure and dynamics in systems containing colloids, polymers, surfactants and biological macromolecules. With a total scientific programme of 35 hours, the academic aim of the "Bombannes" school is to introduce on a fundamental level the current methodology of static and dynamic scattering techniques and their application to "soft matter" systems.

In the course of the week 25 hours of general lectures were given by the team of 14 European experts in the field of soft condensed matter. The lectures were divided into two parts: an introductory session during the first half of the week covered the areas of general introduction to scattering experiments, basic concepts of data treatment, the notion of contrast, general theorems, instrumentation and resolution effects. In the second half of the week, applications of static and dynamic scattering techniques to investigate typical soft matter systems such as colloidal suspensions, microemulsions, micelles and surfactant solutions, polymeric and biological systems, turbid suspensions as well as the use of scattering techniques in chemical industry were presented.

A particularly successful feature of the "Bombannes" school is the combination of the general lectures with the compulsory oral contributions given by the 38 students during the evening after-dinner sessions during the week. These contributions are training for the students to present their specific fields of research (10 min each) and provide a forum for discussion and exchange of experience when using complementary experimental methods. Full-board accommodation of all participants on a remote site, the presence of the lecturers for the whole week and the possibility of the common sailing activity during the afternoon facilitated contact between teachers and students and helped to establish rapidly an open discussion atmosphere.

Sailing preparations: From the left, Caroline Ericsson (U Lund) and Cecile Dreiss (Imperial College, London) were faster with dressing. Ronny Vavrin (U Fribourg) needs the help of Roland May (ILL Grenoble) to fasten the wetsuit.

All "Bombannes" lectures have been edited by P. Lindner and T. Zemb and published in October 2002 as the introductory textbook "Neutrons, X-rays and Light: Scattering Methods Applied to Soft Condensed Matter" in Elsevier's North-Holland Delta series (Amsterdam, 2002).
http://www.ill.fr/Events/bombannes/2002/bombannes2002.html

Joint ILL-ESRF Conference on Materials

From 1 to 3 August the ILL and ESRF organised a joint satellite meeting to the IUCr Geneva Congress entitled "Crystal Chemistry of New Materials & Soft Matter Studied by Synchrotron & Neutron Diffraction". Neutron & Synchrotron diffraction have been essential for the understanding of new materials - hard magnets, superconductors, CMR materials, zeolites and so on. Large position-sensitive detectors, image plates, focussing optics, polarized beams

and new software are all being developed rapidly, opening up new opportunities for chemists, physicists & biologists interested in relating the properties of materials to their structure. This workshop highlighted some of this new science, and the techniques that have made it possible.

A total of 87 participants registered for the meeting, from Australia, Denmark, France, India, Germany, Great Britain, Japan, the Netherlands and the United States. Other participants from ILL and ESRF attended some of the 30 lectures, on subjects as diverse as charge order, spin-ladders, high pressures, real-time chemistry, supra-molecular materials, clathrates and zeolites, quasi-crystals and nano-materials. There were also sessions on materials engineering and new imaging and detection techniques. The standard of lectures was very high, while at the same time at a level suitable for non-specialists. The lectures were organised in the ILL amphitheatre, with a similar number of posters displayed in the ESRF mezzanine, accompanied by refreshments. A reception buffet was provided in the ESRF-ILL restaurant, with the conference dinner the following evening in the Château de la Commanderie. On the Sunday following the 3-day meeting, coach transport was organised to take some of the participants to Geneva, while others enjoyed a hike in the Chartreuse mountains, or a tour of the Beaujolais vineyards; the quantity of wine sampled at the various cellars and brought back on the coach was very impressive, as the photos reveal. We are grateful to our 3 generous sponsors, Bruker Nonius, INEL and AZ-Systèmes.

John and Lucy Stride (ILL and ESRF, respectively) at the posters and wine session.

Altogether a very enjoyable and instructive meeting, demonstrating in a very practical way a happy synergy between the neutron and synchrotron diffraction communities, and especially between ILL and ESRF.

The programme for the meeting, with many photos of the participants, is available on http://www.ill.fr/dif/iucr/.

Bridging the gap between model systems and real systems in molecular science

In molecular science, smaller ("model") systems with a limited number of degrees of freedom allow more precise measurements of structure and dynamics compared to bigger ("real") systems. The same statement is true for numerical modelling of molecules in condensed matter since *ab initio* (quantum chemistry) methods can be applied to smaller systems. Recently it has been demonstrated that a uniquely clear and detailed insight into the structure and dynamics of condensed matter systems can be obtained by combining neutron scattering and numerical investigations. A European Science Foundation Exploratory workshop (ESF) therefore brought together 23 experimentalists and computational experts to investigate the possibilities of "passing-up" information and techniques from model systems to real systems and of defining model systems that are relevant fractions of real systems. Real systems could be broadly categorised as being of biological or technological interest and are often polymeric. A number of key points emerged from the presentations and many lively discussions.

- Numerical modelling techniques, in particular molecular dynamics (MD), gives a microscopic description of systems of almost any size. Using force

Participants in the ESF workshop (L'école de physique, Les Houches, Chamonix, France).

fields, several hundred thousand atoms, for example proteins in solution can be simulated for tens of nanoseconds on typical PC clusters. Whether or not an accurate understanding is obtained depends on the validity of the force field.

• Single *ab initio* calculations can also be performed on several hundred thousand atoms using linear scaling techniques, although an extensive series of calculations would be limited to about one thousand atoms. This size of system corresponds to small proteins and compact structures of DNA.

• One way of passing information up from model to real systems is to optimise the description of force fields, first against *ab initio* calculations and then against experimental data. The large number of atoms that can now be treated by ab initio methods gives considerable scope for defining model systems.

• Experimentally, measurements should discriminate between different numerical models. For example, MD simulations tend to reproduce accurately quasi-elastic neutron scattering data, but inelastic measurements of low frequency collective excitations are less well reproduced by the same simulations, limiting their validity.

• When considering more complex model molecular structures, crystallinity and short-range order become key parameters. Polymer fibres offer a high degree of crystallinity and interesting possibilities exist in this context for working on DNA and related polymers and oligomers.

To summarise, the "value" of experimental data is maximised by experimentalists and computational experts working together.

Collaborations will be pursued between participants and promoted in further meetings and workshops.

Neutron Reflection: Progress in the study of interfaces (REFILL)

The workshop - held at the ILL on 24-26 October - gave an outstanding demonstration that Neutron Reflectivity is providing important answers well-beyond simple depth profiling of layer-thicknesses and compositions at interfaces across a range of problems from biophysics to thin-film devices.

An introductory session for newcomers to the field was held on the day preceding the main meeting. For the main workshop there were 51contributions, including 19 posters from the 64 registered participants from around the world.

Determination of reflection curves is now sufficiently routine that often only the interpretation is displayed. However area detector data have advantages in revealing anomalous sample effects, such as roughness, directly at the time of measurement, as well as providing simultaneous measurement of background.

It is impossible to review all contributions. New instruments were presented, and new insight on instrument resolution and neutron coherence length was offered in theoretical presentations. To give an idea of the breadth of fields represented, the number of talks/posters can be summarised: for model membranes and biophysical systems: 9/7, for surface chemistry: 6/4, and magnetic layers and nano-structures: 6/4. Many studies involved complex multicomponent or multilayer structures.

Interest is growing in all fields, to include off-specular scattering and consequent information on in-plane structure and geometry (notably on magnetic domain walls) and even inelastic effects. Increasingly, now that layer structures have been characterised, studies are being pursued with kinetic measurements, or cyclic magnetization experiments, following hysteresis effects.

Non-equilibrium systems include the newly formed air/liquid interface being studied in a flow cell where the surface was renewed continuously. Visco-elastic properties of bilayers are being examined as affecting transport properties through bio-membranes. Electric properties of bio-sensors, organic thin film devices, and GMR, and self-assembly of nanostructures show the proximity of these reflection studies to the industrial world.

This timely meeting successfully marked the maturity of the technique. A notable conclusion is that there will be increasing pressure on the available instrument time for a vibrant community tackling a wide range of problems.

Bob Cubitt describes EVA's features during the REFILL introductory session.

Contributions from the REFILL meeting have been submitted to Langmuir to appear in a special issue in 2003.

Symposium in honour of Anton Heidemann

Anton Heidemann left the ILL in May 2002, after 30 years of activity at our Institut. He was one of the many thesis students of Maier-Leibnitz, who supervised his thesis on the back-scattering method in Garching. Indeed, Toni was one of the pioneers of this technique, and he has contributed enormously to its development almost from the beginning of the ILL, where he arrived in the early seventies for a sabbatical.

He developed and commissioned the cold neutron back-scattering instrument IN10, on which he continued as instrument responsible when he was employed by the ILL in 1975.

From 1976 to1983 he held the role of Group Coordinator of the so-called "Vercors Group" (equivalent to today's Time-of-flight and Large Scale Structure groups). In the eighties he developed and commissioned another new instrument, the thermal neutron back-scattering spectrometer IN13, and he led the instrument as first responsible until 1984, when he left for a sabbatical year at the Brookhaven National Laboratory, during which he developed a triple-axis back-scattering spectrometer.

Back at the ILL in 1987, Toni took over more general functions: he was first appointed Head of the Instrument Operation Department EDEX (including Sample Environment, Instrument technicians, Central Service, site and building maintenance), and subsequently Head of the Instrumentation Branch of the Projects and Techniques Division (DPT) in 1993. In 1998 he was promoted Deputy to the DPT Director, a position he held until his retirement.

Toni had many scientific interests, witnessed by some 125 scientific papers published since 1968. His papers focus mainly on the applications of nuclear spin-dependent high resolution inelastic neutron scattering, but also on the use of high resolution neutron spectroscopy to study hyperfine interactions and phase transitions and the tunnelling motions of small groups (CH_3, CH_4, NH_4^+, etc).

Werner Press says goodbye to Toni during his leaving pot.

To thank Toni for his technical and scientific contributions, the ILL held a Symposium in his honour on 29 November. The meeting included invited presentations and it was closed by Toni's remarks and anecdotes.

Toni will be missed by many of us at the Institut: we all wish him a long and peaceful moonlit retirement and we hope to see him back often at the ILL!

Workshop on the perspectives in Single Crystal Neutron Spectroscopy (SCNS)

More than 80 scientists gathered together for a workshop on the perspectives in Single Crystal Neutron Spectroscopy (SCNS) held on 12-14 December at the ILL. Experts in both TAS and TOF instrumentation as well as condensed matter and material science contributed to the meeting, which was organised jointly by the ILL and its collaborating research groups of the CEA/ Grenoble and the FZ Jülich. The workshop also got a support from the neutron Round-table and the City of Grenoble.

The scope of the meeting was to discuss the new scientific opportunities for the study of excitations in condensed matter, which arise from recent developments in instrumentation at both reactor-based and spallation neutron sources. The comprehensive programme reflected the symbiosis of instrumentation and science in the field. Some papers focussed on the scientific challenges in magnetism, lattice dynamics, unconventional superconductivity and low-dimensional systems. Other contributions covered instrumental aspects, including wide-angle PSD's, inelastic spin-echo techniques, instrument simulations and science modelling. Christian Vettier, scientific director of the ILL, pointed out that *"this meeting was timely - in view of the new instrumentation efforts at existing sources and also at new spallation sources - and provided a comprehensive review of the scientific challenges in this active and important field"*.

Unsung heroes and heroines

Bernadette Mallassi, secretary of the Associate French Director, will leave us in May 2003 after 32 years in our Institut.

The ILL team which participated in the run for the Michallon Hospital's sick children in December!

On 15 December, Jacques Italia (Health Physicist at the ILL) was elected president of ATSR (Association for radioprotection techniques and sciences). ATSR's objective is to link people professionally interested in ionising radiation's problems and techniques. ATSR members are also personally engaged in education programmes. Visit the ATSR's web site at www.atsr-ri.com.

Our ladies in the translation service: Marie-Eve Meyer (on the left) and Susan Tinniswood.

EXPERIMENTAL & USER PROGRAMME.

Reactor operation

User operation

Instrument list

Beam-time allocation

Instrument performance

Industrial use of neutrons

The ILL's instrument suite *(December 2002)*

ILL's instruments		
D1A (50%)	powder diffractometer	operational
D2B	powder diffractometer	operational
D3*	single-crystal diffractometer	operational
D4*	liquids diffractometer	operational
D7	diffuse-scattering spectrometer	operational
D9*	single-crystal diffractometer	operational
D10	single-crystal diffractometer	operational
D11	small-angle scattering diffractometer	operational
D16	small momentum-transfer diffractometer	operational
D17	reflectometer	operational
D19	single-crystal diffractometer	operational
D20	powder diffractometer	operational
D22	small-angle scattering diffractometer	operational
IN1*	three-axis spectrometer	operational
IN3	three-axis spectrometer	operational
IN4	time-of-flight spectrometer	operational
IN5	time-of-flight spectrometer	under reconstruction
IN6	time-of-flight spectrometer	operational
IN8	three-axis spectrometer	under reconstruction
IN10	backscattering spectrometer	operational
IN11	spin-echo spectrometer	operational
IN14	three-axis spectrometer	operational
IN16	backscattering spectrometer	operational
IN20	three-axis spectrometer	operational
PF1	neutron beam for fundamental physics	operational
PF2	ultracold neutron source for fundamental physics	operational
PN1	fission product mass spectrometer	operational
PN3	gamma-ray spectrometer	operational
Strain Imager	residual stress diffractometer	under construction
VIVALDI	thermal neutron Laue diffractometer	operational

* hot neutrons instruments

Jointly funded instruments		
DB21 (50%)	single-crystal diffractometer	operational *(EMBL)*
LADI (50%)	Laue diffractometer	operational *(EMBL)*
IN15	spin-echo spectrometer	operational *(FZ Jülich and HMI Berlin)*

Test beams	
CT1, CT2	detector test facilities
S42	Laue-crystal alignment facility
T3	neutron optics test facility
T13A, T13C	monochromator test facilities
T17	cold neutron test facility

CRG instruments			
D1B	powder diffractometer	CRG-A	operational *(CNRS)*
IN13	backscattering spectrometer	CRG-A	operational *(INFM Italy)*
ADAM	reflectometer	CRG-B	operational *(Bochum University)*
BRISP	Brillouin spectrometer	CRG-B	under construction *(INFM Italy)*
D15	single-crystal diffractometer	CRG-B	operational *(CEA Grenoble)*
D23	single-crystal diffractometer	CRG-B	operational *(CEA Grenoble)*
EVA	reflectometer	CRG-B	operational *(MPI Stuttgart)*
IN12	three-axis spectrometer	CRG-B	operational *(FZ Jülich)*
IN22	three-axis spectrometer	CRG-B	operational *(CEA Grenoble)*
S18	interferometer	CRG-C	operational *(Atominstitut Wien)*

Instrument layout *(December 2002)*

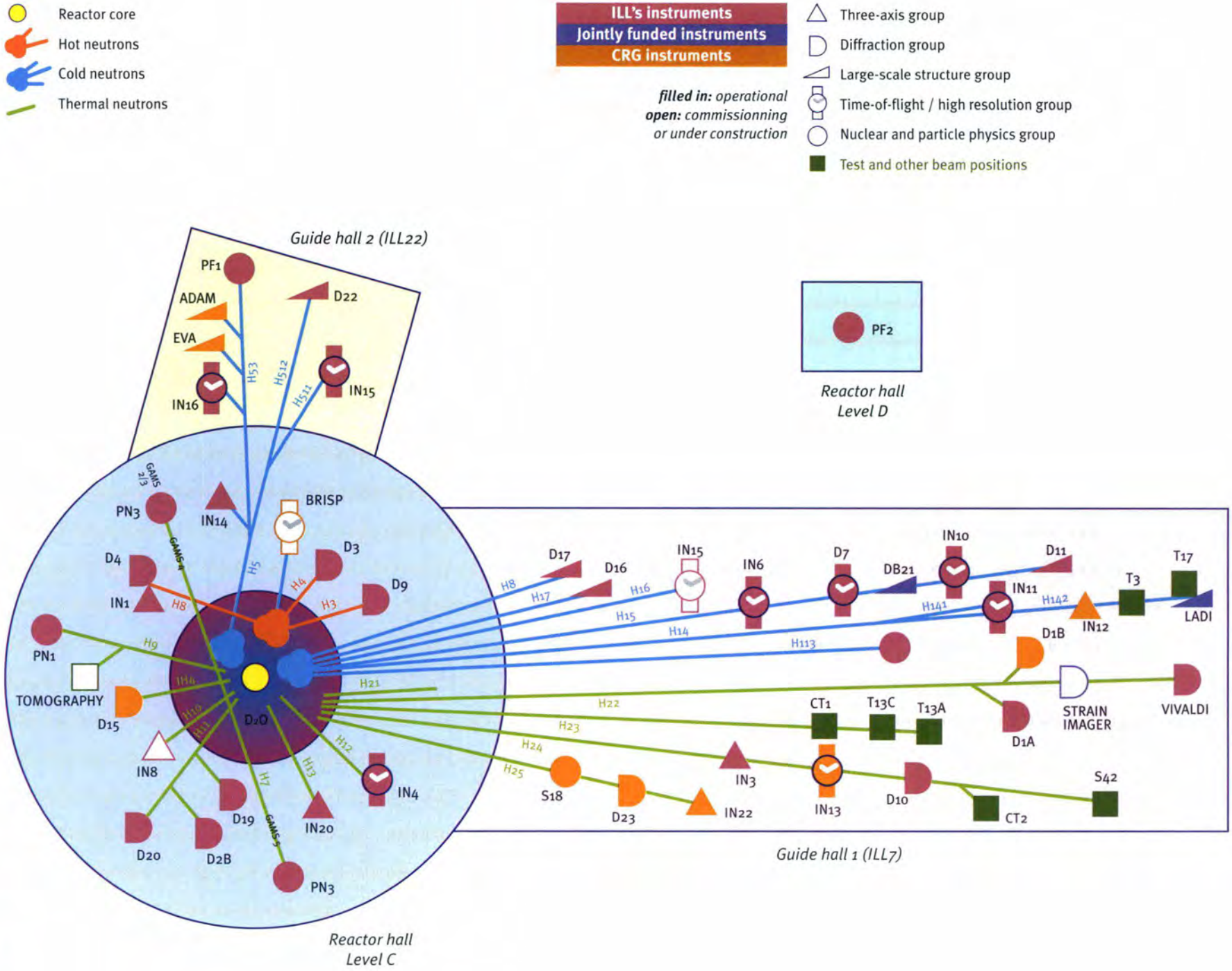

Reactor operation

Four and a half cycles – corresponding to 225 operating days – were originally scheduled for scientific work in the year 2002. The schedule for the first three cycles was respected, with any time lost due to unscheduled shutdowns being made up at the end of the cycle in question. During the planned shutdown between cycles 132-133, a water leak was detected on the H8 beam tube which feeds the instruments IN1 and D4. The beam tube, which is rectangular in cross-section, was removed and inspected visually and by using a revealing dye. The observation revealed a crack of several centimetres along the beam tube. We believe that the crack was due to excessive cyclic stress of the beam tube and it was at the origin of the water leak. The design of the H4 (feeding D3) and H3 (feeding D9) beam tubes is identical, and as a precautionary measure we decided to remove these beam tubes as well. Accordingly, the instruments D9 and D3 were removed and the H8, H4 and H3 beam tubes were closed off in September.

Thanks to the efforts of those concerned (scientists, engineers and technicians of the Projects & Techniques and Reactor Divisions) we were able to reschedule a complete cycle before the close of 2002, resulting in a total of 200 days of reactor operation in the year with a loss of only 25 days compared to the initial schedule.

The meeting of the *"Groupe Permanent"* responsible for the periodic safety review of the HFR and detritiation facility took place on 2 May 2002.

Cycle n°	Start of cycle	End of cycle	Number of days scheduled	Number of days of operation	Number of unscheduled shutdowns
130	05.02.02	27.03.02	50	50	1
131	16.04.02	05.06.02	50	50	0
132	20.06.02	13.08.02	50	50	2
133	16.10.02	07.12.02	50	50	2
Half a cycle (25 days) cancelled because of a leak in the H8 beam tube (see text for details)					
		Total	200	200	4

Table 1: Reactor operation in 2002.

Although the entire installation has been reviewed, the main focus of the examination and its repercussions concerns the seismic behaviour of the civil engineering structures, including the reactor building and interactions with surrounding structures. In order to deal with the issues raised by the *"Groupe Permanent"*, the ILL set up a new structure known as the "Refit Management Committee" (RMC), which consists of engineers and technicians either with an ILL status or sub-contracted to the Institute. This technical support group is attached to the ILL Management and works in close collaboration with the Reactor Division staff. Therefore, the ILL is committed to a 3-year 'refit' programme (see page 140 for details), and as a result of the modifications and upgrades envisaged during this period to the reactor and detritiation facilities, we can be confident of the long term operation prospects for the installation.

In view of the scale of the work to be undertaken, the ILL will reduce the number of reactor cycles from 4.5 down to 3 cycles per year during the next three years. Nevertheless, every effort will be made to offer a larger fraction of the available beam time to our users, compared to what was achieved before.

In addition to the removal of the three beam tubes H3, H4 and H8, the most important work carried out this year involved:

- the replacement of the H12 beam tube and of the three transformers of the secure electrical supply;
- the upgrading of the control system and auxiliary installations of the hot source;
- and the upgrading of the control system of the emergency air lock on level C of the reactor building. Six fuel elements were sent for reprocessing this year.

The detritiation facility was shut down on 8 November 2000. No tritium was produced or despatched this year. The detritiation facility maintenance campaign is drawing to a close. One important programme involving the replacement of all the pressure sensors and temperature detectors and the associated explosion-proof systems has been completed. All the pressure relief valves of the tritiated deuterium circuit have been replaced. The deuterium recompression installation of the detritiation facility and the HFR's cold sources has been completely overhauled.

A new campaign for the detritiation of the HFR's heavy water will begin in mid-January 2003.

User operation

The ILL User Support assists all our users. If you are coming to the ILL to carry out experiments, the User Office is here to give you the organisational and administrative support you need for the successful operation of your experiments. Neutron beams and instrument facilities are free of charge for users of accepted experiments. Scientists affiliated to the ILL member countries will also, in general, be assisted with necessary travel and daily subsistence for a limited period. The User Support Team makes all arrangements for accommodation and transport and will process claims for expenses after you have completed your experiment.

Katja Jenkins (left) and Diana Dijoux, part of the SCO team!

The ILL Visitors Club

All administrative tools for our scientific visitors are now grouped together and directly accessible on the web, thanks to the Visitors Club. All information is presented in a user friendly environment. After having logged in with your own personal identification[1], you will access directly all the available information which concerns you. Users with particular responsibilities have privileged access to other tools, according to their role. The ILL Visitors Club includes the electronic proposal and experimental reports submission procedures and makes available additional services on the web, such as acknowledgement of receipt, subcommittee results, user satisfaction forms and so on.

Moreover, we are in the process of introducing an *Electronic Peer Review* of the proposals submitted to the ILL, with a new application within the Visitors Club, which uses a web-based interface to the SCO Oracle database.

Proposal submission

There are three different ways of submitting a proposal to the ILL:

- standard submission of a research proposal - twice a year (in the first & third quarters).
- fast access to the ILL beam time - twice a year (in the second & fourth quarters).
- Director's discretion time (DDT) – no time restriction.

Special access for proprietary research and industrial users is also possible.

The Visitors Club hot-line is here to assist all users in all computer and server hitches. From the left, Franck Festivi, Sylvie Perroux and Jean Foubert.

1 - If you have submitted a proposal to the ILL from 1998 onwards, you have been automatically registered in the Visitors Club and received an e-mail with your personal username and password. If not and you wish to join the ILL Visitors Club, you can register on the ILL web site or directly at http://vitraill.ill.fr/cv/.

Extensive information about the ILL, its facilities and application for beam-time is available on our web-site (at http://www.ill.fr/).

In 2002, a common ***ILL/EMBL deuteration laboratory*** has been made available to external users. The aim of the laboratory is to provide a focus for European scientists wishing to make their own deuterated materials for neutron scattering or NMR experiments. Information about the availability of this facility for external users is given on the ILL web-site (http://www.ill.fr, Users & Science, user Information, Proposal Submission). Please contact the Head of the Deuteration Facility, Dr Michael Härtlein (haertlein@ill.fr) for further details.

Brigitte Aubert organises the Subcommittee Meetings, held at the ILL in Spring and Autumn every year.

Andrew Harrison (University of Edinburgh, left) and Hervé Jobic (CNR, Villeurbanne), joined the ILL Scientific Council in November 2002.

Submission of a standard research proposal

Applications for beam time should be submitted electronically, via our Electronic Proposal Submission system (EPS), available on the Visitors Club web-site. Proposals can be submitted to the ILL twice a year, at the end of February and September. The web system is activated two months before each deadline.

Submitted proposals are divided amongst the different colleges (see indent), according to their main subject area.

Proposals are judged by a Peer Review Committee of the Subcommittees of the ILL Scientific Council. Subcommittee members are specialists in relevant areas of each College and they evaluate the proposals for scientific merit, assigning priorities and beam time to accepted proposals.

Before the meeting, the subcommittee receives a Report on the technical feasibility and safety of a proposed experiment from the appropriate College at the ILL. Two proposal review rounds are held each year, approximately six weeks after the dead-line for submission of applications.

There are normally 4.5 reactor cycles a year each, of which lasts 50 days. Accepted proposals submitted by February will receive beam time in the second half of the year and those submitted by September, in the first half of the next year. More detailed information on application for beam-time and dead-lines are given on our web-site at http://www.ill.fr/pages/science/User/UProposals.htm.

The ILL scientific life is organised into 10 colleges:

College 1	*Instrumentation*
College 2	*Theory*
College 3	*Nuclear and Fundamental Physics*
College 4	*Structural and Magnetic Excitations*
College 5A	*Crystallography*
College 5B	*Magnetism*
College 6	*Structure and Dynamics of Liquids and Glasses*
College 7	*Materials Science, Surfaces and Spectroscopy*
College 8	*Structure and Dynamics of Biological Systems*
College 9	*Structure and Dynamics of Soft-condensed Matter*

Submission of a proposal by the Fast Access route (FAST)

To be more responsive to user needs where appropriate and where possible, the ILL had introduced in February 2001, Faster Access Special beam Time (FAST) on specific instruments. This covered scientific areas where fast response time was a crucial point. The beam time made available for FAST access was during the period of February-March and August-September. The idea was to create 2 plus 2 submission dead-lines which were broadly speaking separated by three months. The Fast Access mode combined peer-review, confidentiality and short delay time between submission and beam time allocation. Research proposals were submitted through the

web: internal review and peer-review assessment by the appropriate Subcommittee was also conducted electronically. The delay time between the proposal submission and the running of experiments was of the order of two months.

However, from the beginning it was clear that FAST access was not overwhelming. Despite publicity aimed to improve this situation, only a moderate number of proposals was received. In addition, at the Scientific Council meeting in April 2002, serious concern was expressed by a number of College Chairmen that not only was the number of proposals low, the overall quality was not judged to be equal to proposals submitted to the normal rounds. As a result, the ILL Management has decided that the procedure will be discontinued as from 2003.

Submission of a proposal to the Director's Discretion Time (DDT)

This option allows a researcher to obtain beam time quickly, without going through the peer-review procedure. DDT is normally used for hot topics, new ideas, feasibility tests and to encourage new users. Applications for Director's Discretion Time can be submitted to the Head of the Science Division, Dr. Christian Vettier, at any time. However, to offer a larger fraction of the available beam time to our users, DDT will be suspended during the 3-year "refit" programme (see page 130).

Access for proprietary research and industrial users

The ILL's mission is to provide neutrons for both public and industrial research. Our Industrial Liaison and Consultancy Group (ILC) ensures rapid access and total confidentiality to industrial companies, and provides a specialised staff. The ILC Group is in fact composed of scientists with considerable experience and expertise in neutron techniques applied to industrial R&D, and it facilitates and co-ordinates all aspects of industrial R&D at the ILL: initial enquiries, contractual questions, planning, experimental operations. All industrial research programmes are confidential and can be organised at short notice. To apply for proprietary beam time, please contact the ILC at industry@ill.fr or consult the web site under http://www.ill.fr, Industrial Use.

A summary of the industrial experiments performed in 2002 is given on page 138.

Experimental reports

Users are asked to complete an experimental report on the outcome of their experiments. The submission of an experimental report is compulsory when applying for beam time for a continuation proposal: failure in doing so may in fact lead to rejection.

All ILL Experimental Reports are now software-archived and accessible via the web server as PDF files (under http://www.ill.fr, Publications). You can search a report by experimental number, instrument, college, date of experiment, title, experimental team or local contact, institute.

The ILL welcomed 1153 users in 2002. Approximately 85% came from the member countries including 276 from France, 209 from Germany and 243 from the UK (figure 1). Many of our visitors were received more than once.

Feedback from our Users

We value feedback from our users as an indicator of how well our facility is fulfilling their needs and to initiate actions when this is not the case. Therefore, this year we have again organised two *User Forums*, in June and in November. Users who are on-site that day are invited to an informal meeting with the ILL Directors, the User Support Office and Group Leaders of both the Science and the Project and Technique Divisions. The objective is to obtain important feedback on the quality of the instruments and services at the ILL.

We very much appreciate the enthusiasm and co-operation of our users in giving their views, on such topics as instrument upgrading and implementation, new sample environment and instrumentation, quality of the Restaurant and the Guest House, and so on. Every effort will be made to implement suggestions.

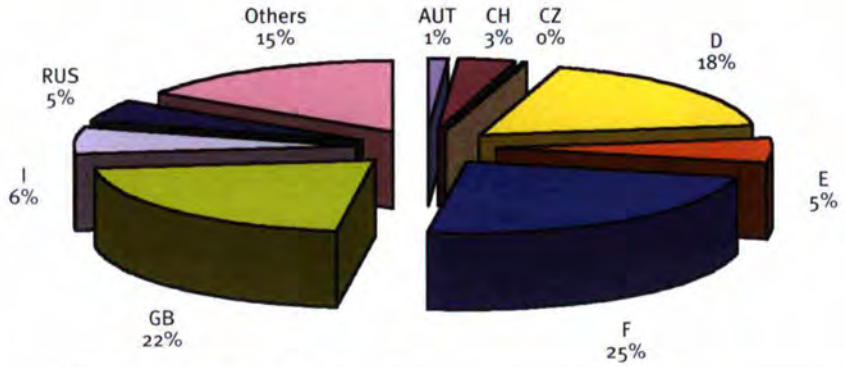

Figure 1: National affiliation of ILL users during 2002.

Experimental reports for experiments performed in 2002 are included in the attached CD-ROM.

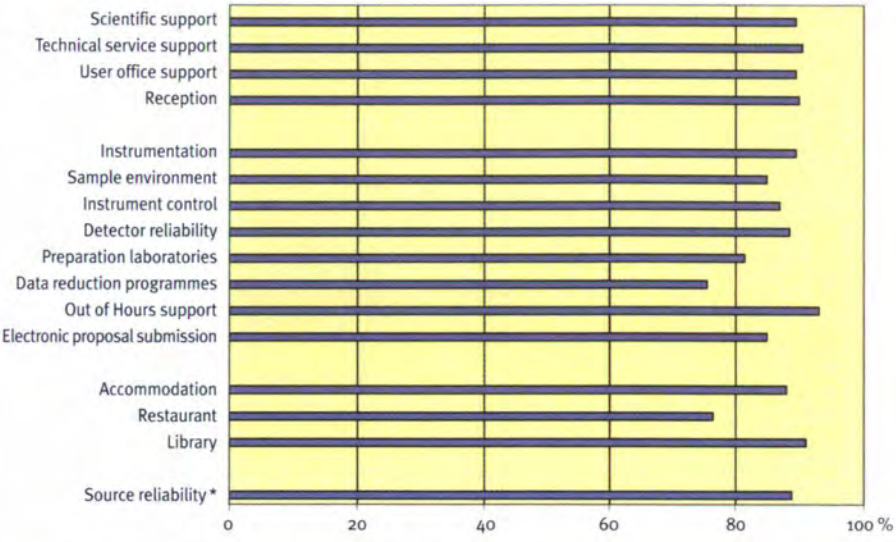

Figure 2: User satisfaction survey results (year 2002).
* The source reliability has been calculated from Table 1.

A happy user! Diana Sanchez from Madrid.

The present system of ***User Feedback Forms***, now dealt with electronically, is another measure of gathering the opinion of our users in order to raise a mirror up to ourselves. Levels of satisfaction are in general high, but we particularly appreciate the written comments on these forms.

We are actively strengthening the level of technical support outside of working hours. ***Out of Hours Support (OHS)*** has been implemented at first within the Instrument Control Service, as a starting point. Comprehensive documentation – web-based – has been put in place. We plan to extend gradually this kind of support to all the other services at the ILL. At the end of 2002, OHS has become operational also within the Neutron Detector Service.
We have being testing user satisfaction via a questionnaire - the ***User Satisfaction Form***. Users who have just finished an experiment at the ILL are asked to complete the questionnaire and to give us their views on different topics. User comments and solutions are entered into a database and summarised for the ILL Directors, the User Support Office, Group Leaders and Instrument Responsibles. The results of the survey during 2002 (see figure 2) showed in most cases very high satisfaction (close to 90%) with the staff support and ILL equipment. The Out of Hours Support – recently established – encountered the approval of most of those who needed it.

The Instrument Control OHS team. From the left: (top) Robert Harrison, John Allibon, Stuart Caunt, Franck Cecillon and Jérôme Locatelli; (bottom) Jean-Antoine Vidal-Garcia, Jean-Jacques Vernier and Abdelali Elaazzouzi. Frédéric Descamps was too shy to be in the picture.

The Neutron Detector OHS team. From the left: Jean-Claude Buffet, Frédéric Millier, Michel Gamon, Jean-François Clergeau, Gilbert Viande, Giuliana Manzin, Patrick Van Esch, Thomas Gahl, Bruno Guerard and Fabrice Horst.

Instruments

The instrumental facilities at the ILL are shown in the schematic diagram on page 129.

Besides the 25 ILL instruments, there are 9 CRG-instruments, which are operated by external Collaborating Research Groups. There are currently three different categories of CRG instruments.

- CRG-A in which the external group leases an instrument owned by ILL. They have 50% of the beam time at their disposal and for the remaining 50% they support ILL's scientific user programme.
- The CRG-B category owns their instrument and retains 70% of the available beam time, supporting the ILL programme for the other 30%.
- Finally, CRG-C instruments are used full time for specific research programmes by the external group, which has exclusive use of the beam.

DB21, LADI and IN15 have a special status, since they are joint ventures of the ILL with other laboratories: in the case of DB21 and LADI with EMBL and for IN15 with FZ Jülich and HMI Berlin.

The list of instruments as of December 2002 is summarised below (CRG instruments are marked with an asterisk *):

- powder diffractometers: D1A, D1B*, D2B, D20
- liquids diffractometer: D4
- polarized neutron diffractometers: D3, D23*
- single-crystal diffractometers: D9, D10, D15*
- large-scale structures diffractometers: D19, DB21, LADI, VIVALDI
- small-angle scattering: D11, D22
- low momentum-transfer diffractometer: D16
- reflectometers: ADAM*, D17, EVA*
- diffuse scattering and polarization analysis spectrometer: D7
- three-axis spectrometers: IN1, IN3, IN8, IN12*, IN14, IN20, IN22*
- time-of-flight spectrometers: IN4, IN5, IN6,
- backscattering and spin-echo spectrometers: IN10, IN11, IN13*, IN15, IN16
- nuclear physics instruments: PN1, PN3
- fundamental physics instruments: PF1, PF2

D1A is shared between powder diffraction and strain scanner applications. S18*, an interferometer, is a CRG-C instrument and is normally not available as a 'user' instrument, although some beam time is made available for prototype tests of USANS.

Details of the instruments can be found on the web under http://www.ill.fr (Users & Science / Instrument groups & Theory).

Beam-time allocation & utilisation for 2002

Overall, the Subcommittees of the Scientific Council scrutinised 935 proposals requesting 7451 days for 2002, out of which 661 proposals received beam time, allocating 4504 days of beam time on the different instruments. In 2002, the member countries of the ILL were: France, Germany, UK, Spain, Switzerland, Austria, Italy, the Czech Republic and Russia. The distribution of beam-time requested and allocated amongst them is shown in Table 2.

In calculating the statistics of beam-time per country, shown in Table 2, the attribution is based on the location of the laboratory of the proposers, not their individual nationality. For a proposal involving laboratories from more than one member country, the total number of days is divided amongst the collaborating countries, and weighted by the number of people for each country. When a proposal involves collaboration with a non-member country, the

			Before national balance		*After national balance*	
Country	**Requested days**	**Requested %**	**Allocated days**	**Allocated %**	**Allocated days**	**Allocated %**
AUT	82.8	1.1	62.5	1.4	62.5	1.4
CH	238.4	3.2	151.3	3.3	151.6	3.4
CZ	69.3	0.9	35.2	0.8	37.7	0.8
D	1 869.7	25.1	1 045.9	23.1	1 056.5	23.5
E	369.8	5.0	235.6	5.2	235.2	5.2
F	1 772.0	23.8	1 158.2	25.6	1 168.8	26.0
GB	2 024.0	27.2	1 285.7	28.4	1 279.2	28.4
I	368.5	4.9	230.2	5.1	231.8	5.1
RUS	656.1	8.8	321.6	7.1	280.5	6.2
Total	**7 450.8**	**100.0**	**4 526.0**	**100.0**	**4 503.8**	**100.0**

Table 2: Distribution amongst the Associate and scientific-member countries of beam-time requested and allocated in 2002 during the Subcommittees of the Scientific Council.

Instruments	Days requested†	Days allocated†	Number of scheduled experiments†	Number of perfomed experiments†	Days used for users††	Days lost	Days for commissioning/ test	Days for internal research
ADAM	*126*	*59*	*11*	*10*	*120*	*2*	*3*	–
D1A	129	119	33	30	108	2	20	30
D1B	*92*	*86*	*34*	*31*	*185*	*6*	*8*	*3*
D2B	247	152	61	63	158	7	24	11
D3*	310	152	16	11	105	12	29	0
D4*	99	62	13	6	48	0	11	0
D7	176	139	15	13	136	2	50	11
D9*	194	139	18	7	94	12	7	36
D10	307	166	17	16	182	7	7	3
D11	234	226	51	46	130	17	47	3
D15	*19*	*7*	*1*	*1*	*37*	*7*	*7*	–
D16	148	134	20	20	144	4	39	14
D17	203	160	38	34	138	3	46	14
D19	182	156	18	15	116	13	69	0
D20	209	163	61	55	154	7	27	13
DB21	31	31	2	*2*	45	4	20	0
D22	364	141	61	52	136	16	38	14
D23	*46*	*50*	*5*	*3*	*187*	*3*	*8*	–
EVA	*61*	*36*	*3*	*3*	*166*	*13*	*11*	–
IN1*	150	78	11	6	53	5	25	7
IN3	76	48	5	4	48	14	137	0
IN4	131	110	23	18	75	7	18	3
IN5*	142	50	10	0	0	0	0	0
IN6	384	177	45	44	166	13	16	10
IN8*	189	66	9	3	15	0	30	5
IN10	174	142	12	19	136	7	54	14
IN11	145	130	12	13	134	5	37	28
IN12	*89*	*43*	*5*	*4*	*97*	*3*	*2*	–
IN13	*152*	*83*	*12*	*11*	*176*	*2*	*22*	–
IN14	248	151	16	15	121	29	34	16
IN15	137	95	11	12	86	44	13	6
IN16	337	163	26	21	154	15	18	17
IN20	240	146	16	16	116	14	48	20
IN22	*98*	*62*	*8*	*7*	*178*	*4*	*10*	–
LADI	179	172	8	2	145	4	50	0
VIVALDI	61	57	15	13	137	8	43	11
PF1	209	160	7	7	125	0	0	0
PF1B	344	104	5	3	148	23	0	19
PF2**	924	555	13	14	710	0	0	0
PN1	380	154	11	9	104	69	26	0
PN3	310	163	9	9	129	5	67	0
Total	8 276	5 087	771	670	5 442 *(74.7%)*	408 *(5.6%)*	1 121 *(15.4%)*	311 *(4.3%)*

Table 3: Beam-time request/allocation (via standard subcommittees, FAST access & DDT altogether) by instrument and instrument performance. CRG instruments are in italic and green.
† The number of performed experiments is lower than the number of accepted ones because of the loss of 0.5 cycle. 'days allocated' refers to only those days reviewed by the subcommittees and FAST access (i.e., excluding CRG days for CRGs).
†† 'days used' refers to the total number of days delivered to users in ILL time, CRG time and DDT.
* D3, D4, D9 and IN1 have not operated in the second half of the year because of the dismantling of the hot beam tubes; IN5 & IN8 were under reconstruction in 2002.
** PF2 consists of 5 different set-ups where several experiments are running simultaneously.

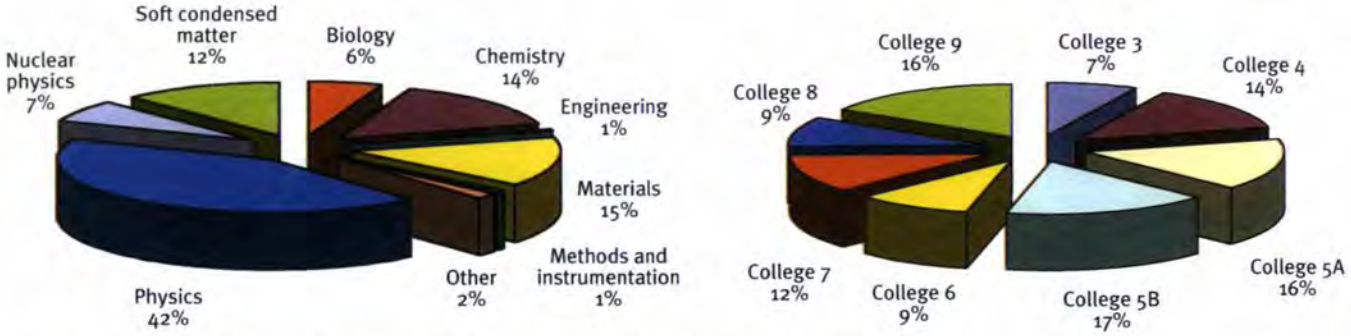

Figure 3: Beam-time allocation in 2002: distribution amongst the different research areas.

allocated time is attributed entirely to the collaborating member country (or countries), and weighted by the number of people for each member country. When ILL scientists are proposers or co-proposers, the allocated ILL time is attributed amongst the member countries according to their financial contributions to the ILL. Local contacts are not counted as proposers except when they are members of the research team.

The distribution of beam time for these experiments amongst the different research areas & colleges is shown in Figure 3.

A more complete view is given in Table 3. Request and allocation of beam time – as well as the number of scheduled experiments – refer to standard submissions to the subcommittee meetings and FAST access. The effective number of days given to our users takes into account also Director's Discretion Time (DDT) and CRG's time for CRG instruments.

In 2002, 29 proposals were submitted to the FAST rounds, requesting 88 days, out of which 18 proposals received beam time, with 46 days allocated on those instruments concerned by the FAST option (D1A, D2B, D20, D11, D22, D16, DB21, LADI, VIVALDI). DDT was given to 14 experiments for a total of 53 days.

The instruments D4 and IN1 share a beam. Note that PF2 consists of 5 different set-ups allowing several experiments to run simultaneously. Normally, for official statistics (as for Table 2) the total number of days requested and allocated is averaged by a factor 5. However, in Table 3 we report the total number of days delivered on all the 5 instruments (EDM, MAM, TES, UCN, VCN).

Instrument performance

Table 3 also gives a summary of instrument performance for 2002. For each cycle, a record is kept of any time lost from the total available beam-time and the reasons for the lost time are analysed for all the instruments. The table gives a global summary for the year.

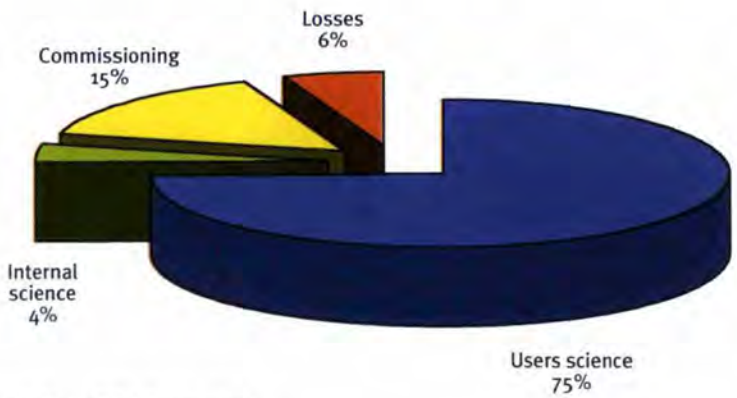

Figure 4: Use of ILL beam time

Overall 5442 days were made available to our users in 2002 on ILL and CRG instruments, which represents about 74.7% of the total days of operation. 311 days were used by ILL scientists to carry out their own scientific research. About 15.3% of the total beam time available on the ILL instruments is allowed for tests, calibrations, scheduling flexibility, minor breakdowns recuperation.

Totally, about 770 experiments were scheduled, but only 670 were effectively carried out. The reason for this is that during 2002 the reactor operated for 4.0 cycles, representing 200 days of

neutrons, instead of the 4.5 cycles initially foreseen (see Reactor Operation, p. 130). Please note that the "days lost" column does not include the half cycle lost due to the beam tube leak (25 days over an average of 30 instruments).
In 2002, about 408 days were lost due to various malfunctions, which represents less than 6% of the total available beam-time.

Detailed comments on the larger beam-time losses (20 days or more) are as follows:

- IN14 had various problems mainly due to failures in critical sample environment conditions (dilution fridge, 4T cryomagnet...); about 10 days were also lost because of a sample which had not been well prepared by the users;
- IN15 lost 28 days because of a serious selector breakdown;
- PF1B could not start a scheduled experiment because the user installation was not ready for measurement;
- PN1's breakdown was due to the failure of the target changer.

Industrial use of neutrons

Relations with high profile industrial companies remained almost stable in 2002. A total of 8.5 days beam time have been sold for 5 different small-angle neutron scattering studies (in 2001: 11 days). 4 experiments (7.5 days) were performed at D11 and one experiment (1 day) at D22. We have attracted one new customer from the field of pharmaceutical research for an experiment at D11.
With a view to increasing plant life the investigation of irradiated reactor steel samples for radiation induced precipitates is a field where UK and French companies are actively using small-angle neutron scattering, both at the instruments D11 and D22 of the ILL.
A direct spin-off from the excellent relation between one of these customers, the D11 instrument team and the ILL's design office has been the development of a new dedicated sample holder for investigating highly radioactive steel tiles in a magnetic field under vacuum. With the old sample holder used until 2001, the samples had been fixed with scotch tape on a plate attached to one of the magnetic pole pieces. Furthermore, the water normalisation of the scattering intensity had to be performed at atmospheric pressure, outside the vacuum container and with a different sample aperture. With the new device in use since May 2002 (see photo), these radioactive samples can now be fixed more precisely and rapidly through a metal clamp. As a consequence, the user's exposure to radiation is reduced, when changing the sample. Another big advantage of the new magnet sample holder is the possibility of using a vacuum-tight standard water cell for normalisation in the same mount, with the same geometry (beam defining aperture) as for the sample run. This example shows the valuable contribution of the ILL's expertise to help our customers to improve their industrial research.
ILL offers industrial users the opportunity to perform a test experiment before ordering beam time in order to examine the feasibility of a measurement. Some customers took advan-

New magnet sample holder for SANS experiments under vacuum at D11, developed at ILL for AEA Technology. The photo shows a 1mm standard water cell at the sample position. The sample holder is shown before fixation to the upper magnet pole piece, the lower pole piece is not shown.

tage of this possibility in the field of residual stress determination.

The appropriate instrument for this type of work is the D1A high-resolution diffractometer, which is used half time for powder diffraction and for neutron stress determination. The neutron method is capable to resolve the residual stress state deep into matter non-destructively and with a lateral resolution of typically 0.5 mm. A speciality of the D1A strain scanning option is its capability to perform measurements at interfaces and surfaces to within a few ten micrometers.

Examples of test measurements were welds in thick stainless steel tubes for nuclear power plants and coated hard metal (Tungsten-Carbide) for the tool making industry. Another industrial test was carried out for Aluminium foil production and became the basis for a scientific proposal for beam time allocation in 2003. Very interesting was an application in the field of aerospace technology. We showed, that it is possible to determine residual stresses in the thin walls (0.5 – 3 mm) of channels surrounding an ARIANE rocket motor. In those, liquid hydrogen and oxygen is evaporated before ignition in the combustion chamber.

In addition, other experiments of industrial relevance have been performed at ILL. Let us take the instrument D20, which is a powder diffractometer with the advantage of high neutron intensity and very fast, simultaneous data acquisition. These characteristics, as well as the penetration power of neutrons, make it a powerful instrument for time-resolved *in situ* measurements. It could demonstrate its capabilities in the fields of hydrothermal synthesis (hardening of autoclaved concrete), self-propagating high-temperature synthesis (production of ceramics with metallic properties for high-temperature applications) and electrochemistry (recharge capabilities of batteries).

More information about our industrial activities and how to apply can be found on the ILL web site http://www.ill.fr/, "industrial use", or by contacting directly our industrial liaison group, industry@ill.fr.

P. Lindner, T. Pirling

The Refit Programme *of the ILL Reactor*

F. Plewinski

During the first half of 2002 detailed safety reviews of the ILL's High Flux Reactor (HFR) and associated facilities were requested by the French nuclear safety authority (DGSNR - Direction Générale de Sûreté Nucléaire et de la Radioprotection). On 2 May 2002, a group of experts (known as the "Groupe Permanent" responsible for nuclear reactors) carried out a review based on a report produced in the first half of the year by the IRSN (Institut de Radioprotection et de Sûreté Nucléaire), in which all aspects relating to nuclear safety and radiation protection were examined. Following the recommendations and requests by DGSNR, a programme of "refit" measures has been agreed over the next 3 years, at a cost of about 20 M€, which will bring the ILL's installations up to the stringent standards foreseen during the coming decade.

The main recommendations concerned the following:

- the structural reinforcement of the HFR and the Institute's buildings in case of a high-intensity earthquake which could affect the Grenoble site;
- the demonstration of the resistance of equipment important for the safety of the installations (reactor cooling and confinement systems) in the event of this safe shutdown earthquake, as well as the demonstration of the resistance, in the event of such an earthquake, of heavy structures likely to damage safety equipment;
- the control system of the High Flux Reactor;
- the safety studies concerning the operation of the HFR and detritiation facility, in particular in the event of a fire or a malfunctioning of safety-related equipment.

The measures to be taken as a result of these recommendations are scheduled to be implemented between 2002 and 2006, with the majority of the work to be completed between the end of 2003 and the end of 2005. During this period we shall operate for 3 cycles per year (instead of the 4.5 cycles normally scheduled) but pledge to deliver 80% of the beam-days of previous years to our scientific partners.

Olivier Aguettaz, technician in the detritiation and source group, at the detritiation station.

The repercussions for the entire installation have prompted the ILL to set up a project management structure, known as the Refit Management Committee, dedicated to the implementation and monitoring of these measures. This structure (see Figure 1), which comprises around a dozen people, also relies on support from the staff of the ILL divisions, in particular the Reactor Division, which brings together the majority of the skills and know-how needed to complete the project successfully within the relatively short time available and taking into account the number and range of tasks to be undertaken.

Olivier Fourrier, chemist at the detritiation and source group in the salle de contrôle.

The following major projects were launched in 2002:

- strengthening of the reinforced concrete structure which supports the transfer canal where used fuel elements are stored. As a result of this reinforcement work, laboratories which handle targets containing alpha emitter radionuclides and the storage area for radioactive sources had to be moved;
- implementation of redundancy measures in the final part of the HFR safety control circuit, to be triply sure that any malfunction would trigger the shut down of the reactor.
- continuation of studies on the resistance of the installation's civil engineering structures in the event of an earthquake. These studies will fully document all actions to be taken and should be completed by the middle of 2003.
- studies of the modifications of buildings in contact with the reactor containment in order to avoid any interaction in the event of an earthquake, between these buildings and the containment. The buildings primarily concerned are the two experimental guide halls (ILL7 and ILL22) and the building which houses the reactor control room and offices (ILL4).

Ladies for science

Part of our library team: (from the left) Maria Jarnias, Sophie Rio and Virginie Teissier.

Satisfait ou remboursé! Isolde Harbich welcomes you at the ILL travel office.

Michèle Correard monitors the doses on scientists' film badges.

Gaëlle Rochex, deputy safety engineer: your security is in good hands!

Vera Gontier and Siriane Lalliat: our smiling welcome to all ILL visitors.

FACTS & FIGURES 2002.

Name Institut Max von Laue - Paul Langevin (ILL)

Founded 1967

Associates

France

Commissariat à l'Energie Atomique (CEA)

Centre National de la Recherche Scientifique (CNRS)

Germany

Forschungszentrum Jülich

United Kingdom

Engineering and Physical Sciences Research Council (EPSRC)

Countries with Scientific membership

Spain

Ministerio de Ciencia y Tecnologìa (MCYT)

Switzerland

Schweizer Bundesamt für Bildung und Wissenschaft (SBBW)

Italy

Istituto Nazionale per la Fisica della Materia (INFM)

Russia

Ministry of the Russian Federation for Atomic Energy (MINATOM)

MENI (Middle European Neutron Initiative) Consortium, composed of

Austria: Österreichische Akademie der Wissenschaften

Czech Republic: Charles University of Prague

Staff

427 people including 60 experimentalists in the scientific sector.
278 French, 51 German, 53 British, 45 others.

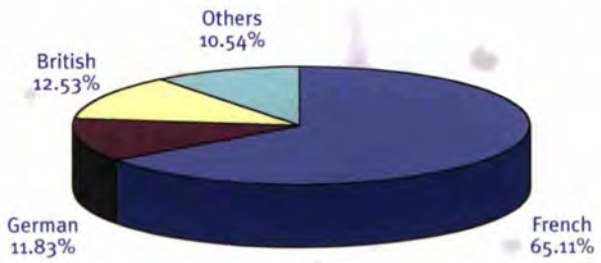

Organisation chart

(December 2002)

DIRECTOR
C. Carlile

DIRECTOR'S SERVICES

HEAD OF HEALTH PHYSICS	SAFETY ENGINEER	MEDICAL	ASSISTANT TO THE DIRECTION
J. Tribolet	H. Schweitzer	J.F. Trzmiel	A. Wright

REFIT MANAGEMENT COMMITTEE
F. Plewinski

SCIENCE DIVISION
C. Vettier
(Associate Director)

- THEORY — E. Kats
- SENIOR ILL FELLOWS — F. Tasset
- SCIENTIFIC COMPUTING — M. Johnson
- INDUSTRIAL LIAISON and CONSULTANCY — P. Lindner, T. Pirling (Assistant)

SCIENTIFIC SUPPORT
G. Cicognani

- SCIENTIFIC COORDINATION
- JOINT ILL/ESRF LIBRARY — V. Teissier

NUCLEAR and PARTICLE PHYSICS
H. Börner

- DIFFRACTION GROUP — A. Hewat
- LARGE SCALE STRUCTURE GROUP — P. Timmins
- BIOLOGY/CHEM. LABORATORY
- THREE-AXIS SPECTROMETER GROUP — R. Currat
- TIME-OF-FLIGHT, HIGH RESOLUTION GROUP — H. Schober

PROJECTS and TECHNIQUES DIV.
W. Press
(Associate Director)
R. Gähler (Deputy)

- NEUTRON DISTRIB., MECHANICS — P. Malbert
- INSTRUMENT CONTROL — F. Descamps
- COMPUTING — A. Barthélémy
- NEUTRON-OPTICS — K. Andersen
- DETECTORS — B. Guérard
- SAMPLE ENVIRONMENT — S. Pujol

REACTOR DIVISION
H. Guyon
J.M. Astruc (Deputy)

- SHIFT TEAMS, SITE SECURITY — L. Brayer
- ELECTRICITY and ELECTRONICS — L. Pacallet
- MECHANICAL SERVICE — J. Bazin

ADMINISTRATION DIVISION
N. König
I. Feuersenger
(Assistant)

- FINANCE — Ph. Guérin
- PURCHASING — B. Donnelly
- PERSONNEL and HUMAN RES. — R. Mulot
- BUILDING and MAINTENANCE — C. Bouton
- MANAGEMENT INFORMATION SYSTEMS — M. Grevaz

Budget 60 M€ (excluding taxes)

Income (M€)

from Associates	50.2	*83.67%*
from scientific members	8.6	*14.33%*
own income	1.2	*2.00%*
	60.0	***100.00%***

Expenditure (M€)

staff costs	32.0	*53.33%*
operating costs	9.7	*16.17%*
investment costs	8.5	*14.17%*
fuel cycle	6.9	*11.50%*
Refit Programme	2.9	*4.83%*
	60.0	***100.00%***

Distribution of ILL purchases (M€, excluding taxes)

France	10.96	*68.46%*
Germany	1.13	*7.07%*
United Kingdom	1.46	*9.13%*
Others	2.46	*15.37%*
	16.01	***100.00%***

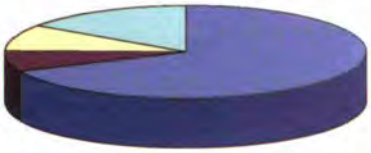

Bodies

Steering Committee, meeting twice a year
Subcommittee on Administrative Questions, meeting twice a year
Scientific Council with 8 subcommittees, meeting twice a year
Instrument Subcommittee, meeting once a year

Reactor 58 MW, running 4 cycles in 2002 (with cycles of 50 days)

Experimental Programme

670 experiments (allocated by subcommittees) on 25 ILL-funded and 9 CRG instruments
1153 visitors coming from 34 countries
935 proposals submitted and 661 accepted

Experiment Selection by the Scientific Council *via* its 8 subcommittees

Nuclear and fundamental physics (college 3)
Structural and magnetic excitations (college 4)
Crystallographic structures (college 5a)
Magnetic structures (college 5b)
Structure and dynamics of liquids and glasses (college 6)
Materials science, surface and spectroscopy (college 7)
Structure and dynamics of biological systems (college 8)
Structure and dynamics of soft-condensed matter (college 9)

Scientific Life

Based on 10 colleges
8 of which map on to the subcommittees plus 2 others:
instruments and techniques (college 1)
theory (college 2)

Neutrons and Art

The London Institute has initiated a series of projects in England, Portugal, France and Italy under the title *"Signatures of the Invisible"* to coincide with International Science Week 2002. Within this frame, the exhibition 'Particle Fabrics' was held in Milano on 8-20 November and presented the result of the collaboration between a group of textile designers from Chelsea College of Art and Design at the London Institute (supervised by Kay Politowicz), and a group of scientists from the ILL (Clive Wilkinson). Particle Fabrics was a groundbreaking exhibition of textiles in which fabrics transform interior space through the use of VIVALDI neutron diffraction patterns, light and shade.

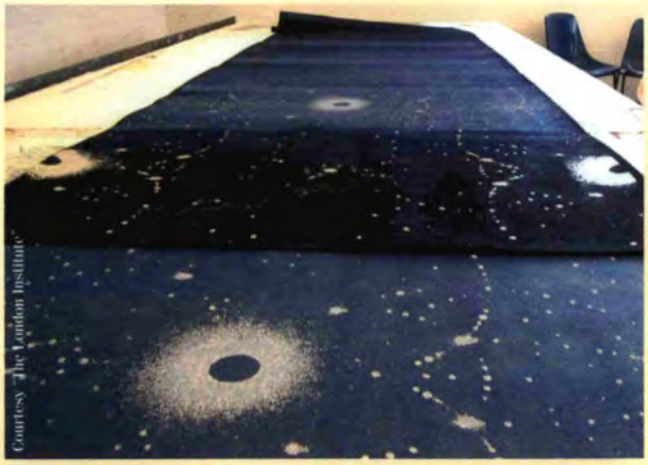

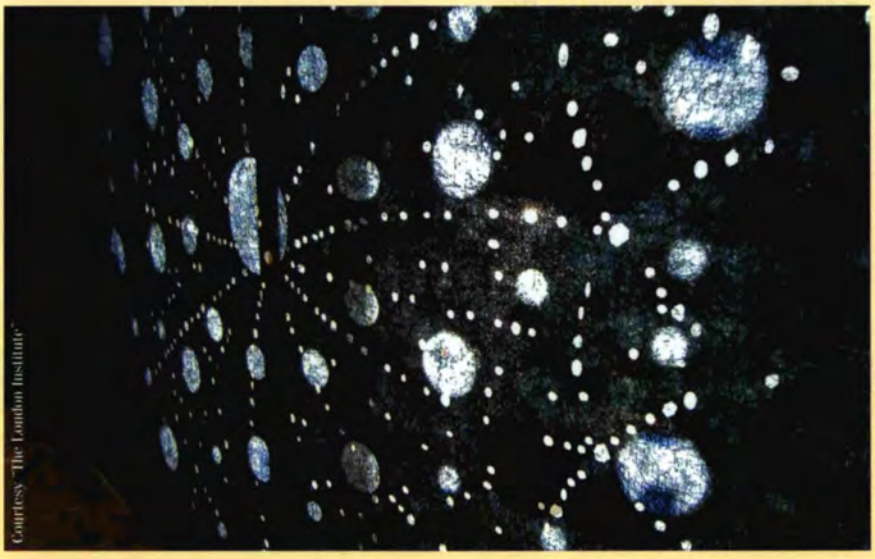

THE LONDON INSTITUTE **CHELSEA COLLEGE OF ART AND DESIGN** CAMBERWELL COLLEGE OF ARTS CENTRAL SAINT MARTINS COLLEGE OF ART AND DESIGN LONDON COLLEGE OF FASHION LONDON COLLEGE OF PRINTING

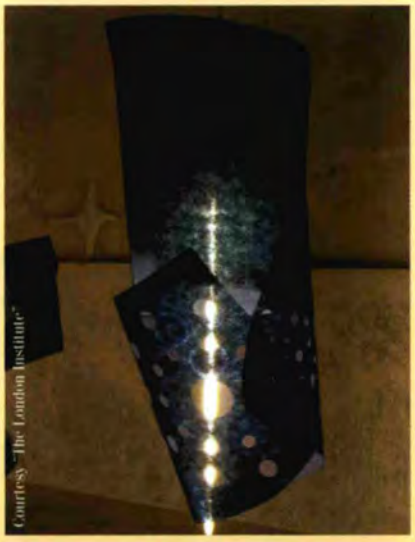

Man accomplishing Unity (1971-1972), sculpture by Ipoustéguy at the ILL entrance.

PUBLICATIONS.

In 2002, the ILL received notice of 429 publications by ILL staff and users of which 378 were published as journal articles, and 51 as conference proceedings in journals, books, cd-roms or reports.

The distribution by subject is as follows: 31 in neutron instruments and methods, 12 in theory, 24 in nuclear and particle physics, 84 in structural and magnetic excitations, 67 in crystallography, 80 in magnetic structures, 31 in structure and dynamics of liquids and glasses, 35 in materials science, surfaces and spectroscopy, 19 in structure and dynamics of biological systems, 46 in structure and dynamics of soft-condensed matter.

From this year onwards, the detailed publications list is included in the attached CD-ROM.

ILL 2002 CD-ROM (Mac/PC)

The enclosed CD-ROM contains both the ILL 2002 Annual Report and the ILL Experimental reports as Portable Document Format (PDF) files. You will need a PDF file reader (Adobe® Acrobat® Reader®) to view it.

The CD-ROM also includes an interactive virtual visit of the ILL instrument hall and of the two guide halls[1]. You can also enjoy a panoramic view of the beautiful landscape surrounding the ILL. Once the visit is launched you can click in the map to select a starting point. Then click in the image to get the cursor ✣ with which you can move right, move left, look up and down. You can move to another view point each time the cursor turns to ⌂. This virtual visit requires QuickTime 5 or later to be installed on your computer. Free Windows and Mac OS downloads are available from www.apple.com/quicktime.
Have a nice visit!

(1) The ILL is usually a very busy place but, for technical reasons, as few people as possible were present during the shooting.

NEUTRONS
FOR SCIENCE

Institut Laue-Langevin
6, rue Jules-Horowitz - BP 156
38042 Grenoble Cedex 9 - France

www.ill.fr